Author:
Sowter, Matthew James

Title:
Macro-scale interaction of hillslope erosion and sediment redistribution.

MACRO-SCALE INTERACTIONS OF HILLSLOPE EROSION AND SEDIMENT REDISTRIBUTION

By

MATTHEW JAMES SOWTER

A thesis submitted to the University of Bristol

in accordance with the requirements of the degree of

Doctor of Philosophy in the Faculty of Science

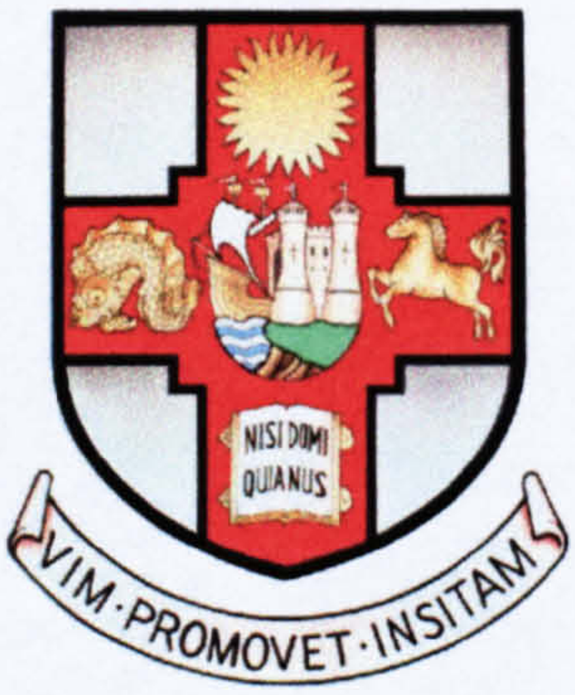

Department of Earth Sciences

November 1999

ABSTRACT

This thesis investigates the macro-scale processes of sediment liberation from orogenic mountain belts and its delivery to adjacent sedimentary basins. Large scale quantitative data for study areas in the Italian Apennines, and the Santa Cruz Mountains, Death Valley, Marin County and the Wheeler Ridge in California are presented.

Data from study areas in the United States and Italy demonstrate that changes in channel long profile morphology consistently change downstream in the transitional zone from areas of long term erosion to deposition. Data are provided which examine the accuracy of such profiles derived from a 230 metre digital terrain model (DTM) of Italy. Profiles derived show a gross morphology similar to that from 1:10,000 scale topographic maps, but slope analyses show a poorer correlation. The Enza River in Italy is an 'alluvial veneer bedrock channel', and is shown to have a narrow range of dimensionless shear ($\tau*$) stresses along its length. Abrupt changes in the value of $\tau*$ and mean grain size along the upper Enza are related to a change in lithology from resistant Tuscan to erodible mudstone formations.

Fieldwork in the Italian Apennines has shown the widespread presence of steep, linear ridge terrain. Such slope forms are also evident in the Santa Cruz Mountains of California. Relief and slope analyses on a 30 metre DTM show that such slopes cluster about characteristic values of 16-24° and 50 to 70 metres respectively, and occur on resistant formations such as the Great Valley Sequence and Santa Cruz Mudstones. Across the Apennines, linear hillslopes are shown to correspond to areas with resistant Tuscan and Marnosa Arenecea formations outcropping. Basins with such slope forms are shown to have high mean slope and relief values and low denudation rates. Such rates result from the critical slope forms present. Areas with weaker Miocene lithologies have higher denudation rates and lack linear hillslopes, and show evidence of bedrock landsliding. Bedrock landsliding is shown to dominate the Apennines, both in terms of sediment delivery and gross morphology. Previous studies which show linear relationships between local relief and denudation are believed to be inadequate for the Apennines, where bedrock lithologies is one of the major controls on landscape form and the erosional processes operating upon it.

ACKNOWLEDGEMENTS

The work contained in this thesis results from the help and assistance of a great number of people, without whom I could not possibly have carried out and completed the work. I must first of all thank Pete Talling for devising the project in the first place and sending details to Edinburgh, where I first saw it advertised. His help in carrying out the work and speedy reading of drafts of work presented to him have been invaluable. I must also thank the University of Bristol for providing me with a scholarship to carry out the work and the Department of Earth Sciences for offering me the grant in 1996. The University of Bristol Alumni Foundation is also thanked for providing a grant which enabled me to visit the United States and attend the AGU conference.

On a more personal level, I would like to thank the various members of G48 for their friendship, support and help over the last three years. Wim, Fraukje, Hugh, Eric, Alex, Paul, Rhona, Isabella, Davide and even Yann - you're all stars, even if you do think that I'm a Geographer!! Scott Orford is thanked for being a great help with Arc/Info and in general for assisting me with things geographical! I also owe a debt to the Department of Geographical Sciences for allowing me to use GMA, without which I could not have carried out most of the work presented. Various other folk have helped me out with getting DTMs, getting references and learning how to use software packages: Eric Fielding for the Wheeler Ridge DTM, Josh Roering for the Santa Cruz models, Richard Pike for helping me in getting to grips with morphometry and the Marin County work and Alex Densmore for being easy to chat to about work. I'd also like to thank Paola Reichenbach and Fausto Guzzetti for making me welcome in Italy and assisting me greatly in my early days with Arc/Info.

Finally, of course, I owe the most to my parents and grandparents who have assisted me over the last seven years in more ways and to a level which I can never repay. Without their help and encouragement I could never have finished this! Thanks to you all!

DECLARATION

I declare that the work in this dissertation was carried out in accordance with the regulations of the University of Bristol. The work is original except where indicated by special reference in the text and no part of the dissertation has been submitted for any other degree.

Any views expressed in the dissertation are those of the author and in no way represent those of the University of Bristol.

The dissertation has not been presented to any other University for examination either in the United Kingdom or overseas.

Matthew J. Sowter 25th November 1999.

TABLE OF CONTENTS

CHAPTER 1 AIMS, OBJECTIVES AND THESIS ORGANISATION 1

1.1 INTRODUCTION 1

1.2 THESIS ORGANISATION 4

CHAPTER 2 EROSION, DEPOSITION AND SEDIMENT REDISTRIBUTION IN ALLUVIAL BASINS AND ADJACENT MOUNTAIN BELTS 7

2.1 INTRODUCTION 7

2.2 CHANNEL LONGITUDINAL PROFILES 10

2.2.1 Previous Work 10

2.2.1.1 Graded River Profiles 11

2.2.1.2 Fluvial Dynamic Equilibrium and Dis-Equilibria Features 11

2.3 DOWNSTREAM CHANGES IN CHANNEL GRADIENT 13

2.3.1 Measurement Strategy 13

2.4 OBSERVED CHANGES IN CHANNEL LONG PROFILES AND GRADIENT 18

2.4.1 The Italian Northern Apennines 18

2.4.1.1 Long Profile Morphology 21

2.4.1.2 Downstream Changes in Channel Gradient 21

2.4.2 Death Valley, California, U.S.A. 29

2.4.2.1 Long Profile Morphology 31

2.4.2.2 Downstream Changes in Channel Gradient 31

2.4.3 Wheeler Ridge, California, U.S.A. 47

2.4.3.1 Long Profile Morphology 49

2.4.3.2 Downstream Changes in Channel Gradient 49

2.4.4 South-Western Britain 59

2.4.3.1 Long Profile Morphology 59

2.4.4.2 Downstream Changes in Channel Gradient 59

2.4.5 Summary of Findings 64

2.5 LONG PROFILES DERIVED FROM DIGITAL TERRAIN MODELS (DTMS) 65

2.5.1 Introduction 65

2.5.2 The Use of DTMs in Hydrological Analyses 66

2.5.3 Problems Associated with DTMs 66

2.5.4 Depressions in Digital Terrain Models 67

2.5.5 Flow Routing Across DTMs 68

2.5.6 Derivation of Channel Long Profiles and Network Properties 69

2.5.7 Comparison of DTM and Map Derived Channel Long Profiles 72

2.6 Bed Shear Stress and Bedload Transport in the Northern Apennines 80

2.6.1 Introduction 80

2.6.2 Bedload Transport Rates 80

2.6.2.1 Bedload Transport in Alluvial Channels 81

2.6.2.2 Sand-Bed Alluvial Channels 82

2.6.3 Grain Size Variations Along Channels 82

2.6.4 Case Study: The Enza River, Northern Apennines, Italy 83

2.6.4.1 Channel Slope 84

2.6.4.2 Channel Depth 84

2.6.4.3 Mean Annual Discharge, Channel Cross-Sectional Area and Flow Velocity 84

2.6.4.4 Mean Annual Discharge and Basin Area 85

2.6.4.5 *Basin Area and Channel Depth* 87

2.6.4.6 Grain Size 87

2.6.5 Effects of Varying Value of Exponent 'p' on Estimated Values of Bed Shear Stress and Dimensionless Critical Shear Stress 87

2.6.6 Downstream Trends in Bed Shear Stress and Dimensionless Shear Stress 89

2.6.7 Implications for Modelling of Channel Networks 92

CHAPTER 3 MODELLING THE SPATIAL DISTRIBUTION OF EROSIONAL PROCESSES WITHIN OROGENIC MOUNTAIN BELTS 94

3.1 INTRODUCTION 94

3.2 MODELLING THE EVOLUTION OF MOUNTAINOUS REGIONS 95

3.2.1 Mountain Belt Erosion 95

3.2.2 Sediment Routing in Orogens 96

3.3 MORPHOLOGY OF HILLSLOPES AND PROCESSES OF HILLSLOPE EROSION 97

3.3.1 Slope Diffusion 98

3.3.2 Regolith Landsliding 100

3.3.3 Bedrock Landsliding 100

3.4 MODELLING SEDIMENT TRANSPORT IN MOUNTAINOUS REGIONS 101

3.4.1 Linear Sediment Transport 102

3.4.2 Nonlinear Sediment Transport 103

CHAPTER 4 CHARACTERISING THE NATURE OF STEEP, LINEAR-RIDGE TERRAIN, SANTA CRUZ MOUNTAINS, CALIFORNIA, USA 106

4.1 INTRODUCTION 106

4.2 PHYSIOGRAPHY AND TECTONIC SETTING OF THE SANTA CRUZ MOUNTAINS 109

4.2.1 Geography and Climate 109

4.2.2 Physiography of the Study Areas 109

4.2.3 Geologic Setting 114

4.3 TERRAIN VARIATION WITHIN THE SANTA CRUZ MOUNTAINS 117

4.3.1 Data and Methods 117

4.3.1.1 Slope 117

4.3.1.2 Local Relief 117

4.3.1.3 Dispersion of Altitude 118

4.3.1.4 ZR Ratio 118

4.3.1.5 Elevation-Relief Ratio / Hypsometric Integral 119

4.3.1.6 Dissection Index 120
4.3.1.7 Nogami Index 120
4.3.1.8 Slope Variability Index 120
4.3.2 Bedrock Lithology and Terrain Form 121
4.4 RESULTS 122
4.4.1 Slope Analysis 122
4.4.2 Local Relief 125
4.4.3 Dispersion of Altitude 129
4.4.4 ZR Ratios 129
4.4.5 Elevation-Relief Ratio and Dissection Index 129
4.4.6 Nogami Index 133
4.4.7 Slope Variability Index 137
4.5 SUMMARY OF RESULTS 139
4.6 BEDROCK VARIATION AND HILLSLOPE FORM IN THE SANTA CRUZ MOUNTAINS 141
4.6.1 Slope-Lithology Interactions 141
4.6.2 Summary of Findings 145
4.7 DISCUSSION 146
4.7.1 Linear Ridge Terrain, Bedrock Landsliding and Surface Process Modelling 146
4.7.1.1 Linear Hillslope Transport 146
4.7.1.2 Bedrock Landsliding 147
4.7.2 Bedrock Controls on Relief Development 149
4.8 CONCLUSIONS AND SUGGESTIONS FOR FUTURE RESEARCH 150

CHAPTER 5 HILLSLOPE EROSION, TERRAIN VARIATION AND SEDIMENT FLUX IN THE ITALIAN APENNINE MOUNTAINS 151
5.1 INTRODUCTION 151
5.2 CONTROLS ON DENUDATION RATES AND SEDIMENT FLUXES FROM MOUNTAINOUS REGIONS 153
5.2.1 Relief and Denudation Rates 153
5.2.2 Basin Physiography and Denudation Rates 154
5.2.3 Climatic Controls on Denudation Rates 157

5.3 ESTIMATING DENUDATION RATES 155
5.3.1 Problems Associated with Calculating Denudation Rates from Sediment Yield Data 159
5.4 INTERACTIONS OF EROSIONAL PROCESSES, LITHOLOGY, SEDIMENT FLUX AND DENUDATION RATES IN THE NORTHERN APENNINES, ITALY 162
5.5 GEOLOGY, TECTONICS AND PHYSIOGRAPHY OF THE NORTHERN APENNINES 164
5.5.1 General Introduction to the Apennine System 164
5.5.2 Tectonic Framework of the Northern Apennines 164
5.5.3 Geologic Framework of the Apennines 165
5.5.4 Physiography of the Northern Apennine Study Area 168
5.6 OBSERVATIONS OF THE INTERACTIONS OF PROCESS, LITHOLOGY AND TERRAIN FORM IN THE NORTHERN APENNINES 169
5.6.1 Field Observations in the Northern Apennines 169
5.6.2 Comparison of Field Observations With Surface Process Modelling 175
5.6.3 DTM Analysis of the Northern Apennines 177
5.7 SEDIMENT FLUX FROM THE NORTHERN APENNINES 180
5.8 COMPARISON OF OBSERVED TRENDS WITH SEDIMENT YIELD DATA 182
5.9 RELIEF AND DENUDATION RATES IN THE NORTHERN APENNINES 186
5.9.1 Introduction 186
5.9.2 Relief - Denudation Rate Relationships in the Apennines 186
5.9.3 Relief, Denudation Rate and Bedrock Lithology 187
5.10 CONCLUSIONS 191

CHAPTER 6 LANDSLIDING AND HILLSLOPE FORM, MARIN COUNTY, CALIFORNIA, USA 193
6.1 INTRODUCTION 193
6.2 SLOPE PROCESSES OPERATING IN THE MARIN COUNTY AREA 194
6.2.1 Earthflows and Earthslides 194
6.2.2 Debris Flows 194
6.3 STUDY AREA 195

6.3.1 Tennessee Basin 196
6.3.2 Redwood Creek 198
6.3.3 Rodeo Basin 200
6.3.4 Mill Valley 201
6.3.5 Larkspur Valley 203
6.3.6 Webb Creek 205
6.4 DATA AND METHODS 208
6.4.1 Terrain Variables 208
6.4.2 Calculation of 'Landslide Potentials' 210
6.5 RESULTS 211
6.5.1 Elevation 211
6.5.2 Gradient 211
6.5.3 Aspect 213
6.5.4 Curvatures 213
6.5.5 Slope Shape 215
6.5.6 Relief 215
6.6 INVESTIGATING THE RELATIONSHIP BETWEEN LANDSLIDING, TERRAIN FORM AND LITHOLOGICAL VARIATION 217
6.6.1 Tennessee Basin 217
6.6.2 Redwood Creek 217
6.6.3 Rodeo Basin 218
6.6.4 Mill Valley 218
6.6.5 Larkspur Valley 218
6.6.6 Webb Creek 219
6.7. DISCUSSION 220
6.7.1 Topographic Variability and the Occurrence of Mass Movement 220
6.7.1.1 Elevation 221
6.7.1.2 Gradient 222
6.7.1.3 Aspect 223
6.7.1.4 Curvature and Slope Shape 224
6.7.1.5 Local Relief 225
6.7.1.6 Summary 22

6.7.2 Lithological Variation, Terrain Parameters and the Occurrence of Mass Movement in Marin County 226

CHAPTER 7 CONCLUSIONS AND SUGGESTIONS FOR FUTURE RESEARCH 228

REFERENCES 233

APPENDIX 1 ARC MACRO LANGUAGE SCRIPTS (AMLS) 247

A1.1 FILL AML 247

A1.2 LOCAL RELIEF AML 248

A1.3 DISPERSION OF ALTITUDE AML 249

A1.4 ELEVATION-RELIEF RATIO AML 250

A1.5 DISSECTION INDEX AML 252

A1.6 NOGAMI INDEX AML 253

A1.7 SLOPE VARIABILITY AML 254

APPENDIX 2 LITHOLOGICAL INFORMATION, SANTA CRUZ MOUNTAINS STUDY AREAS, CALIFORNIA 255

A2.1 COASTAL STUDY AREA 255

A2.2 MID STUDY AREA 256

A2.3 NEW STUDY AREA 256

A2.4 NEW2 STUDY AREA 257

A2.5 NEW3 STUDY AREA 257

A2.6 NEW4 STUDY AREA 258

A2.7 NEW5 STUDY AREA 258

A2.8 NEW6 STUDY AREA 259

LIST OF FIGURES

Figure		Page
1.1	Map Showing Location of Study Areas in Thesis	6
2.1	Differences in Calculated Slope Values from Topographic Maps According to 1, 3 or 5 Point Sampling	15
2.2	Long Profile, Enza River, Italy	16
2.3	Distance from Drainage Divide Versus Local Slope, Enza River, Italy	16
2.4	Distance from Drainage Divide Versus Log Local Slope, Enza River, Italy	17
2.5	Log Distance from Drainage Divide Versus Log Local Slope, Enza River, Italy	17
2.6	Shaded Relief Image of the Northern Apennines Demonstrating Transition from High Relief Mountain Belt to Low Relief Po Plain Area.	19
2.7	Grey Shaded DTM Image of the Northern Apennines Showing Major Drainage Outlets and Transition from Upland Areas (Grey and White Colours) to Depositional Plain (Black Area) to the North-East	19
2.8	Map Showing Northern Apennine Rivers and Locations Mentioned in the Text	20
2.9	Longitudinal River Profiles, Northern Apennine Rivers, Italy	22-24
2.10	Logarithmic Plots of Local Slope Against Distance from Drainage Divide Measured from Topographic Maps for Po Tributaries Draining the Northern Apennines, Italy	26-28
2.11	Location Map, Eastern Death Valley, California	30
2.12	Location Map, Western Death Valley, California	30
2.13	Longitudinal River Profiles, Eastern Death Valley, California, USA	32-34
2.14	Logarithmic plots of local slope against distance from drainage divide measured from topographic maps for rivers draining the eastern side of Death Valley, California, USA	35-37
2.15	Longitudinal river profiles, western Death Valley, California, USA	40-42
2.16	Logarithmic Plots of Local Slope Against Distance from Drainage Divide Measured from Topographic Maps for Rivers Draining the Western Side of Death Valley, California, USA	45-47
2.17	Location Map, Wheeler Ridge, California	48

2.18	Longitudinal River Profiles, Wheeler Ridge, California, USA	50-53
2.19	Logarithmic Plots of Local Slope Against Distance from Drainage Divide Measured from Topographic Maps for Rivers Draining the Wheeler Ridge, California, USA	55-58
2.20	Location Map, North Devon, England	60
2.21	Longitudinal River Profiles, North Devon, England	61
2.22	Logarithmic Plots of Local Slope Against Distance from Drainage Divide Measured from Topographic Maps for Rivers Draining North Devon, England	63
2.23	The Effect of Pit-Filling on Stream Network Derivation, Enza River, Northern Apennines, Italy	71
2.24	Comparative Plots of Long Profiles Derived from 1) Topographic Maps, 2) Unfilled DTM Data and 3) Pit-Filled DTM Data	74
2.25	Comparative Plots of Long Profiles Derived from 1) Topographic Maps, 2) Unfilled DTM Data and 3) Pit-Filled DTM Data	75
2.26	Map of Control Point Locations, Enza River Basin,. Italy	76
2.27	Plot of Downstream Distance and Elevation for Control Points, Enza Basin, Italy	76
2.28	Smoothed River Profile Taken Along Lower Unfilled Elevation Points, Enza River	77
2.29	Slope Values Along the Enza River Calculated from 1:10,000 Scale Topographic Map (red) and 230 Metre DTM (blue) Data	79
2.30	Mean Annual Discharge Versus Width, Italian Basins	86
2.31	Mean Annual Discharge Versus Depth, Italian Basins	86
2.32	Mean Annual Discharge Versus Velocity, Italian Basins	86
2.33	Basin Area Versus Mean Annual Discharge	86
2.34	Variation in Calculated Values of Dimensionless Shear Stress, With Exponent 0.5 (red), 0.21 (blue) and 0.36 (green)	88
2.35	Distribution of Bed Shear Stress Along the Enza River	91
2.36	Grain Size Variation Along the Enza River, Italy	91
2.37	Distribution of Dimensionless Shear Stress Along the Enza River, Italy	91
3.1	Linear Slope Diffusion and its Relationship to Sediment Flux	99
3.2	Critical Threshold Sliding	105

4.1	Shaded Relief Map of the Santa Cruz Mountains, California	110
4.2	Slope Map, Santa Cruz Mountains	110
4.3	Hillslope Profiles of Mountains in the Santa Cruz Mountains Sampled from 30 Metre Digital Terrain Model	112
4.4	Fault Map of the Santa Cruz Mountains	114
4.5	Slope Distribution Plots	124
4.6	Cumulative Slope Distribution Plots	124
4.7	Cumulative Local Relief (3 Pixel Radius)	127
4.8	Cumulative Local Relief (3 Pixel Radius)	127
4.9	Cumulative Local Relief (20 Pixel Radius)	128
4.10	Cumulative Local Relief (50 Pixel Radius)	128
4.11	Dispersion of Altitude Plots	131
4.12	ZR Ratio Plots	131
4.13	Elevation-Relief Ratio Plots	132
4.14	Dissection Index Plots	132
4.15	Nogami Index Plots	133
4.16	Nogami Index Plots Continued	134
4.17	Slope Variability Plots	137
4.18	Slope Variability Plots Continued	138
4.19	Mean Slope of Bedrock Lithologies in Santa Cruz Study Areas	143
4.20	Slope Gradient Distributions Resulting from Linear Slope Diffusion (1) and Bedrock Landsliding (2)	148
5.1	Relationship of Local Relief and Mechanical Denudation Rate	155
5.2	Relationship of Local Relief and Mean Denudation Rate	155
5.3	Relationship of Local Relief to Mean Denudation Rate, Hydrographer's Range, Papua New Guinea	155
5.4	Comparison of Sediment Flux Versus Mean Local Relief Through Time for the Zagros Fold Belt	155
5.5	Relationship of Basin Area and Sediment Yield	156
5.6	Relationship of Basin Area and Mechanical Denudation Rate	156
5.7	Relationship Between Precipitation Rate and Denudation Rate	158
5.8	Map Showing Location of Northern Apennines in Context of Europe and Apennine Rivers Mentioned in the Text	163

5.9	Generalised Geological Map of the Northern Apennines, Italy	166
5.10	Mean Slope (Blue) and Local Relief (Red) Values Calculated for Basins Draining the Northern Apennines, Italy	179
5.11	Sediment Yields Along Rivers Draining the Northern Apennines	181
5.12	Denudation Rates Along Rivers Draining the Northern Apennines	181
5.13	Relationship Between Local Relief and Denudation Rate, Northern	189
5.14	Apennines, Based on 1) Ahnert's Law (Blue) and 2) Sediment Load Data (Red).	
5.15	Rates of Denudation in the Northern Apennines Based on Empirical Relationships Determined by Ahnert (1970) in Blue and After Bartolini et al., 1996 in Red	190
6.1	Location Map of Tennessee Basin, Marin County	197
6.2	Location Map of Redwood Creek, Marin County	199
6.3	Location Map of Rodeo Basin, Marin County	201
6.4	Location Map of Mill Valley, Marin County	203
6.5	Location Map of Larkspur Creek, Marin County	205
6.6	Location Map of Webb Creek, Marin County	205
6.7	Elevation Landslide Potentials, Marin County	211
6.8	Gradient Landslide Potentials, Marin County	211
6.9	Aspect Landslide Potentials, Marin County	213
6.10	Curvature Landslide Potentials, Marin County	213
6.11	Slope Shape Landslide Potentials, Marin County	215
6.12	Local Relief Landslide Potentials, Marin County	215
A2.1	Coastal Study Area Lithological Chart	
A2.2	Mid Study Area Lithological Chart	
A2.3	New Study Area Lithological Chart	
A2.4	New2 Study Area Lithological Chart	
A2.5	New3 Study Area Lithological Chart	
A2.6	New4 Study Area Lithological Chart	
A2.7	New5 Study Area Lithological Chart	
A2.8	New6 Study Area Lithological Chart	

LIST OF TABLES

Table		Page
2.1	Gradient and Intercept Values for Log-Log Plots of Slope Versus Downstream Distance for Rivers Draining the Northern Apennines, Italy	25
2.2	Gradient and intercept values for log-log plots of slope versus downstream distance for rivers draining the eastern side of Death Valley, California, U.S.A.	35
2.3	Gradient and Intercept Values for Log-Log Plots of Slope Versus Downstream Distance for Rivers Draining the Western Side of Death Valley, California, U.S.A.	43
2.4	Gradient and Intercept Values for Log-Log Plots of Slope Versus Downstream Distance for Rivers Draining the Wheeler Ridge, California, U.S.A.	54
2.5	Gradient and Intercept Values for Log-Log Plots of Slope Versus Downstream Distance for Rivers Draining North Devon, England	62
4.1	General lithological trends and noted for study areas, Santa Cruz Mountains	115
4.2	Descriptive Statistics for Study Areas in Santa Cruz Mountains	123
4.3	Summary table of morphometric indices' ability to identify linear ridge topography	140
5.1	Mean Slope and Local Relief Measurements for Northern Apennine	178
6.1	Example Data Set Used to Illustrate Calculation of 'Landslide Potentials'	210

LIST OF PLATES

Plate		Page
5.1	Linear Ridge Topography, near Santa Sofia, Bidente River Basin, Italy	170
5.2	Rounded Hillslope Forms in the Trebbia Valley	170
5.3	Landslide, Corniglio, Parma Valley	171
5.4	Triangular Facets, Collina, Tuscany	173
5.5	Linear Hillslopes, Trebbia River Valley	175
5.6	Linear Hillslopes and Triangular Front Facets, Upper Marecchia Valley	175
5.7	Bedrock Channel in the Lamone Basin, near Fognano	185
5.8	Braided River Channel, Taro River	185
6.1	Rounded Earthflow Topography, Redwood Creek, East of Shoreline Highway, Marin County, California	200
6.2	Rounded Earthflow Topography, Redwood Creek, East of Shoreline Highway, Marin County, California	200

TO MY PARENTS

CHAPTER 1

AIMS, OBJECTIVES AND THESIS ORGANISATION

1.1 INTRODUCTION

Tectonically active mountain belts such as the Alps, Himalayas, Andes and Apennines are frequently bounded by actively subsiding sedimentary basins. Critical links and feedback mechanisms operate between the erosional and depositional processes which operate in these two distinct domains, such that changes in one can have effects on the other. Tectonic uplift in the orogen is frequently accompanied by downwarping of the adjacent basin, resulting in both heightened erosion in the former and increased depositional space in the latter. The interactions of the processes operating within orogens and basins are of interest for both geomorphologists and sedimentologists, yet at present these interactions are poorly understood. This lack of understanding has developed both as a result of the inherent difficulty in studying such processes at large spatial scales, and because of the post-war trend to focus on small scale process studies. Powerful computer-based simulations have been proposed which model the feedbacks between mountain belts and sedimentary basins, and whilst they are sometimes capable of producing realistic output, they are frequently based on inadequate or poorly constrained process studies.

Strong links exist between the form of hillslopes, or their morphology, and the types of processes operating upon them. A variety of recent studies in the fields of geophysics and geomorphology have indicated that the macro scale morphology of orogenic areas represent the interplay of a suite of tectonic and geomorphic processes, influenced by the interactions and feedbacks of climatic, tectonic and erosional processes amongst others (for example, Burbank and Pinter, 1999; Ellis *et al.*, 1999; Montgomery, 1994; Anderson, 1994; Molnar *et al.*, 1993). As this awareness has grown, the importance of understanding how different types of erosional process affect mountainous regions has heightened. At a large scale, denudation of uplands removes material from hillslopes and transports it to the sedimentary system. The removal of sediment has been suggested to influence patterns of crustal uplift in

orogens and global patterns of climate (Raymo and Ruddiman, 1992). However, again, our present understanding of what types of process are operating, where, and to what extent in large scale orogens is relatively limited. In addition, the roles played by factors such as tectonics and lithological variation in determining the types of erosional process operating in orogens is also in its infancy. The importance of understanding how these processes interact at an orogenic scale has led to the development of a number of surface process and landscape evolution models, which attempt to capture the coupling between crustal and geomorphic processes operating at a variety of temporal and spatial scales. For example, Howard's (1997) model simulates landscape evolution at the scale of a drainage basin, whilst that of Ellis *et al.* (1999) examines the development of mountainous topography at larger spatial scales. However, as with models simulating the development of sedimentary basins, the types of equations employed are often based on small scale studies with limited bearing on the processes operating at larger scales.

Recently, studies have indicated the importance of bedrock landsliding as an erosional process in many mountainous regions (for example, Densmore *et al.*, 1999, Densmore and Hovius, 1998b, Hovius *et al.*, 1997; Burbank *et al.*, 1996). The dominance of these landslides means that they control not only the large scale form of many upland areas, but also the flux of sediment released from hillslopes into the sediment transport system. Despite this growing awareness, such a process has largely been ignored by models simulating the development of orogenic areas. In addition, there are few studies which have examined what controls the spatial distribution of bedrock landsliding at the scale of orogens, and what the implication of such slides are for denudation and sediment flux calculations.

This thesis addresses a number of the issues raised above by examining the ways in which sediment is both liberated into the geomorphic system from hillslopes and redistributed by the sedimentary system. By focusing on macro scale process interactions and feedbacks, many of the problems associated with employing smaller scale empirically based observations in simulating large scale mountain belt and sedimentary basin development may be overcome. Furthermore, by examining the factors controlling the spatial distribution of bedrock landsliding in orogenic areas, better constraints on the importance of different surface processes may be acquired,

which, in turn, will allow for more accurate simulations of the development of mountain belts.

Specifically, the seven primary aims of this thesis are:

- To examine whether channel long profile morphology changes in the transitional area from long term erosion to deposition
- To determine whether channel long profiles may be derived from 230 metre digital terrain models at an accuracy comparable with those derived from 1:10,000 scale topographic maps
- To derive changes in bed shear stress along a channel network, determine downstream changes in bedload transport rates, and assess the factors controlling such changes.
- To develop a method for detecting mountainous areas affected by bedrock landsliding based on analyses of digital terrain data rather than small scale field studies.
- To assess the factors controlling the spatial distribution of bedrock landsliding
- To determine the significance of bedrock landsliding for rates of denudation and sediment flux from orogens.
- To determine whether topography susceptible to earthflow-type landslides can be distinguished on the basis of terrain morphometry.

The work contained in this thesis is novel in a variety of ways. By examining how sediment is both liberated from, and transported through, the orogenic system, it provides data at a scale large enough to be incorporated into many surface process models (for example, Ellis *et al.*, 1999), overcoming criticism that many such models lack field observations at a similar scale (Willgoose, 1994). Secondly, by examining how changes in channel properties, such as shear stress, derived from large scale digital elevation models change both along channels and across orogens, this thesis not only addresses the implications of such changes for sediment transport, but also provides an insight into the validity of using such models for large scale process studies. A novel approach is adopted in this thesis in which field observations of erosional processes in California and Italy are combined with detailed morphological analysis of an orogenic digital terrain model in studies which show how linear

hillslopes affected by bedrock landsliding demonstrate characteristic slope and relief values.

1.2 THESIS ORGANISATION

Chapter 2 examines how long term patterns of erosion and deposition are reflected by changes in river longitudinal profile morphology. Results of a study by Yatsu (1955) indicate that the erosion-deposition transition along Japanese rivers is marked by a rapid drop in channel slope gradient. This study examines whether this general observation is valid for the erosion-deposition transition in the Northern Apennines of Italy, Death Valley and Wheeler Ridge, California, USA and North Devon in Great Britain. Patterns of erosion and deposition along graded channel networks are accompanied by downstream increases and decreases in bedload transport rates, which are proportional to changes in bed shear stress along the channel. The work in this chapter determines changes in bed shear stress, with shear stress calculated as proportional to the product of channel slope and contributing area$^{0.5}$, along the Enza River in Italy. Downstream trends in bedload transport rate are compared with field observations which document how grain size varies along the Enza River. Finally, the implications of the chapter's findings for fluvial network models, such as Rigon *et al.*'s (1994) are discussed.

Chapter 3 serves as an introduction to the themes of significance in the two following chapters. An outline to the interactions of terrain form and erosional process is provided, before a detailed overview of the various processes operating on mountainous hillslopes is discussed. The chapter then moves on to look at how these processes are modelled by linear and nonlinear sediment transport laws. Finally, large scale surface process and landscape evolution models are outlined, which attempt to simulate both the ways in which upland areas are formed and eroded, as well as how the sediment denuded from hillslopes is routed from the system.

Chapter 4 provides a case study of the Santa Cruz Mountains in central California, USA (Figure 1.1). This area shows widespread linear hillslope forms (Anderson, 1994). Field observations in the Basin and Range province of the United States (Ellis *et al.*, 1999) and computer modelling (Densmore *et al.*, 1998) have shown that the

form of such hillslopes results from widespread bedrock landsliding (Anderson, 1994; Densmore *et al.*, 1998; Schmidt and Montgomery, 1995). This work examines the different ways of fingerprinting these erosional linear slopes by comparing terrain form in areas which do and do not exhibit such hillslopes. The Santa Cruz area is outlined, both in terms of its topography and geology. Next, eight different terrain variables are outlined which are tested for their ability to discriminate between areas showing linear, bedrock landslide topography and those which do not. The role of bedrock lithology on terrain form is examined using digital geological maps. Results of the terrain analyses are outlined. Variations in hillslope form and slope gradient on different lithological outcrops are discussed. Finally, the implications of bedrock controls on relief development and terrain analysis, and bedrock landsliding on sediment transport are outlined.

Chapter 5 combines field observations of hillslope form and process, sediment yield and denudation rate data and digital terrain model analyses of the Northern Apennines (Figure 1.1) to examine the role played by different erosional processes on terrain form, and the flux of sediment from mountainous regions. Controls on denudation rates and sediment fluxes are discussed, as are the different ways of estimating the former and problems associated with doing so. Previous sediment flux and denudation rate studies in the Northern Apennines are outlined with an introduction to the physiographic and geologic setting of the area. Results of field observations of erosional hillslope processes and terrain morphology are discussed, as are results of DTM analyses in the Northern Apennine study area. Field observations are compared with sediment yield and denudation rate data. Denudation rates based on local relief measurements (Ahnert, 1970) are then compared with observed yield data. Finally, the implications of the study for how the interactions of erosional processes and sediment liberation at large spatial scales are, and should be, dealt with in models of mountain belt development are discussed.

Chapter 6 shows an investigation into the relationship of hillslope form, erosional process and lithological variation in Marin County, California. This area is subject to earthflow type landslides, which result in rounded topography differing from the linear hillslope forms discussed in Chapters 4 and 5.

Chapter 7 provides an overall conclusion to the six previous chapters and outlines potential avenues which future research could follow to develop on the themes and results presented in this thesis.

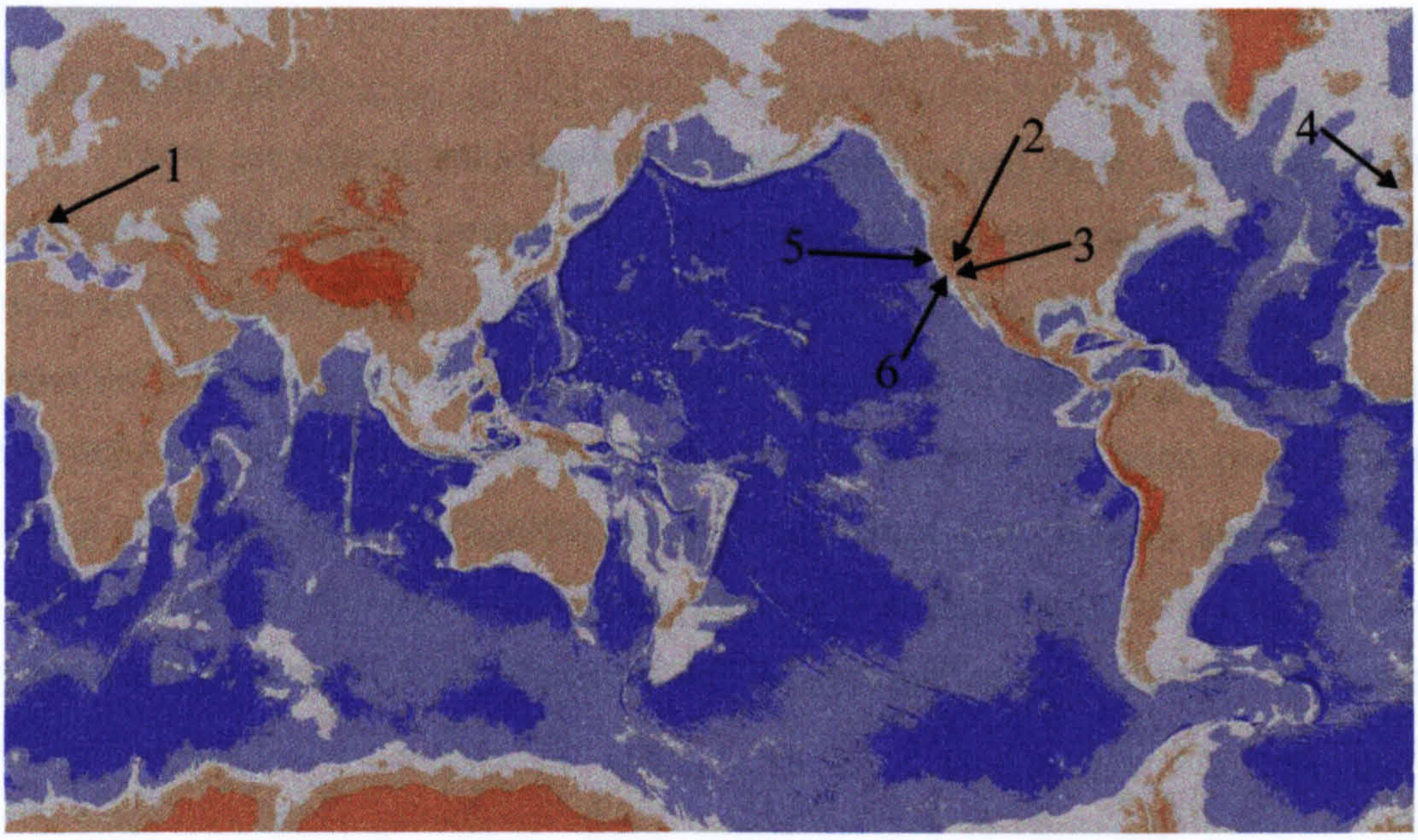

Figure 1.1 Map Showing Location of Study Areas in Thesis.

1. **Northern Apennines, Italy**
2. **Death Valley, California, USA**
3. **Wheeler Ridge, California, USA**
4. **North Devon, Great Britain**
5. **Marin County, California, USA**
6. **Santa Cruz Mountains, California, USA**

CHAPTER 2

EROSION, DEPOSITION AND SEDIMENT REDISTRIBUTION IN ALLUVIAL BASINS AND ADJACENT MOUNTAIN BELTS

2.1 INTRODUCTION

There are critical links between the processes which act to erode and deposit sediment on the Earth's surface, and the tectonic processes which uplift mountain belts and create sedimentary basins (e.g. Montgomery, 1994; Burbank *et al.*, 1996). A better understanding of the ways these forces interact is crucial for geomorphologists wanting to comprehend the ways orogens evolve, for meteorologists examining the role of mountain belt development on climate change (e.g. Raymo and Ruddiman, 1992), as well as for sedimentologists interested in how basins fill and thus why sedimentary sequences were deposited in the geologic record (Talling and Sowter, 1998).

River channels are frequently classified as having bedrock, loose-bed alluvial and mixed-bed morphologies (Howard *et al.*, 1994). Whilst the former exists where more than 50% of the channel boundary is exposed bedrock (Tinkler and Wohl, 1999), loose-bed channels are free to cut into poorly consolidated alluvial deposits (Knighton, 1987). It has been proposed that rates of bedrock incision and sediment transport in alluvial channels are controlled not by channel discharge alone, but by its associated flow characteristics of stream power (Bagnold, 1980) and bed shear stress (Meyer Peter and Müller, 1948). Stream power is proportional to the product of the density of water (ρ_w), gravitational acceleration (g), channel slope (S) and mean annual discharge (Q) along a channel and represents the mean rate of potential energy expenditure per unit length of channel (Richards, 1982). Bed shear stress is calculated as the product of the density of water, gravitational acceleration, channel slope and channel bankfull depth.

Incision into bedrock channels has been modelled as proportional to both stream power (Seidl *et al.*, 1994) and bed shear stress (Burbank *et al.*, 1998), with the former approach also being used to model channel incision into bedrock in broad scale landscape evolution models (for example, Kooi and Beaumont, 1994; Tucker

and Slingerland, 1996). Empirical data from flume tank experiments and short term field observations (Bagnold, 1980, Gomez and Church, 1989) have demonstrated evidence for strong links between stream power, bed shear stress and sediment transport rates. Assuming a conservation of bedload sediment mass in a downstream direction, downstream increases in bedload transport rates will result in erosion, whilst downstream decreases will result in deposition. Whilst these trends appear to be valid over the relatively limited spatial and temporal scales of the studies involved (for example, Bagnold, 1980), studies focusing on the interactions of stream power, bed shear stress and sediment transport rates at broader scales are lacking. Hence, despite the widespread adoption of laws by which sediment transport rates are governed by downstream changes in parameters such as shear stress in landscape evolution (for example, Tucker and Slingerland, 1996) and basin development models (for example, Paola *et al.*, 1992), empirical support for the use of such equations is lacking.

By determining whether large scale changes in sediment transport from erosional to depositional areas are accompanied by downstream changes in slope gradient and shear stress, this study addresses the lack of broad scale empirical data. The work in this chapter examines the relationship between channel profile characteristics, bed shear stress and bedload transport rates in four study areas in Italy, the USA and Great Britain using a combination of topographic map and digital terrain model (DTM) data. DTM data allows for the rapid measurement of channel network properties across broad spatial scales and is thus ideal for the large scale nature of this study.

Previous studies have demonstrated how changes in river longitudinal profiles can be related to tectonic (Goldrick and Bishop, 1995; Merrits and Vincent, 1987), lithologic (Sowter, 1996; Hack, 1957, 1973) and base level changes (Seidl and Dietrich, 1992) along the channel. Furthermore, a previous study in Japan showed that the relationship between downstream distance along a channel and channel slope gradient changed as one moved downstream from areas exhibiting long term erosion to deposition (Yatsu, 1955). As both stream power and bed shear stress are heavily dependent on channel slope properties (Hancock *et al.*, 1999), identifying whether Yatsu's (1955) observation is valid for other locations is crucial in order to better

understand how bedload transport rates are related to parameters such as stream power and bed shear stress. Results from small scale studies (for example, Gomez and Church, 1989) indicate that as one moves from areas of erosion to deposition, bedload transport rates (as indicated by stream power and bed shear stress measurements) should show a transition from downstream increases to downstream decreases. Previous studies have not documented changes across such a transition using data from more than one study area. This study thus determines whether such changes are a general phenomenon related to sediment transport or a more local relationship valid only for the channels studied by Yatsu (1955).

This study thus has three main objectives:

1) To determine whether changes in channel slope always occur at the transition from long term erosion to deposition.
2) To assess the suitability of DTMs in deriving channel long profiles.
3) To compare downstream trends in bed shear stress, grain size and implications for bedload transport rates

The work involved in obtaining the data for this chapter was carried out both by the author (MJS) alone and in collaboration with Dr Peter Talling (PJT). River profiles for Italy were obtained by MJS and PJT, those for the American profiles by the MS, and those from Devon by PJT. Profiles and work involving data collection from digital terrain models was carried out by MJS. Grain size data collection was carried out by MJS and PJT, with the subsequent analyses furthering the work of both Rigon *et al.* (1996) and Talling (in review).

The study begins by examining the relationship between channel profiles and patterns of late Quaternary erosion and deposition in the Northern Apennines, Italy, Death Valley in California, the Wheeler Ridge, California, and North Devon, England. This will allow for an assessment of Yatsu's (1955) observations at a broader scale than initially undertaken. Secondly, channel profiles are derived from DTM data. Despite limited use of DTM derived river profiles (for example, Weissel and Seidl, 1999), no previous study has systematically compared profiles derived from conventional map and DTM data sources. By carrying out such a comparison, this study also allows for an assessment of the ability of DTM derived profiles to

reproduce fundamental channel network properties, such as slope and drainage area. Finally, estimates of bed shear stress are made along the Enza River in the Northern Apennines. Predicted trends are compared with field data constraining grain size variation along the channel, and subsequent implications for bedload transport rates and the development of fluvial networks are discussed.

2.2 CHANNEL LONGITUDINAL PROFILES

This study aims to examine the relationships between the form of channel long profiles and patterns of long-term erosion and deposition over periods of greater than 1ka. For the purpose of this work, long-term erosion is inferred to be operating where the topography surrounding the channel is of an erosional, rugged relief. By contrast, areas of lower relief topography, levees, avulsed channels and significant Quaternary alluvium are taken to be indicative of long-term deposition. Although fill terraces within mountainous regions represent periods of sediment deposition, the rugged type topography dominating such areas must be the result of longer term erosional incision (Talling and Sowter, 1998). This study differs from the majority of research examining fluvial channel morphology (for example, Hack, 1957; Mackin, 1948) by holistically examining channel profile development in both the erosional, upper basin and the depositional, lower basin. This approach was used by Yatsu (1955) who noted that when plotted on semi-logarithmic axes, the exponential function of channel gradient against downstream distance for a series of Japanese rivers changed dramatically as one moved from areas of long term erosion to deposition. This study examines whether Yatsu's (1955) observation is a general property demonstrated by channel profiles as rivers flow from areas of erosion to deposition. Such observations have important implications for the factors governing the location of erosion and depositional boundaries, and thus the large scale redistribution of sediment on the Earth's surface over geological time scales.

2.2.1 Previous Work

The longitudinal profile of a river is taken to represent the elevation of a point in the middle of the stream bed, plotted along the ordinate, against the distance at that point from the stream mouth, plotted along the abscissa (Merrits & Vincent, 1987). Long profiles resemble a number of graphical curves produced by simple mathematical functions, including logarithmic, exponential and power (Snow and

Slingerland, 1987; Yatsu, 1955). Assuming average conditions of grade (see below), Snow and Slingerland (1987) stated that deviations from such mathematical curves may be indicative of external geomorphic controls. However, Seidl *et al.*(1994) question not only their usage of a single mathematical function to describe an entire channel, but also their assumption of conditions of grade representing their model's realism.

2.2.1.1 Graded River Profiles

The early work of G.K. Gilbert (1877) explained the general concavity demonstrated by many rivers as resulting from progressively increasing downstream discharge, enabling the transportation of the river's sediment load on slopes of decreasing gradient downstream (Richards, 1982; Pazzaglia *et al.*, 1998). Gilbert's declivity work was developed upon by W.M. Davis (1902) and Mackin (1948) in his conceptual work on the 'graded river'. Adopting Gilbert's assertion that channel slope is inversely proportional to river discharge, Mackin proposed that a river system evolves over time to attain a state of equilibrium, or 'grade', between the erosional and depositional processes acting within it (Ohmori & Saito, 1993). Gilbert stated that grade is "...a condition of equilibrium..." (1948, p.464), whereby slopes within the drainage system are adjusted, with the available discharge and channel characteristics, to result in the velocity required to transport the material provided from the valley slopes and upstream (Howard *et al.*, 1994).

2.2.1.2 Fluvial Dynamic Equilibrium and Dis-equilibria Features

Stream long profiles represent the long term geological development of a region influenced by recent channel pattern adjustments and longer term morphogenetic and tectonic factors (Leopold *et al.*, 1964). Studies of such profiles are therefore of use in both neotectonic and long-term analyses of landscape evolution (Goldrick & Bishop, 1995). Hack (1957) developed the work of Gilbert and proposed that lithology is the single most important factor governing stream slope and concavity. Hack's 'Dynamic Equilibrium' is a state attained by rivers whereby their slopes are roughly adjusted to the lithological substrate over which they flow. Furthermore, Hack contested the assertion of certain authors, for example Davis (1902), that relief and lithological controls on landscape form decline over time, and instead argued for their persistent influence on the morphology of the landscape. Hack

(1957; 1973) believed that the close relation between lithology and stream long profiles resulted in a state of dynamic equilibrium between the relief, form of the channel and resistance of the bedrock to erosion, meaning that long profile analysis represents as a highly powerful method of landscape interpretation. Hack's work, developed partly upon Gilbert's belief that channel gradient depends upon discharge and rock type, assumed that a stream graded to its substrate would have a smooth, equilibrium profile. Deviations from this smooth profile were taken to represent equilibrium features created by differing lithologies, anomalous drainage patterns, or the effect of long term disequilibria features, such as knickpoint migration upstream resulting from base level changes (Fried *et al.*, 1992; Bonneau and Snow, 1992). Base level being viewed as "...the lowest level to which a river bed could be reduced <which> would be the extension of sea level surface beneath the land " (King, 1951, p.34) - the 'geoid'.

Breaks from an ideally graded, concave upwards longitudinal profile are significant elements which have been the focus of many investigations (for example, Mackin, 1948). Such slope breaks have been interpreted in a variety of ways; for example, Rhea (1993) related convex breaks along such profiles to uplift in Oregon, whilst Hack (1957) believed such deviations in Appalachian profiles were created by lithological variation (see also Miller, 1991 and Morisawa, 1985). Recently, Seidl (*et al.*, 1994; and Dietrich, 1992) related profile breaks along Hawaiian channels to base level changes. Merrits and Vincent (1987) outlined the problem of distinguishing between the roles of uplift and rock resistance in morphological analyses. Difficulties differentiating between the causes of channel profile changes were outlined and a technique was proposed by Goldrick and Bishop (1995) who outlined a method of differentiating between profile steepening due to lithological variation and that caused by surface uplift.

2.3 DOWNSTREAM CHANGES IN CHANNEL GRADIENT

The aim of this work is to determine whether changes from long term sediment erosion to deposition are reflected in changes in the shape of channel long profiles. In order to achieve this, data from four different areas were collected and the assumption of conservation of bedload sediment mass is made (Reid and Laronne, 1995). Assuming that no loss of bedload or water from the channel occurs, downstream changes in bedload transport rate integrated across the channel (Q_{bed}) will change the channel bed elevation (H). Assuming bedload sediment mass is conserved downstream, downstream increases in bedload transport will result in erosion, whilst decreases will result in deposition. Of the study areas chosen, three are undergoing active tectonic deformation: the Po Basin, Italy (Figures 2.6 and 2.7) (Pieri and Groppi, 1981), Death Valley in California (Figures 2.11 and 2.12) (Hooke, 1972), and Wheeler Ridge in California (Figure 2.17) (Mueller and Talling, 1996). All three areas have undergone late Quaternary erosion and deposition (Talling and Sowter, 1998). The fourth area, North Devon in south-western England (Figure 2.20) has experienced only late Quaternary erosion, and will thus be used to test whether changes in profile shape occur where no erosion-deposition transition occurs in the field.

2.3.1 Measurement Strategy

For each of the four areas, elevation and downstream distance were measured using an opisometer along topographic map 'blue-lines'. Channel elevations were recorded where the river crossed contour lines, and the distance between the intervals recorded. In addition, where extensive low gradient reaches exist along Po tributaries in northern Italy, elevations were also recorded at spot heights supplementing the rather sparse contour data existing there. The maps used had a scale of 1:24,000 for Death Valley and Wheeler Ridge, and were published in 1989 and 1991 by the United States Geological Survey (USGS). The maps used for the Italian rivers were published by the Instituto Geografico Militaire at a scale of 1:10,000. The North Devon profiles were taken from 1:25,000 maps published by the British Geological Survey in 1992.

For each channel profile, the slope gradient (S in m km^{-1}) along the channel was derived using the difference between the upper and lower calculation points, the points above and below the calculation point, and the points two above and below the calculation points, thereby giving gradient estimates for two, three and five adjacent

points (Figure 2.1). It was decided that the three-point measure be used to reduce measurement uncertainty. The five-point method resulted in a reduction of the data set at the upper and lower extremes due to the sampling technique, and this method was rejected in favour of three-point sampling. The channel profiles were then plotted as downstream distance (x in km) against channel slope on logarithmic plots. Best fit straight line segments were calculated from the plots with the form

(2.1) $\log_{10}S = \phi \log_{10}x + \psi,$

and therefore,

(2.2) $S = 10^{\psi}x^{\phi}$

where ϕ and ψ are the gradient and axis intercept of the best-fit regression line plots. Log-log plots were selected as they best demonstrate the changes in slope gradient between upper and lower profile segments (Figures 2.2 to 2.5) (Talling and Sowter, 1998), as shown by Figure 2.5. For the erosional upper and depositional lower reaches, best fit regression analyses were performed on data within each segment, with gradient (ϕ), intercept (ψ) and r^2 values being calculated.

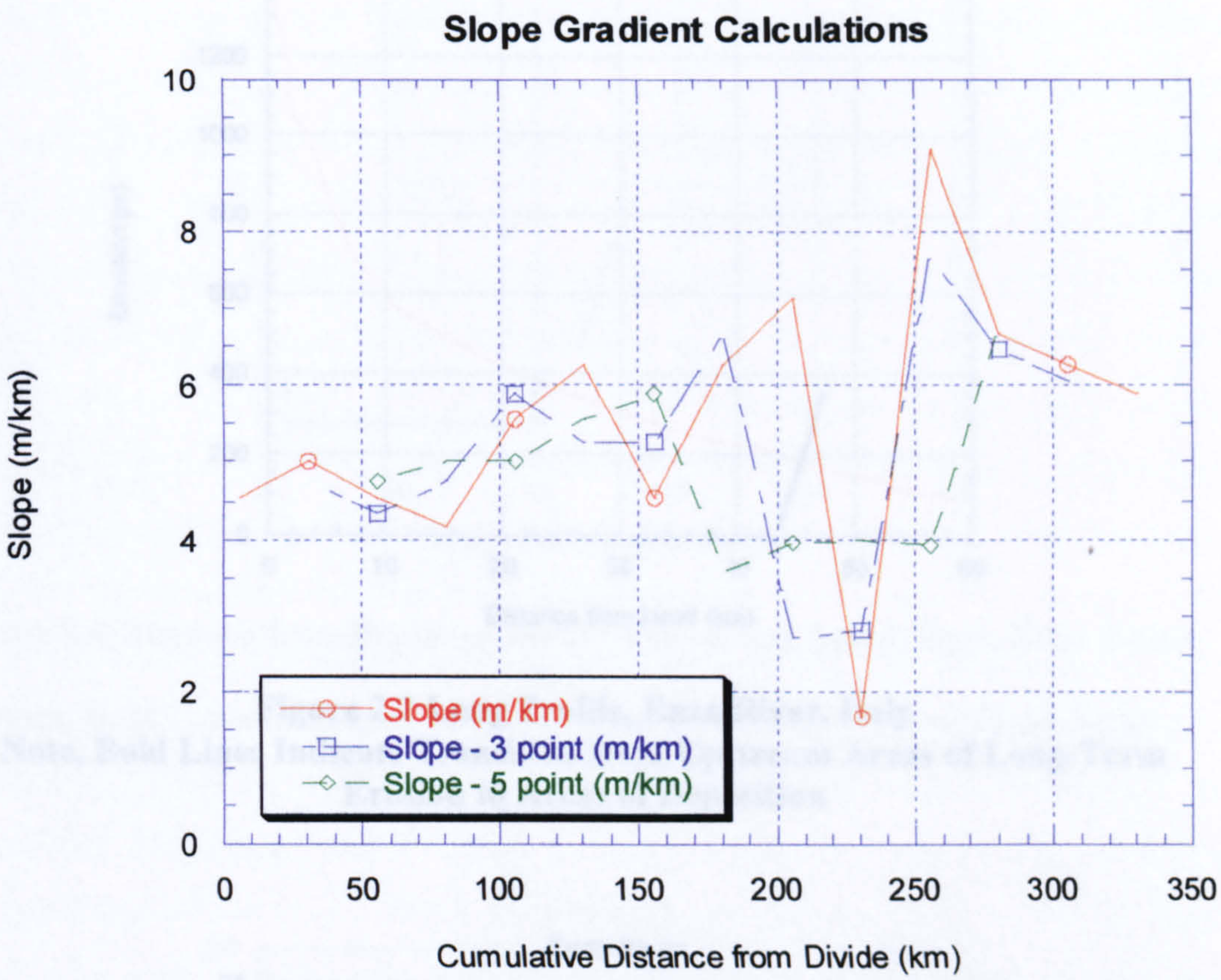

Figure 2.1 Differences in Calculated Slope Values from Topographic Maps According to 1, 3 or 5 Point Sampling

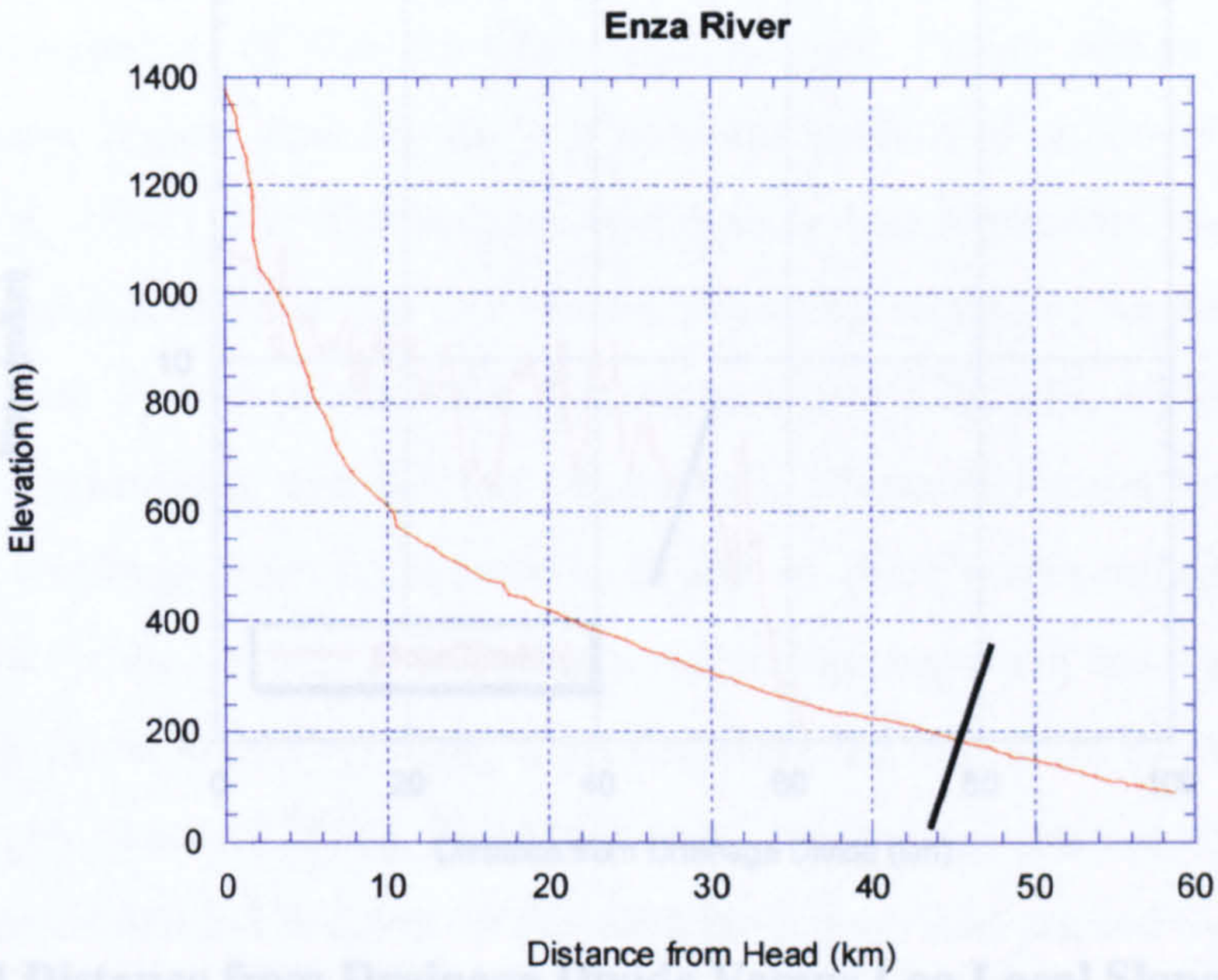

Figure 2.2 Long Profile, Enza River, Italy
Note, Bold Lines Indicate Transition from Upstream Areas of Long-Term Erosion to Areas of Deposition

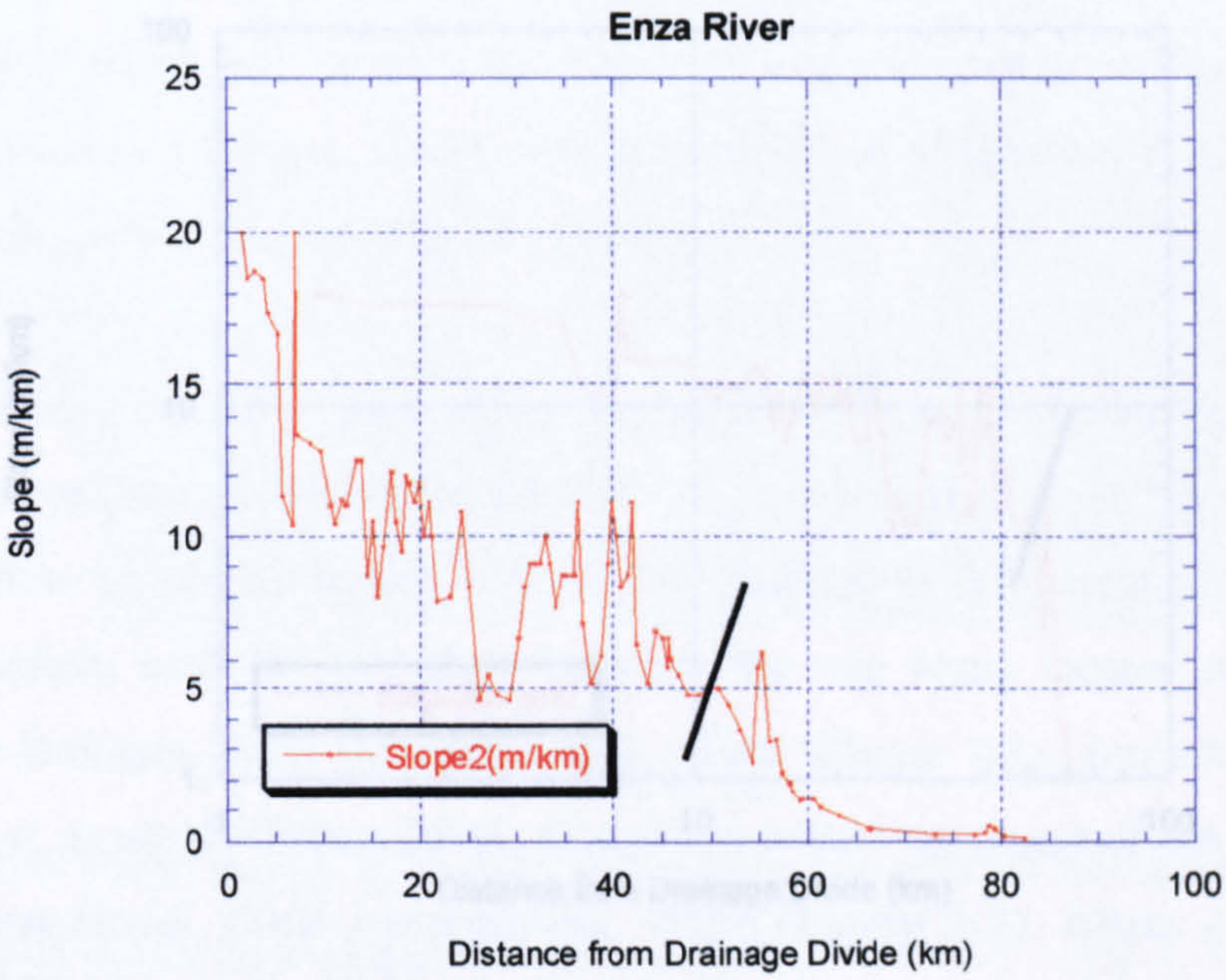

Figure 2.3 Distance from Drainage Divide Versus Local Slope, Enza River, Italy.
Note, Bold Lines Indicate Transition from Upstream Areas of Long-Term Erosion to Areas of Deposition

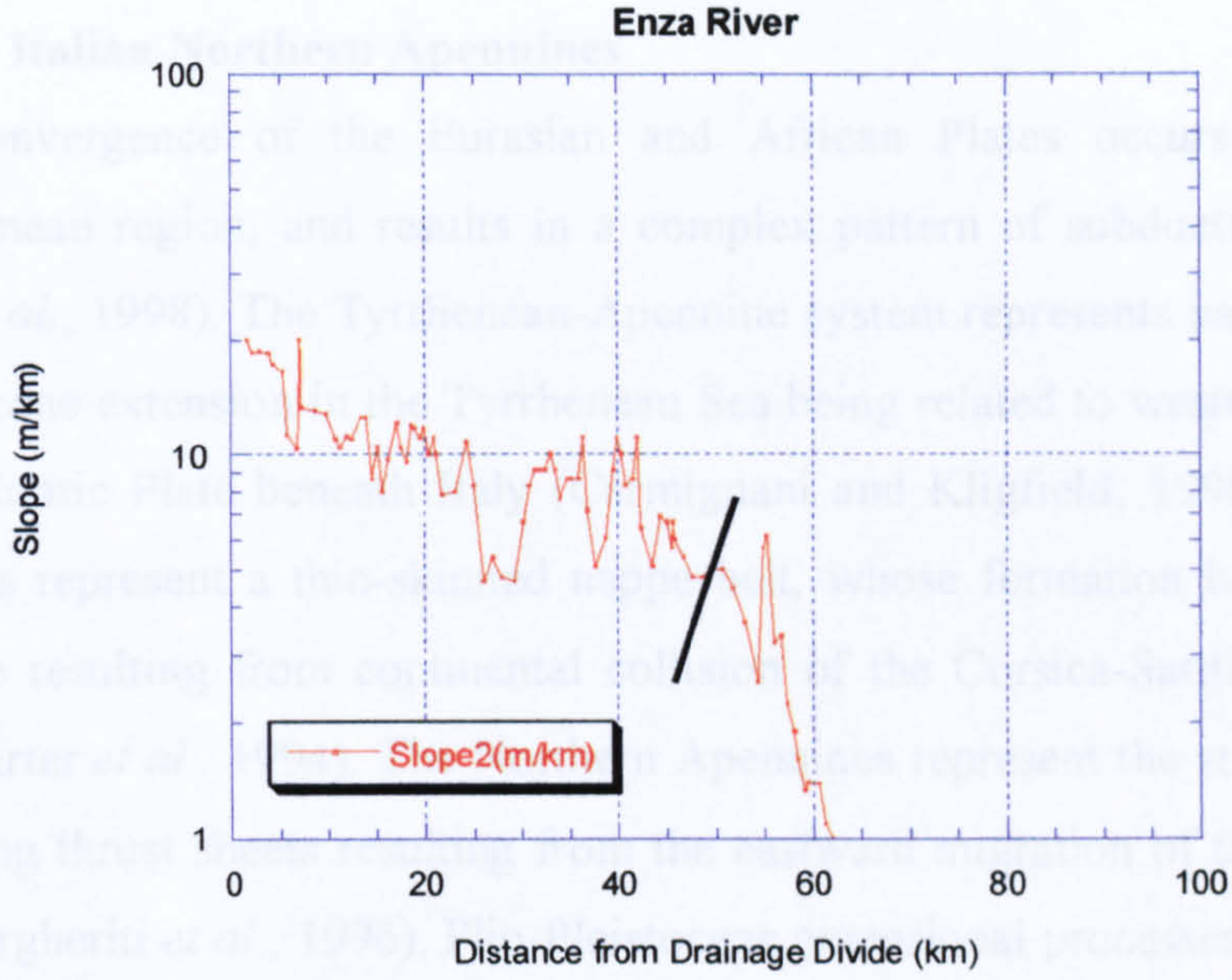

Figure 2.4 Distance from Drainage Divide Versus Log Local Slope, Enza River, Italy.
Note, Bold Lines Indicate Transition from Upstream Areas of Long-Term Erosion to Areas of Deposition

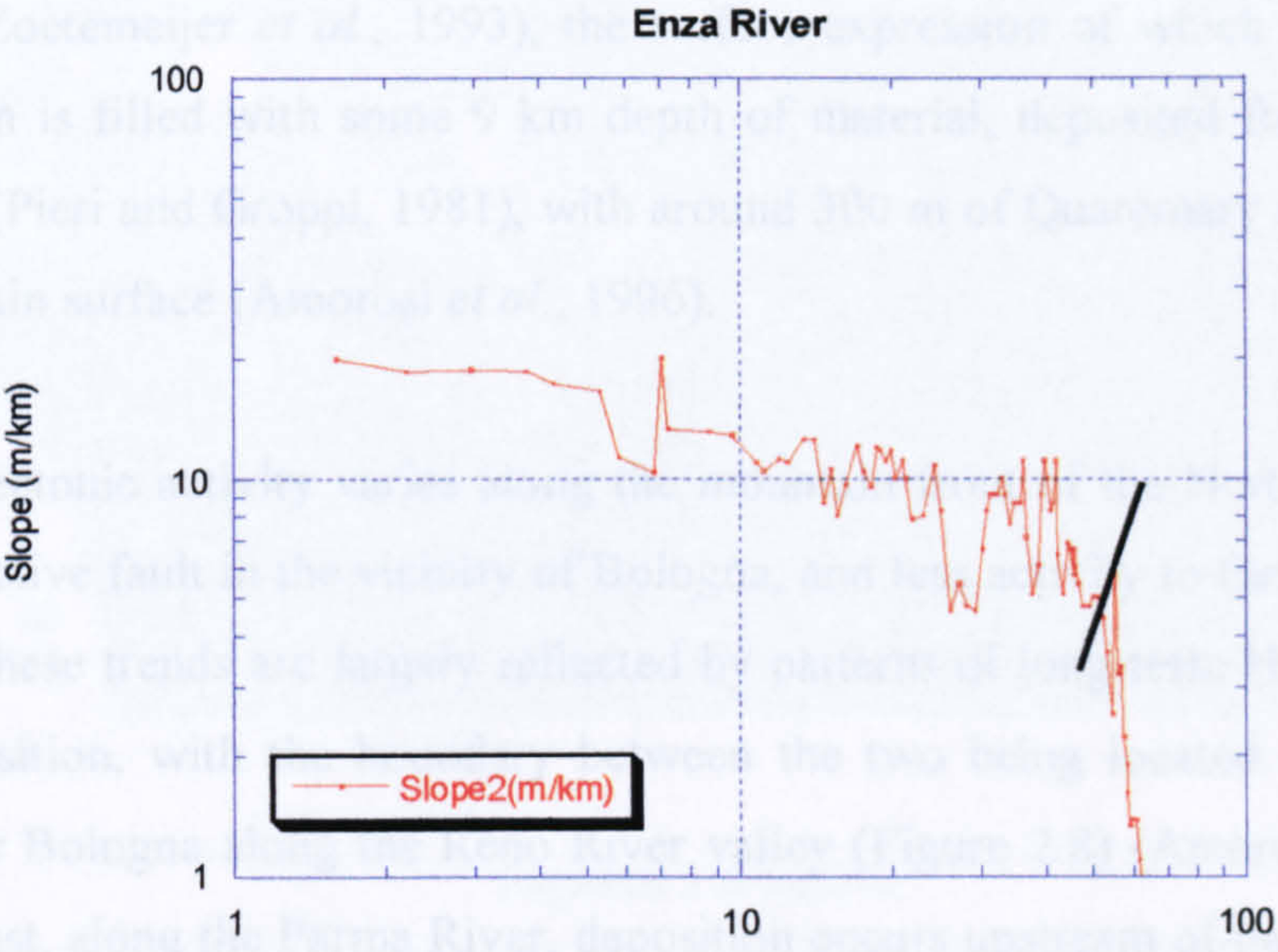

Figure 2.5 Log Distance from Drainage Divide Versus Log Local Slope, Enza River, Italy.
Note, Bold Lines Indicate Transition from Upstream Areas of Long-Term Erosion to Areas of Deposition

2.4 OBSERVED CHANGES IN CHANNEL LONG PROFILES AND GRADIENT

2.4.1 The Italian Northern Apennines

Convergence of the Eurasian and African Plates occurs throughout the Mediterranean region, and results in a complex pattern of subduction and collision (Buiter *et al.*, 1998). The Tyrrhenean-Apennine system represents part of this system, with Miocene extension in the Tyrrhenean Sea being related to westwards subduction of the Adriatic Plate beneath Italy (Carmignani and Kligfield, 1990). The Northern Apennines represent a thin-skinned nappe belt, whose formation began in the Late Oligocene resulting from continental collision of the Corsica-Sardinia and Adriatic plates (Carter *et al.*, 1994). The Northern Apennines represent the stacking of several NE-verging thrust sheets resulting from the eastward migration of the compressional front (Margheriti *et al.*, 1996). Plio-Pleistocene extensional processes have meant that many of the collisional features in the west have been overprinted by a series of N-S and NW-SE grabens as seen in southern Tuscany (Carmignani and Kligfield, 1990; Margheriti *et al.*, 1996). The large, foreland basin situated to the north and east of the Apennines (Figure 2.6) has been suggested to result from the downward flexure of the lithosphere (Beaumont, 1981), resulting from the load emplaced by the evolving orogen (Zoetemeijer *et al.*, 1993), the surface expression of which is the Po Plain. This basin is filled with some 9 km depth of material, deposited from the Pliocene onwards (Pieri and Groppi, 1981), with around 300 m of Quaternary alluvium nearest the Po Plain surface (Amorosi *et al.*, 1996).

Tectonic activity varies along the mountain front of the Northern Apennines, with an active fault in the vicinity of Bologna, and less activity to the north-west near Parma. These trends are largely reflected by patterns of long-term Holocene incision and deposition, with the boundary between the two being located at the mountain front near Bologna along the Reno River valley (Figure 2.8) (Amorosi *et al.*, 1996). By contrast, along the Parma River, deposition occurs upstream of the mountain front around Langhirano (field observations, 1997) (Figure 2.8). Many Apennine rivers have incised into the Po Plain (Castaldini and Panizza, 1988), and their fluvial terraces, for example the Reno and Bidente Rivers, with much of this incision believed to have resulted from anthropogenic activities, such as channel bed dredging (Castaldini and Panizza, 1988).

1

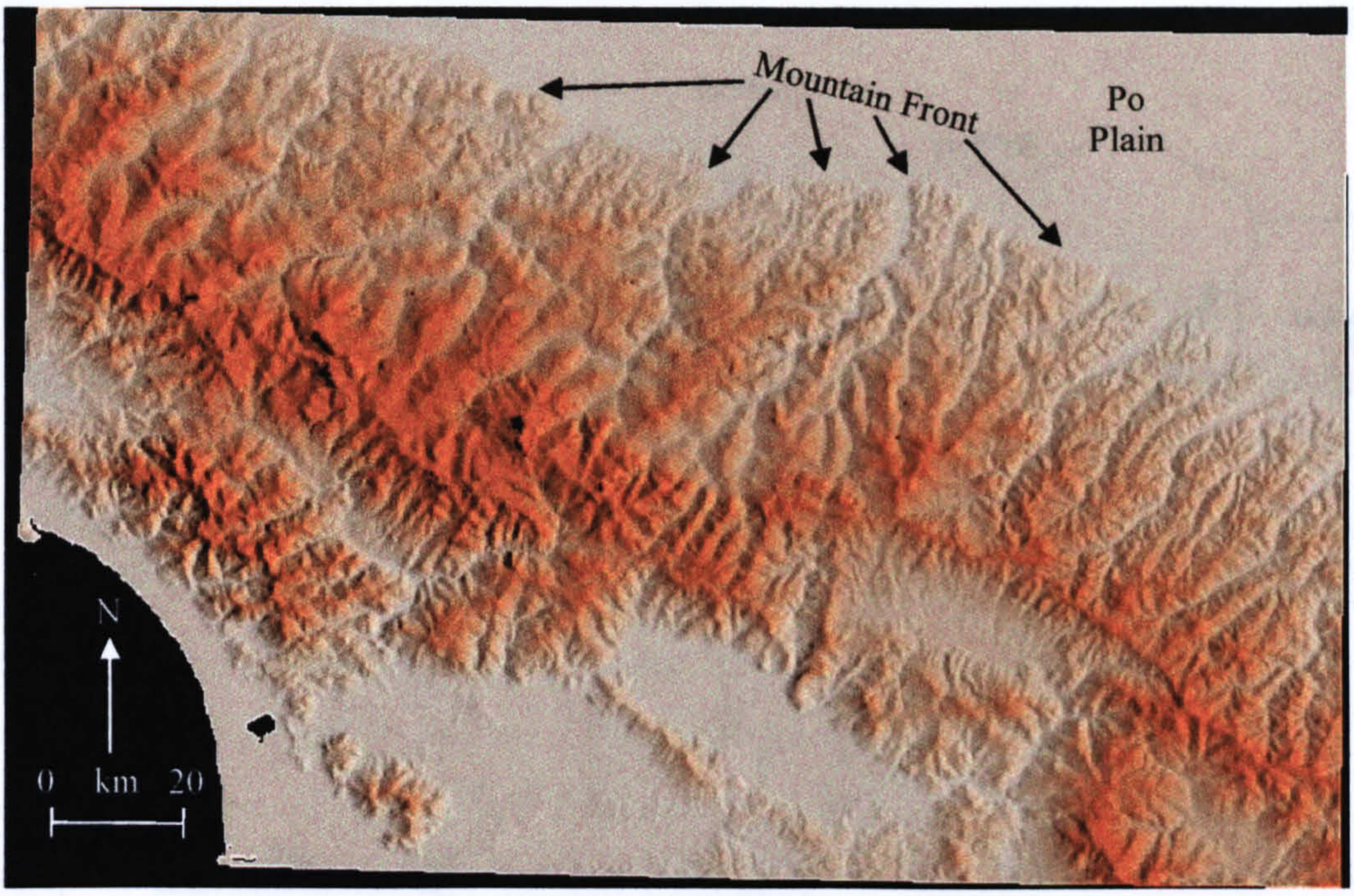

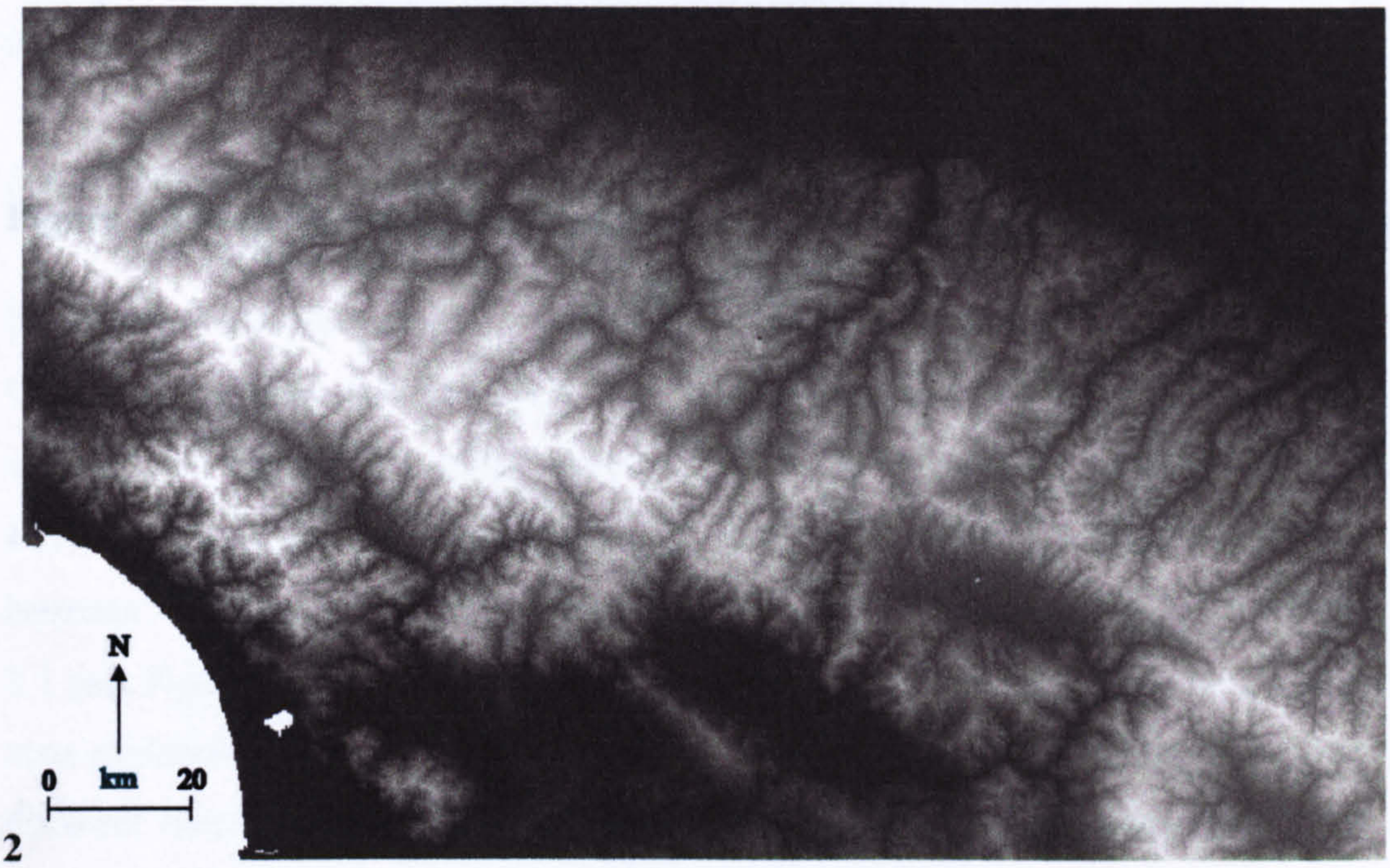

2

Figures 2.6 and 2.7

1) Shaded Relief Image of the Northern Apennines Demonstrating Transition from High Relief Mountain Belt to Low Relief Po Plain Area. 2) Grey Shaded DTM Image of the Northern Apennines Showing Major Drainage Outlets and Transition from Upland Areas (Grey and White Colours) to Depositional Plain (Black Area) to the North-East

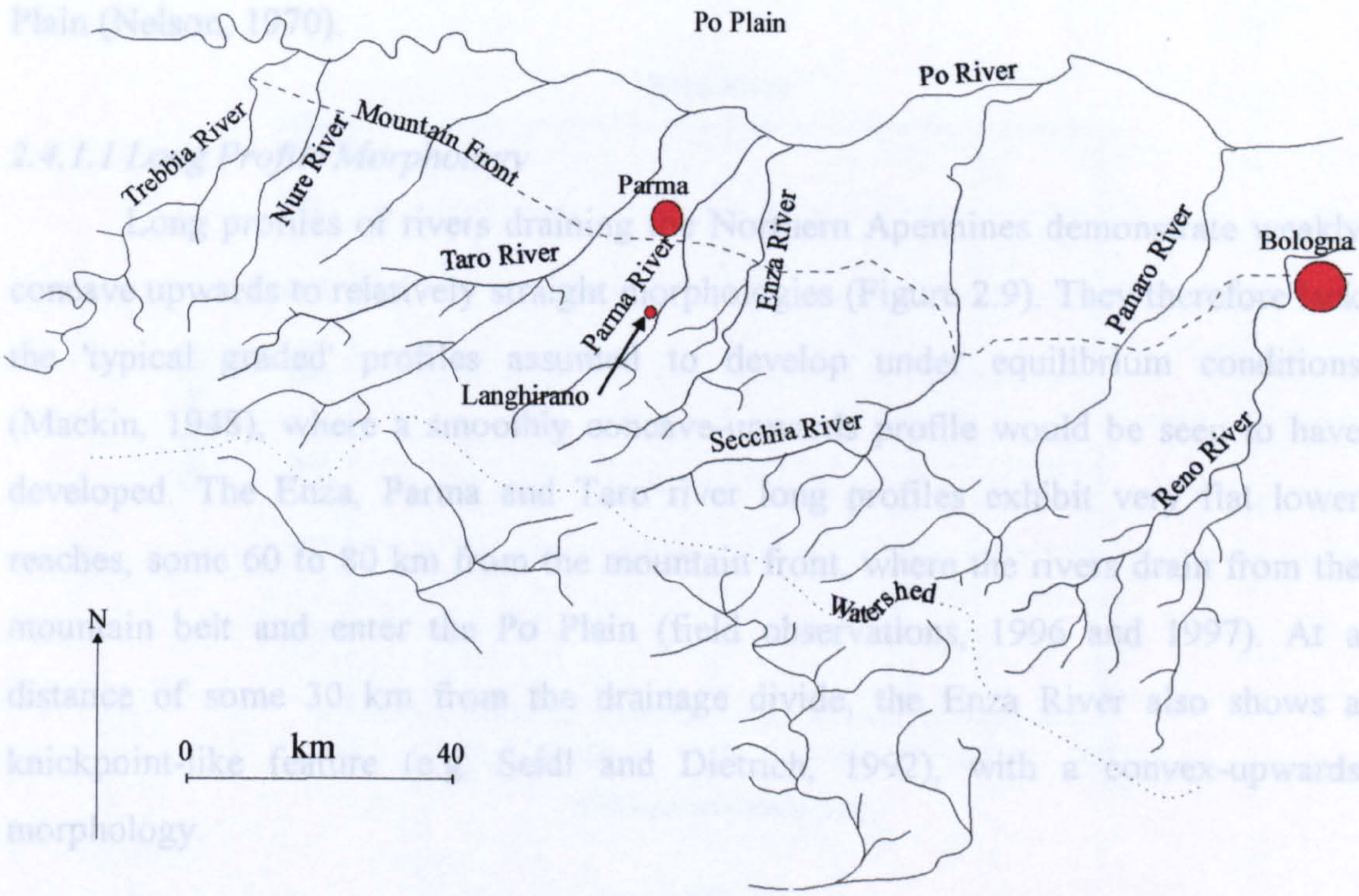

Figure 2.8 Map Showing Northern Apennine Rivers and Locations Mentioned in the Text

Longer term deposition nearer the Po River confluence is indicated by historical channel avulsions and by the Po River's channel bed being elevated above the Po Plain (Nelson, 1970).

2.4.1.1 Long Profile Morphology

Long profiles of rivers draining the Northern Apennines demonstrate weakly concave upwards to relatively straight morphologies (Figure 2.9). They therefore lack the 'typical graded' profiles assumed to develop under equilibrium conditions (Mackin, 1948), where a smoothly concave-upwards profile would be seen to have developed. The Enza, Parma and Taro river long profiles exhibit very flat lower reaches, some 60 to 80 km from the mountain front, where the rivers drain from the mountain belt and enter the Po Plain (field observations, 1996 and 1997). At a distance of some 30 km from the drainage divide, the Enza River also shows a knickpoint-like feature (e.g. Seidl and Dietrich, 1992), with a convex-upwards morphology.

2.4.1.2 Downstream Changes in Channel Gradient

Rivers draining the northern Apennines and flowing as tributaries into the Po River show distinct trends in downstream gradient which reflect patterns of late Quaternary erosion and deposition. For the rivers taken as a whole, areas of incision and channel degradation within the erosional, upper basin above the mountain front show gradients (ϕ) on log-log plots of local slope and distance downstream of between -0.86 and -0.26, with intercept values (ψ) of between 2.19 and 9.65 (Table 2.1 and Figure 2.9). As one moves downstream of the mountain front and enters the zone of deposition where the tributaries enter the Po Plain before joining the Po River, different trends are observed. In areas of Late Quaternary deposition, the Northern Apennine tributaries show log-log gradients of between -9.48 and -3.62, contrasting with the higher values of between -1 and 0 for erosional reaches. Also in contrast to values in erosional reaches, values of ψ vary from 13.15 to 42.21, much higher than the values of less than 5 found further upstream.

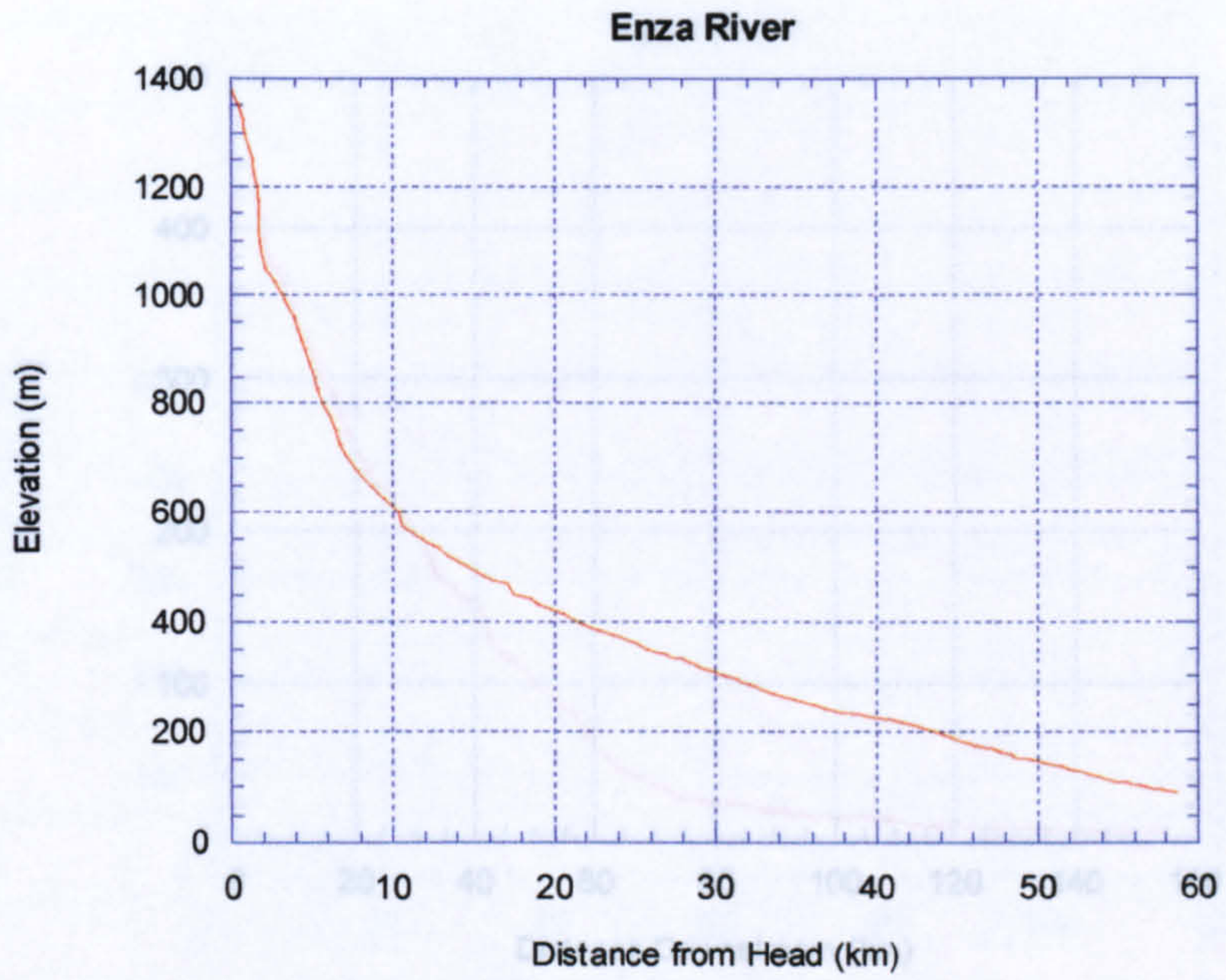

Enza River

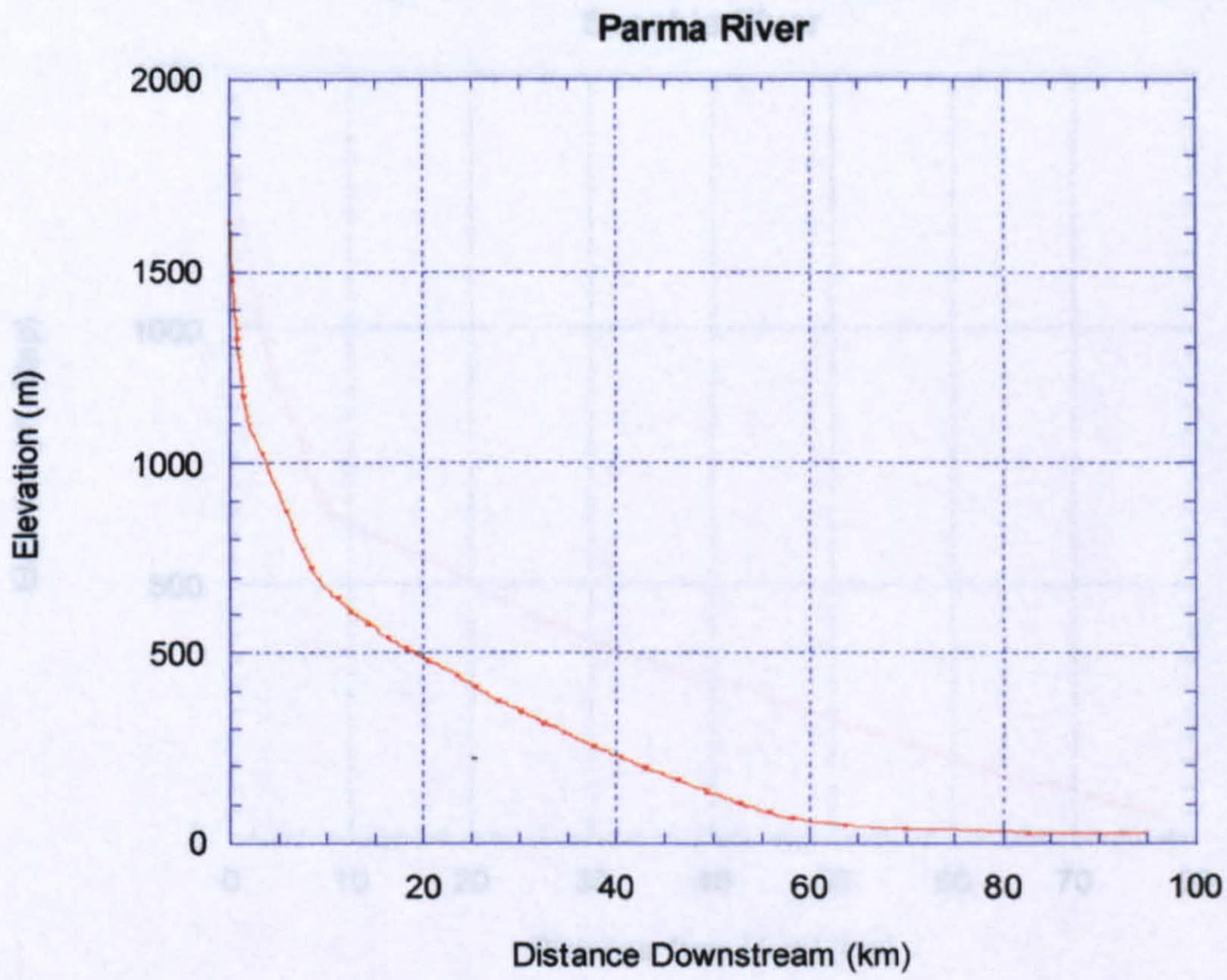

Parma River

Figure 2.9 Longitudinal River Profiles, Northern Apennine Rivers, Italy

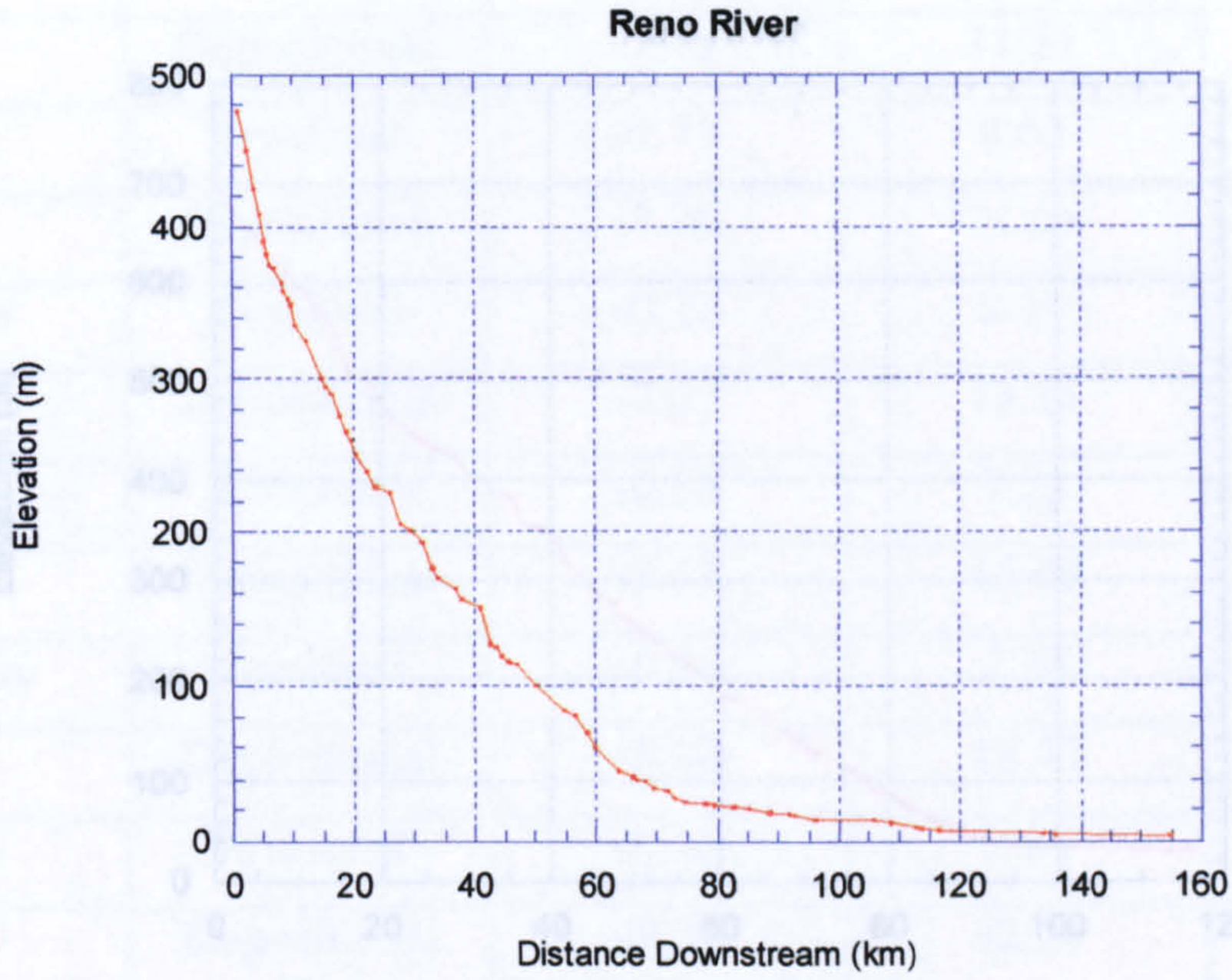

Reno River

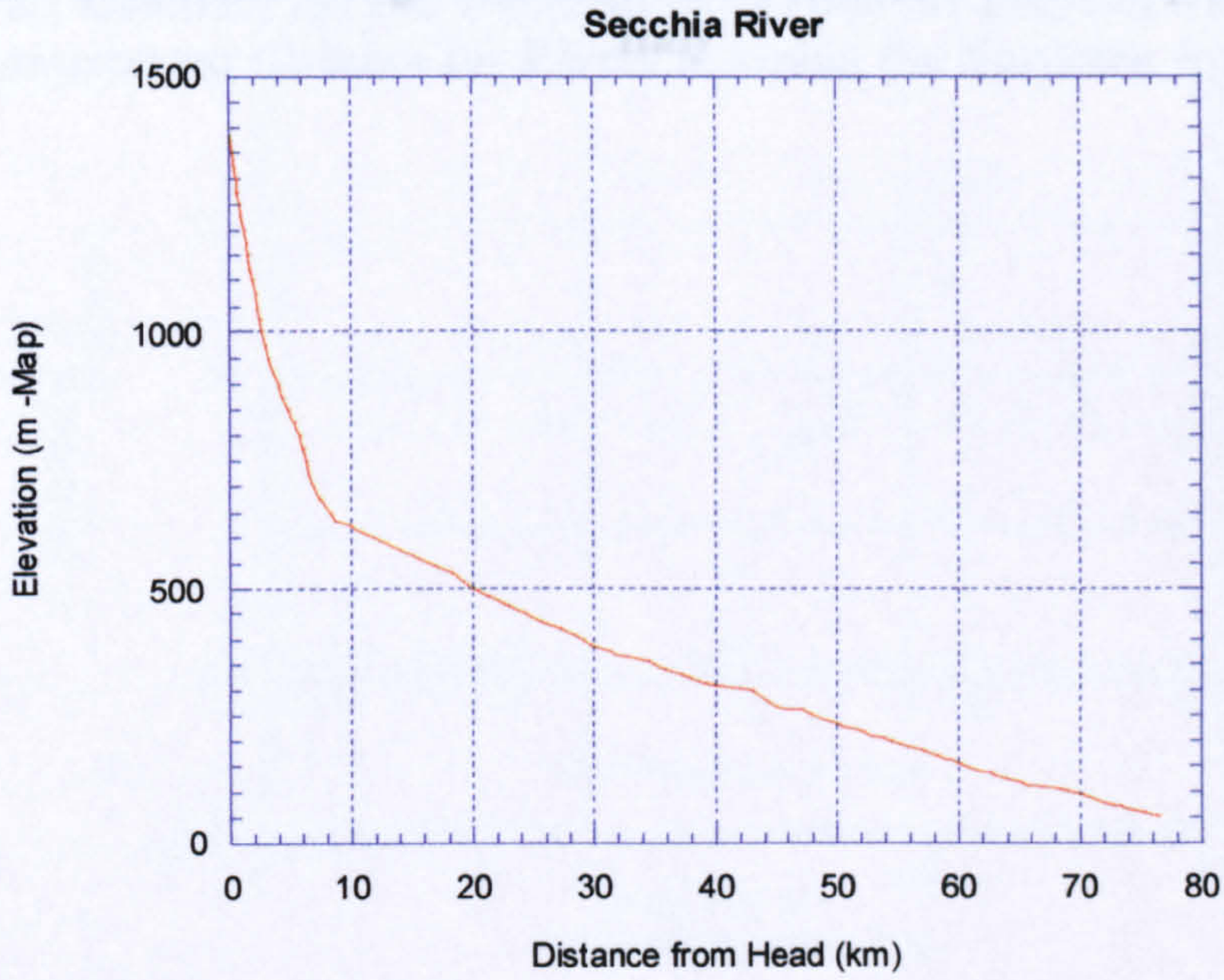

Secchia River

Figure 2.9 Continued Longitudinal River Profiles, Northern Apennine Rivers, Italy

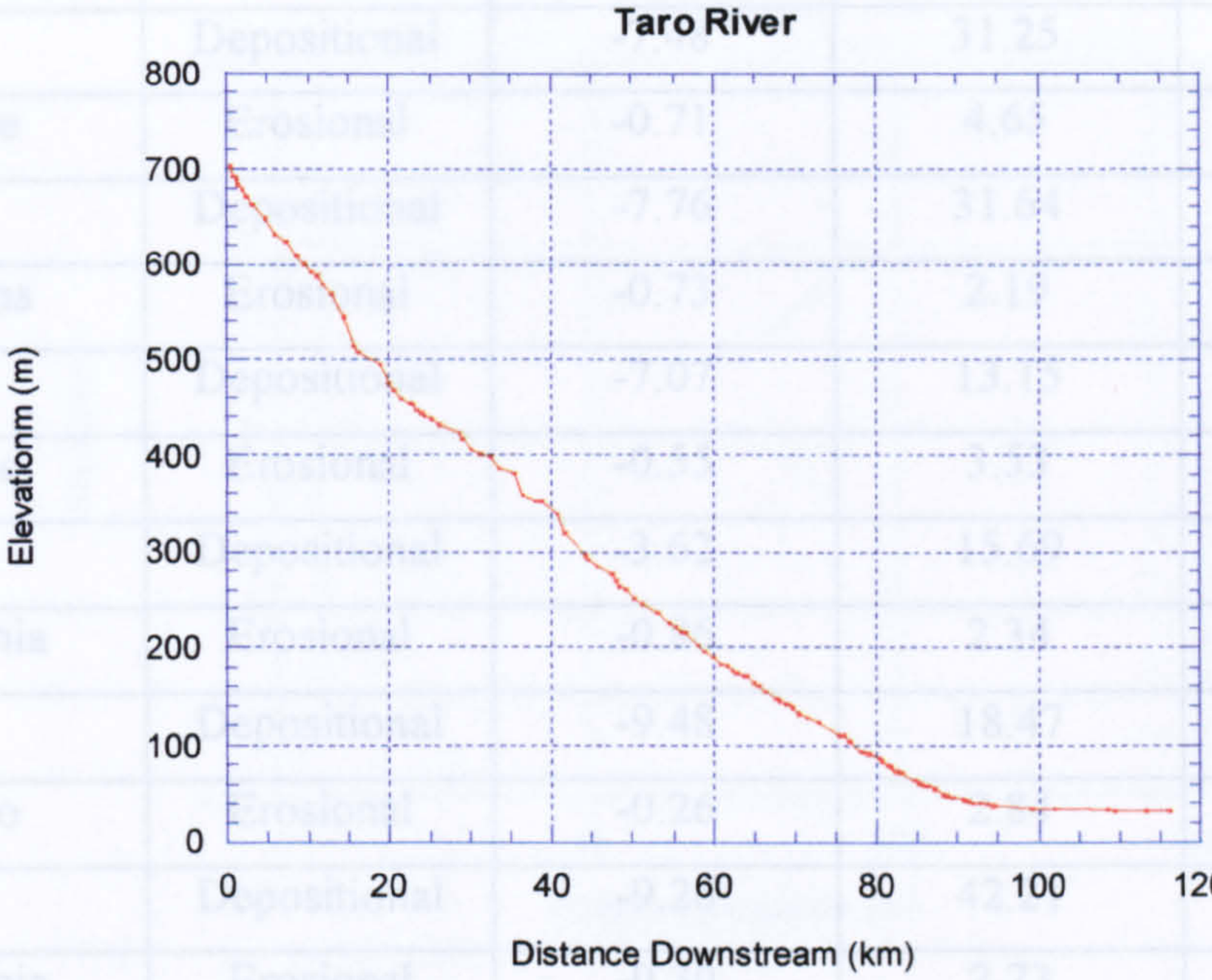

Figure 2.9 Continued Longitudinal River Profiles, Northern Apennine Rivers, Italy

Basin	Regime	Gradient	Intercept	r^2
Enza	Erosional	-0.44	3.54	0.48
	Depositional	-7.48	31.25	0.86
Nure	Erosional	-0.71	4.65	0.83
	Depositional	-7.76	31.64	0.56
Parma	Erosional	-0.73	2.19	0.94
	Depositional	-7.07	13.15	0.87
Reno	Erosional	-0.55	3.53	0.63
	Depositional	-3.62	15.69	0.69
Secchia	Erosional	-0.86	2.34	0.94
	Depositional	-9.48	18.47	0.81
Taro	Erosional	-0.26	2.84	0.38
	Depositional	-9.26	42.21	0.79
Trebbia	Erosional	-0.30	2.73	0.54
	Depositional	-9.25	41.82	0.79

Table 2.1 Gradient (ϕ) and Intercept (ψ) Values for Log-Log Plots of Slope Versus Downstream Distance for Rivers Draining the Northern Apennines, Italy.

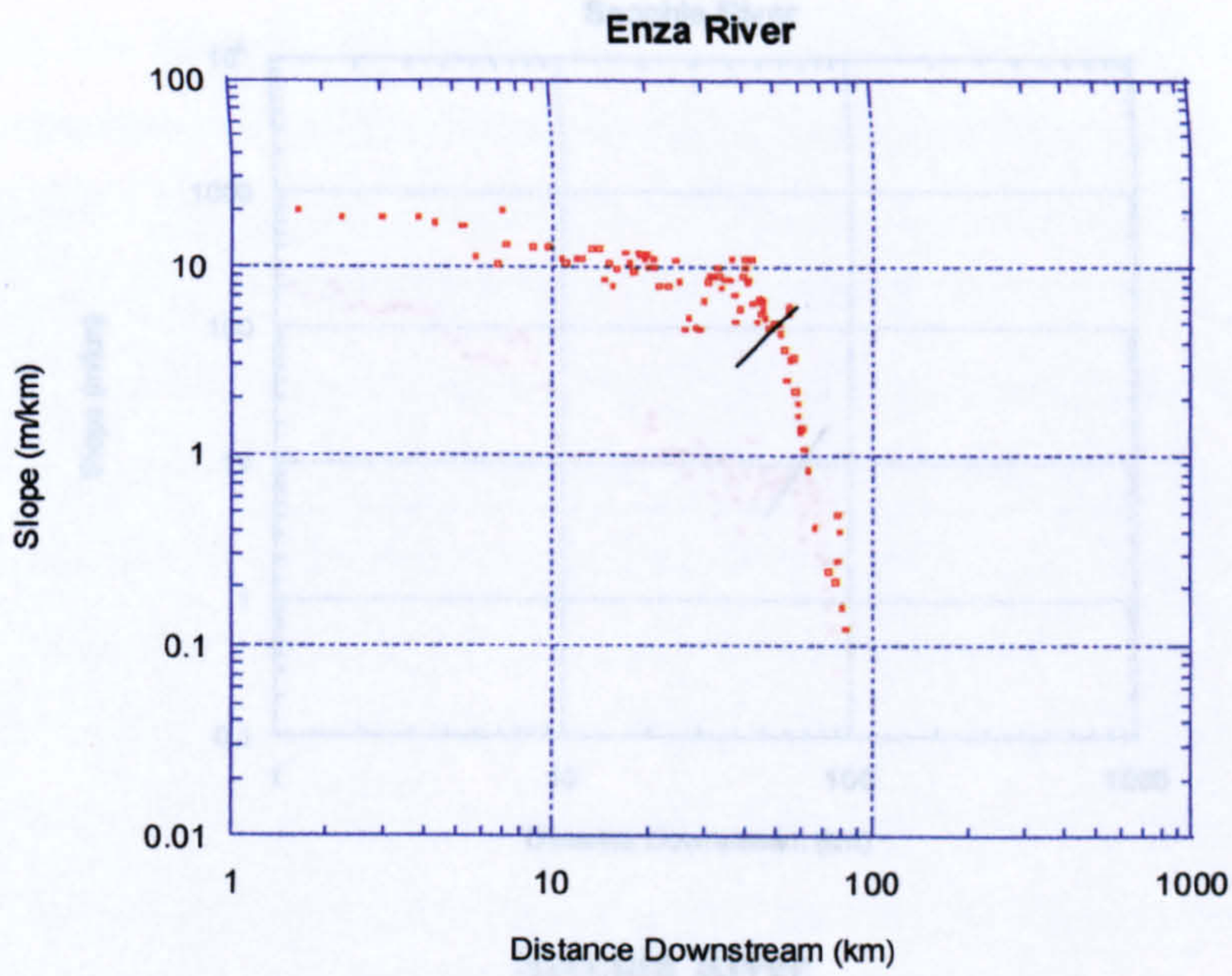

Enza River

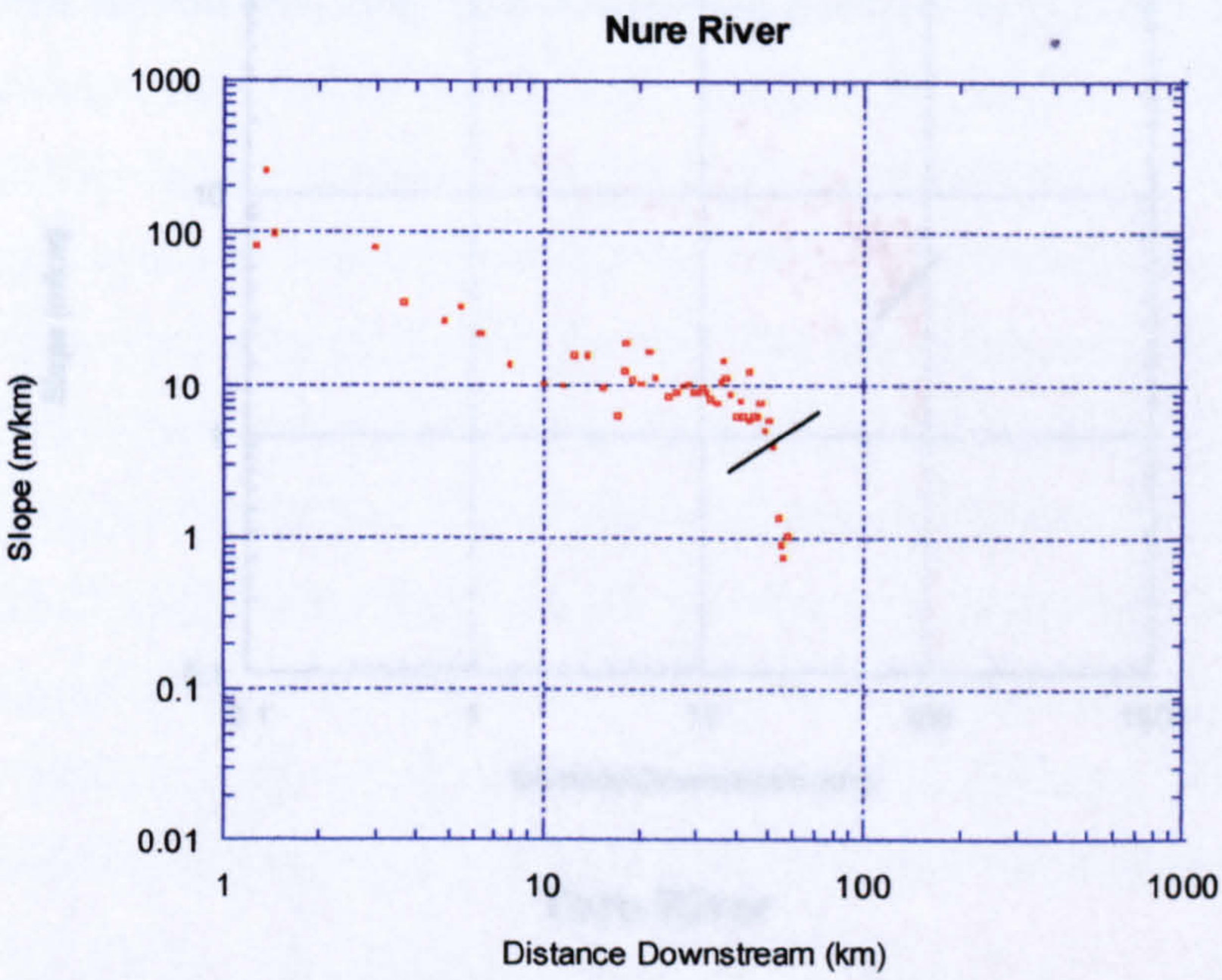

Nure River

Figure 2.10 Logarithmic Plots of Local Slope Against Distance from Drainage Divide Measured from Topographic Maps for Po Tributaries Draining the Northern Apennines, Italy (Lines Indicate Erosion/Deposition Transition)

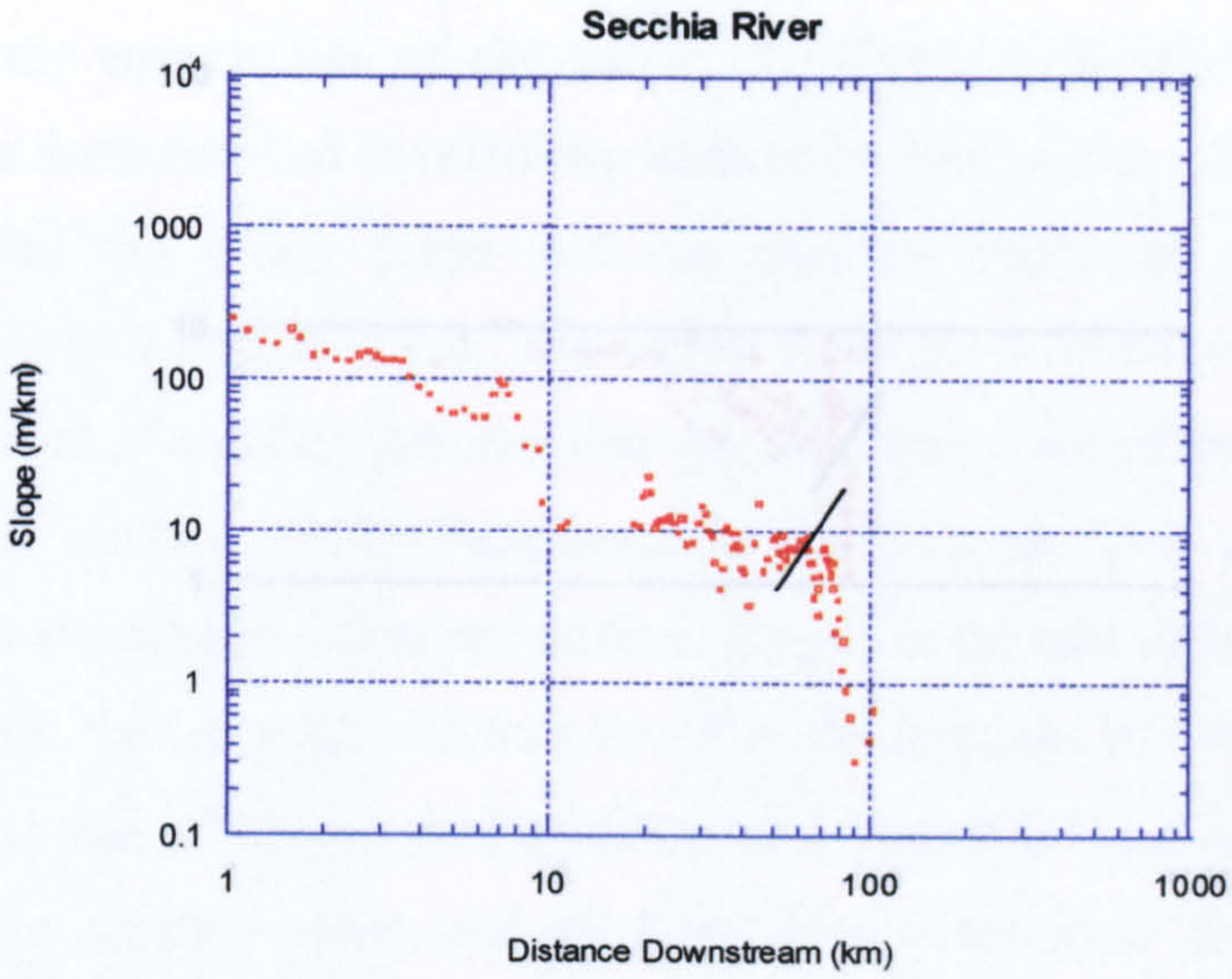

Secchia River

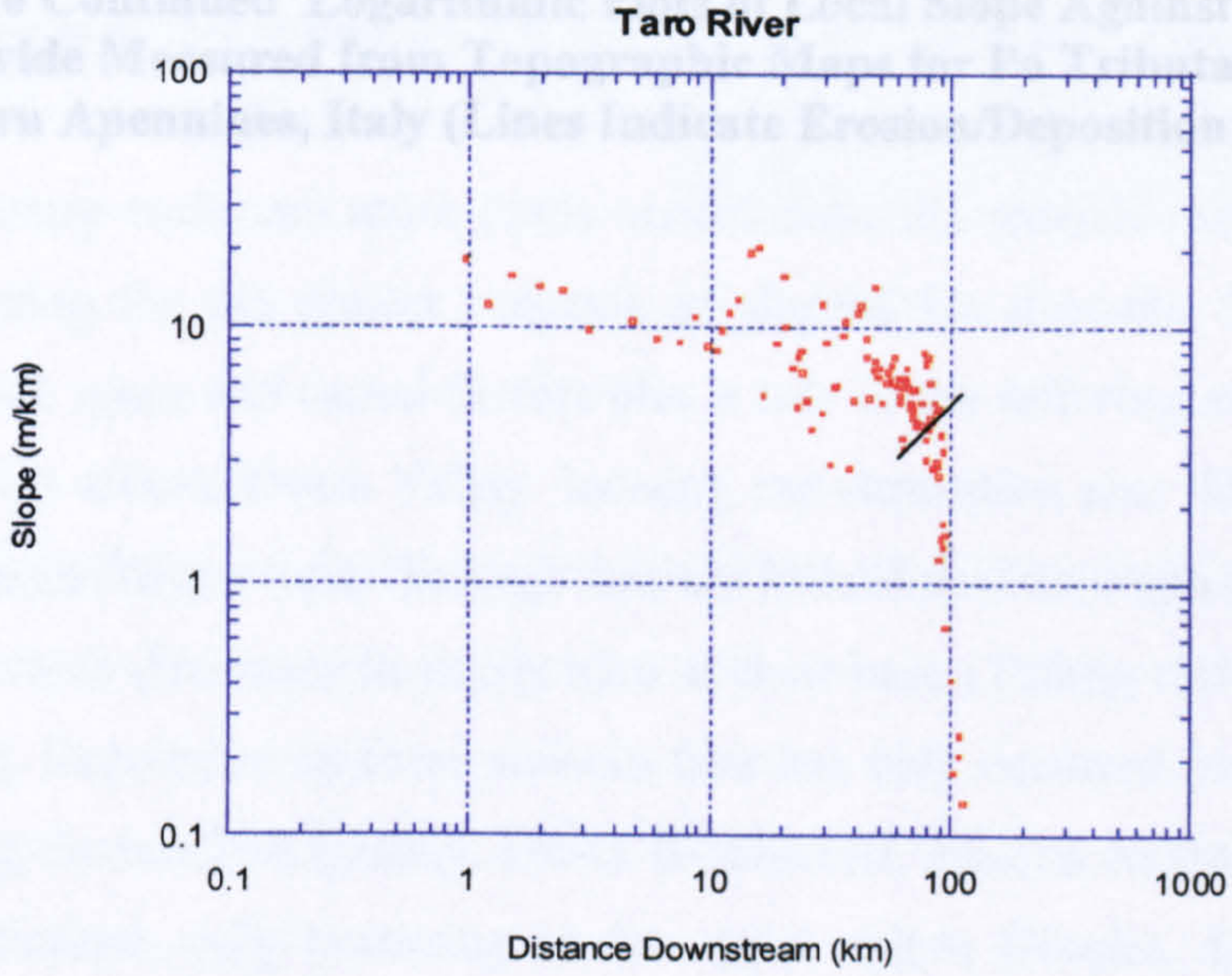

Taro River

Figure 2.10 Continued Logarithmic Plots of Local Slope Against Distance from Drainage Divide Measured from Topographic Maps for Po Tributaries Draining the Northern Apennines, Italy (Lines Indicate Erosion/Deposition Transition)

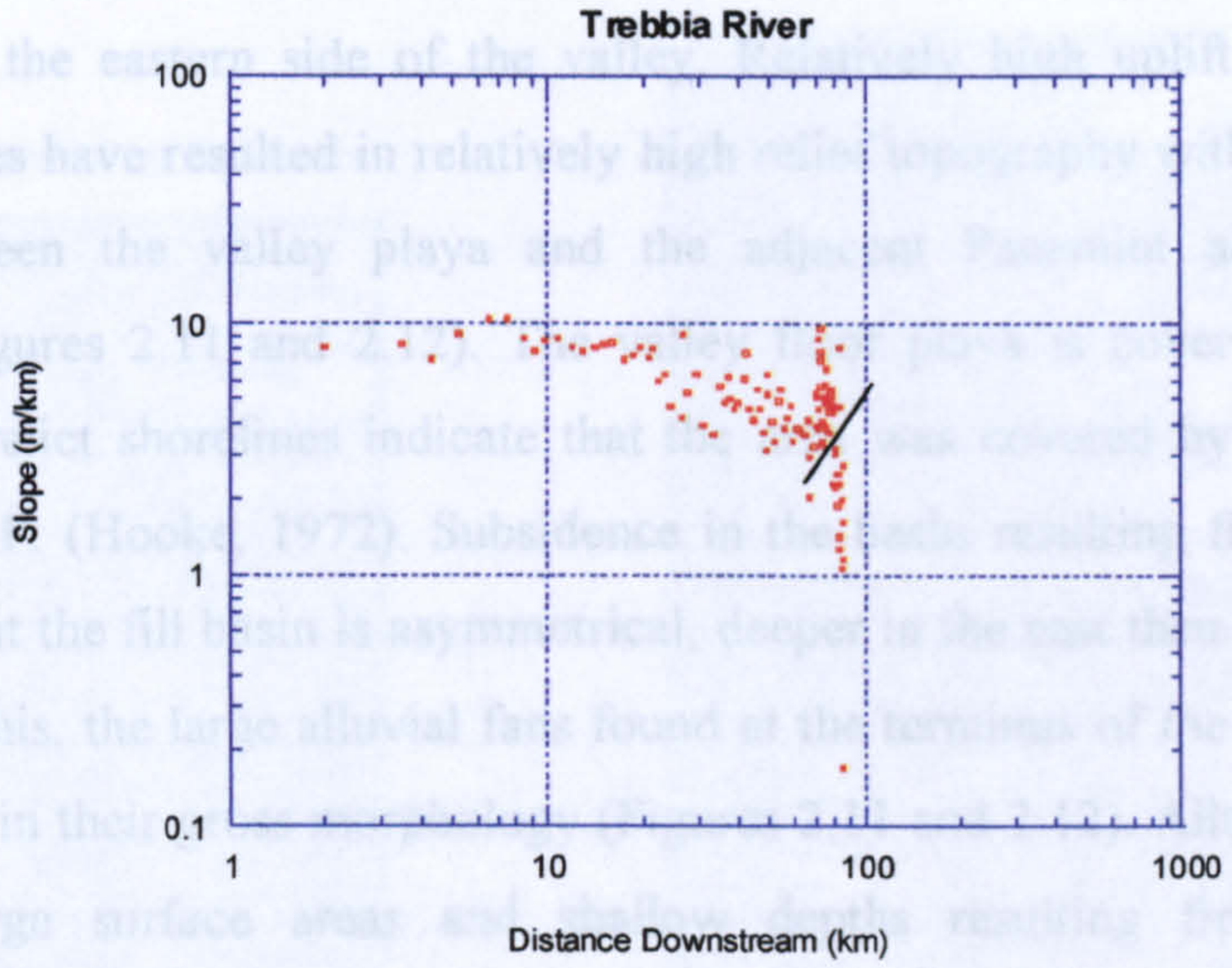

Trebbia River

Figure 2.10 Continued Logarithmic Plots of Local Slope Against Distance from Drainage Divide Measured from Topographic Maps for Po Tributaries Draining the Northern Apennines, Italy (Lines Indicate Erosion/Deposition Transition)

2.4.2 Death Valley, California, U.S.A.

Extensional faulting has been occurring in Death Valley for some 8 Ma (Topping, 1993). This faulting is prominently displayed by a normal reverse fault running along the eastern side of the valley. Relatively high uplift rates and low denudation rates have resulted in relatively high relief topography with relief of up to 3500 m between the valley playa and the adjacent Panamint and Greenwater Mountains (Figures 2.11 and 2.12). The valley floor playa is covered in evaporite deposits, and relict shorelines indicate that the area was covered by an inland lake some 10 ka B.P. (Hooke, 1972). Subsidence in the basin resulting from the eastern fault means that the fill basin is asymmetrical, deeper in the east than the west. Partly as a result of this, the large alluvial fans found at the terminus of the Death Valley's canyons differ in their gross morphology (Figures 2.11 and 2.12). Alluvial fans to the west have large surface areas and shallow depths resulting from the limited depositional space in the western fill basin. By contrast, basins on the eastern side drain into a basin with substantially increased fill depth, resulting in fans with smaller surface areas, but have higher subsidence rates than their western counterparts. These differences are also influenced by the differences in lithological types, terrain form and, to a lesser extent, climatic variation between the two sides of the basin. To the west, sedimentary rocks are more easily eroded than the granitic rocks to the east, partly accounting for the greater volumes of alluvial fan deposits. Therefore both accommodation space and causal factors play a role in the differing morphologies of the alluvial fans around Death Valley. Incision and deposition also differ on the two sides of the basin. To the west, the large fans are incised near their apices to a depth of some 50 m, which decreases to nearly zero at their base (Talling and Sowter, 1998; Hooke, 1972). Deposition on these western fans has only occurred in the lowermost reaches during the last 2 ka (Denny, 1964). By contrast, incision on the eastern fans is much more limited, only occurring at the upper apices (Hooke, 1972), with the majority of the eastern fans being purely depositional during the Holocene.

Eastern Side of Death Valley, California

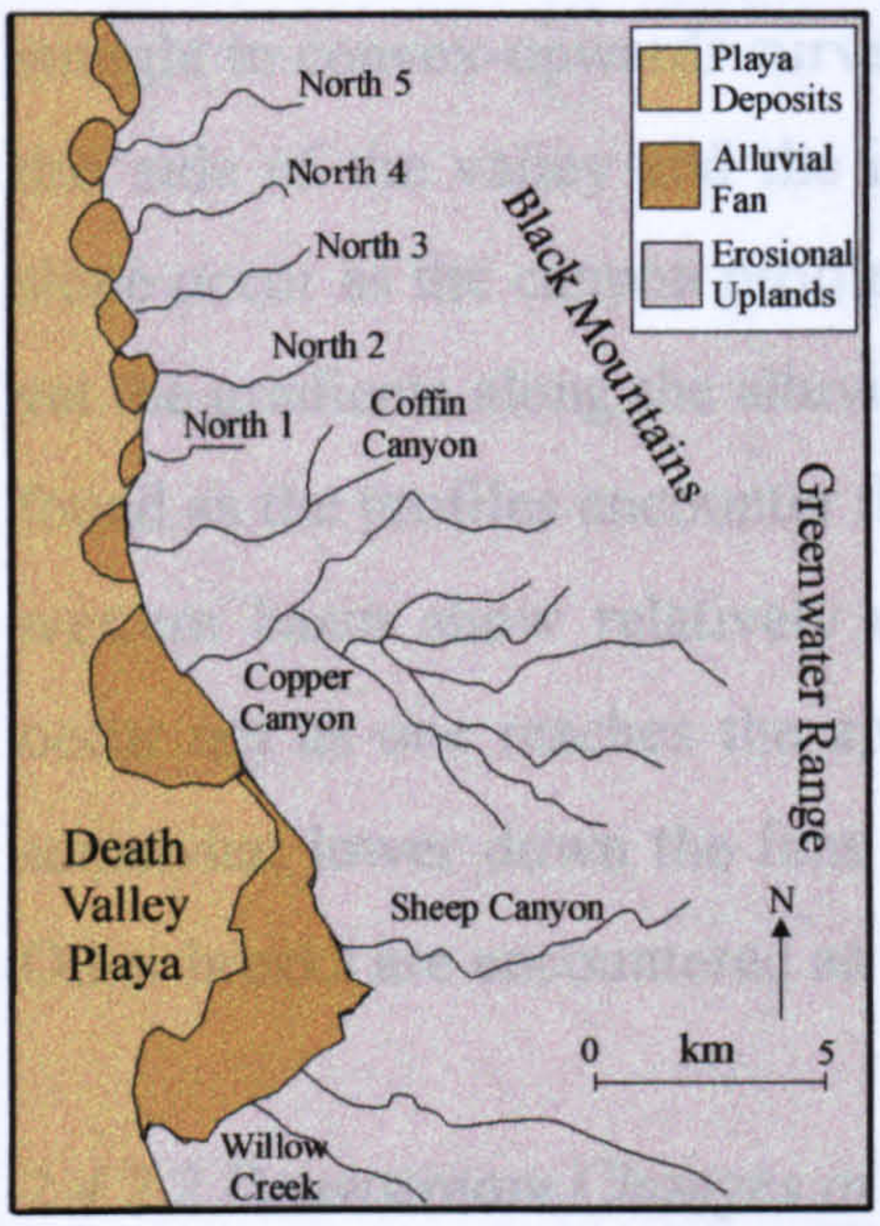

Western Side of Death Valley, California

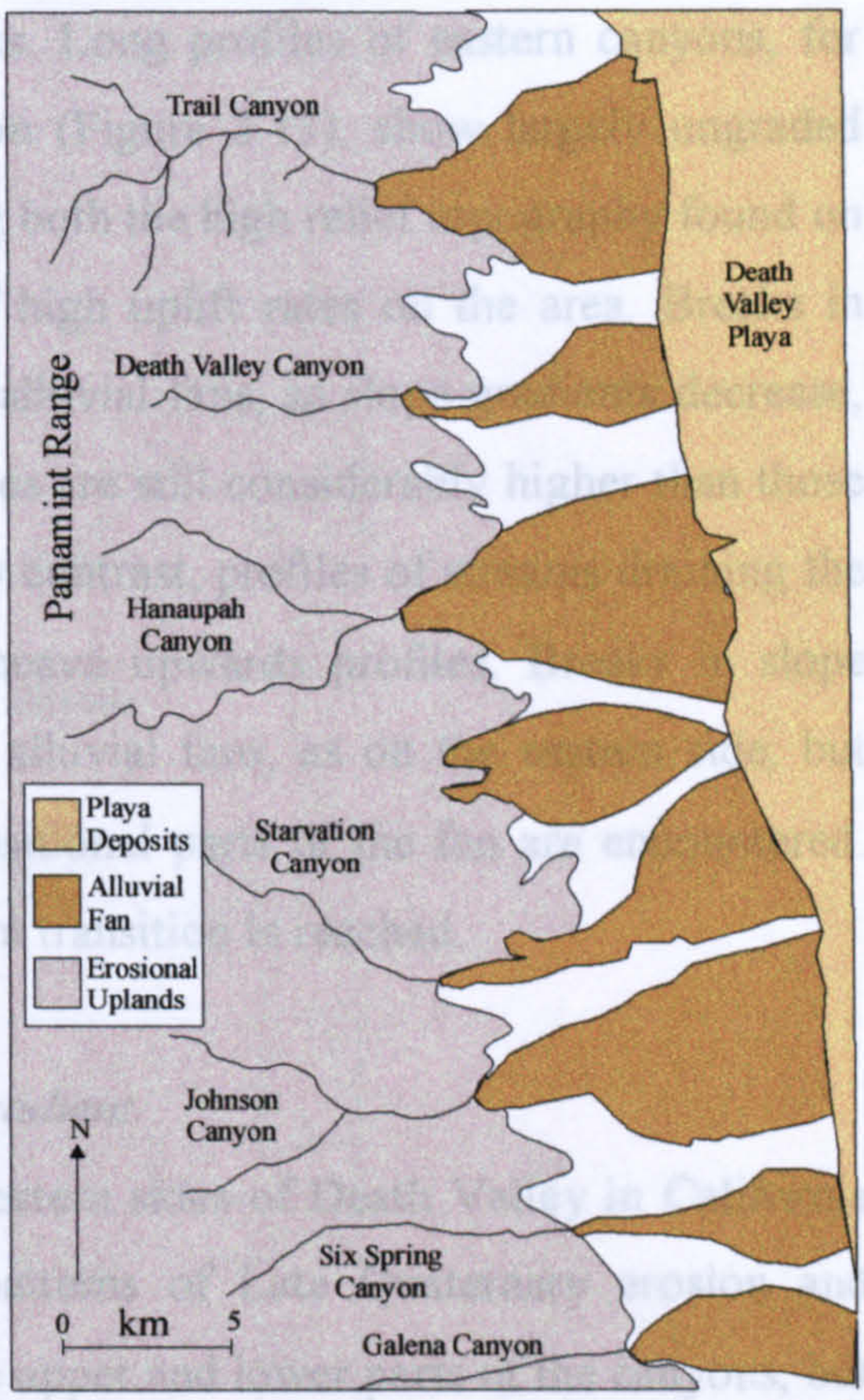

Figures 2.11 and 2.12 Location Maps, Death Valley, California

2.4.2.1 Long Profile Morphology

Long profiles of canyons exiting the uplands of Death Valley show characteristics which reflect both the nature of erosion and deposition, and also the effects of external controls such as tectonics. Long profiles of eastern canyons, for example Willow Creek and North 3 Canyon (Figure 2.13), show largely ungraded straight to convex-upwards curves, reflecting both the high relief topography found on this side of the valley and the influence of high uplift rates on the area. Breaks in slope occur as the canyon profile enters the alluvial fans, as slope gradients decrease, yet the gradients along the alluvial fan reaches are still considerably higher than those found as the profiles encounter the playa. By contrast, profiles of streams draining the western basin show relatively uniform concave upwards profiles. Breaks in slope occur not as one reaches the apices of the alluvial fans, as on the eastern side, but somewhat lower down the fans as the depositional parts of the fan are encountered. Other breaks are encountered as the fan-playa transition is reached.

2.4.2.2 Downstream Changes in Channel Gradient

Canyons draining the eastern and western sides of Death Valley in California again show distinctive trends reflecting patterns of Late Quaternary erosion and deposition. These trends not only vary in the upper and lower parts of the canyons, but also differ from one side to the other, reflecting differing erosional and tectonic regimes.

Death Valley East

The eastern side of Death Valley is drained by a series of relatively short canyons, many of which are bounded by depositional alluvial fans at their lower end, which occur where a normal reverse fault reaches the valley surface. These fans are reflected in the log-log plots of slope and downstream distance as gradients decrease as one moves from the erosional canyons into the depositional alluvial fans. The gradients along the fans are, however, still significantly higher than on the valley floor playa, resulting in two distinct breaks in slope (Figure 2.14). In the upper, erosional reaches of the canyons draining the eastern side of Death Valley, values of ϕ vary from -0.91 to 0.1, with values of ψ varying from -32.89 to -6.10 (Table 2.2). In contrast, areas of deposition in eastern Death Valley show values of ϕ from -4.38 to

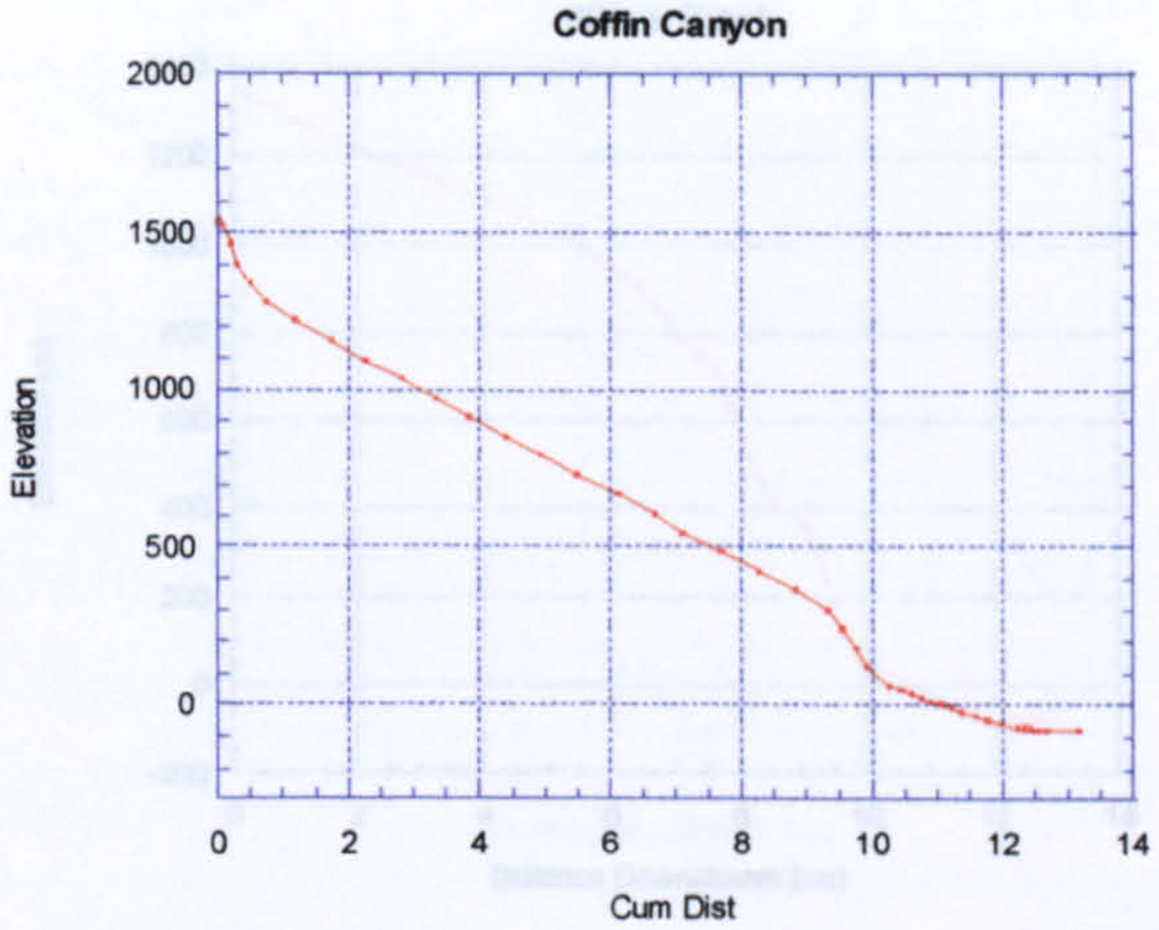

Coffin Canyon

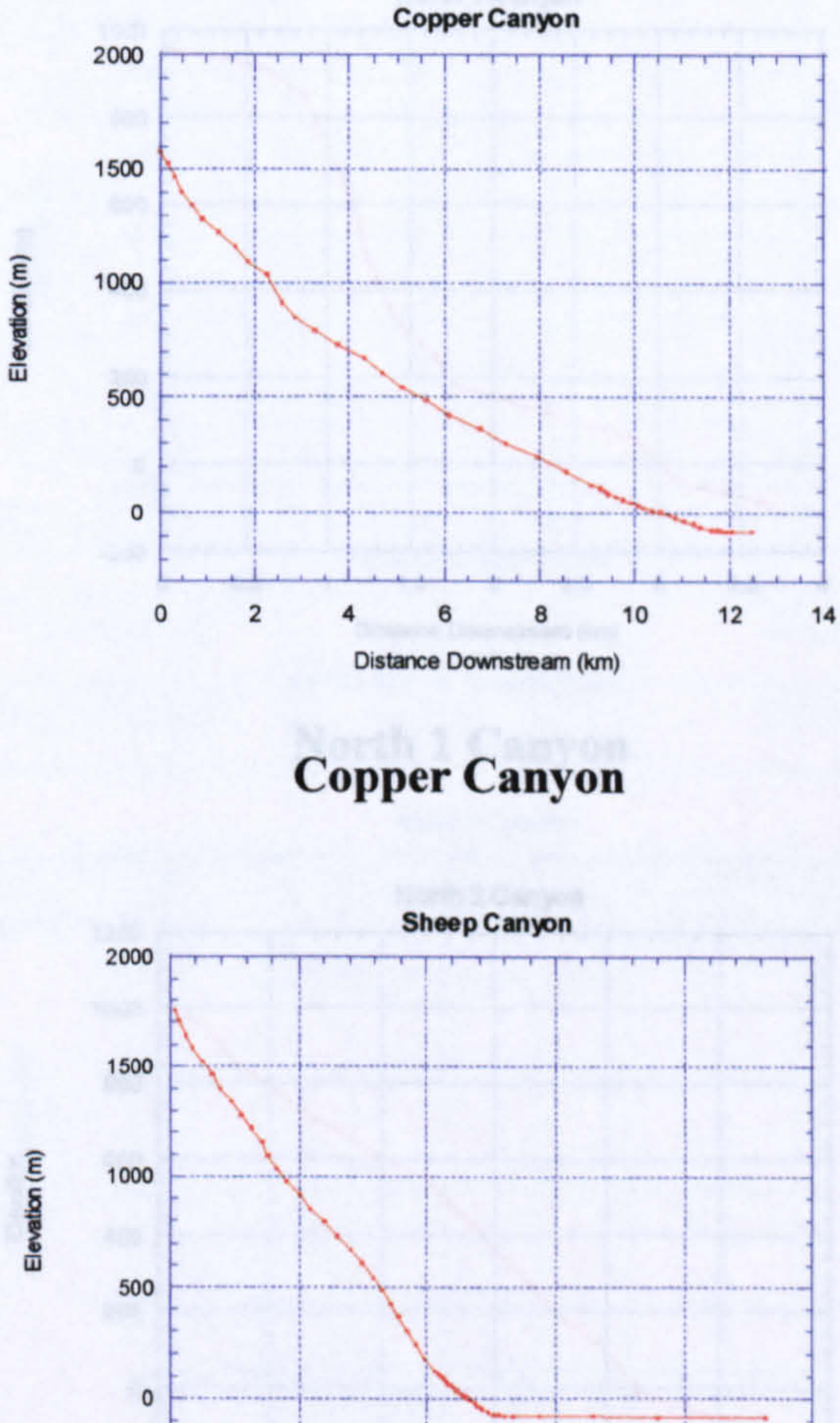

Copper Canyon

Sheep Canyon

Figure 2.13 Longitudinal River Profiles, Eastern Death Valley, California, USA

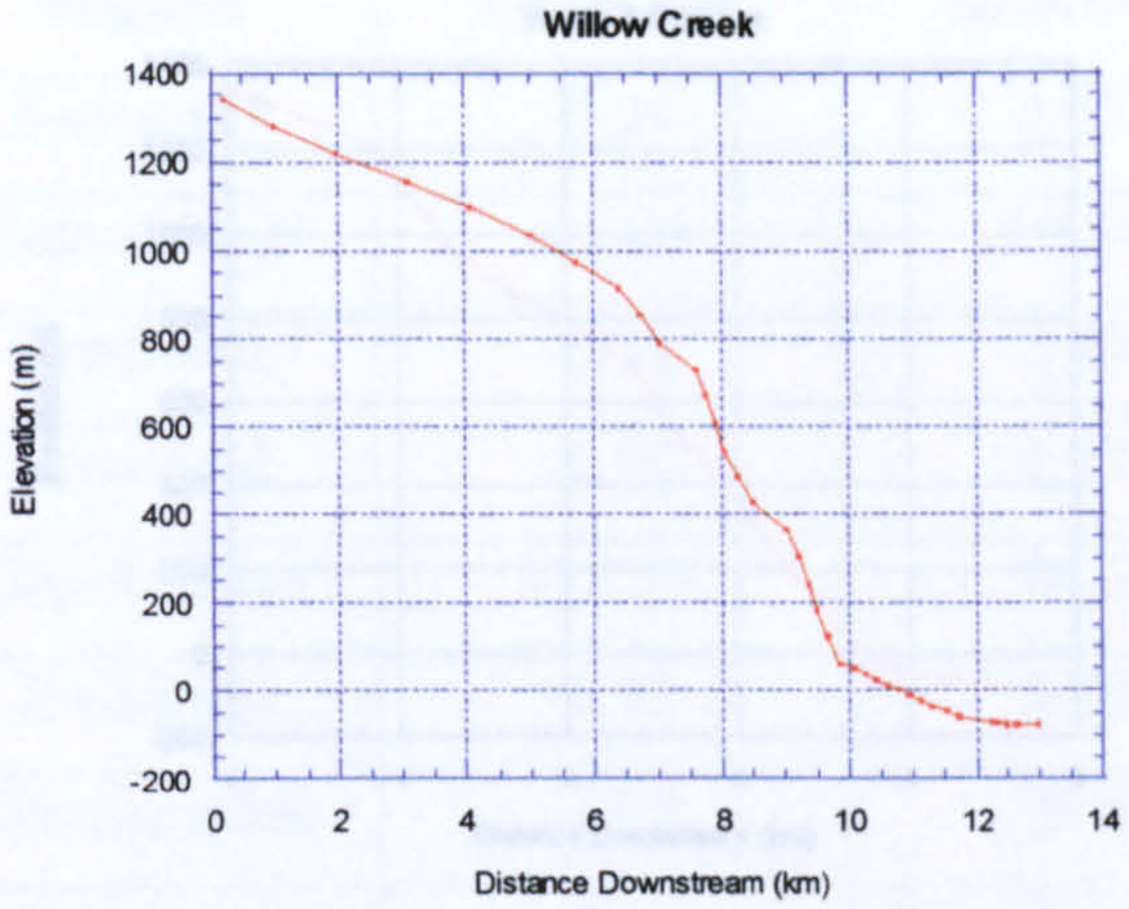

Willow Creek

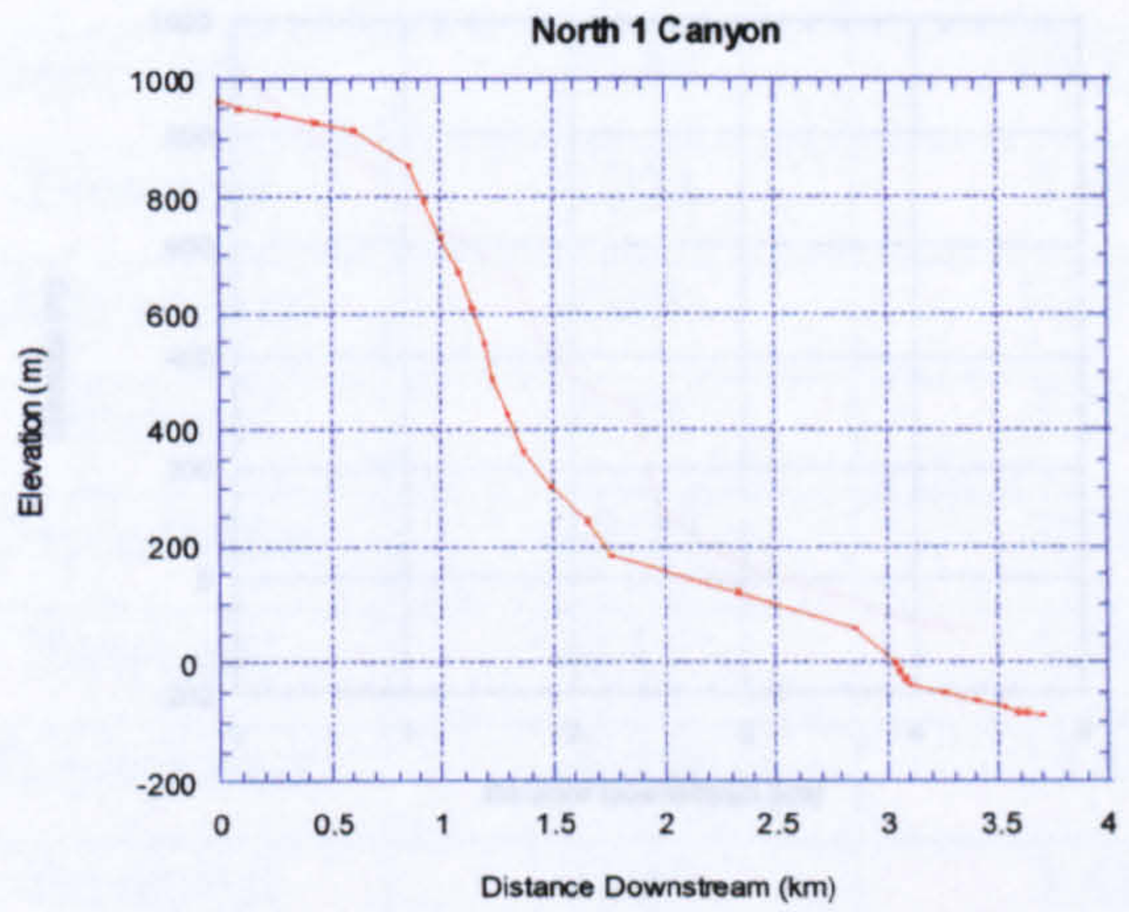

North 1 Canyon

North 2 Canyon

Figure 2.13 Continued Longitudinal River Profiles, Eastern Death Valley, California, USA

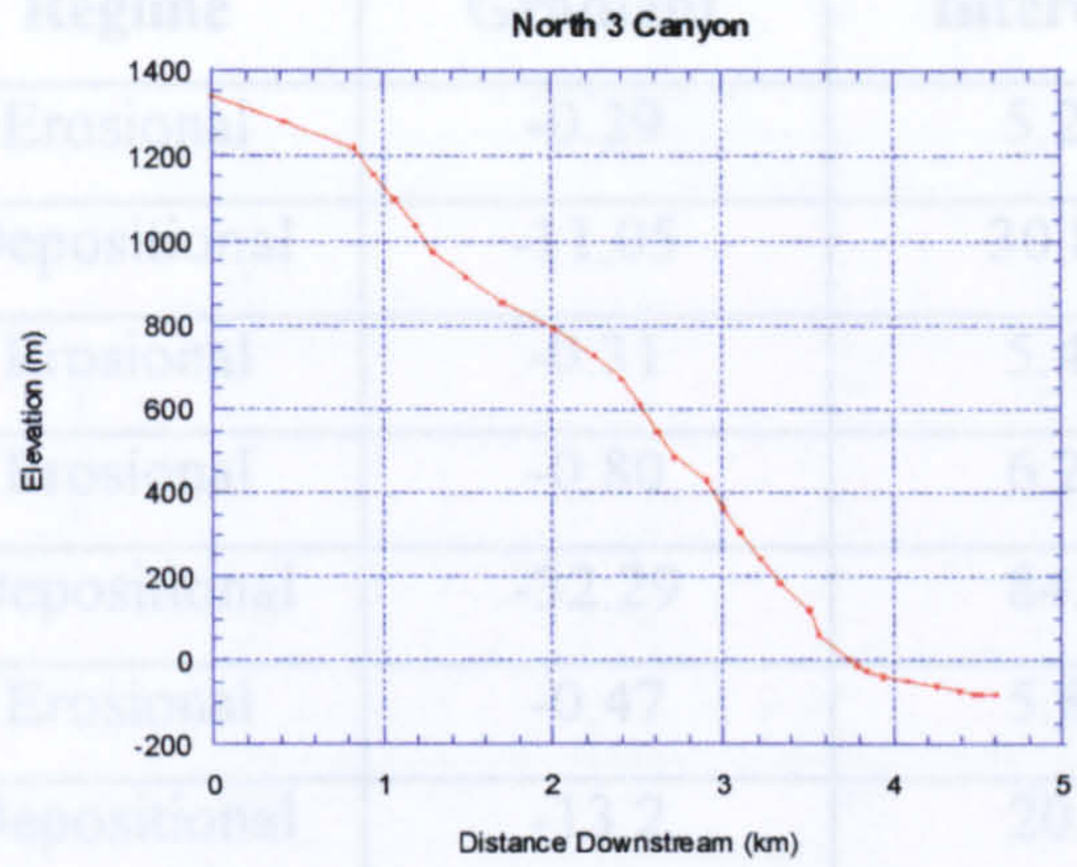

North 3 Canyon

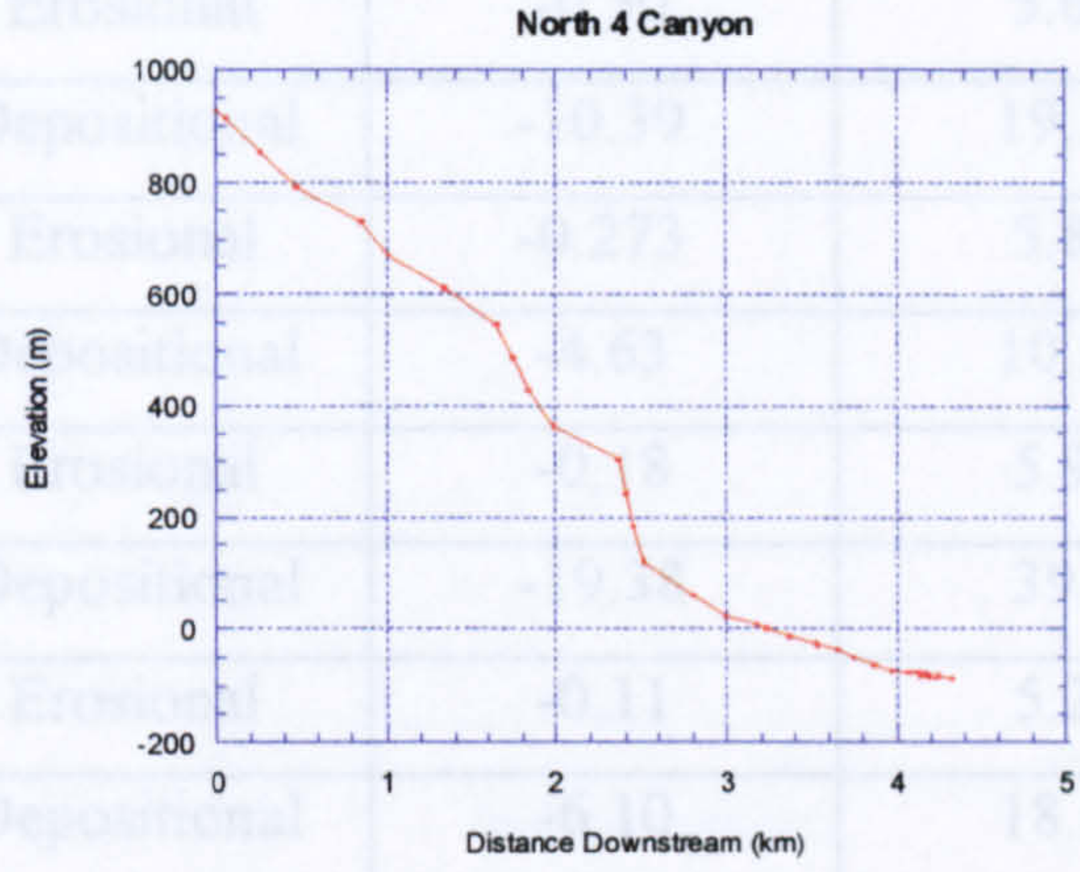

North 4 Canyon

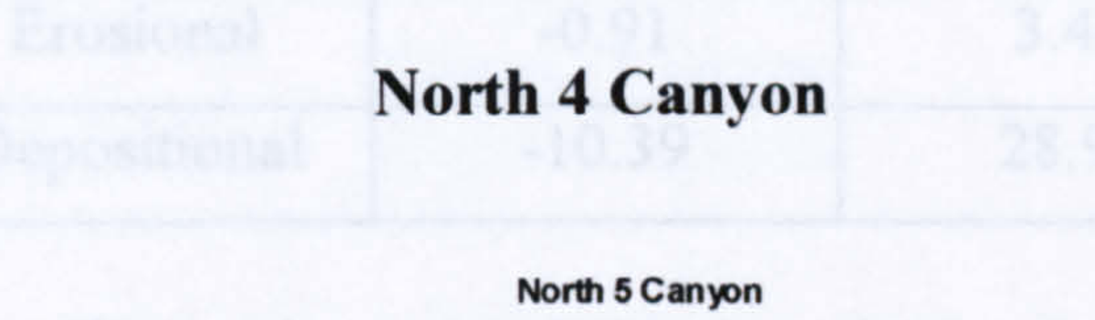

North 5 Canyon

Figure 2.13 Continued Longitudinal River Profiles, Eastern Death Valley, California, US

Canyon	Regime	Gradient	Intercept	r^2
Coffin	Erosional	-0.29	5.23	0.59
	Depositional	-11.05	30.86	0.82
Copper	Erosional	-0.31	5.49	0.55
	Erosional	-0.80	6.27	0.39
	Depositional	-32.29	84.3	0.88
North 1	Erosional	-0.47	5.89	0.15
	Depositional	-13.2	20.9	0.74
North 2	Erosional	-0.10	5.44	0.06
	Depositional	-8.68	18.19	0.52
North 3	Erosional	-0.50	5.69	0.32
	Depositional	-10.39	19.39	0.81
North 4	Erosional	-0.273	5.89	0.15
	Depositional	-4.63	10.37	0.49
North 5	Erosional	-0.18	5.91	0.11
	Depositional	-19.38	39.8	0.54
Sheep	Erosional	-0.11	5.21	0.17
	Depositional	-6.10	18.54	0.53
Willow	Erosional	-0.91	3.48	0.50
	Depositional	-10.39	28.93	0.76

Table 2.2 Gradient (ϕ) and intercept (ψ) values for log-log plots of slope versus downstream distance for rivers draining the eastern side of Death Valley, California, U.S.A.

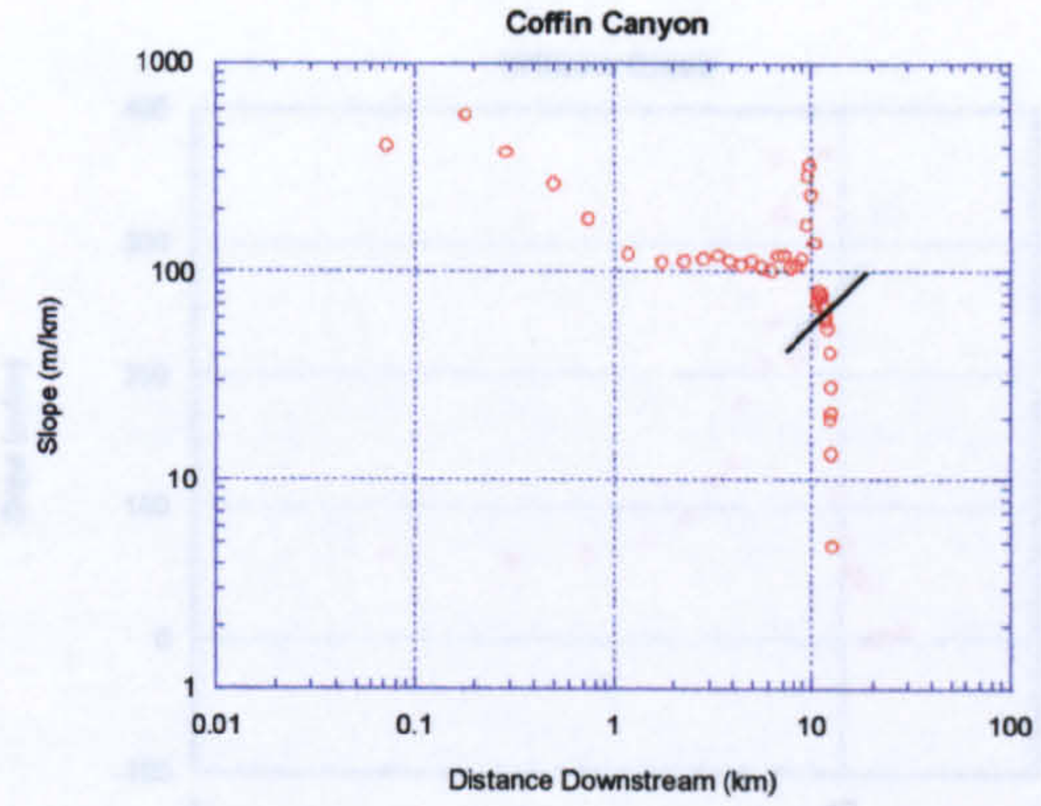

Coffin Canyon

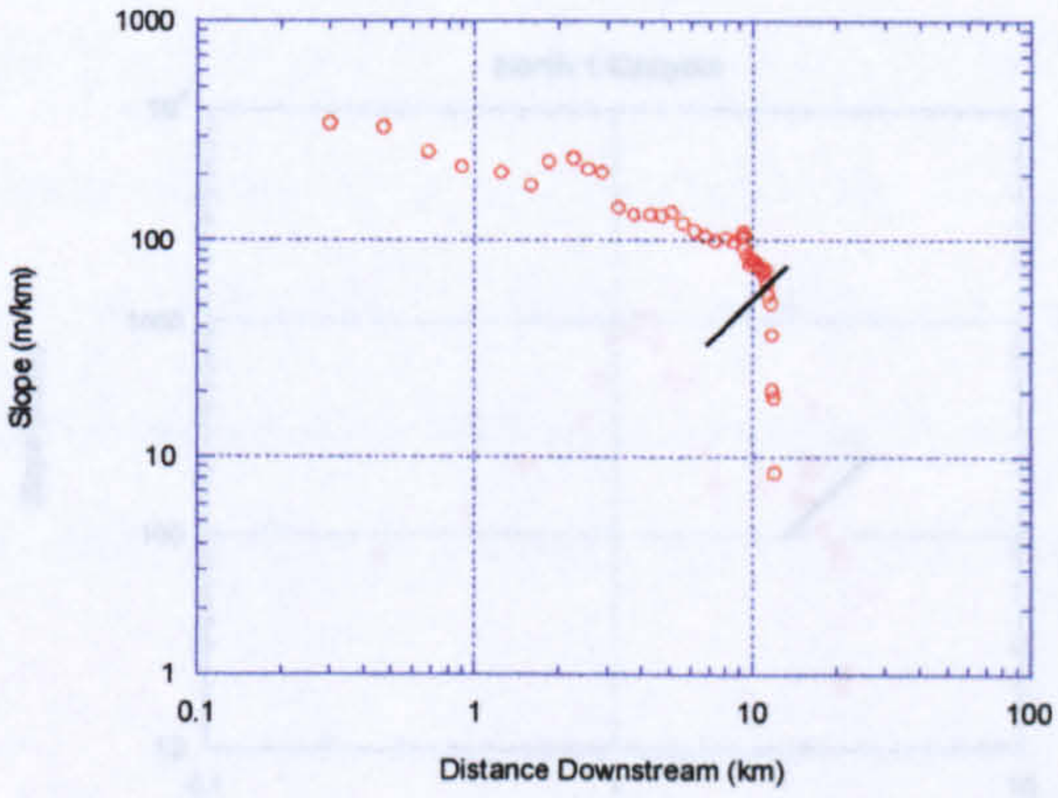

Copper Canyon

Sheep Canyon

Figure 2.14 Logarithmic plots of local slope against distance from drainage divide measured from topographic maps for rivers draining the eastern side of Death Valley, California, USA (lines indicate erosion/deposition transition)

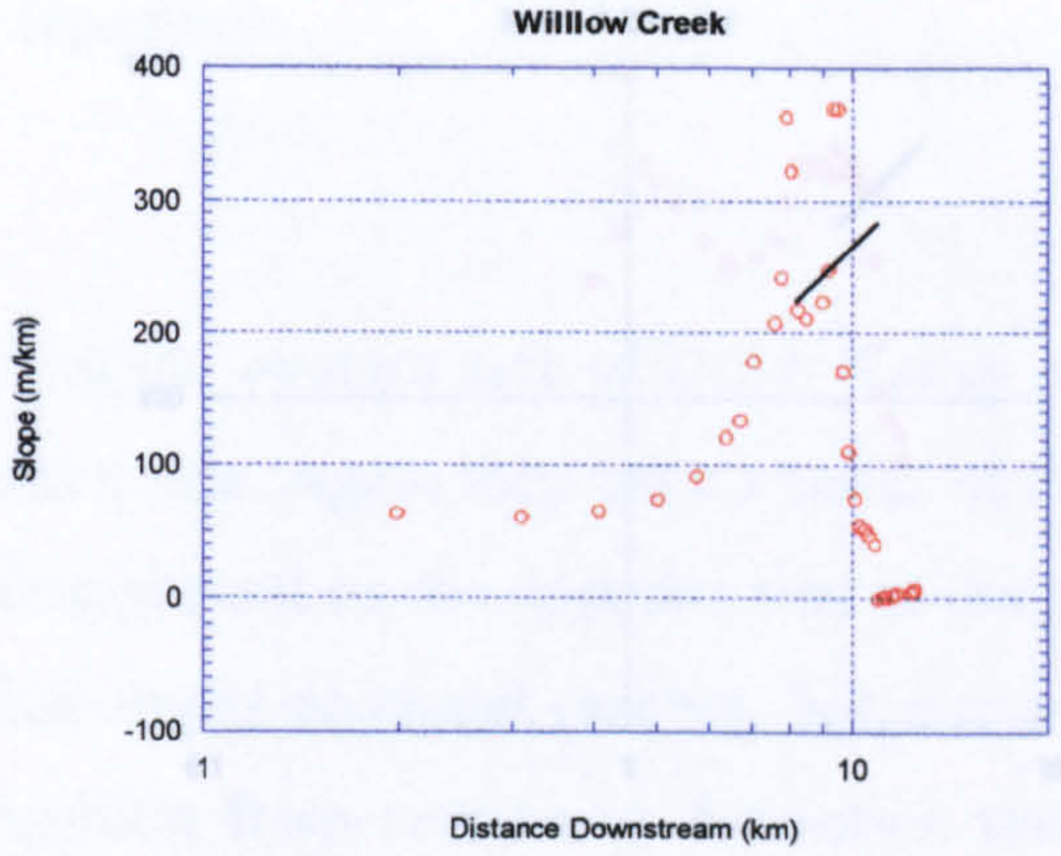

Willow Creek

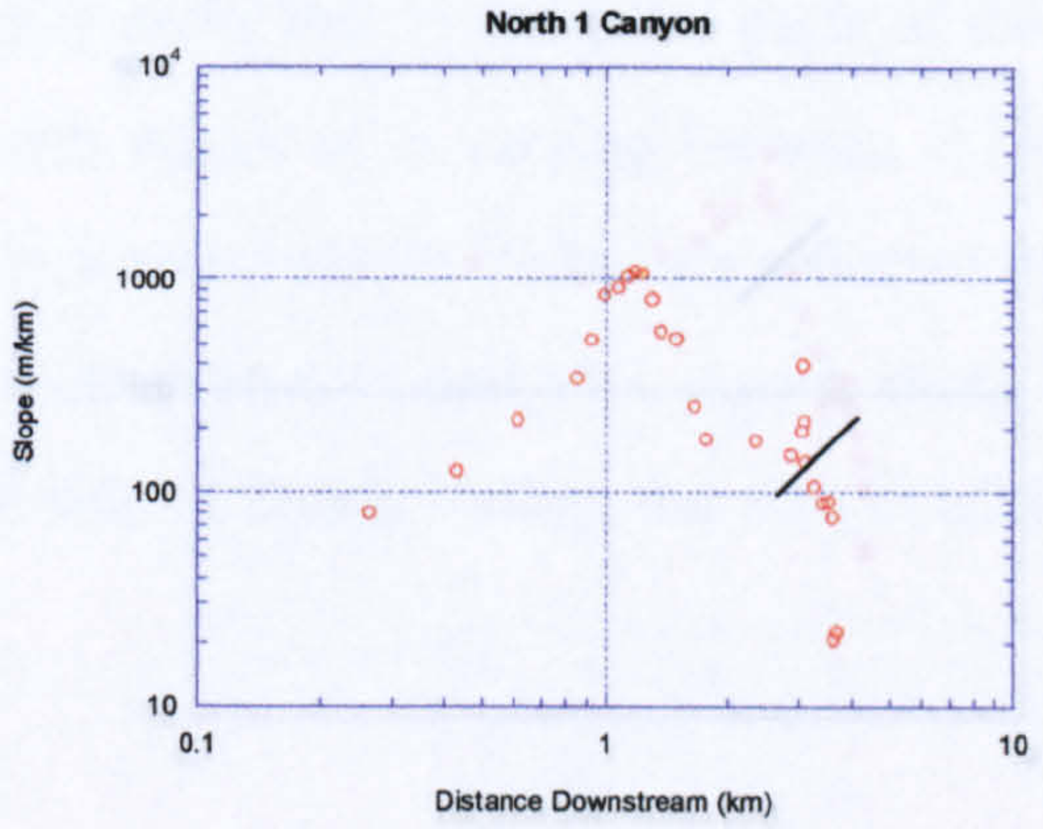

North 1 Canyon

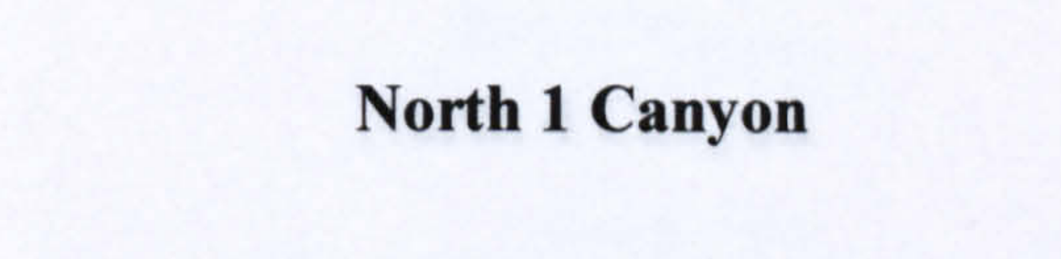

North 2 Canyon

Figure 2.14 Continued Logarithmic plots of local slope against distance from drainage divide measured from topographic maps for rivers draining the eastern side of Death Valley, California, USA (lines indicate erosion/deposition transition)

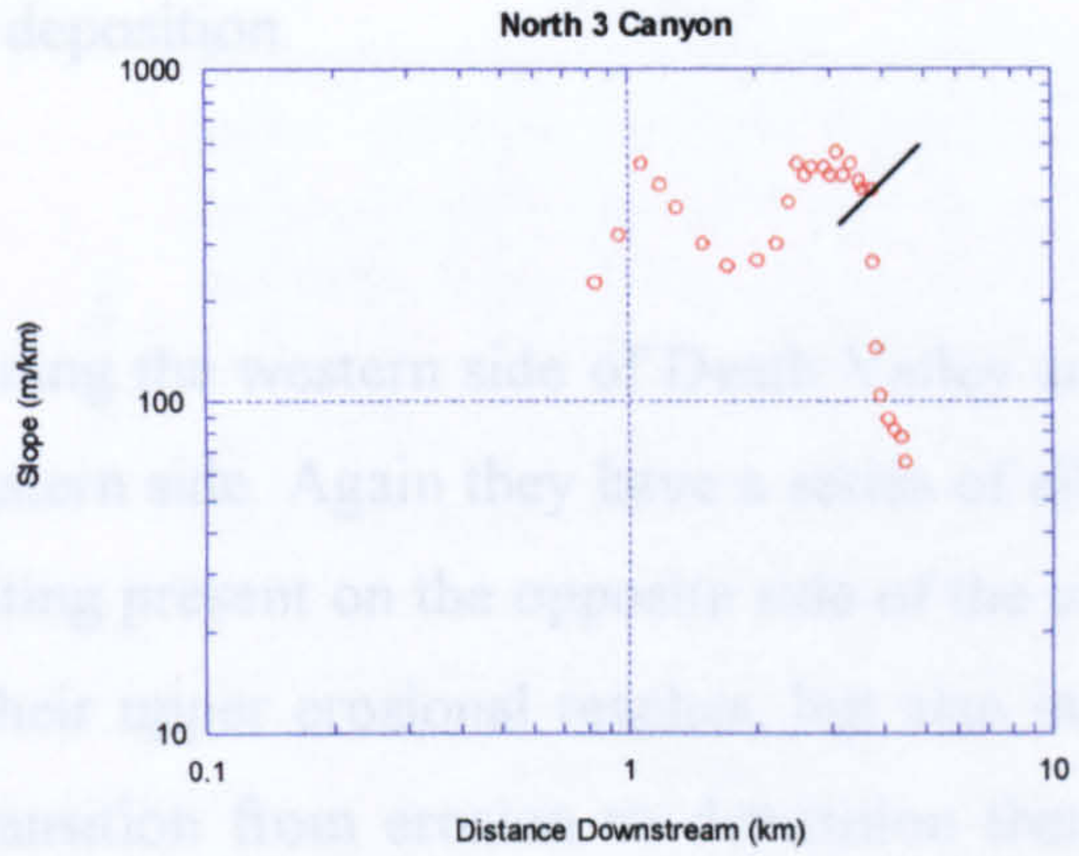

North 3 Canyon

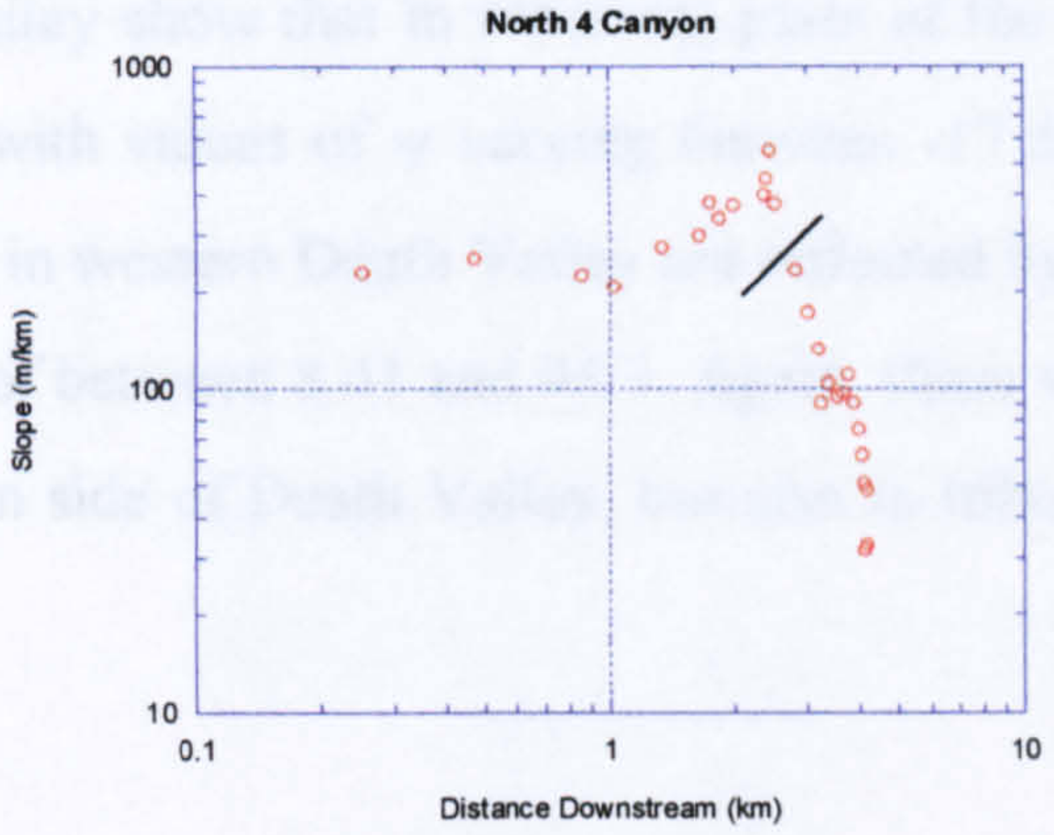

North 4 Canyon

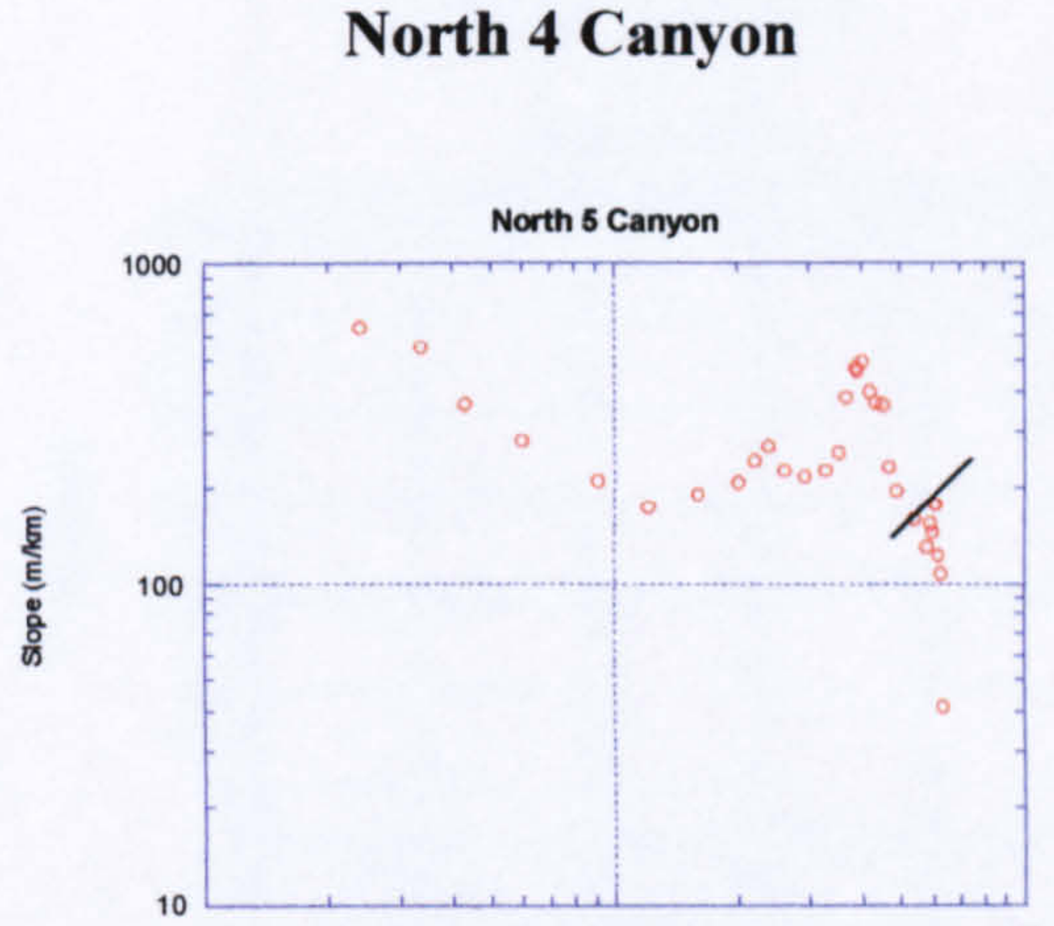

North 5 Canyon

Figure 2.14 Continued Logarithmic plots of local slope against distance from drainage divide measured from topographic maps for rivers draining the eastern side of Death Valley, California, USA (lines indicate erosion/deposition transition)

-1.33 and values of ψ from 5.94 to 16.51. These values therefore follow on from trends seen in Italy for areas of erosion and deposition, with much higher values of ϕ and ψ in the areas of deposition.

Death Valley West

Canyons draining the western side of Death Valley are somewhat longer then those draining the eastern side. Again they have a series of alluvial fans at their lower end, but lack the faulting present on the opposite side of the valley. These canyons are incised not only in their upper erosional reaches, but also in the upper parts of their alluvial fans. The transition from erosion to deposition therefore does not coincide with the change from bedrock canyon to alluvial fan as on the eastern side, but rather lower down along the alluvial fans. Log-log plots of slope and downstream distance for western Death Valley show that in erosional parts of the basins, values of ϕ vary from -0.59 to -0.13, with values of ψ varying between -17.68 and -1.62 (Table 2.3). Depositional regimes in western Death Valley are reflected by values for ϕ of between 5.36 and 5.91 and ψ of between 8.41 and 84.3. Again, these values reflect trends seen not only in the eastern side of Death Valley, but also in tributaries of the Po River in Italy.

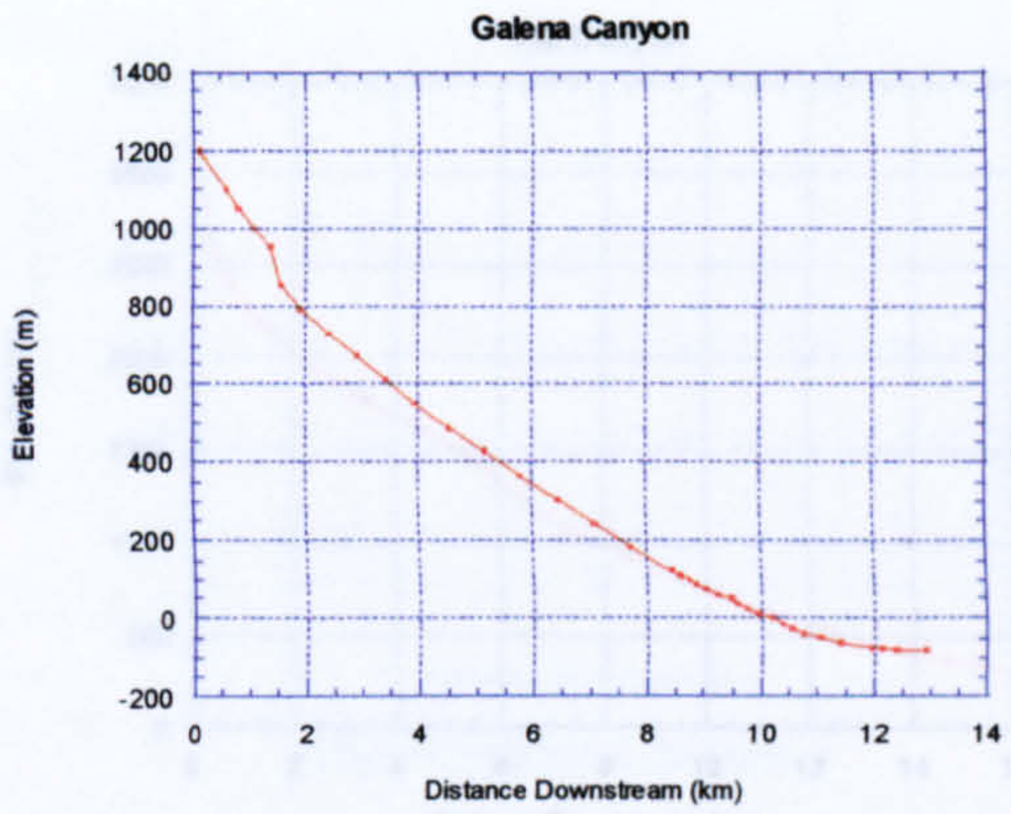

Galena Canyon

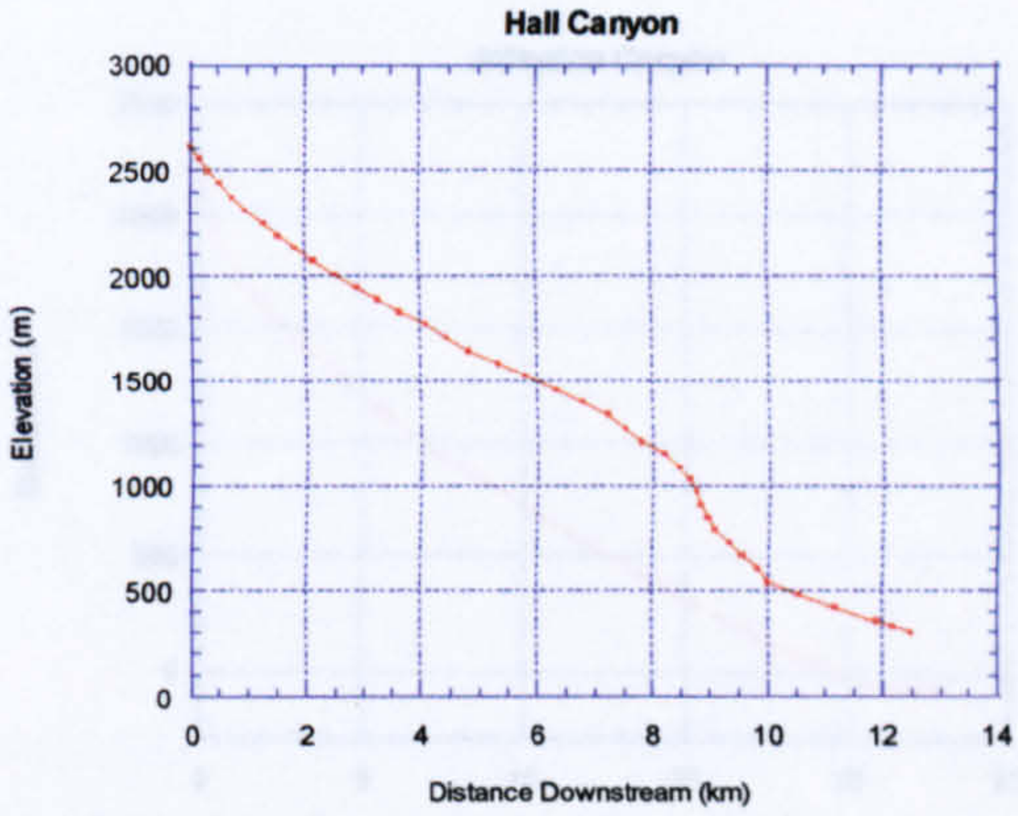

Hall Canyon

Hanaupah Canyon

Figure 2.15 Longitudinal river profiles, western Death Valley, California, USA

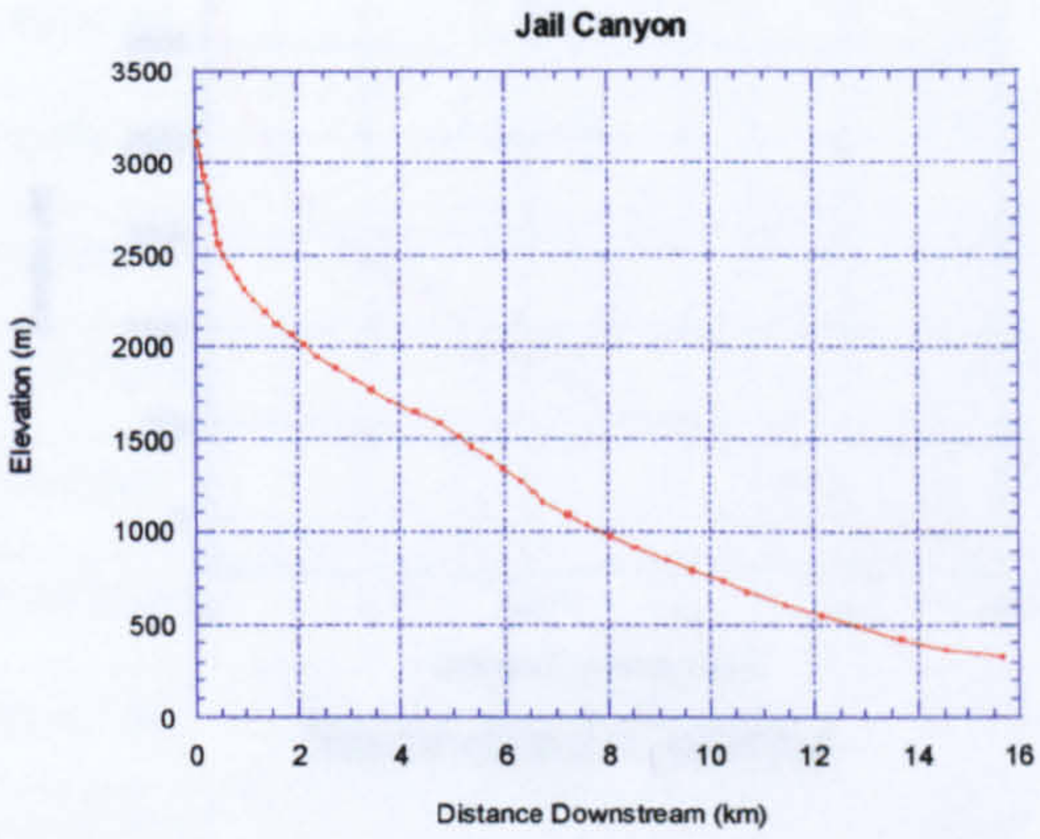

Jail Canyon

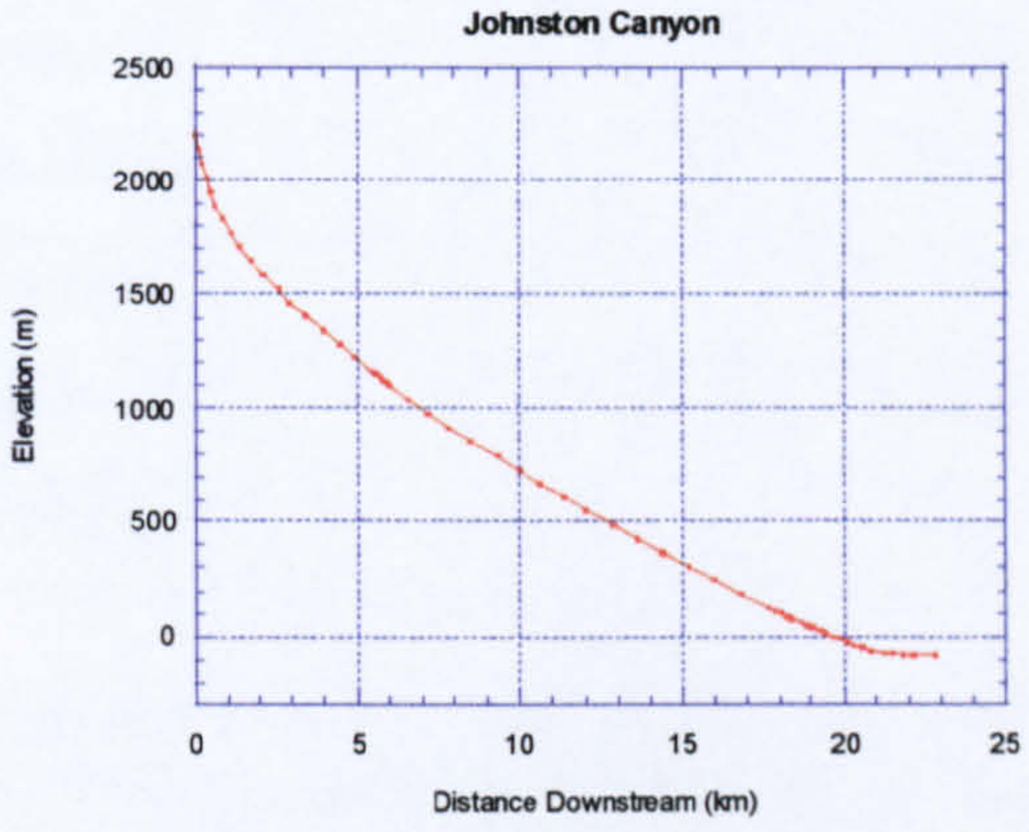

Johnston Canyon

Sixspring Canyon

Figure 2.15 Continued Longitudinal river profiles, western Death Valley, California, USA

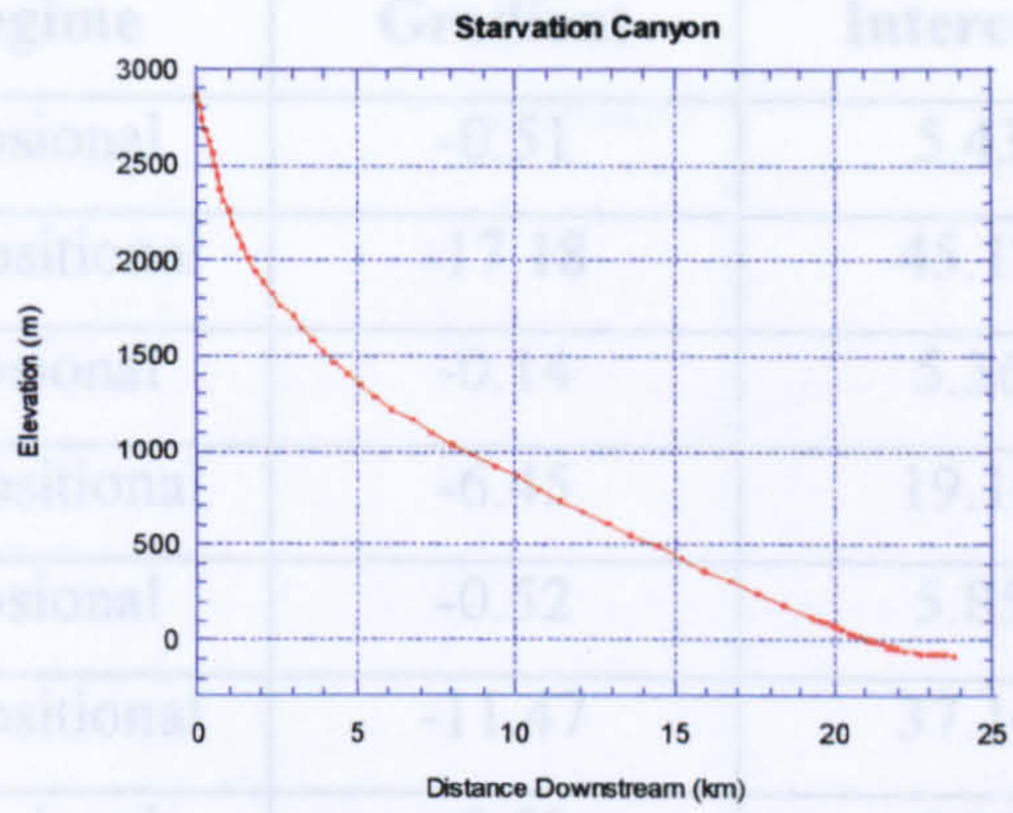

Starvation Canyon

Figure 2.15 Continued Longitudinal river profiles, western Death Valley, California, USA

Canyon	Regime	Gradient	Intercept	r^2
Galena	Erosional	-0.51	5.43	0.71
	Depositional	-12.19	48.17	0.94
Hall	Erosional	-0.14	5.36	0.36
	Depositional	-6.25	19.14	0.86
Hanaupah	Erosional	-0.32	5.86	0.92
	Depositional	-14.27	57.26	0.79
Jail	Erosional	-0.69	6.10	0.83
	Depositional	-1.62	8.41	0.77
Johnston	Erosional	-0.42	5.55	0.94
	Depositional	-12.58	41.07	0.88
Six Spring	Erosional	-0.48	5.68	0.91
	Depositional	-10.63	34.29	0.62
Starvation	Erosional	-0.13	6.3	0.18
	Erosional	-0.57	5.91	0.93
	Depositional	-17.68	57.99	0.81

Table 2.3 Gradient (ϕ) and Intercept (ψ) Values for Log-Log Plots of Slope Versus Downstream Distance for Rivers Draining the Western Side of Death Valley, California, U.S.A.

Canyon	Regime	Gradient	Intercept	r^2
Galena	Erosional	-0.51	5.43	0.71
	Depositional	-17.18	45.17	0.94
Hall	Erosional	-0.14	5.36	0.36
	Depositional	-6.45	19.14	0.86
Hanaupah	Erosional	-0.52	5.85	0.92
	Depositional	-11.47	37.16	0.79
Jail	Erosional	-0.59	6.10	0.83
	Depositional	-1.62	8.41	0.77
Johnston	Erosional	-0.46	5.55	0.94
	Depositional	-12.58	41.07	0.88
Six Spring	Erosional	-0.48	5.68	0.91
	Depositional	-10.63	34.29	0.62
Starvation	Erosional	-0.13	6.3	0.18
	Erosional	-0.57	5.91	0.93
	Depositional	-17.68	57.99	0.81

Table 2.3 Gradient (ϕ) and Intercept (ψ) Values for Log-Log Plots of Slope Versus Downstream Distance for Rivers Draining the Western Side of Death Valley, California, U.S.A.

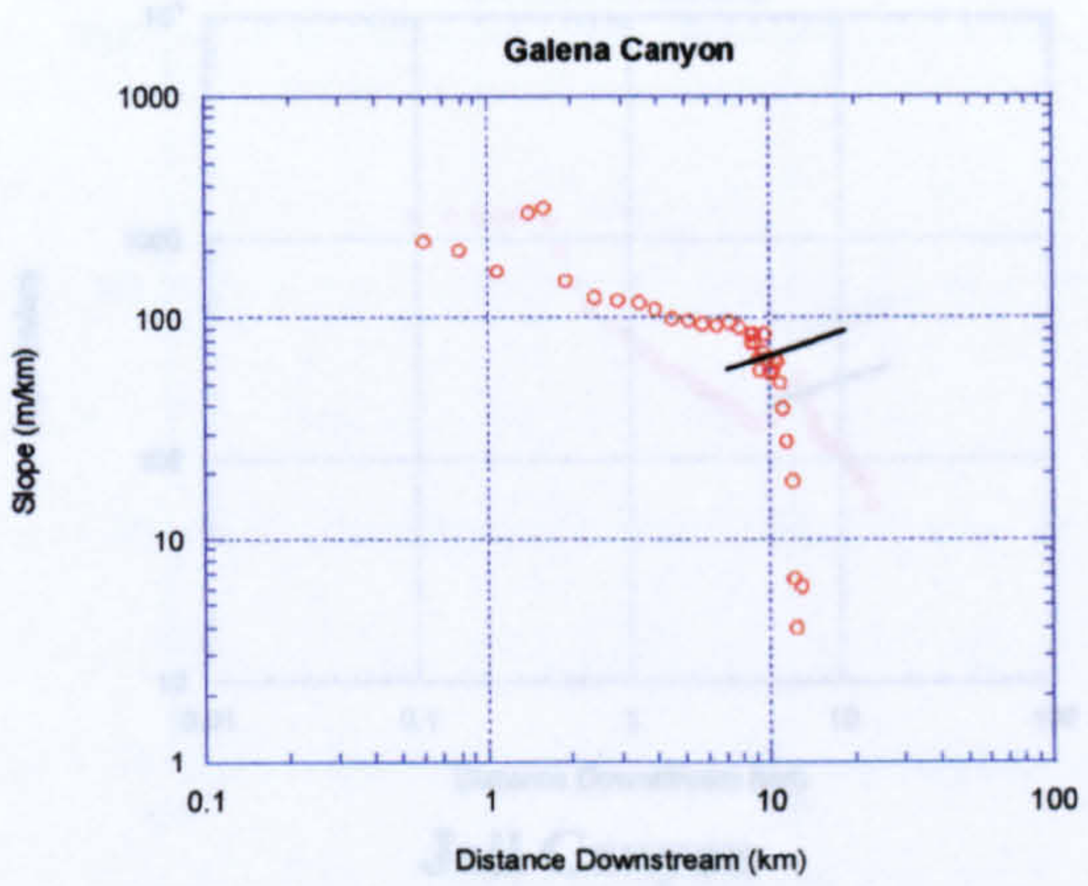

Galena Canyon

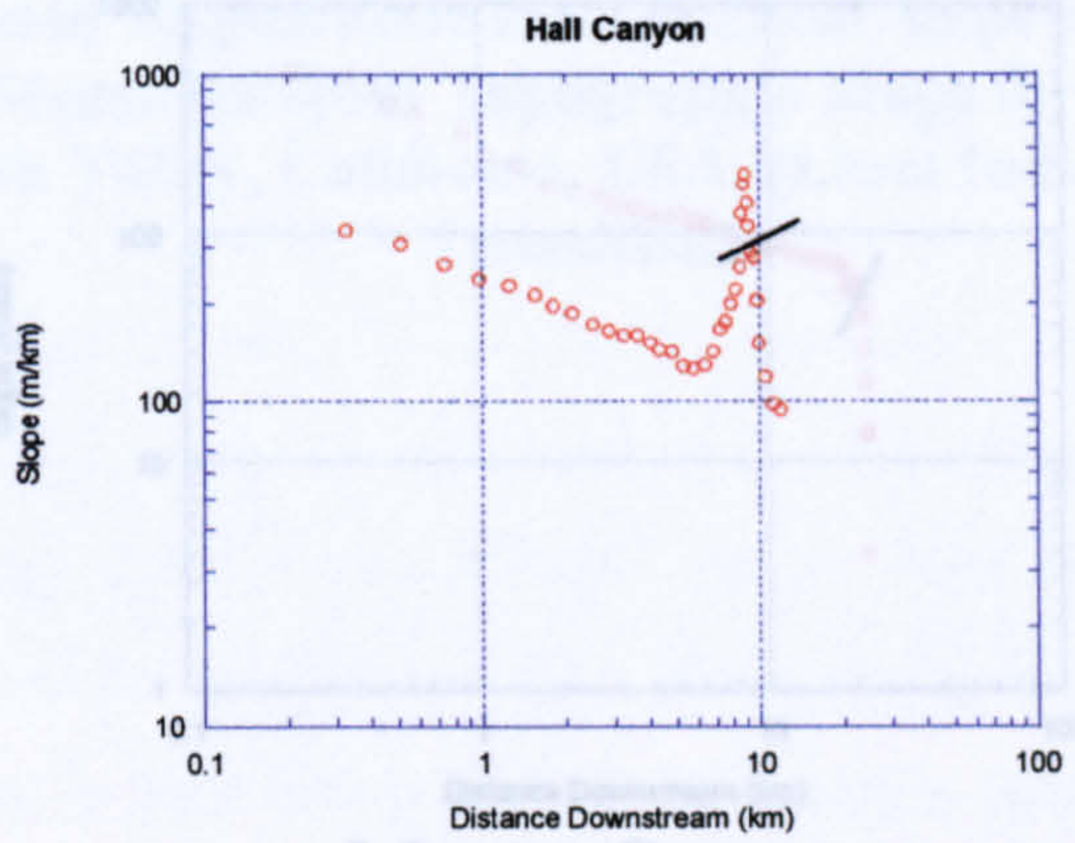

Hall Canyon

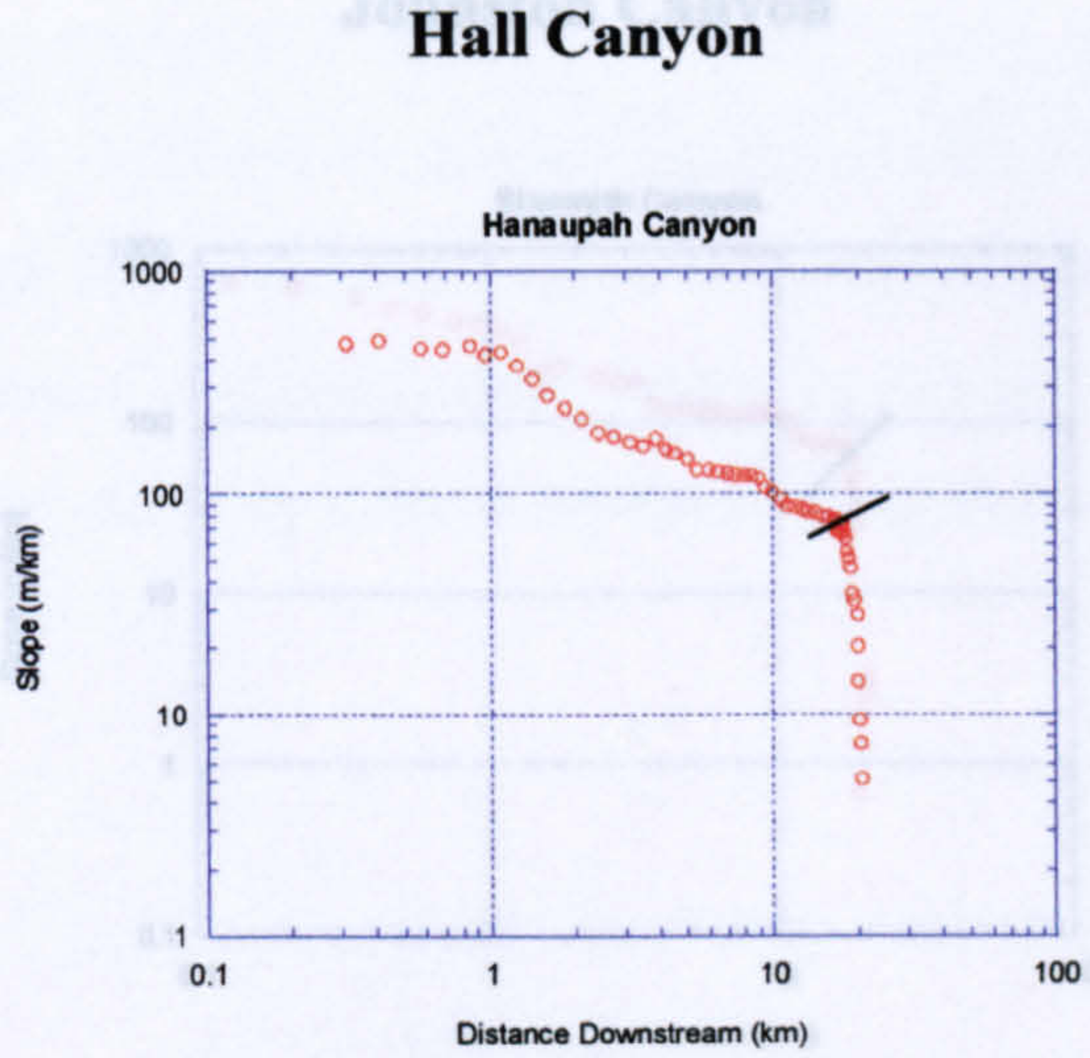

Hanaupah Canyon

Figure 2.16 Logarithmic Plots of Local Slope Against Distance from Drainage Divide Measured from Topographic Maps for Rivers Draining the Western Side of Death Valley, California, USA. (Lines Indicate Erosion/Deposition Transition)

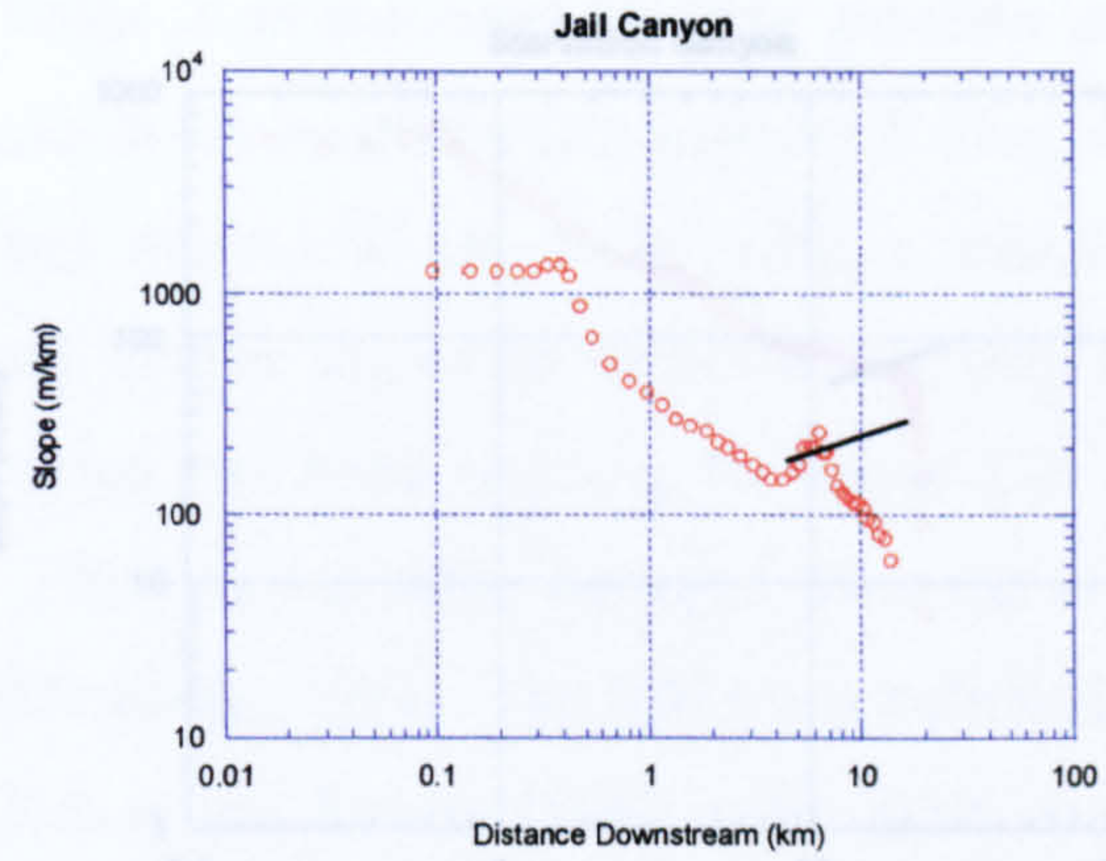

Jail Canyon

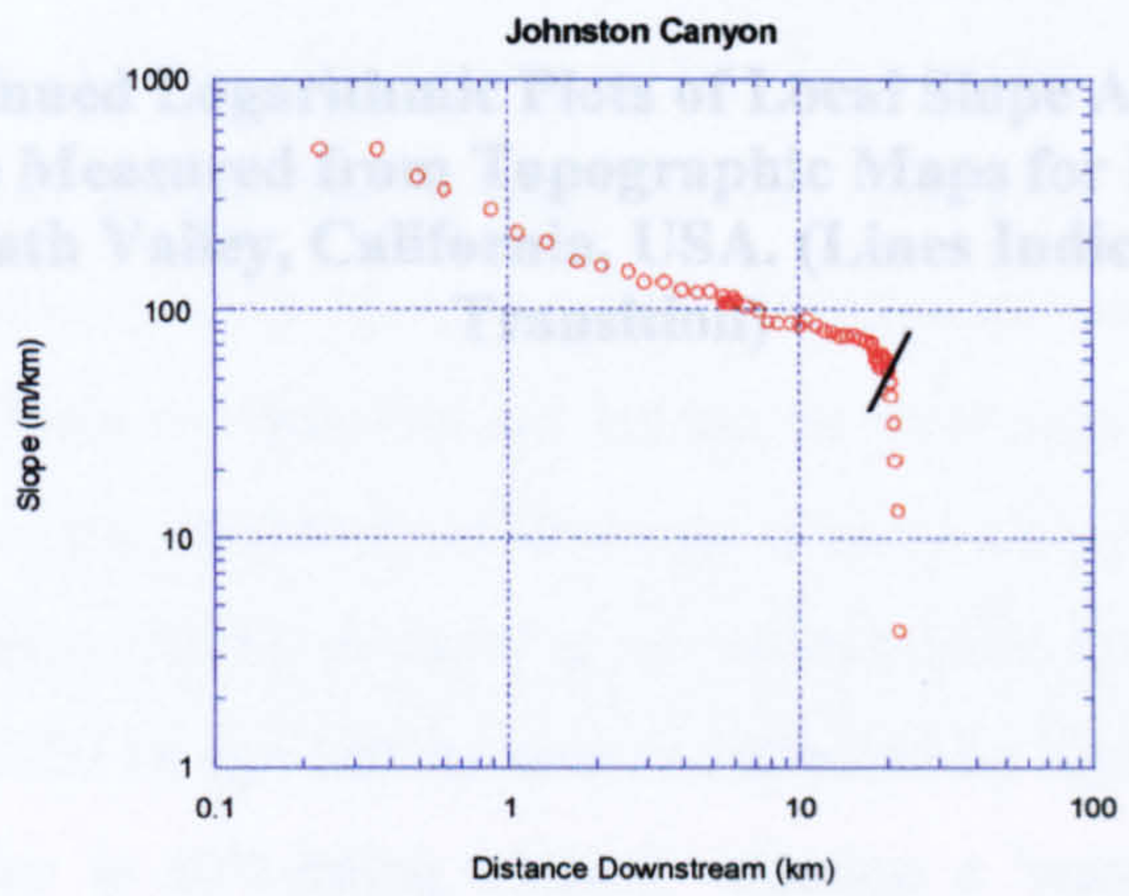

Johnston Canyon

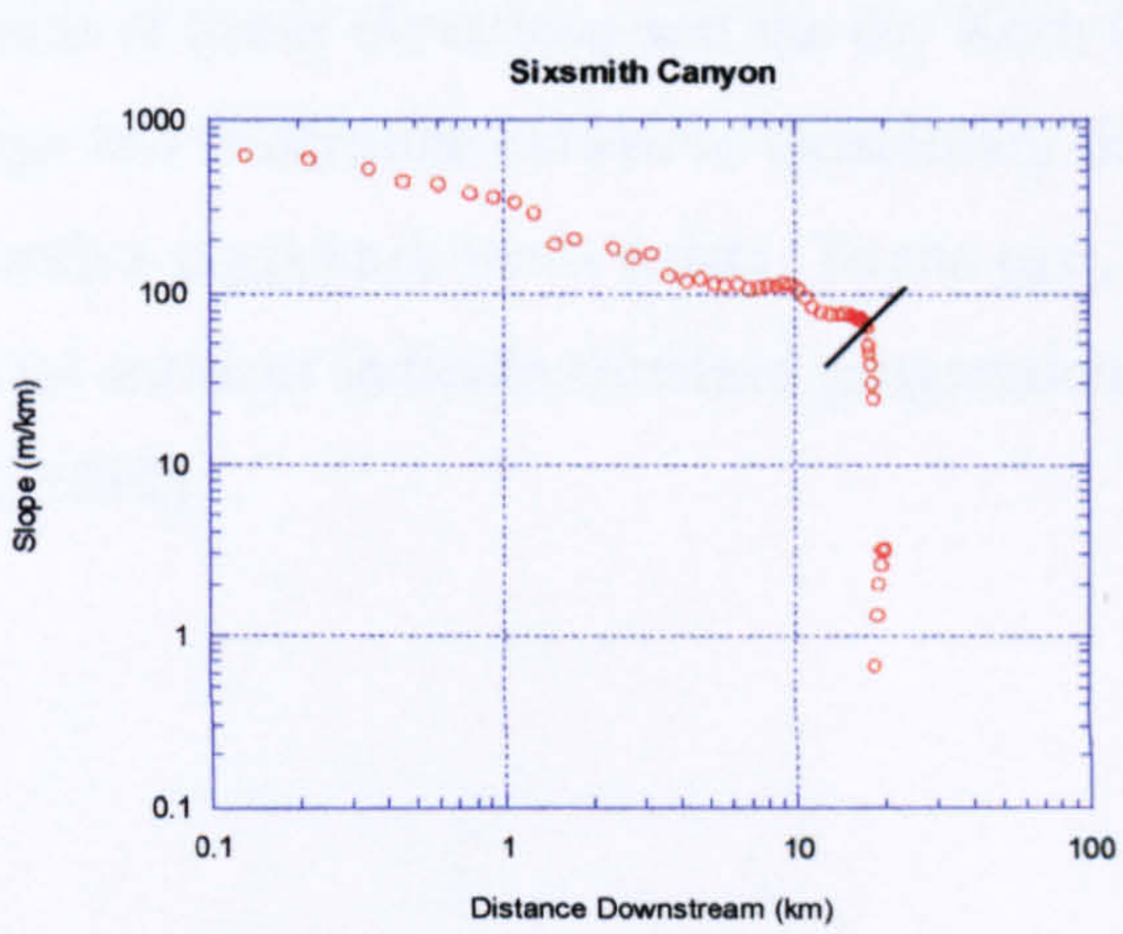

Sixspring Canyon

Figure 2.16 Continued Logarithmic Plots of Local Slope Against Distance from Drainage Divide Measured from Topographic Maps for Rivers Draining the Western Side of Death Valley, California, USA. (Lines Indicate Erosion/Deposition Transition)

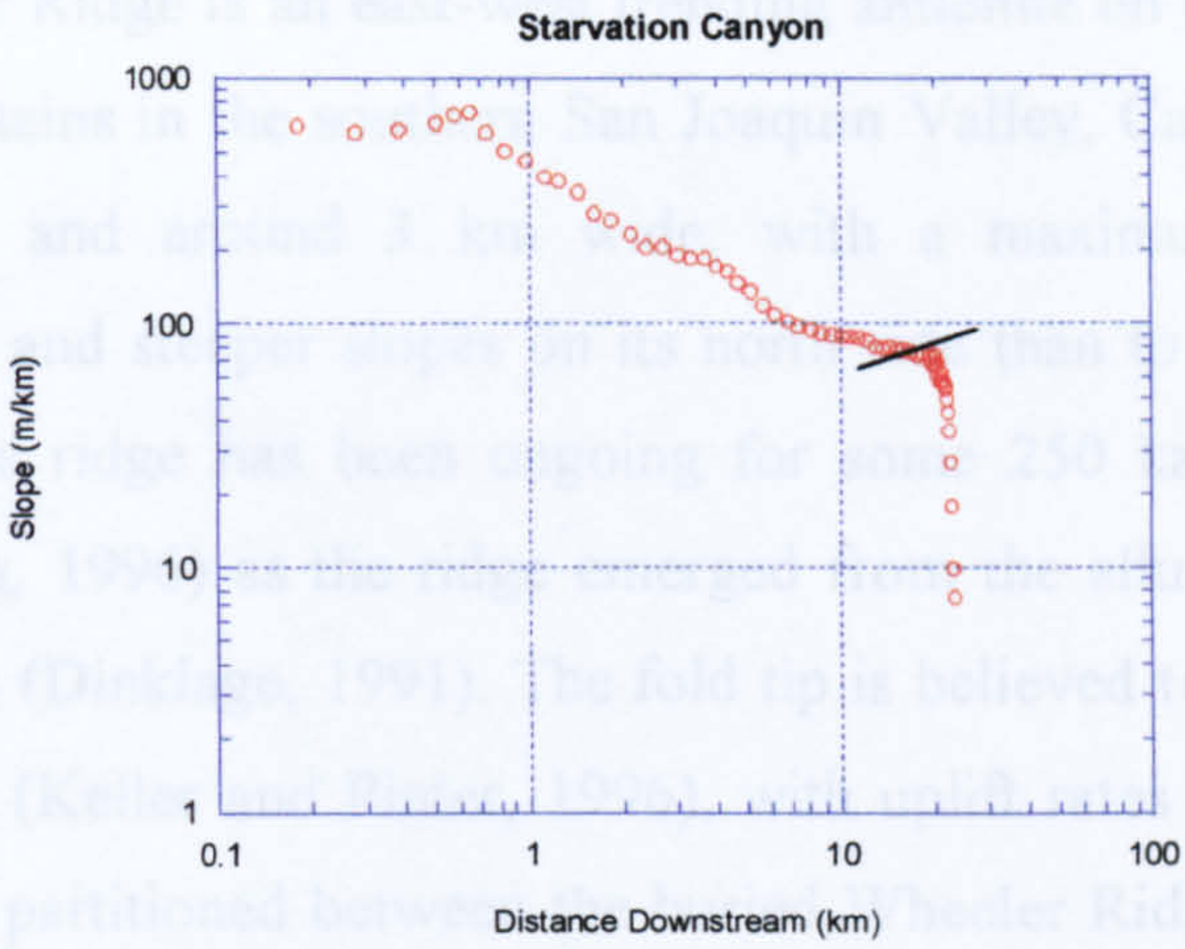

Starvation Canyon

Figure 2.16 Continued Logarithmic Plots of Local Slope Against Distance from Drainage Divide Measured from Topographic Maps for Rivers Draining the Western Side of Death Valley, California, USA. (Lines Indicate Erosion/Deposition Transition)

2.4.3 Wheeler Ridge, California, U.S.A.

The Wheeler Ridge is an east-west trending anticline on the north flank of the San Emigdio Mountains in the southern San Joaquin Valley, California. The ridge is some 10 km long and around 3 km wide, with a maximum relief of 500 m (Medwedeff, 1992) and steeper slopes on its north side than to the south (Dinklage, 1991). Uplift of the ridge has been ongoing for some 250 ka (Medwedeff, 1992; Mueller and Talling, 1996) as the ridge emerged from the alluvial plain of the San Emidgio Mountains (Dinklage, 1991). The fold tip is believed to be propagating east at around 29 mm/a (Keller and Pinter, 1996), with uplift rates of around 3.2 mm/a. Tectonic activity is partitioned between the buried Wheeler Ridge Fault on the north side of the anticline, and the Pleito Fault to the south (Figure 2.17), where uplift rates are around 0.5 mm/a (Keller and Pinter, 1996). In contrast to the buried Wheeler Fault, the Pleito Fault breaks the surface to the south of Wheeler Ridge. Well constrained differences in uplift rates and fault propagation along the ridge make it ideal to study the effects of tectonics on landscape evolution and morphology, for example by looking at the evolution of drainage density along the fault (Talling and Sowter, 1999; Dinklage, 1991). A number of valleys have eroded into the ridge; a 'wind gap' of some 30-60 ka age had its stream deflected by high uplift rates, whilst to the east a deep valley is still being incised, creating a 'water gap'. The area has relatively low rainfall (around 150 mm)(Keller *et al.*, 1998), with ephemeral streams flowing into alluvial fans at lower elevations and the dry Kern County Lake. The area to the north of the ridge has undergone extensive Quaternary deposition (Medwedeff, 1992), whilst to the south a piggyback basin exists. To the east, uplifted Holocene and Late Pleistocene alluvial surfaces indicate eastward progression of the Wheeler Ridge anticline (Medwedeff, 1992).

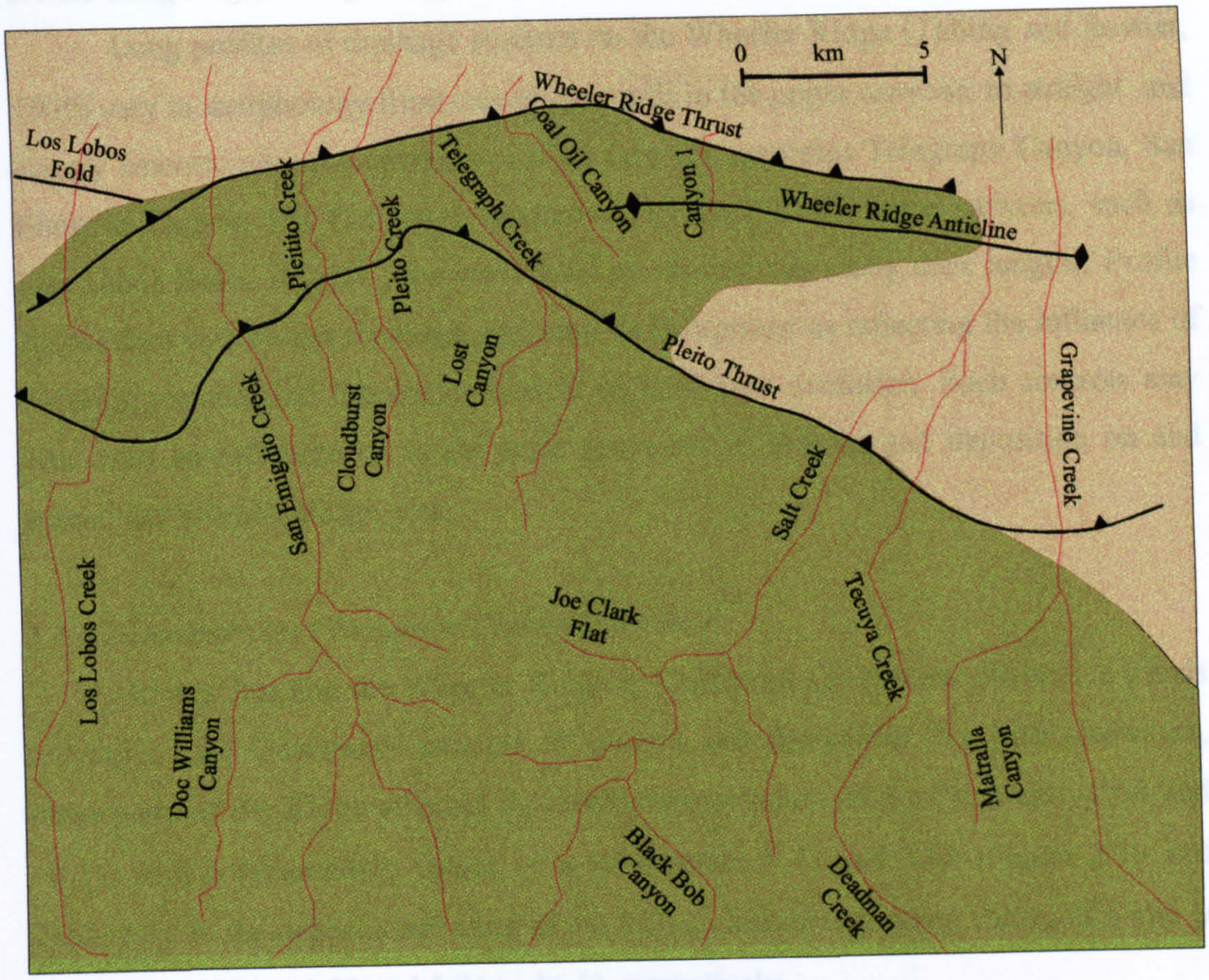

Figure 2.17 Location Map, Wheeler Ridge, California

2.4.3.1 Long Profile Morphology

Long profiles of drainage systems on the Wheeler Ridge (Talling and Sowter, 1999) vary in morphology from convex-upwards in the upper canyons, to straight and largely smooth, concave upwards profiles (see for examples Telegraph Canyon, San Emigdio Canyon and Canyon 1 respectively)(Figure 2.18). Some canyons, such as Los Lobos Basin, display prominent knickpoints midway along their lengths. Profile shapes thus vary across the ridge, and may be interpreted as reflecting the influence of differing tectonic and lithologic controls on landscape evolution. Such controls may also exert an influence on larger scale processes of erosion and deposition on and around the Wheeler Ridge area.

2.4.3.2 Downstream Changes in Channel Gradient

Rivers draining the Wheeler Ridge in California again show distinctive trends reflecting Late Quaternary patterns of erosion and deposition. As with elsewhere, those parts of the Ridge affected by erosion show values of ϕ of between -0.65 and +0.21, with corresponding values of ψ of between 3.73 and 5.64 (Figure 2.19 and Table 2.4). In the depositional parts of the Ridge, the corresponding values of ϕ and ψ vary from -4.38 to -1.33 and 5.94 to 16.51 respectively.

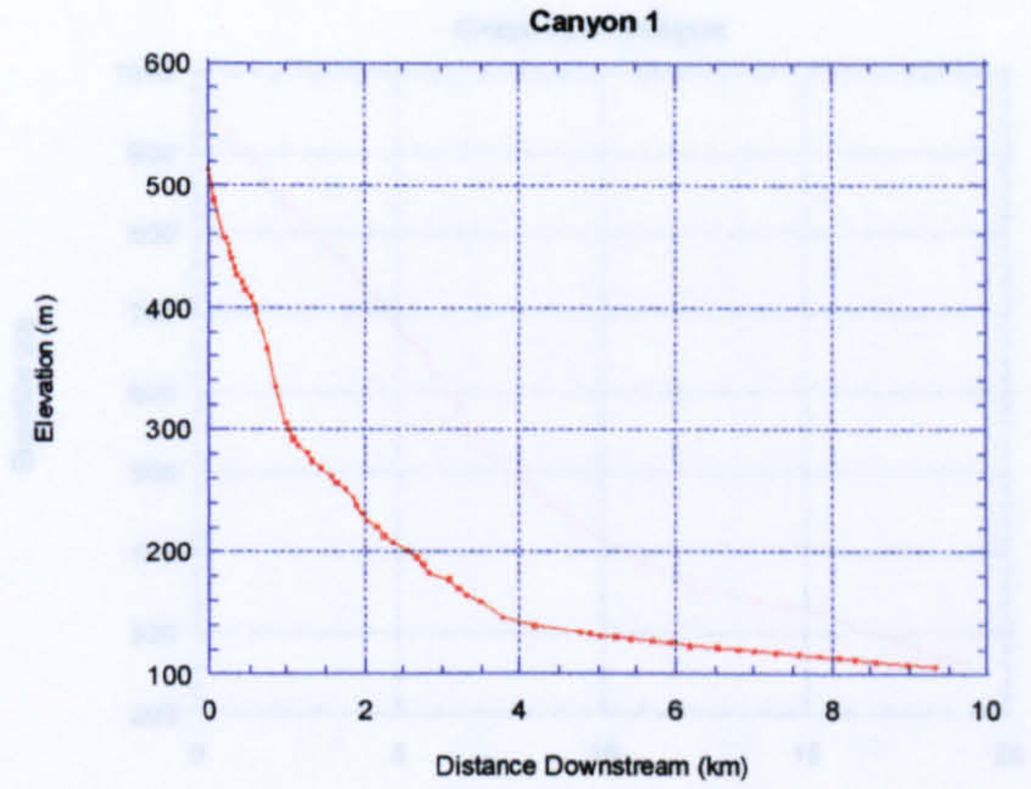

Canyon 1

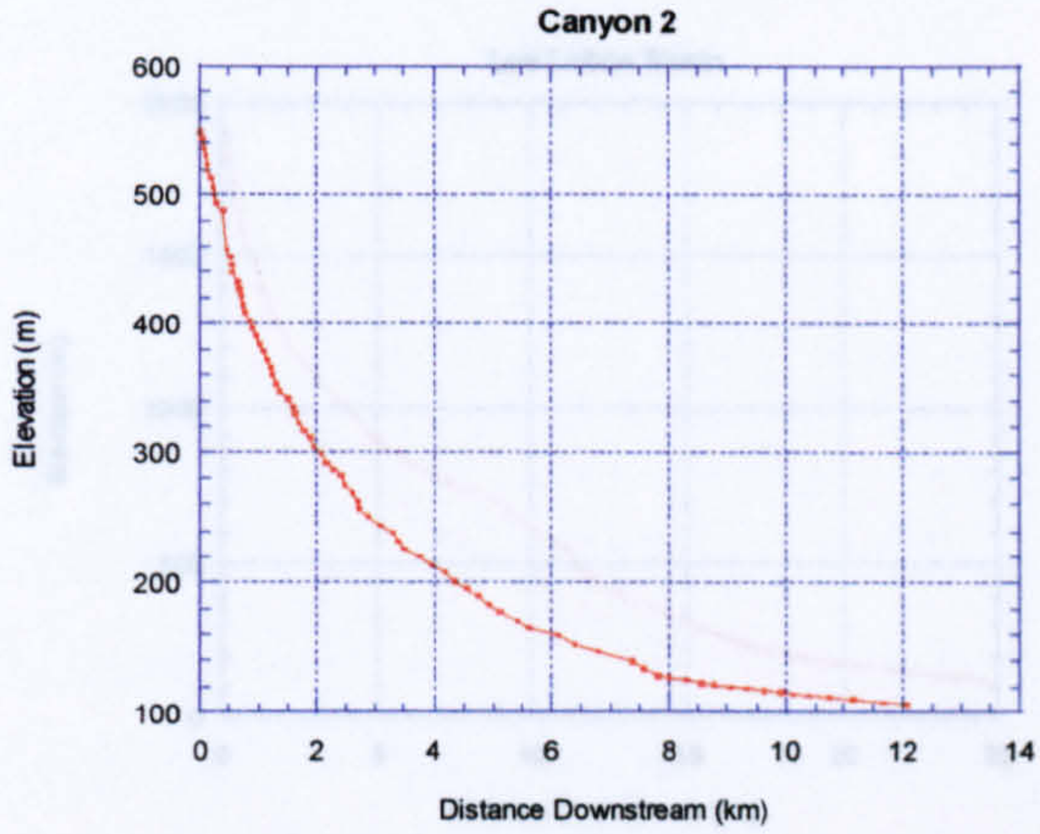

Canyon 2

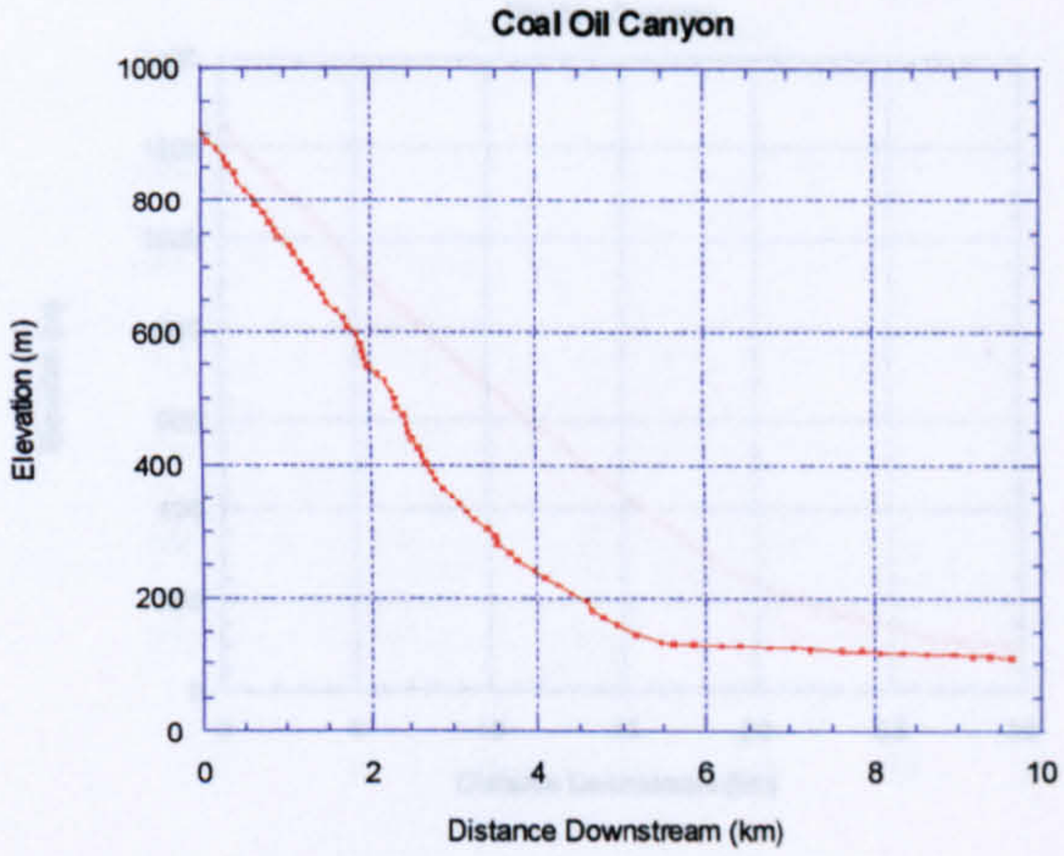

Coal Oil Canyon

Figure 2.18 Longitudinal River Profiles, Wheeler Ridge, California, USA

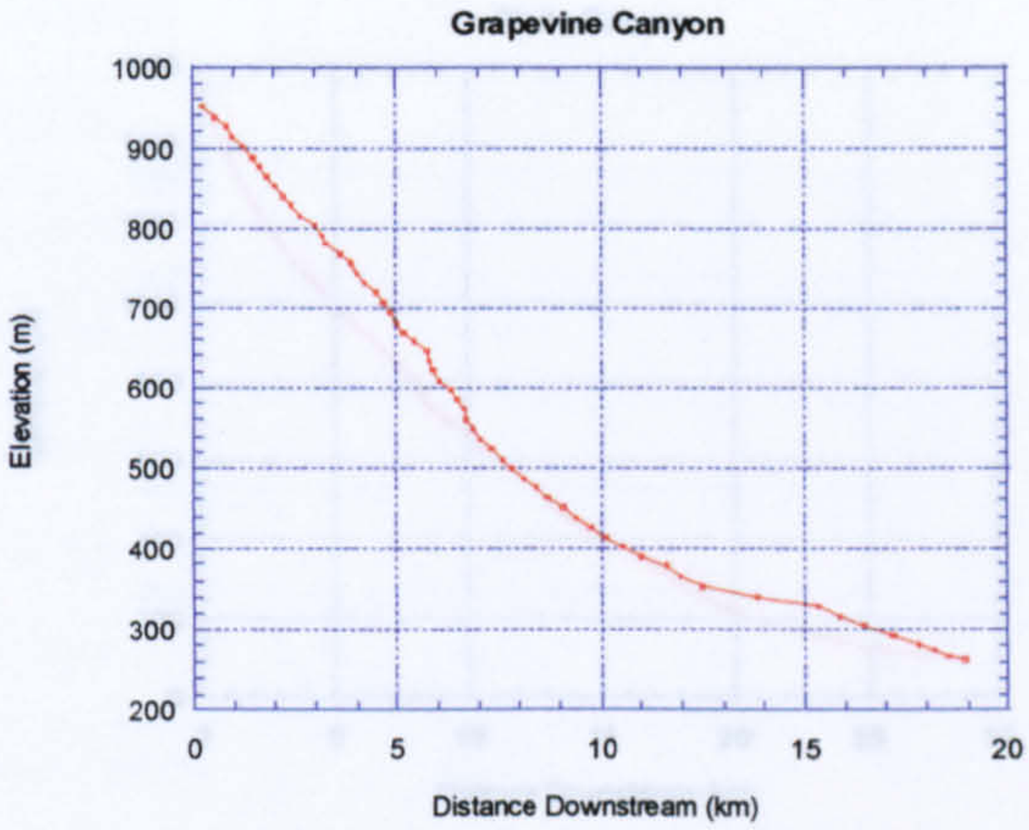

Grapevine Canyon

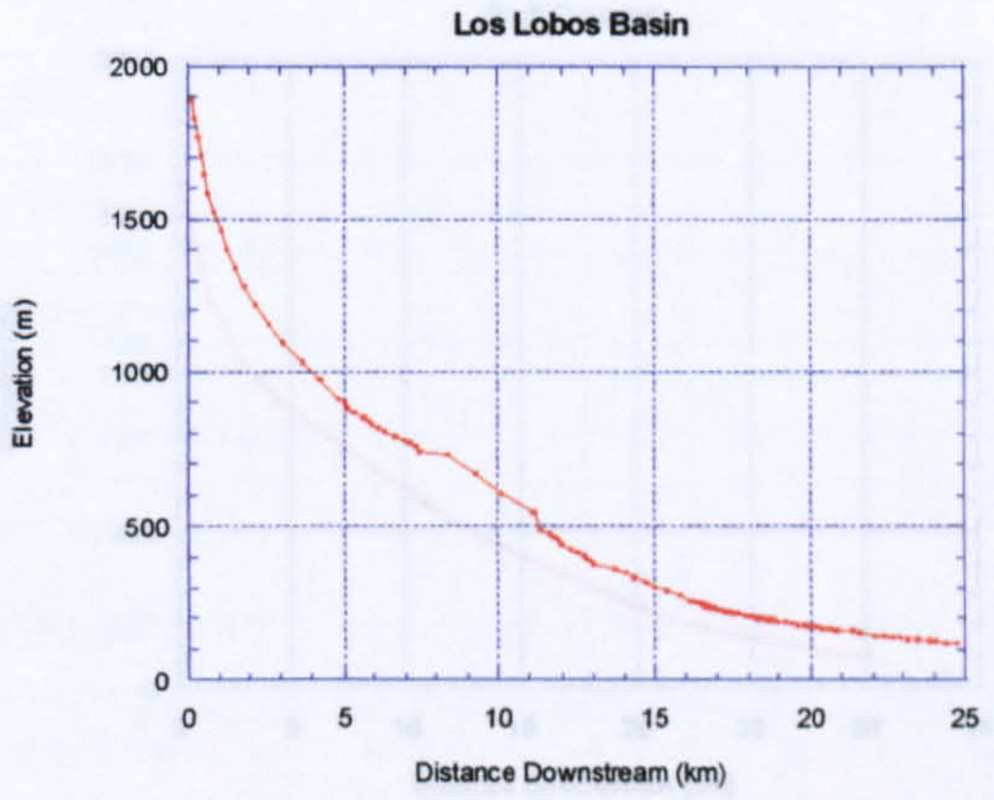

Los Lobos Basin

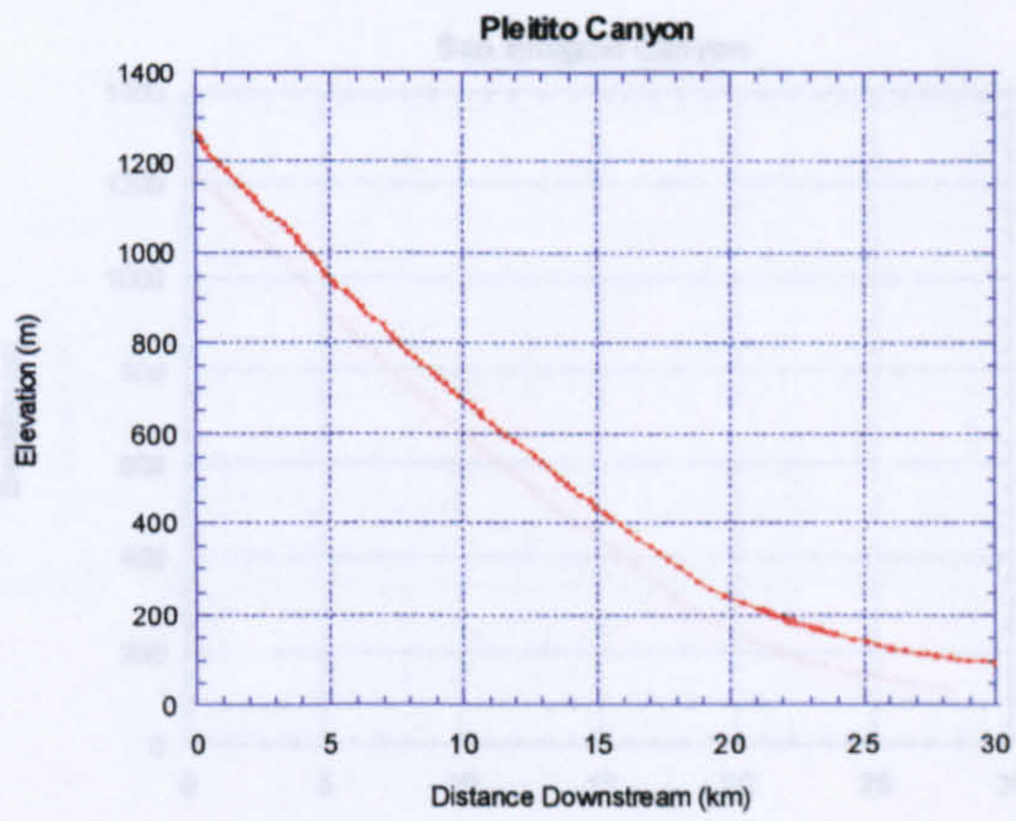

Pleitito Canyon

Figure 2.18 Continued Longitudinal River Profiles, Wheeler Ridge, California, USA

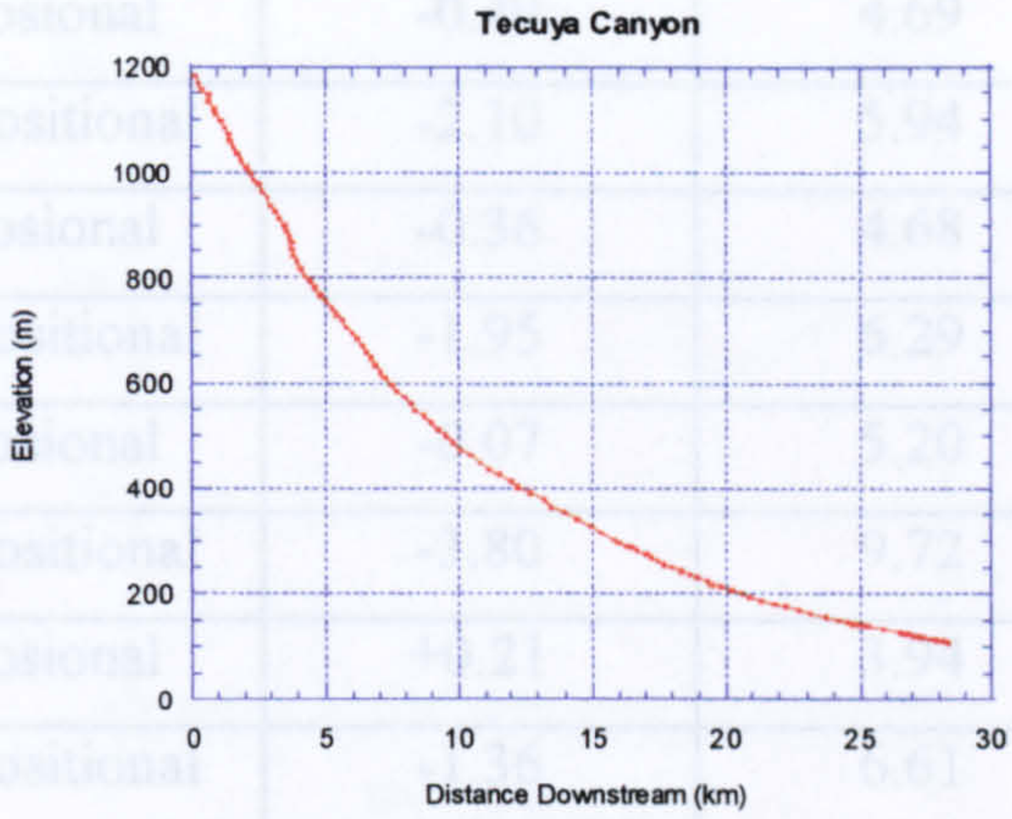

Tecuya Canyon

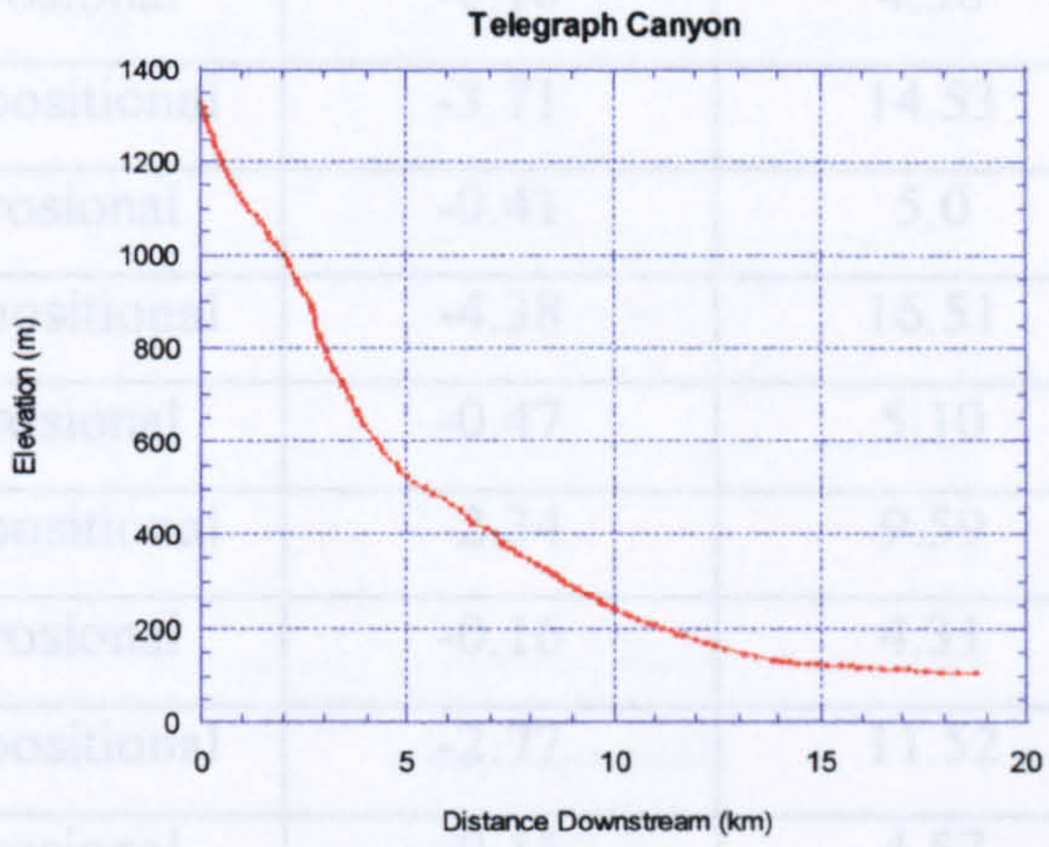

Telegraph Canyon

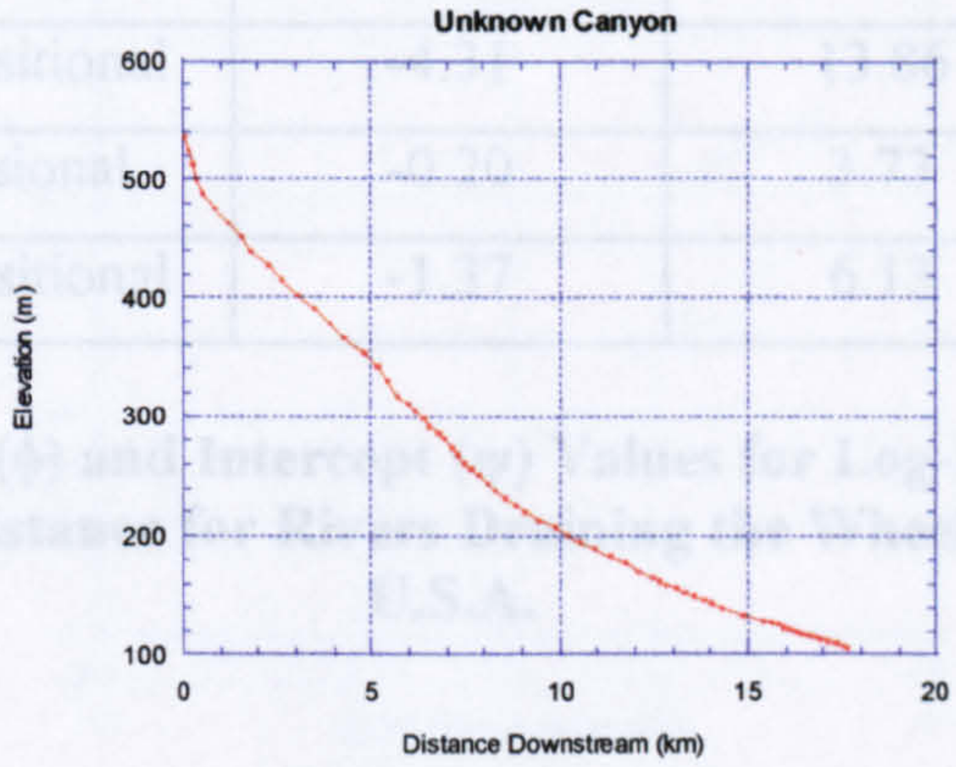

Unknown Canyon

Figure 2.18 Continued Longitudinal River Profiles, Wheeler Ridge, California, USA

Basin	Regime	Gradient	Intercept	r^2
Canyon 1	Erosional	-0.49	4.69	0.46
	Depositional	-2.10	5.94	0.89
Canyon 2	Erosional	-0.36	4.68	0.35
	Depositional	-1.95	6.29	0.80
Coal Oil	Erosional	-0.07	5.20	0.01
	Depositional	-3.80	9.72	0.61
Grapevine	Erosional	+0.21	3.94	0.09
	Depositional	-1.36	6.61	0.72
Los Lobos	Erosional	-0.65	5.64	0.65
	Depositional	-3.38	12.91	0.81
Pleitito	Erosional	-0.16	4.30	0.31
	Depositional	-3.71	14.53	0.87
Pleito	Erosional	-0.41	5.0	0.60
	Depositional	-4.38	16.51	0.91
Salt	Erosional	-0.47	5.10	0.55
	Depositional	-2.34	9.59	0.48
San Emigdio	Erosional	-0.16	4.31	0.30
	Depositional	-2.77	11.52	0.81
Tecuya	Erosional	-0.11	4.57	0.04
	Depositional	-1.33	6.82	0.85
Telegraph	Erosional	-0.40	5.23	0.55
	Depositional	-4.31	13.86	0.88
Unknown	Erosional	-0.20	3.73	0.25
	Depositional	-1.37	6.13	0.88

Table 2.4 Gradient (ϕ) and Intercept (ψ) Values for Log-Log Plots of Slope Versus Downstream Distance for Rivers Draining the Wheeler Ridge, California, U.S.A.

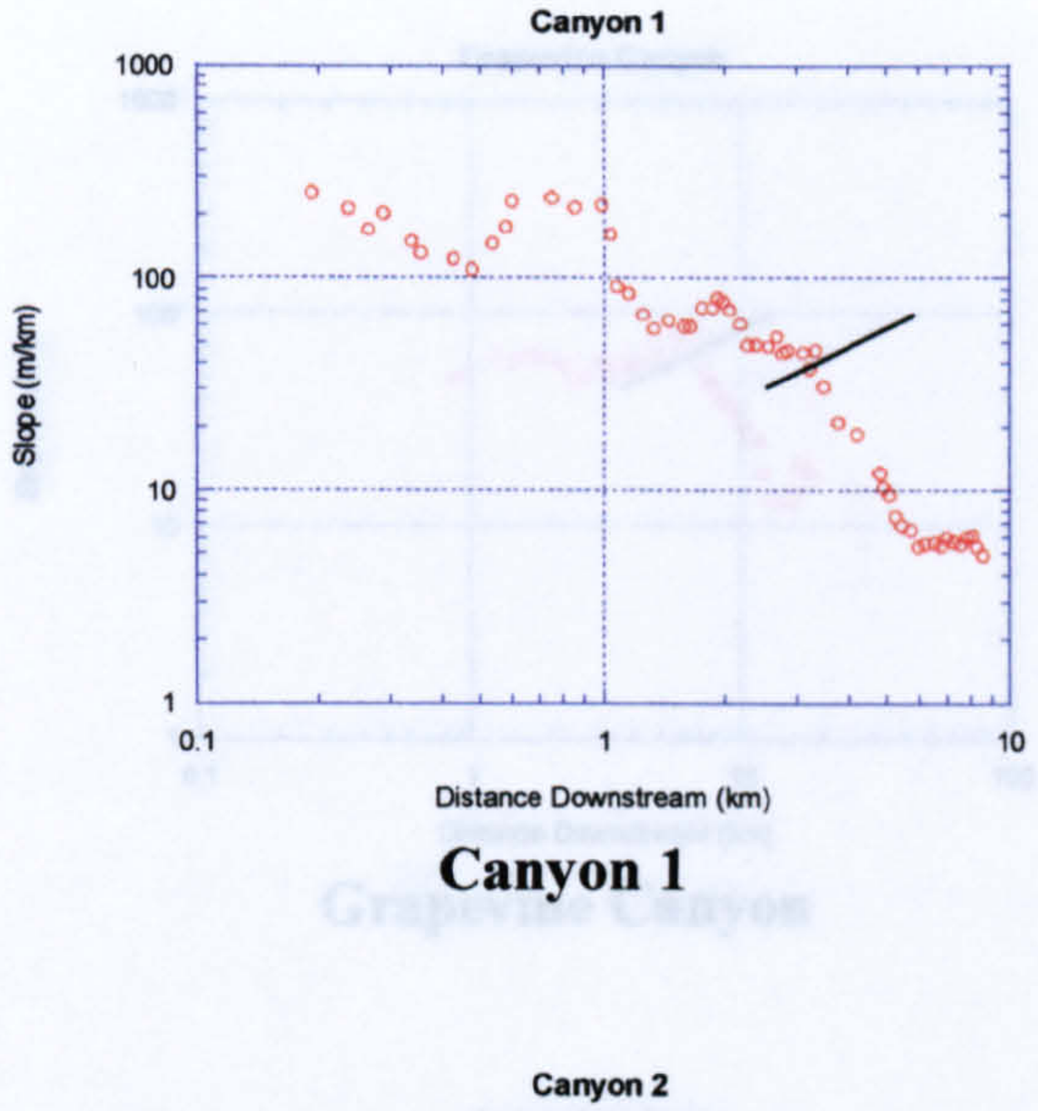

Canyon 1

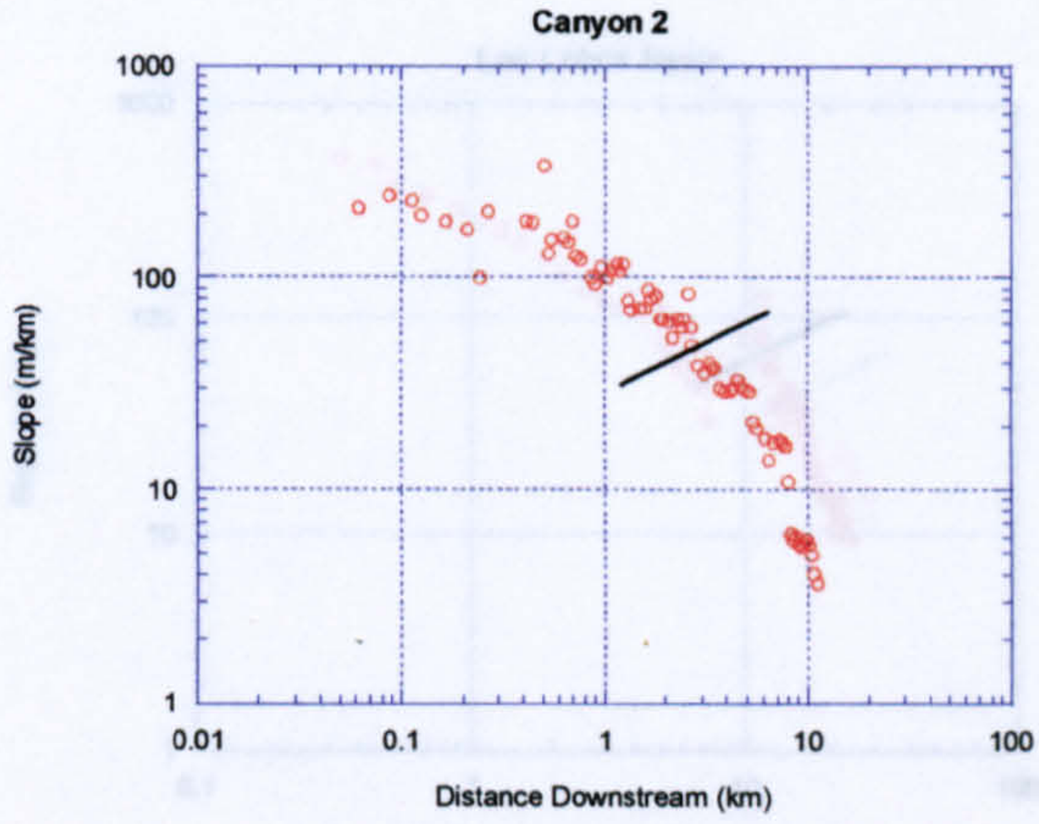

Canyon 2

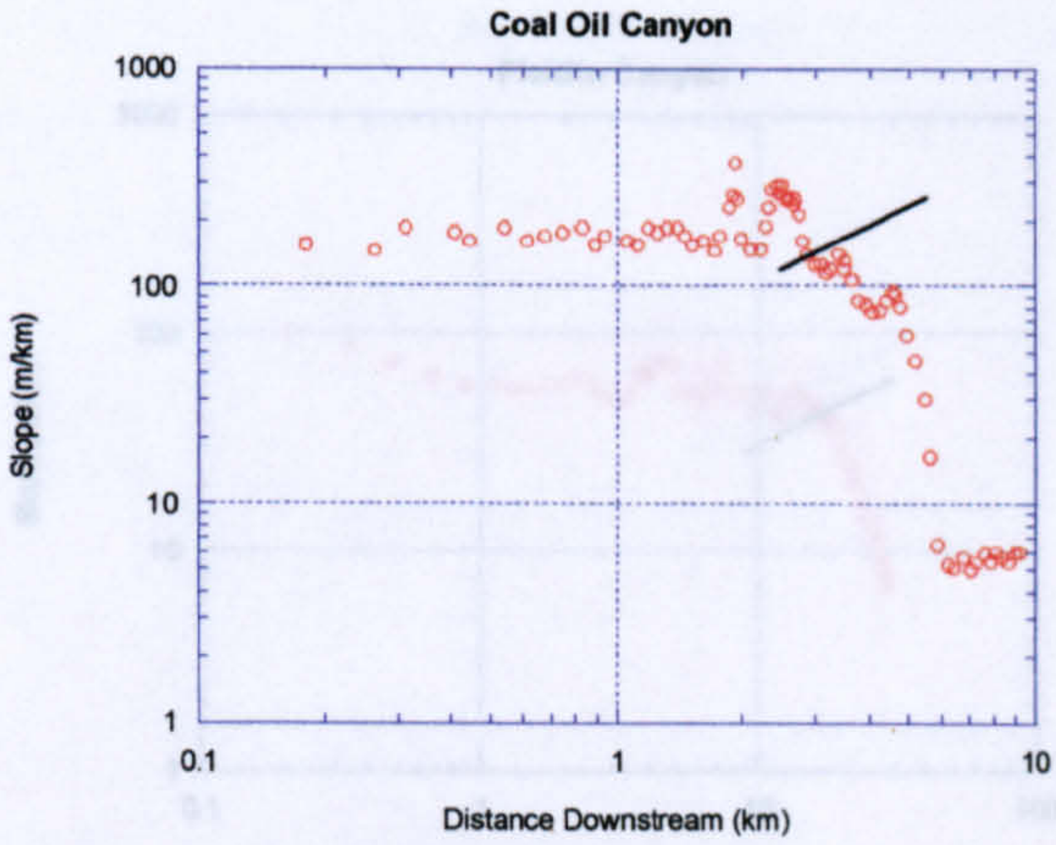

Coal Oil Canyon

Figure 2.19 Logarithmic Plots of Local Slope Against Distance from Drainage Divide Measured from Topographic Maps for Rivers Draining the Wheeler Ridge, California, USA (Lines Indicate Erosion/Deposition Transition)

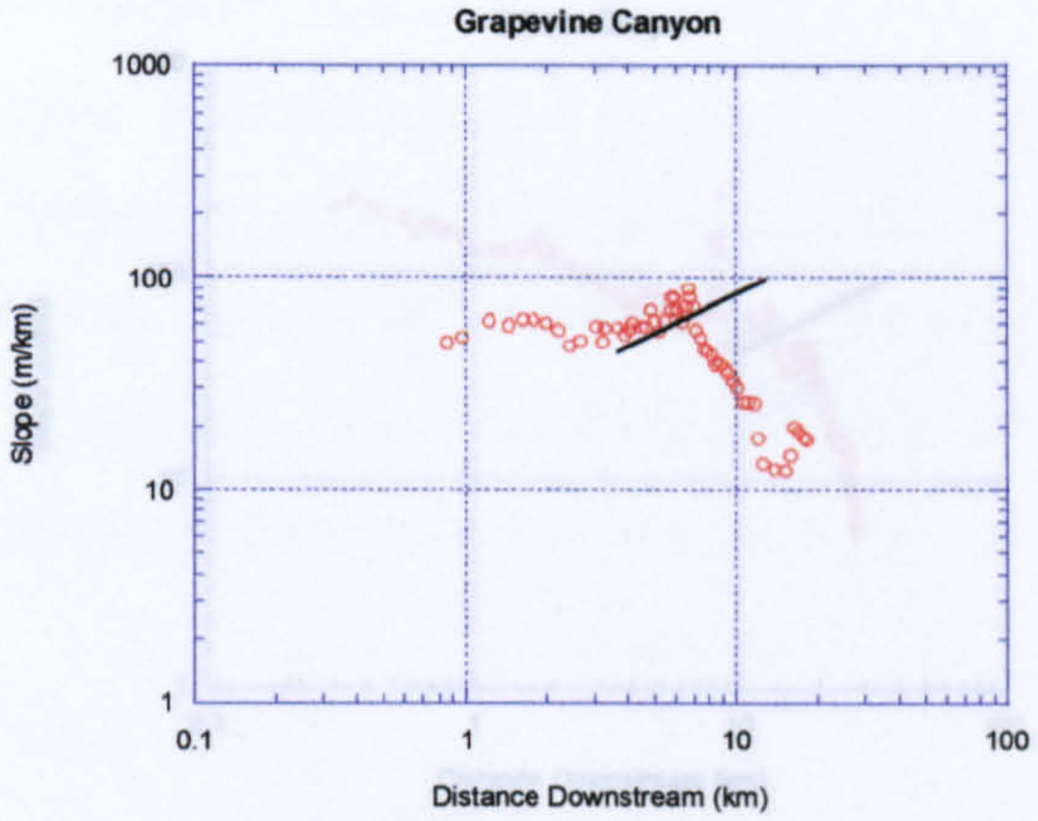

Grapevine Canyon

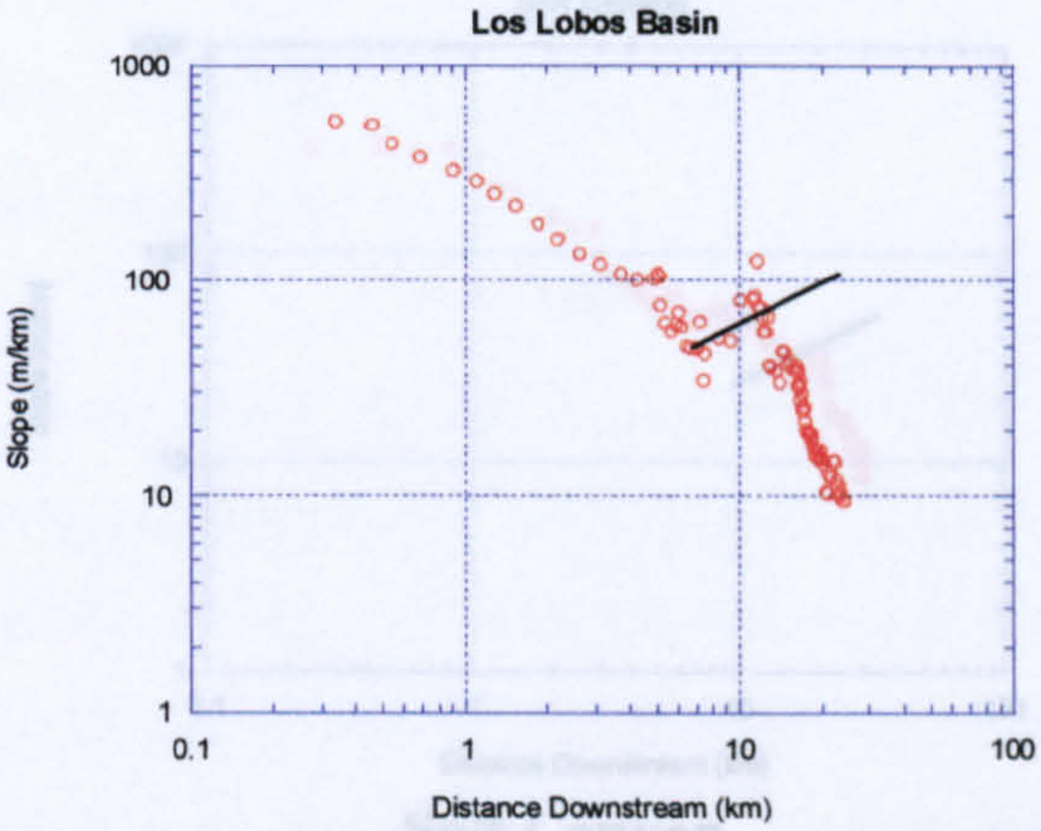

Los Lobos Basin

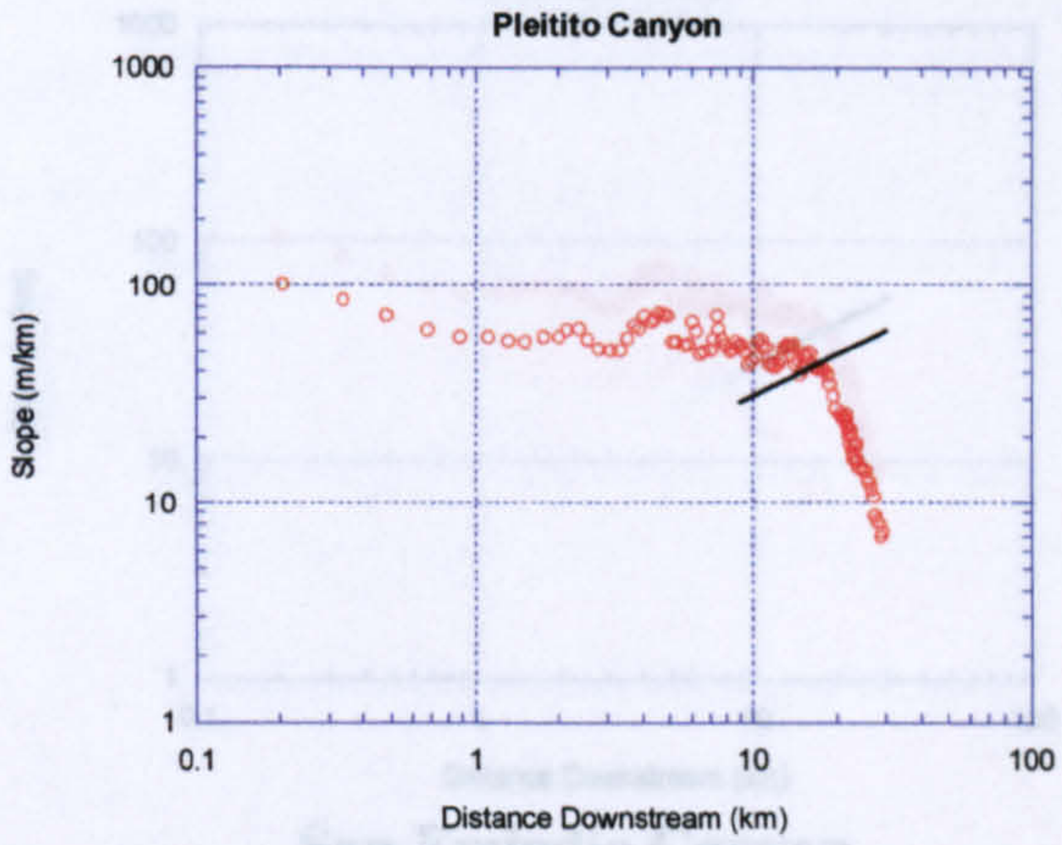

Pleitito Canyon

Figure 2.19 Continued Logarithmic Plots of Local Slope Against Distance from Drainage Divide Measured from Topographic Maps for Rivers Draining the Wheeler Ridge, California, USA (Lines Indicate Erosion/Deposition Transition)

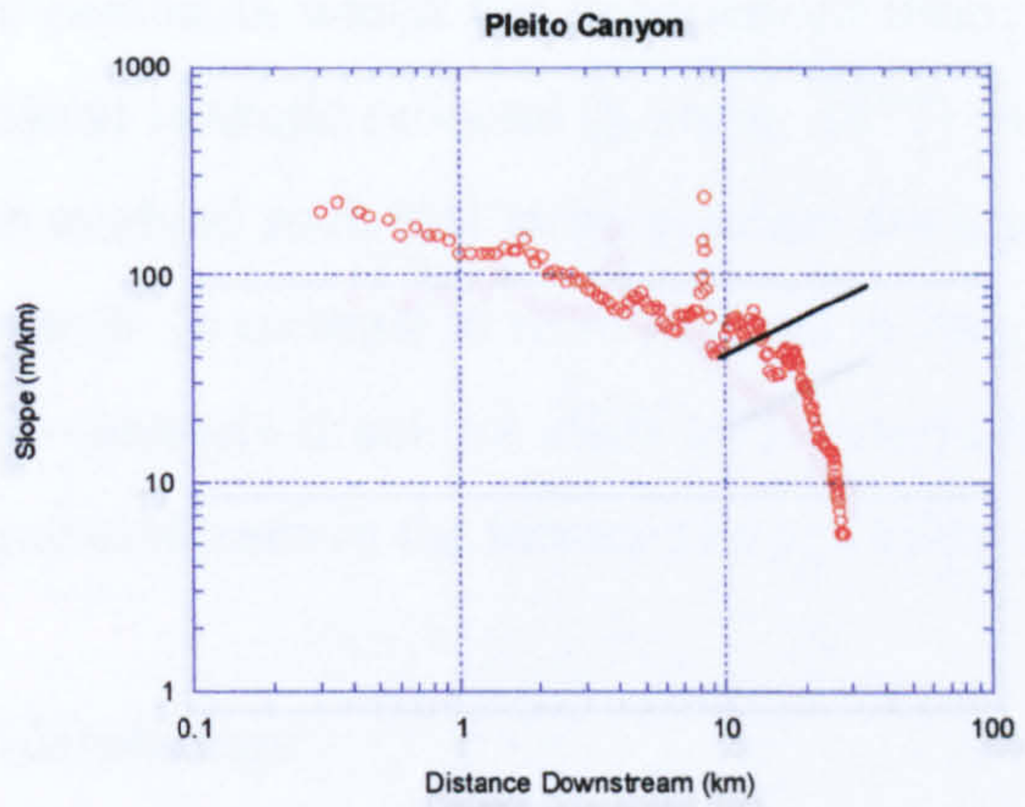

Pleito Canyon

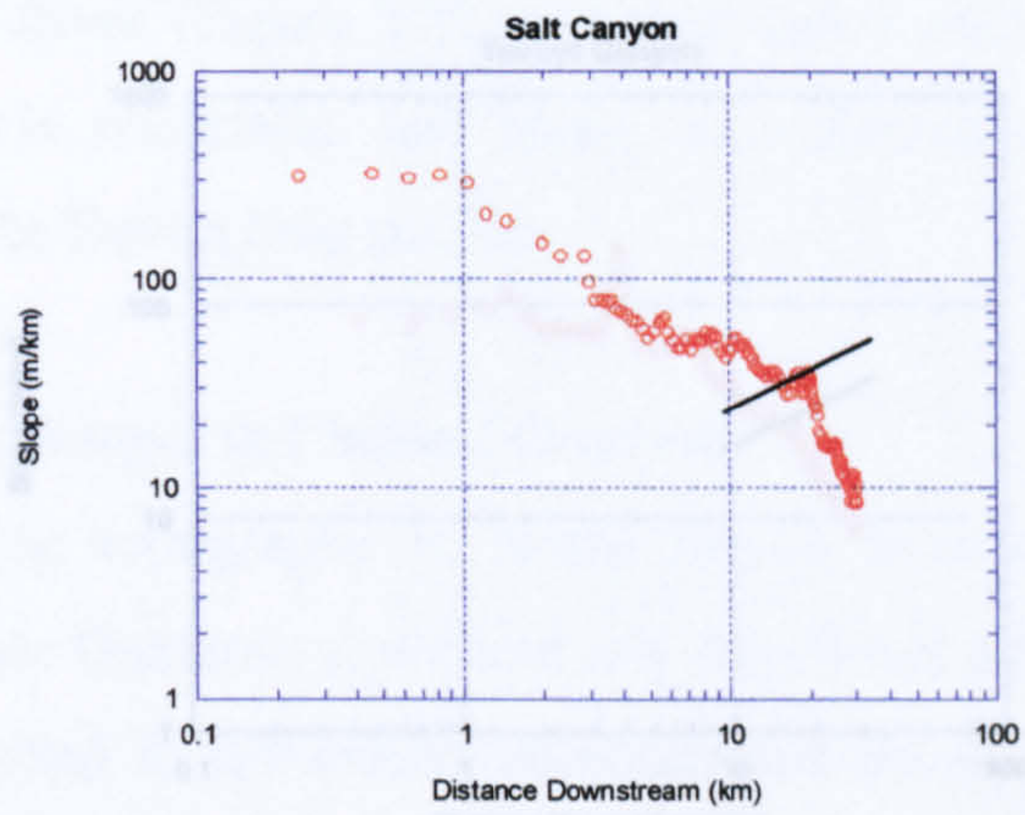

Salt Canyon

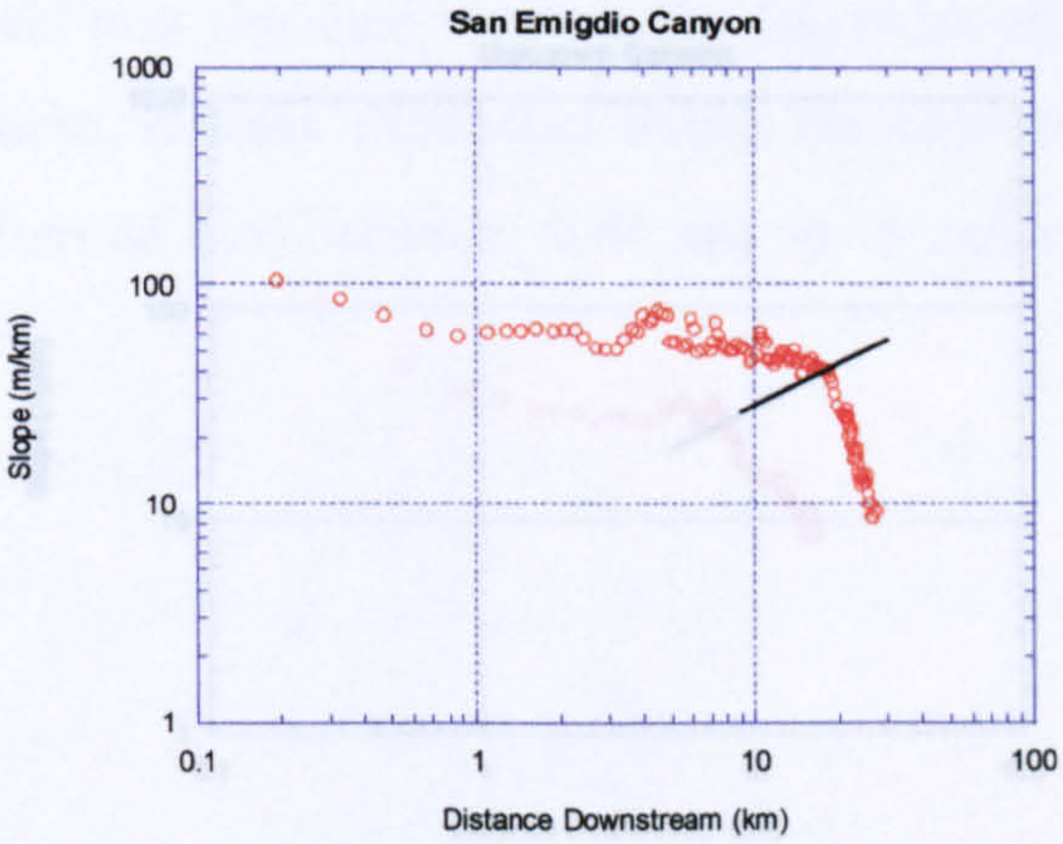

San Emigdio Canyon

Figure 2.19 Continued Logarithmic Plots of Local Slope Against Distance from Drainage Divide Measured from Topographic Maps for Rivers Draining the Wheeler Ridge, California, USA (Lines Indicate Erosion/Deposition Transition)

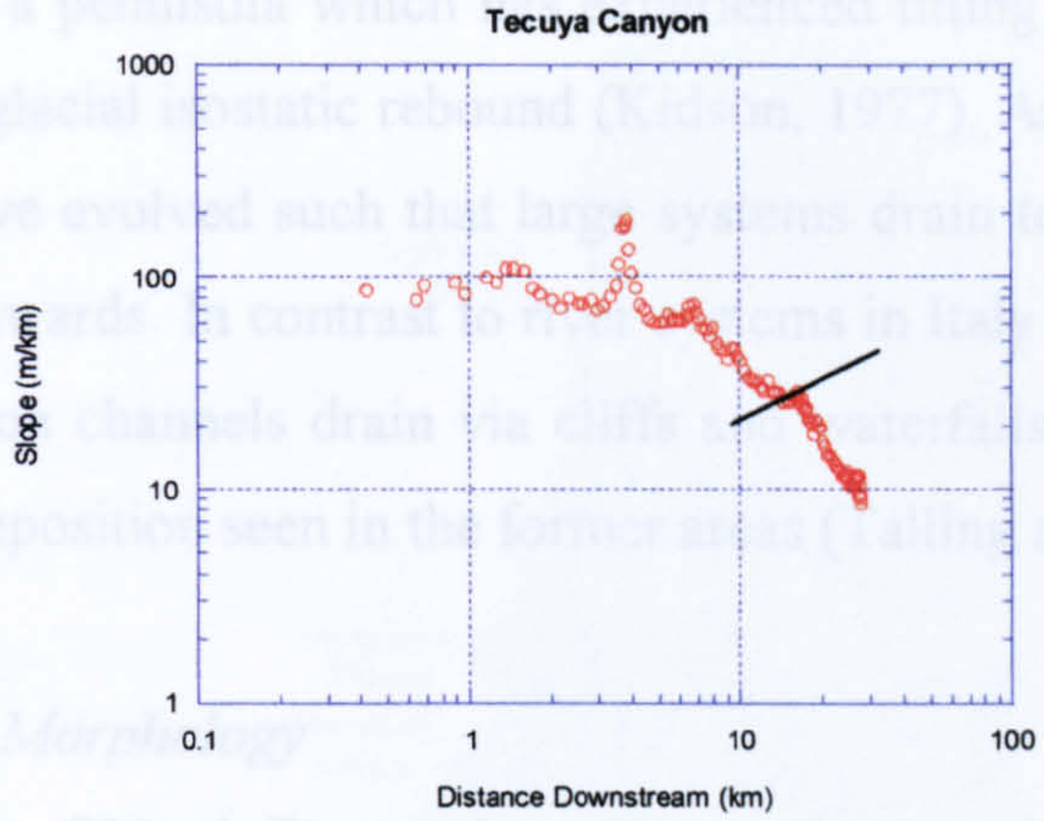

Tecuya Canyon

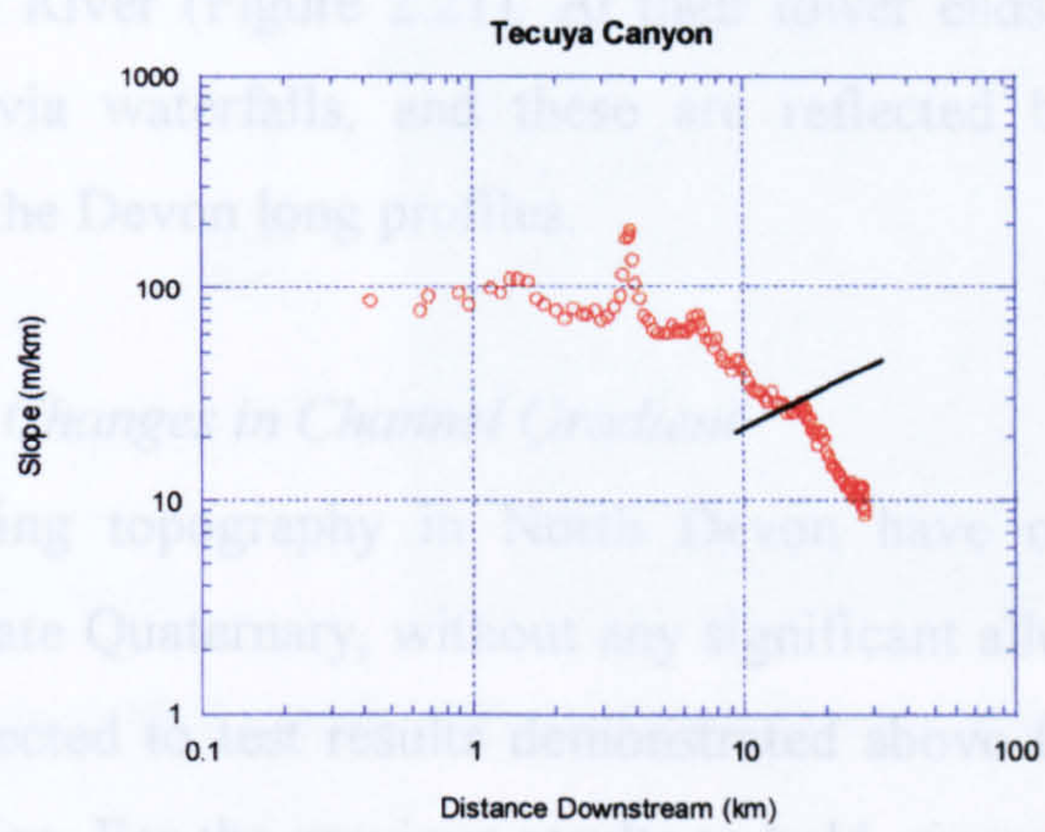

Telegraph Canyon

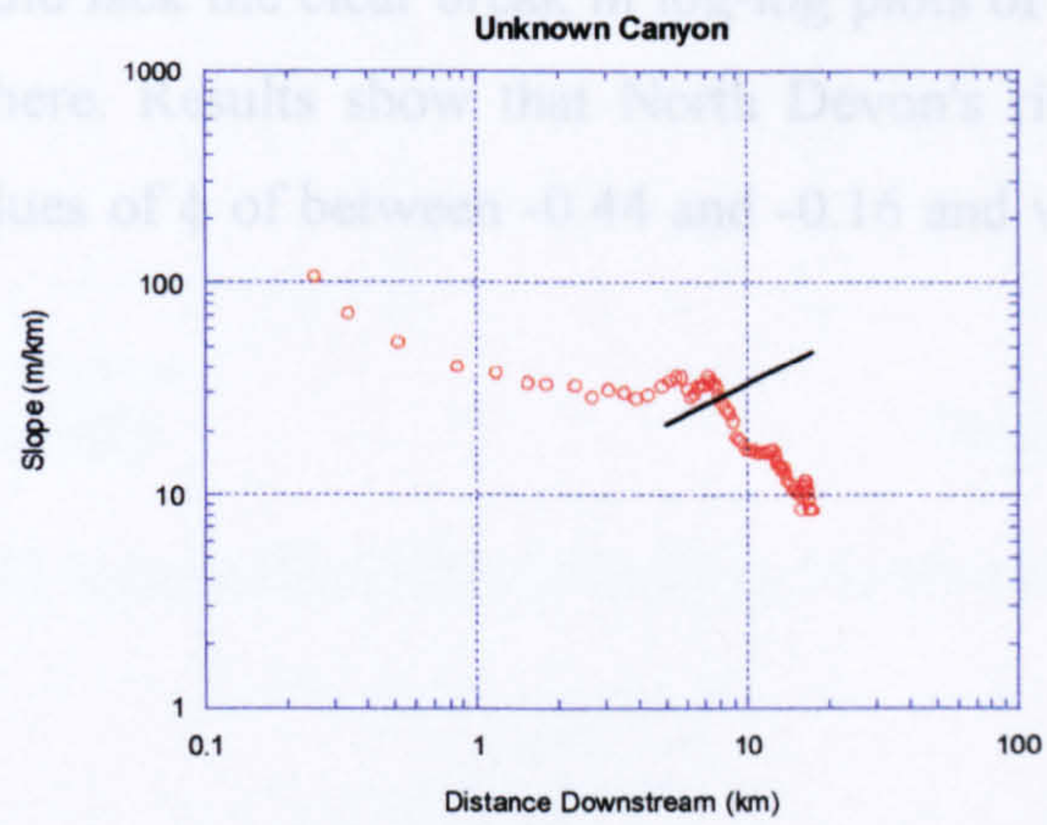

Unknown Canyon

Figure 2.19 Continued Logarithmic Plots of Local Slope Against Distance from Drainage Divide Measured from Topographic Maps for Rivers Draining the Wheeler Ridge, California, USA (Lines Indicate Erosion/Deposition Transition)

2.4.4 South-Western Britain

Profiles selected for study in North Devon in south-western England (Figure 2.20) are located on a peninsula which has experienced tilting during the Quaternary resulting from post-glacial isostatic rebound (Kidson, 1977). As a consequence of this tilting, drainages have evolved such that large systems drain to the south and shorter drainages flow northwards. In contrast to river systems in Italy and the U.S.A. studied here, the North Devon channels drain via cliffs and waterfalls into the sea, and lack areas of long term deposition seen in the former areas (Talling and Sowter, 1998).

2.4.4.1 Long Profile Morphology

Long profiles of North Devon rivers demonstrate straight to slightly concave upwards morphologies, many with convex upwards knickpoints, for example Black Valley and Coombe River (Figure 2.21). At their lower ends, many of these rivers drain into the sea via waterfalls, and these are reflected by the vertical profile morphologies of all the Devon long profiles.

2.4.4.2 Downstream Changes in Channel Gradient

Rivers draining topography in North Devon have only been affected by erosion during the Late Quaternary, without any significant alluvial deposition. These rivers were thus selected to test results demonstrated above for Italy, Death Valley and the Wheeler Ridge. For the previous results to hold, rivers draining North Devon should demonstrate values for ϕ of between -1 and 0, and values of ψ of less than 5.94 (Table 2.5), and should lack the clear break in log-log plots of slope and downstream distance seen elsewhere. Results show that North Devon's rivers do indeed follow such trends, with values of ϕ of between -0.44 and -0.16 and values of ψ of between 3.37 and 4.24.

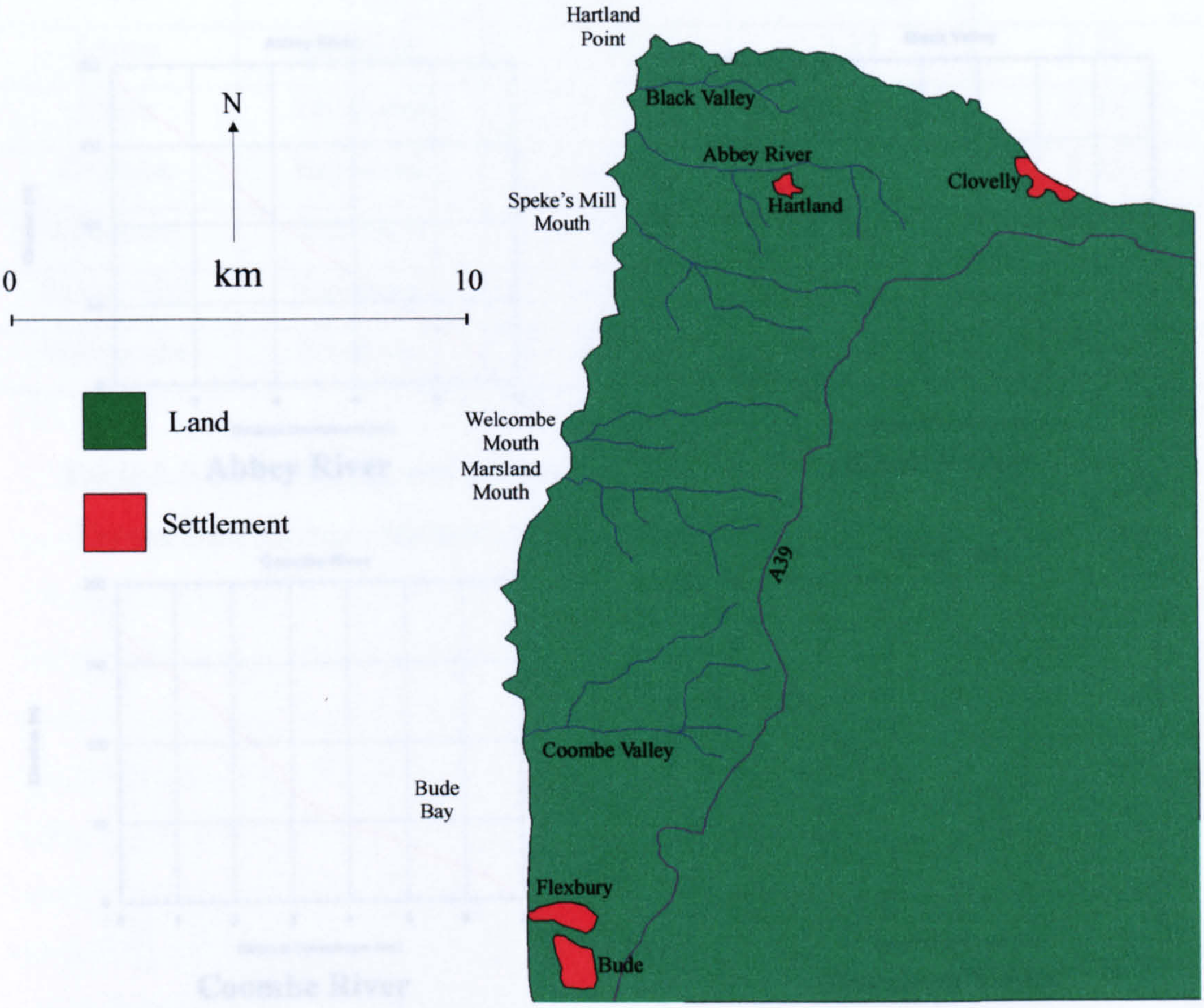

Figure 2.20 Location Map, North Devon, England

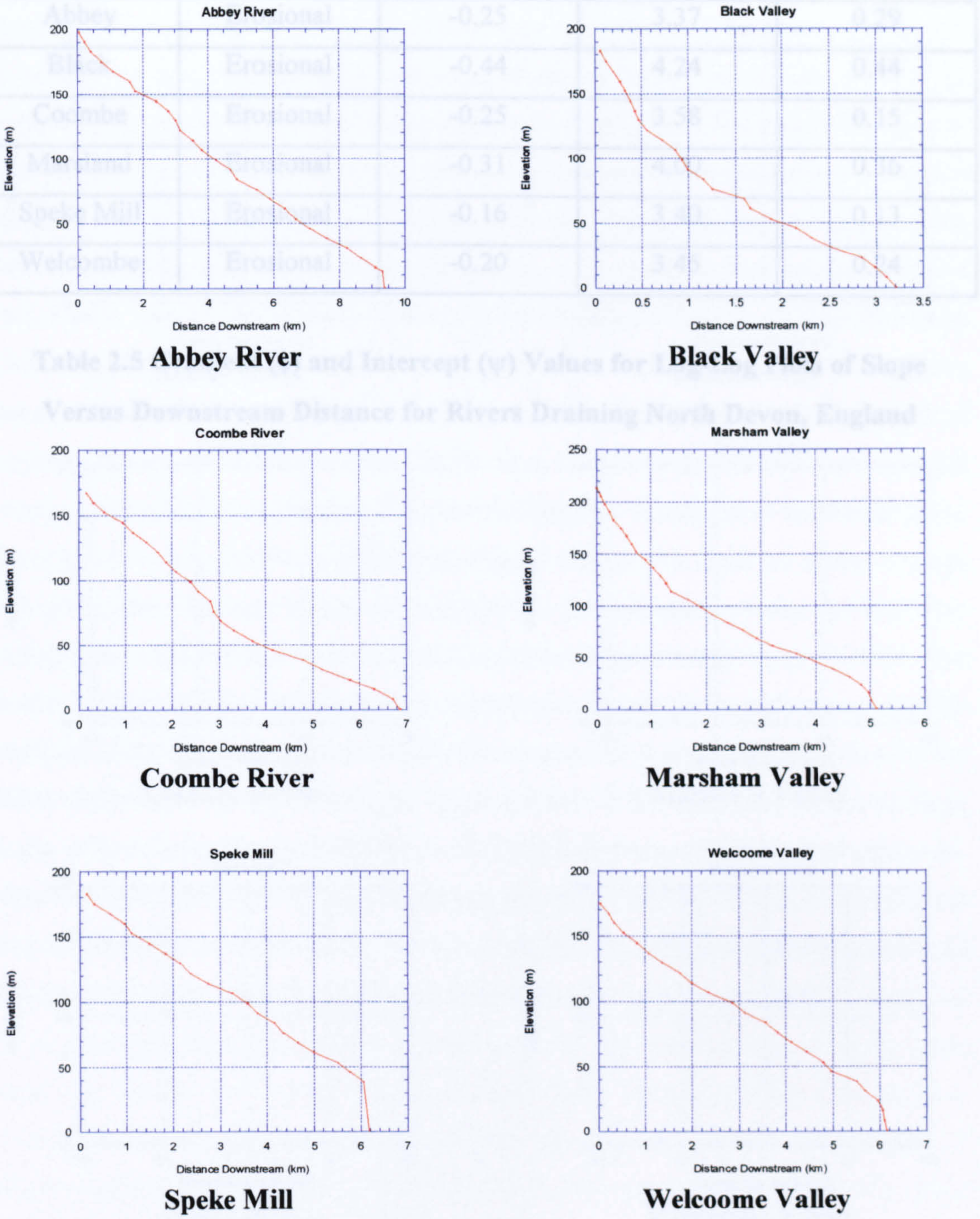

Figure 2.21 Longitudinal River Profiles, North Devon, England

Basin	Regime	Gradient	Intercept	r^2
Abbey	Erosional	-0.25	3.37	0.29
Black	Erosional	-0.44	4.24	0.44
Coombe	Erosional	-0.25	3.58	0.15
Marsland	Erosional	-0.31	4.00	0.36
Speke Mill	Erosional	-0.16	3.40	0.13
Welcombe	Erosional	-0.20	3.45	0.24

Table 2.5 Gradient (ϕ) and Intercept (ψ) Values for Log-Log Plots of Slope Versus Downstream Distance for Rivers Draining North Devon, England

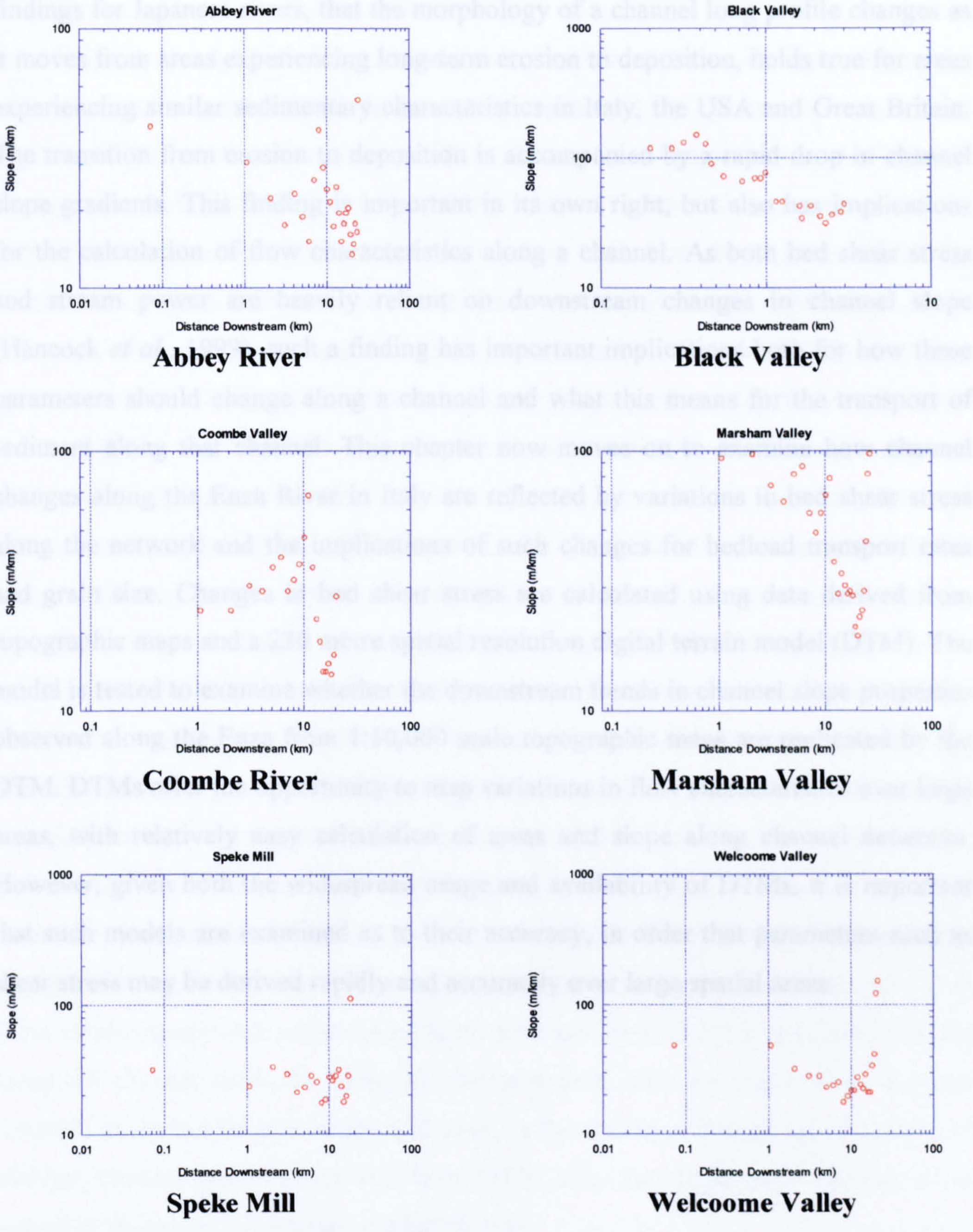

Figure 2.22 Logarithmic Plots of Local Slope Against Distance from Drainage Divide Measured from Topographic Maps for Rivers Draining North Devon, England
(Note, No Break in Slope, Hence No Transitional Line)

2.4.5 Summary of Findings

The work presented so far in this chapter has demonstrated that Yatsu's (1955) findings for Japanese rivers, that the morphology of a channel long profile changes as it moves from areas experiencing long-term erosion to deposition, holds true for areas experiencing similar sedimentary characteristics in Italy, the USA and Great Britain. The transition from erosion to deposition is accompanied by a rapid drop in channel slope gradients. This finding is important in its own right, but also has implications for the calculation of flow characteristics along a channel. As both bed shear stress and stream power are heavily reliant on downstream changes in channel slope (Hancock *et al.*, 1999), such a finding has important implications both for how these parameters should change along a channel and what this means for the transport of sediment along that channel. This chapter now moves on to examine how channel changes along the Enza River in Italy are reflected by variations in bed shear stress along the network and the implications of such changes for bedload transport rates and grain size. Changes in bed shear stress are calculated using data derived from topographic maps and a 230 metre spatial resolution digital terrain model (DTM). The model is tested to examine whether the downstream trends in channel slope properties observed along the Enza from 1:10,000 scale topographic maps are replicated by the DTM. DTMs offer the opportunity to map variations in flow characteristics over large areas, with relatively easy calculation of areas and slope along channel networks. However, given both the widespread usage and availability of DTMs, it is important that such models are examined as to their accuracy, in order that parameters such as shear stress may be derived rapidly and accurately over large spatial areas.

2.5 LONG PROFILES DERIVED FROM DIGITAL TERRAIN MODELS (DTMS)

2.5.1 Introduction

In the previous section it was shown that downstream changes in channel slope gradient correspond with large scale patterns of Late Quaternary erosion and deposition. The work in this chapter will now move on to examine how smaller scale changes in bedload transport rates along channel networks are determined by variations in parameters such as stream power and bed shear stress. Work in subsequent sections will show how the fundamental parameters required to derive estimates of stream power and bed shear stress can be determined from empirical relationships between basin and channel characteristics such as area, distance from the drainage divide and slope. These parameters can be determined relatively easily and quickly from digital terrain data. In addition to these benefits, derivation of channel and network properties from DTM data has the added advantage over conventional topographic map-based analyses of being able to calculate properties over much larger areas (given the constraints of the spatial area covered by the DTM). As such, in a later section, channel network properties along the Enza River are used to determine changes in bed shear stress and the implications such changes have for bedload transport rates and grain size changes along the river. Constraints are also determined regarding the resolution of the DTM data required for such analyses to be carried out. In order for this to be achieved, the DTM data must be able to replicate the channel properties, such as trends between downstream distance and elevation, observed both in the field and from conventional topographic map analyses. Calculations of bed shear stress require that estimates of basin area and channel slope gradient be made along the channel network. Although the latter have been calculated from detailed 1:10,000 scale topographic maps and used in the previous section, the question of whether channel profiles derived from DTM data can accurately provide slope measures along networks remains unanswered.

This section will thus examine a number of questions. Firstly, channel long profiles will be derived from DTM data based on both the original and pit-filled data sets. Pit filling is a widely applied pre-analysis technique employed in DTM-based analyses (for example, Pratson and Ryan, 1996; Weissel and Seidl, 1999), yet its employment has also received increasing attention (for example, Rieger, 1998). The

derived original and pit-filled DTM long profiles are thus analysed to assess the impact of pit filling on profile shape and the implications this has for subsequent analyses on the profiles. Calculations of distance from the drainage divide and basin area along the channel network are also assessed to compare how these measures differ from those calculated from topographic maps. Finally, channel slope gradients are derived along the DTM channel profiles in the manner outlined in Section 2.3.1. Thus the suitability of DTM derived long profiles and the calculations of stream network properties based upon these data are assessed, allowing for an evaluation of their reliability of use in subsequent calculation of bed shear stress.

2.5.2 The Use of DTMs in Hydrological Analyses

Digital terrain models have received wide usage in hydrological and terrain analyses (see Moore *et al.*, 1991). The capability of such models to delineate drainage paths and divides provides an ideal method with which to track water as its migrates across the surface of the Earth. The speed with which such analyses can be performed and the broad areas over which such calculations can be made offer considerable benefits over analyses based upon conventional topographic maps. However, despite their widespread usage and enormous potential, there are a large number of problems associated with using DTMs in hydrological analyses. These problems are associated both with the generation and accuracy of the DTM itself as well as with the algorithms used to derive channel networks and subsequent properties. Before outlining the methods used to derive channel long profiles and network properties used in this chapter, a brief overview of the problems associated with DTM derivation and usage is provided.

2.5.3 Problems Associated with DTMs

A variety of problems and errors are associated with the initial derivation of DTMs (Martz and Garbrecht, 1998). Of these problems, input data errors, errors resulting from the interpolation algorithms used, and the limited spatial and vertical resolution of the DTM are believed to be the most widespread and significant (Tribe, 1992; Zhang and Montgomery, 1994). These errors are believed to result mainly from errors in the data acquisition process (Band, 1986; Carrara, 1988). For example, in areas with high contour curvature (valleys and ridges), interpolation algorithms have difficulty in deriving accurate DTMs (Rieger, 1998). In combination, these errors

result in a widespread and controversial aspect of DTM-based analyses: depressions or pits.

2.5.4 Depressions in Digital Terrain Models

Depressions or 'pits' in DTMs are low points which are surrounded by higher pixels in all nine surrounding pixels. Such features create considerable difficulty in DTM-based hydrological analyses as they hinder flow routing across the surfaces in question (section 2.5.5). As discussed subsequently, flow routing algorithms employed in many computational packages, such as Arc/Info, require that flow directions be assigned for all cells within a grid, thus requiring pre-analysis pit filling. Such a pre-processing stage is widely undertaken (Pratson and Ryan, 1996; Weissel and Seidl, 1998; Jensen and Domingue, 1988) yet the application of such a technique has recently been questioned (Rieger, 1998). Pits are seen as errors which result from the grid resolution being too low for the morphological features under examination or being due to the inadequacy of the interpolation algorithms utilised to derive the DTM (Carrara, 1988). Although it is acknowledged that pits do occur naturally in glaciated and arid karst terrains, they are thought to be relatively rare in erosional topography with a spatial grid resolution of greater than 10 metres (Tarboten *et al.*, 1991). Recent work has indicated alternative methods to dealing with pits in DTM data, with the suggestion that they may in effect represent *real* features which should be dealt with in a "*hydrologically meaningful manner*" (Martz and Garbrecht, 1998, p.845). This conclusion is also supported by Rieger (1998), who suggests that pits may actually be more representative of the elevation of a channel, for example, than those pixels surrounding it. Thus, by filling the central, 'pit', pixel, artificially high elevations result. This has consequences not only for the channel properties derived from such pit-filled profiles, but also for flow routing algorithms which have to deal with the newly created, artificially flat, filled areas (Pilotti *et al.*, 1996). Thus by filling pits, another problem is created as flow routing over flat areas results in artificial parallel flow lines instead of more natural convergent ones. Tribe (1992) has suggested a convergent flow algorithm which overcomes this latter problem, yet it is currently not employed in common packages such as Arc/Info. Subsequent analyses in this chapter will assess the implications of pit filling on long profile derivation in the Apennines, allowing for a critical evaluation of the various ideas proposed to deal with depressions in DTM data.

2.5.5 Flow Routing Across DTMs

A variety of methods have been proposed with which to delineate and measure channel network properties from DTM data (Band, 1986; Jensen and Domingue, 1988; Tribe, 1992; Martz and Garbrecht, 1998). Three methods have been commonly used in grid-based analyses to compute surface flow directions. These algorithms are used to determine whether depressions are present in the data, which can then be dealt with using the techniques outlined above. The three most commonly used flow routing algorithms are: 1) flagging of local high points in moving 2*2 windows (Peuker & Douglas, 1975), 2) detection of high opposing pairs in windows (Jensen and Domingue, 1988) to detect V-shaped valleys, 3) the commonly used steepest-descent flow algorithm using the D-8 method (Deterministic 8 neighbour) to route flow to the lowest downslope neighbour (O'Callaghan & Mark, 1984; Jensen & Domingue, 1988). These methods are common in that they all assign a single flow direction to the output cell. It has been suggested that such output may be unrealistic in some situations where multiple output flow directions would be more accurate (Tarboten *et al.*, 1991), yet once again such advanced algorithms are beyond the current capabilities of Arc/Info.

Having derived flow directions from the DTM, the next stage is to delineate the channel network itself. Once again, the methods employed are numerous (Tarboten *et al.*, 1991; Montgomery and Foufoula-Georgiou, 1994). Three methods reviewed by Ijjasz-Vasquez & Bras (1995) are 1) those using a constant thresholds of drainage area (constant critical support areas-CSA) to delineate the network (Tarboten *et al.*, 1991; Jensen, 1995; Gardner *et al.*, 1990; Vogel *et al.*, 1995), 2) those using inflection points in plots of link area versus slope (Tarboten *et al.*, 1991), and 3) those using a combined local slope-area product to define the network extent, each having different criteria for channel initiation (Montgomery & Foufoula-Georgiou, 1993). Whilst it has been suggested that variable slope-area thresholds are required for defining channel heads (Montgomery and Dietrich, 1992, 1994; Dietrich *et al.*, 1992, 1993; Dietrich and Dunne, 1993; Montgomery & Foufoula-Georgiou, 1993; Pratson and Ryan, 1996), others have suggested that varying such thresholds has little impact on the derived channel networks and properties and that a constant support area (CSA) threshold should be employed across catchments (Pilotti *et al.*, 1996). The

latter conclusion is important as employing a constant threshold reduces the time required to perform the analyses required on the resulting channel network.

2.5.6 Derivation of Channel Long Profiles and Network Properties

Channel networks were derived from a 230 metre spatial resolution digital terrain model of the Northern Apennines. Despite better resolution models being available in areas such as the United States (Chapter 4), and the planned NASA radar inferometry mission, which will map the globe between 60° north and south at 30 metre resolution (E. Fielding, pers. comm.), at present the 230 metre model is the only DTM available for the entire Northern Apennines. In order to obtain reliable measures of downstream distance and basin area, it was necessary to derive a continuous channel network from the DTM. By performing flow routing algorithms and deriving channels from the original DTM, discontinuous networks resulted (Figure 2.23). Whilst such features may be present in ephemeral streams in arid environments, the channel networks in the Northern Apennines are continuous and thus the sources of the discontinuities had to be removed. Arc/Info allows for pit filling and peak removal of DTMs and whilst the former revealed many pits along the derived channel networks, the latter failed to identity possible 'high points' along the networks. However, as the aim here is to derive a continuous network along which channel properties could be derived, the pit filling algorithm was applied to the Italian DTM. A constant support area of 50 pixels was applied to the DTM (as in Ryan and Pratson, 1996). Most of the debate surrounding the selection of an appropriate support area focuses on definition of the channel head, thus as the emphasis here is on the channel network and not defining the upper extent of the network, such issues may be ignored. Problems associated with routing drainage across flat areas, such as the Po Plain area in Northern Italy (Figure 2.7), mean that drainage could not be defined at elevations lower than the mountain front (approximately 100 m elevation). By deriving continuous networks, calculations of downstream distance, elevation, slope and contributing area along the channels could be determined. The effect of pit filling on the resultant DTM long profile could also be measured by overlaying the continuous stream network derived from the pit-filled DTM onto the original unfilled DTM. This in turn would allow both for an assessment of the level of pit filling performed along the network, as well as a measure of the ability of both the original and filled long

profiles to replicate the morphology and slope measures derived from the conventional topographic map profiles.

1.

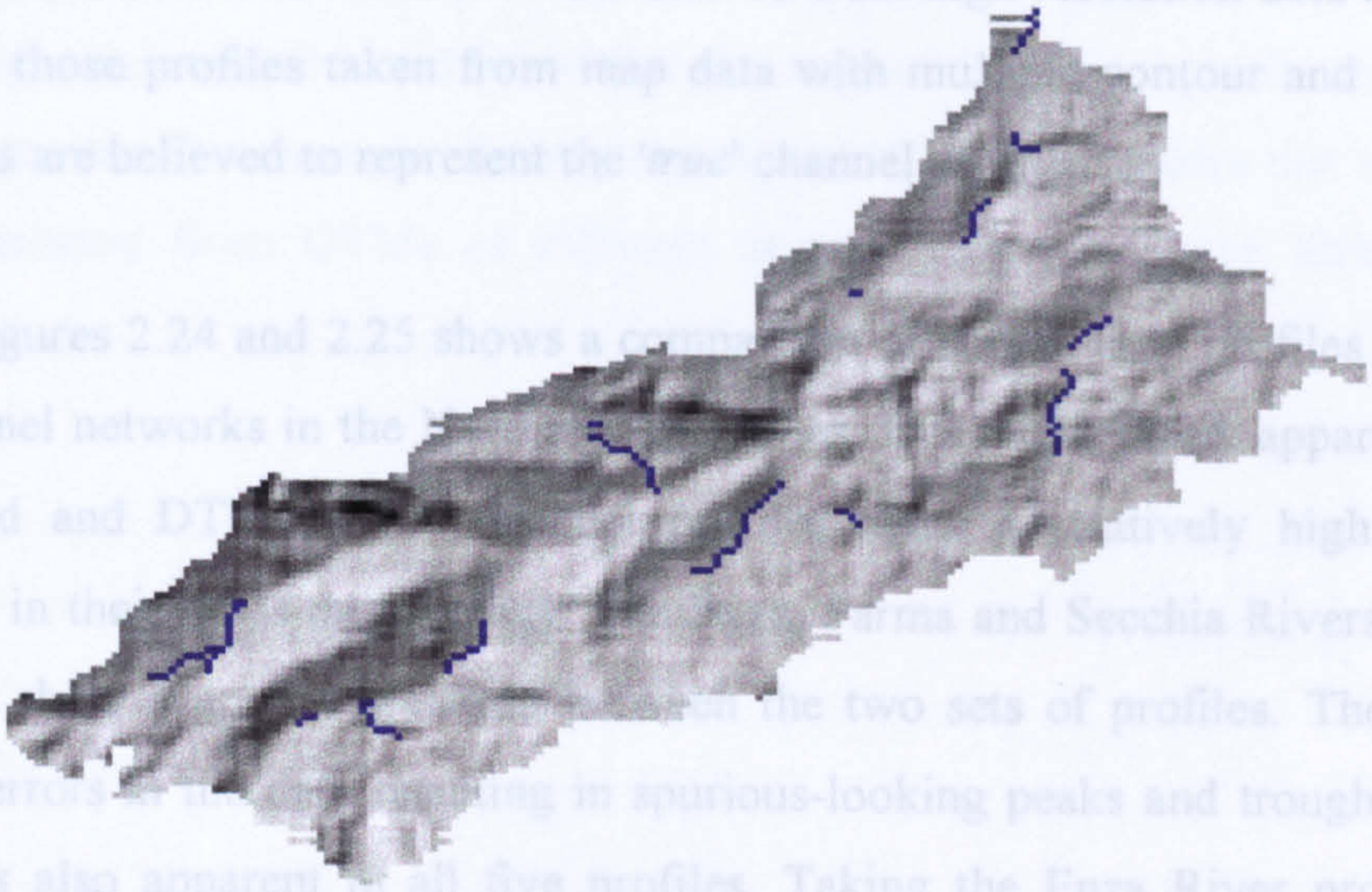

2.

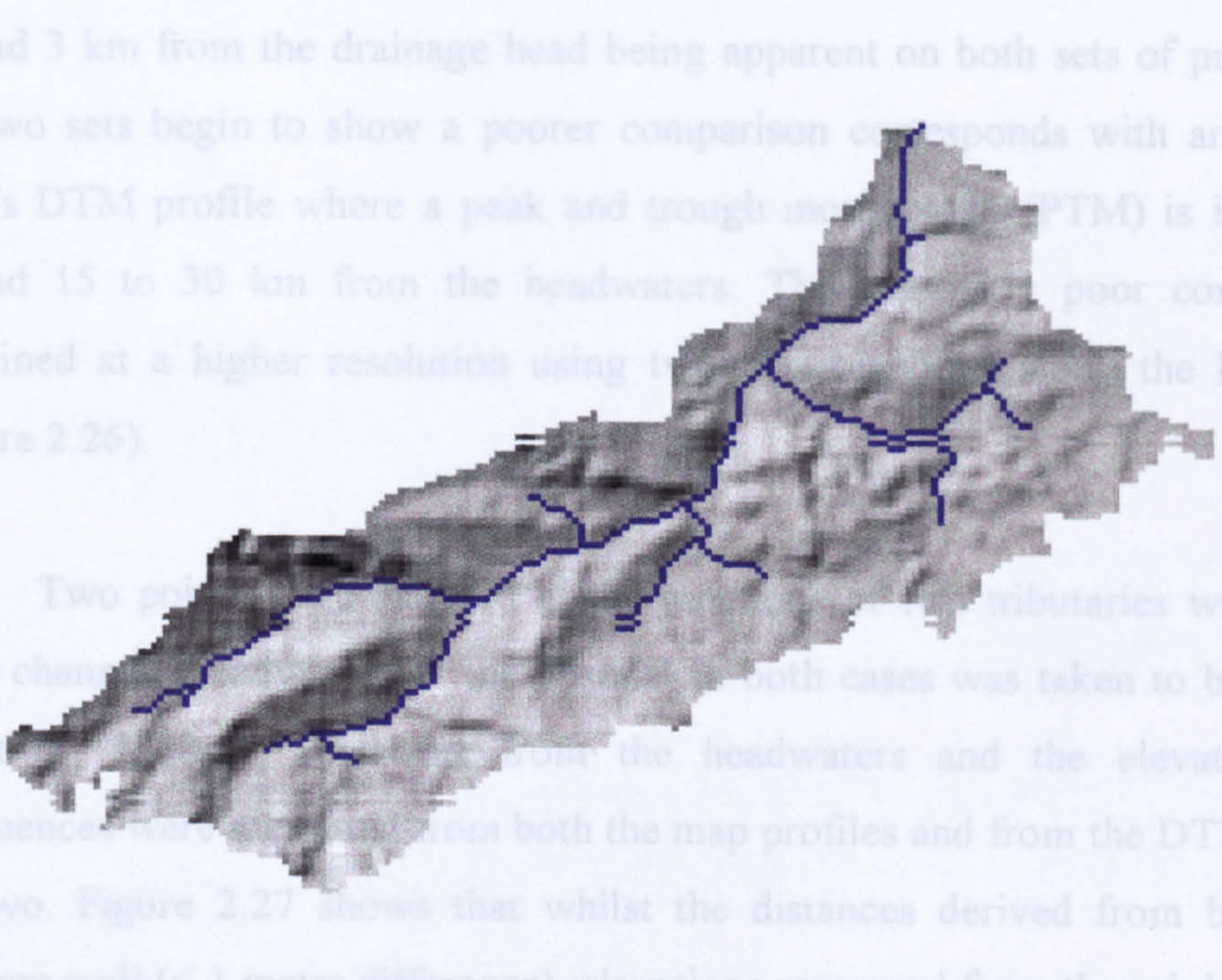

Figure 2.23 The Effect of Pit-Filling on Stream Network Derivation, Enza River, Northern Apennines, Italy.

1) Discontinuous Network Resulting from Pits in DTM Data

2) Continuous Network Resulting from Pit-Filled DTM

2.5.7 Comparison of DTM and Map Derived Channel Long Profiles

The Italian DTM data were derived from manual and computer-aided scanning of map contour data (Reichenbach *et al.*, 1993), in which the data were arranged to give average elevations within 230 metre grid cells. Given that in the topographic map profiles taken for Italian channels were derived from high resolution data at a scale of 1:10,000, those profiles taken from map data with multiple contour and spot height recordings are believed to represent the '*true*' channel profile.

Figures 2.24 and 2.25 shows a comparison of stream long profiles derived for five channel networks in the Northern Apennines. It is immediately apparent that the map-based and DTM-derived channel profiles show a relatively high degree of similarity in their gross morphology. The Enza, Parma and Secchia Rivers profiles in particular show a good correlation between the two sets of profiles. The effects of possible errors in the data resulting in spurious-looking peaks and troughs along the profiles is also apparent in all five profiles. Taking the Enza River profiles as an example, it can be seen how the uppermost and lowermost reaches of the profile show a good correlation between the two data sets, with features such as knickpoints at around 3 km from the drainage head being apparent on both sets of profiles. Where the two sets begin to show a poorer comparison corresponds with areas along the Enza's DTM profile where a peak and trough morphology (PTM) is in evidence at around 15 to 30 km from the headwaters. This relatively poor comparison was examined at a higher resolution using two control points along the Enza network (Figure 2.26).

Two points were selected at the junctions of two tributaries with the Enza's trunk channel. Headwaters of the channel in both cases was taken to be at the same elevation (1370m). Distances from the headwaters and the elevation of these confluences were measured from both the map profiles and from the DTM to compare the two. Figure 2.27 shows that whilst the distances derived from both data sets compare well (< 1 metre difference), elevations measured from the original DTM data set are found to be 53 and 60 metres above those measured from the map profiles. Such problems can be attributed to problems associated with deriving DTMs in areas of high contour curvature (Rieger, 1998) as, for example, in the gorges in evidence along the Enza River (field observations, 1998). An examination of Figure 2.24 shows

that along the Enza River, the lower points along the original DTM profile are closer to the elevations of the higher resolution topographic map profile. By removing the higher points and smoothing the profile between the lowermost points (Figure 2.28), a DTM profile with a higher degree of similarity to that map profile can be obtained. This finding supports the proposal by Rieger (1998), who suggests that the elevation of the 'pit' pixel may be correct whilst the surrounding nine pixels are too high. Previous studies (for example, Pratson and Ryan, 1996) have shown that contributing areas calculated from DTMs of different spatial resolutions have little variation.

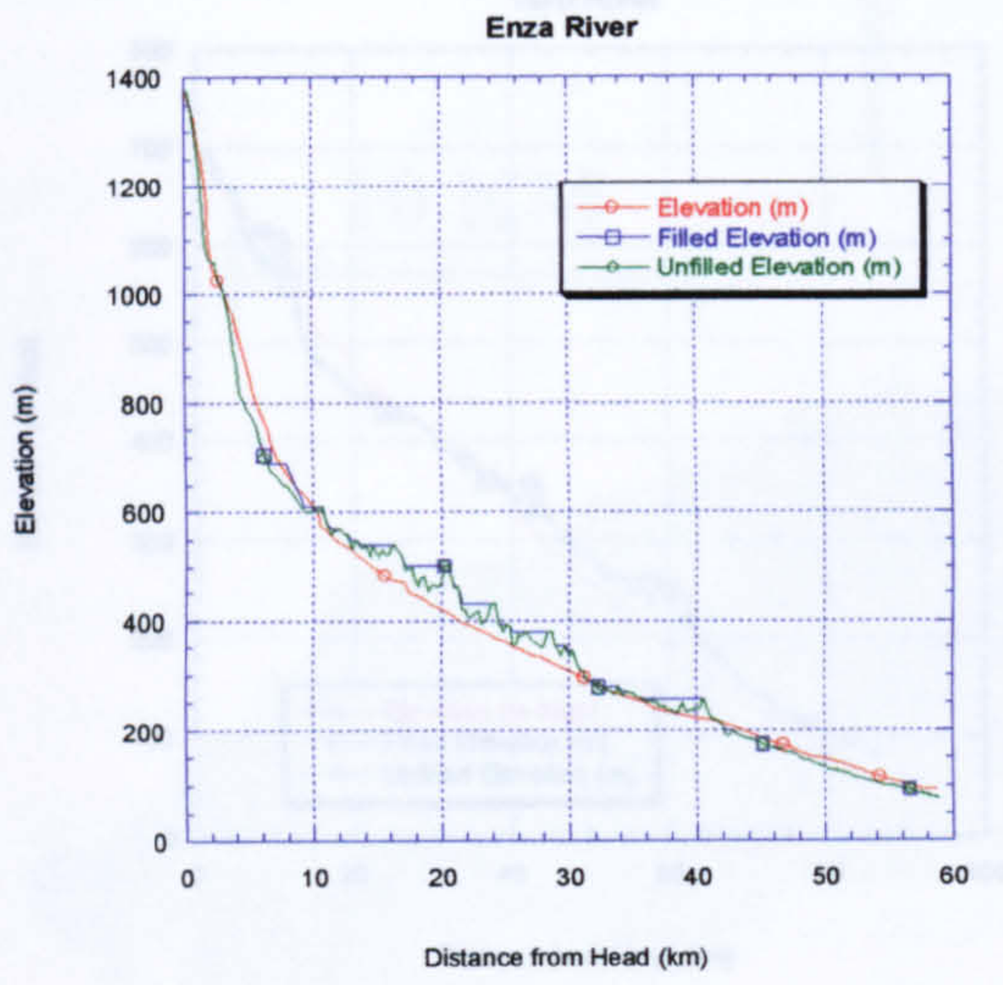

Enza River

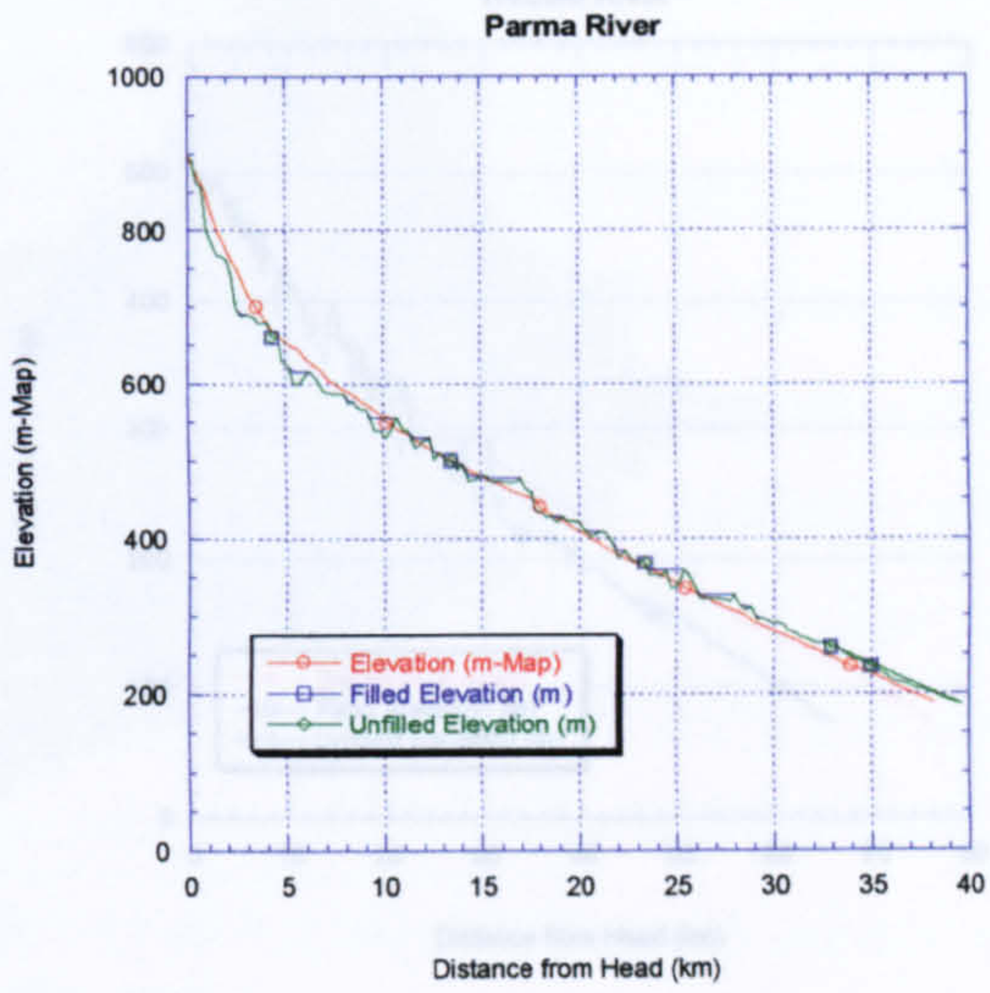

Parma River

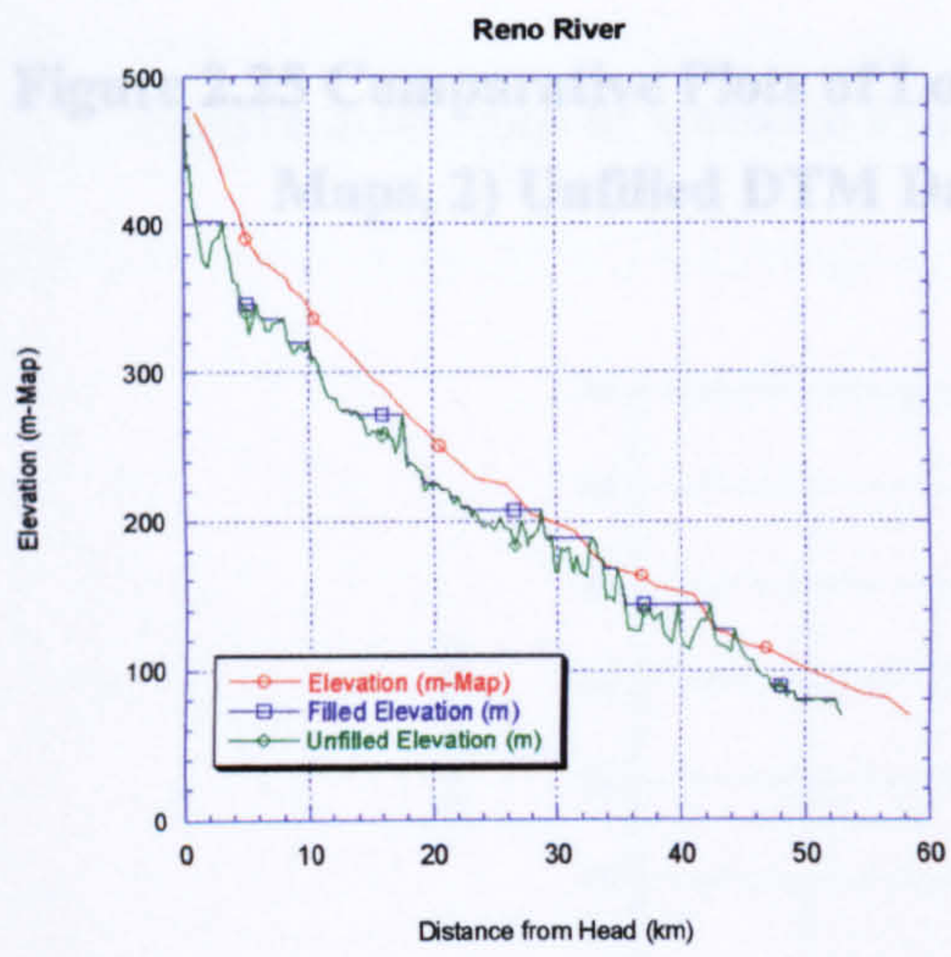

Reno River

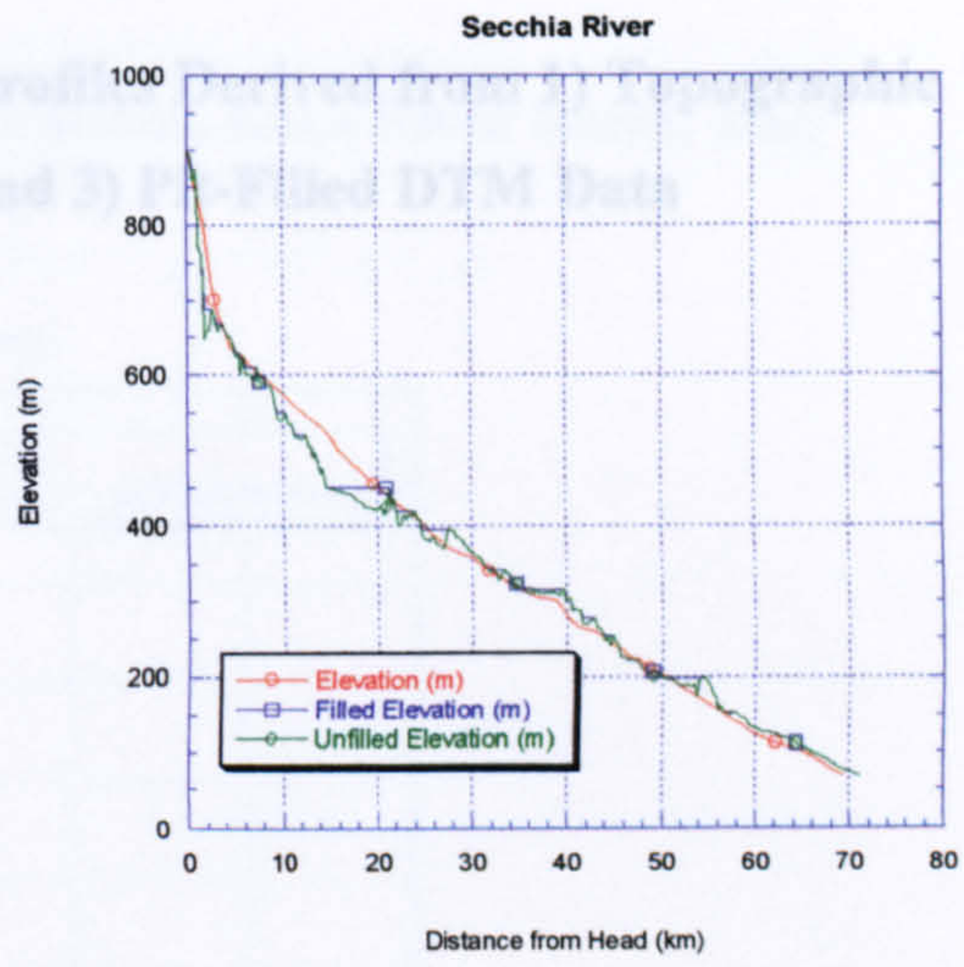

Secchia River

Figure 2.24 Comparative Plots of Long Profiles Derived from 1) Topographic Maps, 2) Unfilled DTM Data and 3) Pit-Filled DTM Data

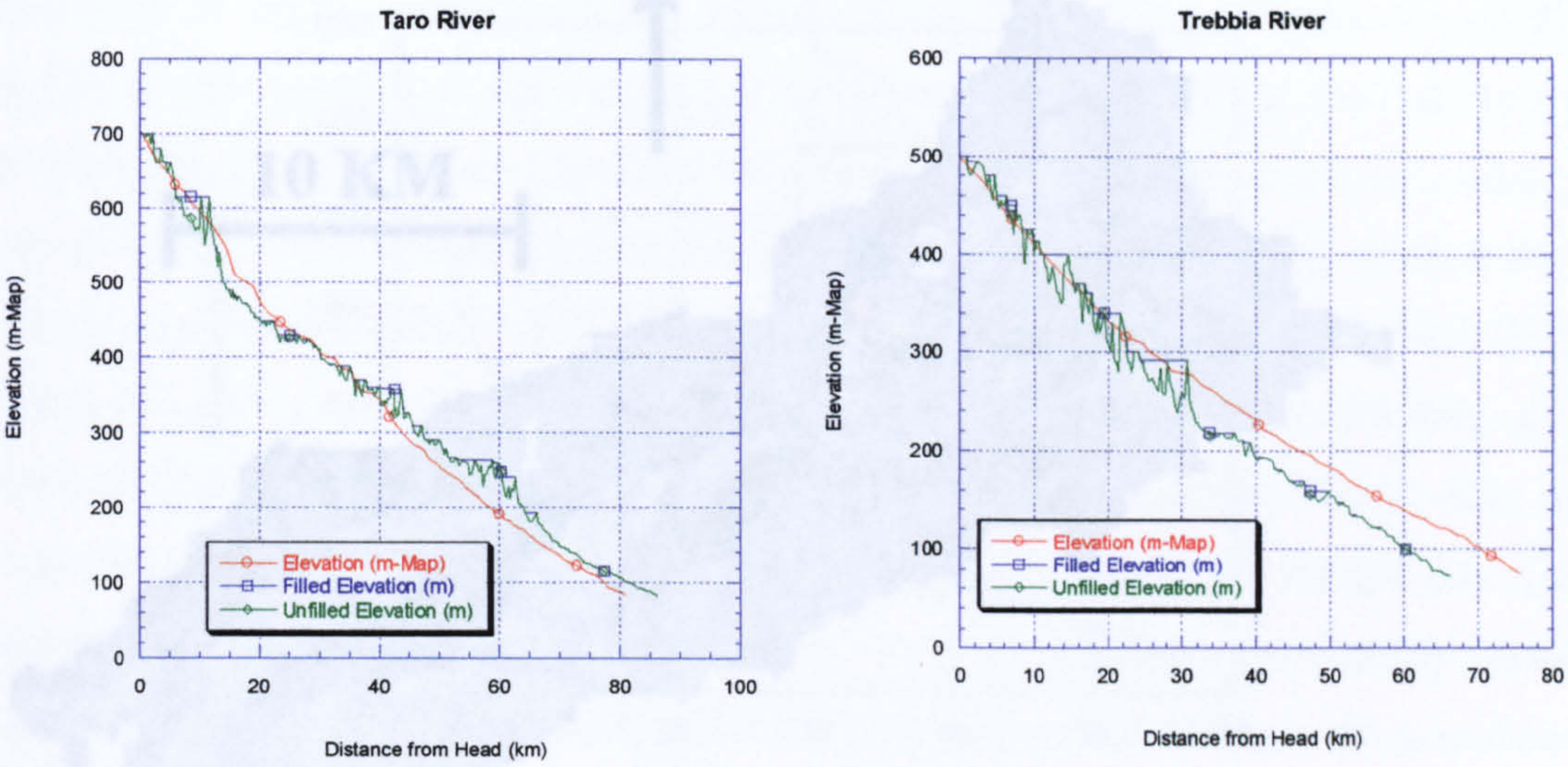

Taro River **Trebbia River**

Figure 2.25 Comparative Plots of Long Profiles Derived from 1) Topographic Maps, 2) Unfilled DTM Data and 3) Pit-Filled DTM Data

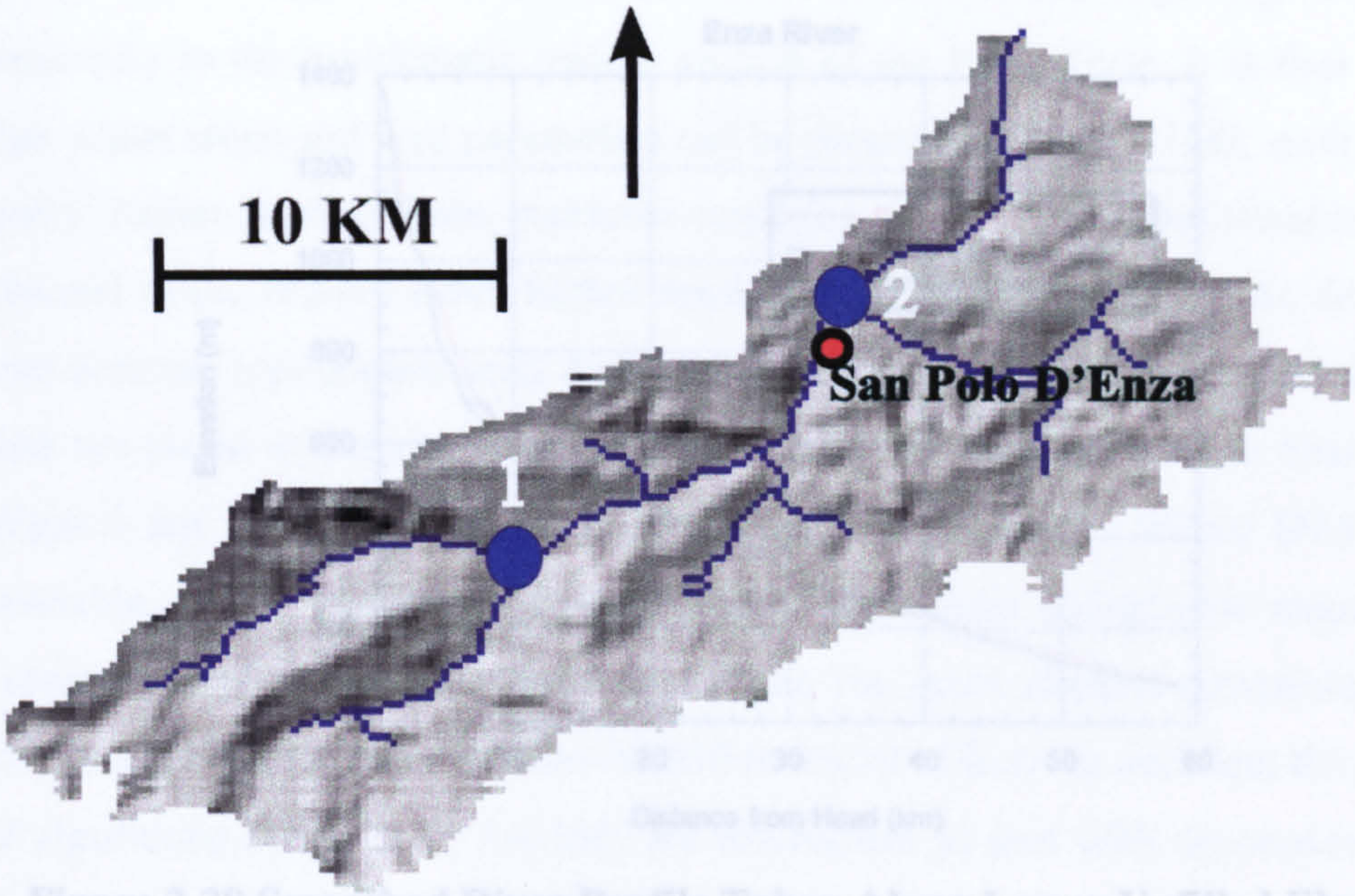

Figure 2.26 Map of Control Point Locations, Enza River Basin, Italy

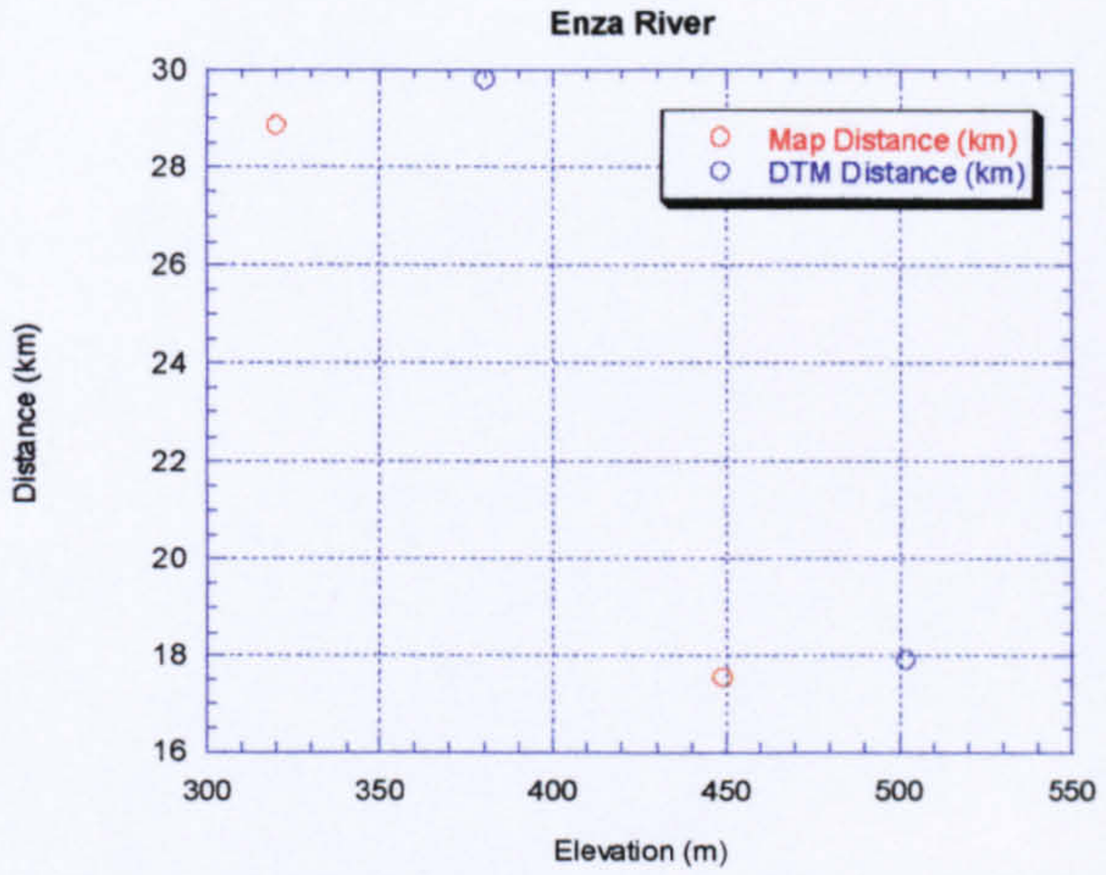

Figure 2.27 Plot of Downstream Distance and Elevation for Control Points, Enza Basin, Italy

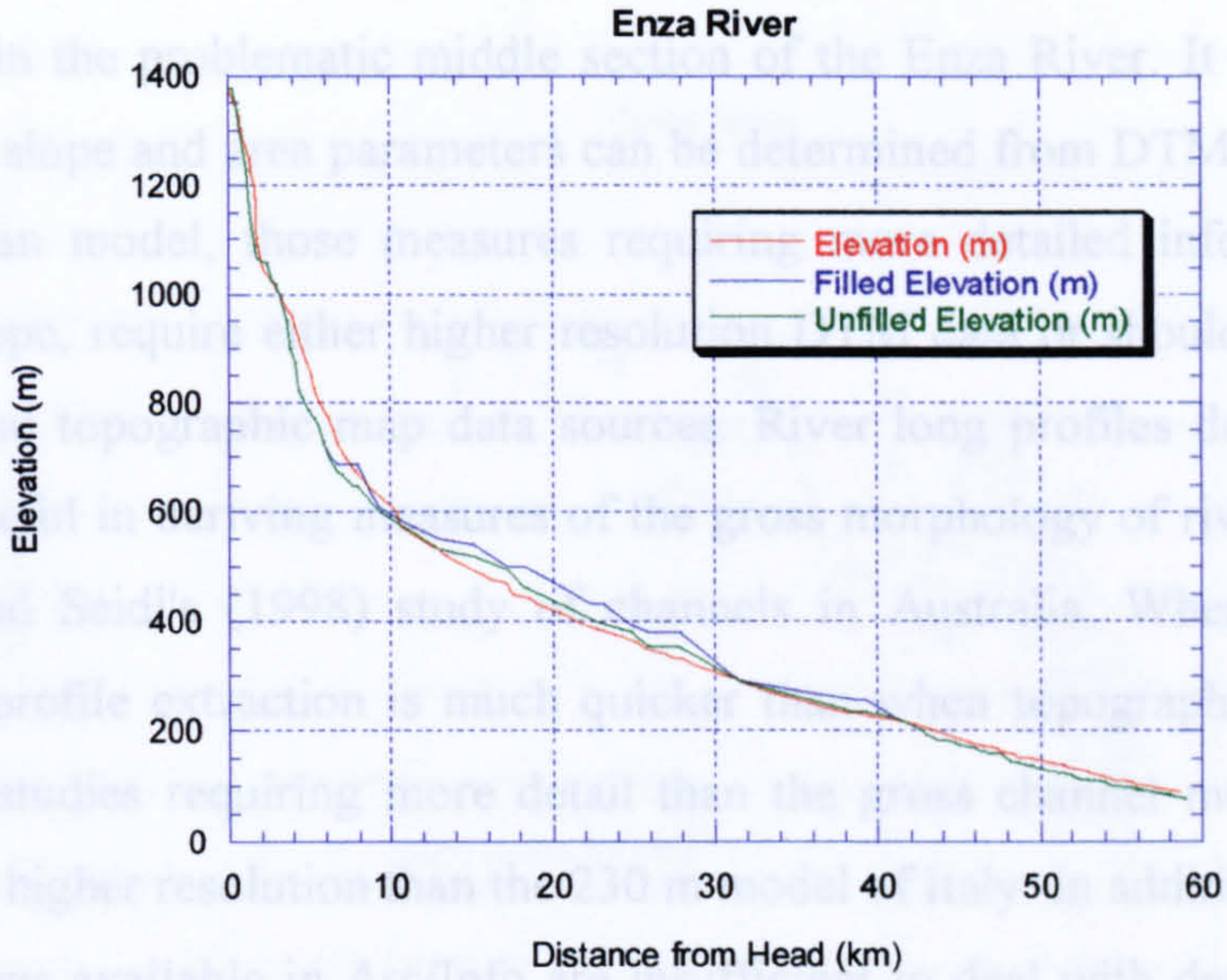

Figure 2.28 Smoothed River Profile Taken Along Lower Unfilled Elevation Points, Enza River

Slope values were calculated along the Enza River in the manner outlined in section 2.3.1. Figure 2.29 shows that they demonstrate a high degree of scatter, especially in the problematic middle section of the Enza River. It is thus concluded that whilst slope and area parameters can be determined from DTMs, such as the 230 metre Italian model, those measures requiring more detailed information, such as channel slope, require either higher resolution DTM data or should be defined from conventional topographic map data sources. River long profiles derived from DTM data are useful in deriving measures of the gross morphology of river channels, as in Weissel and Seidl's (1998) study of channels in Australia. Where DTM data are available, profile extraction is much quicker than when topographic maps are used. However, studies requiring more detail than the gross channel morphology require DTMs at a higher resolution than the 230 m model of Italy. In addition, the present set of algorithms available in Arc/Info are insufficient to deal with depressions in DTM data, where they are dealt with as errors. The results of this study indicate that depressions should be dealt with in the manner outlined by Rieger (1998), lowering the higher points surrounding the *pit* pixel, rather than increasing the elevation of the latter. Such algorithms require implementation in packages such as Arc/Info if they are to be used as tools to derive channel profiles from DTM data.

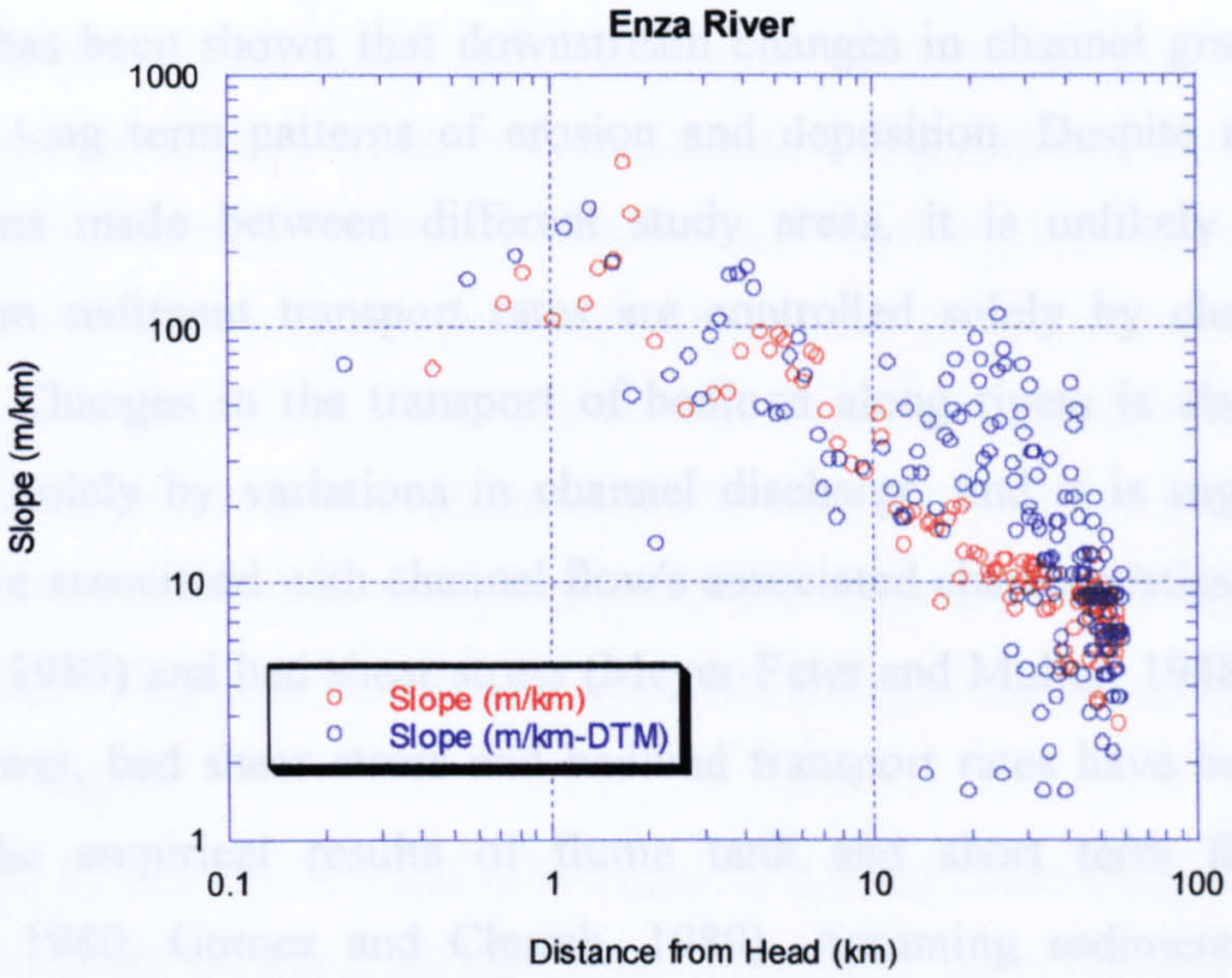

Figure 2.29 Slope Values Along the Enza River Calculated from 1:10,000 Scale Topographic Map (red) and 230 Metre DTM (blue) Data

2.6 BED SHEAR STRESS AND BEDLOAD TRANSPORT IN THE NORTHERN APENNINES

2.6.1 Introduction

It has been shown that downstream changes in channel gradient are closely related to long term patterns of erosion and deposition. Despite the agreement of observations made between different study areas, it is unlikely that changes in downstream sediment transport rates are controlled solely by changes in channel gradient. Changes in the transport of bedload along rivers is also unlikely to be controlled solely by variations in channel discharge, and it is suggested that such changes are associated with channel flow's associated characteristics of stream power (Bagnold, 1980) and bed shear stress (Meyer-Peter and Muller, 1948). Links between stream power, bed shear stress and bedload transport rates have been demonstrated through the empirical results of flume tank and short term field observations (Bagnold, 1980; Gomez and Church, 1989). Assuming sediment continuity in a downstream direction (Reid and Laronne, 1995), downstream increases and decreases in bedload transport rates result in erosion and deposition of sediment on the channel bed. Previous work has shown how downstream variations in stream power are correlated to changes in sediment transport rates and patterns of erosion and deposition (Bull, 1979). Although the previous work in this chapter examined channel gradient changes in four study areas, the focus will now shift to focus on the Northern Apennines, where more detailed field studies have been undertaken and measurements along channel networks made.

2.6.2 Bedload Transport Rates

Assuming that there is no loss of bedload or water from the channel downstream, changes in bedload transport rates result in erosion or deposition of sediment on the channel bed - the sediment continuity equation (Lane *et al.*, 1995). Under conditions of grade (Section 2.2.1.1), alluvial gravel-bed channels adjust such that sediment transport rates are kept constant in a downstream direction, i.e. there is no net erosion or deposition on the channel bed. Although large amounts of sediment are transported in suspended or solute form in some channels (Milliman and Syvitski, 1992), such transport does not directly influence the channel bed elevation, and as such their effects are ignored in this study. The transport of sediment requires that a threshold flow strength be equalled or exceeded such that particles may move (Powell

and Ashworth, 1995; Richards, 1982). However, despite this intuitively correct observation, the processes and mechanisms responsible for sediment transport remains highly controversial (Reid and Laronne, 1995). For particles to be moved, for example during a flood, the lift and drag forces exerted on sediment particles must be great enough to overcome the sediment's restraining forces due to its weight and interparticular friction (Powell and Ashworth, 1995). Early work was largely based on Shields (1936) laboratory observations in which the critical shear stress required for sediment entrainment varied directly as a function of particle size - 'size-selective entrainment', whilst more recent studies have attempted to relate bedload entrainment and transport to bed shear stress (τ_o) estimated from a channel depth-slope product (Ashworth and Ferguson, 1989). Bed shear stress (τ_o) is calculated as

(2.3) $\tau_o = \rho_w g d S$,

where ρ_w is the density of water (1000 kgm^{-3}), d is the channel depth, S is the channel slope (m) and g is the gravitational acceleration (9.81 ms^{-2}). Shields' (1936) work has been challenged by studies which have shown that all grain sizes in nonuniform sediment mixes are entrained within a narrow range of shear stresses - 'equal mobility' (Parker *et al.*, 1982; Ashworth and Ferguson, 1989). Parker *et al.* (1982) indicate that hiding and protrusion effects along channel networks are so important that the critical shear stress (τ_c) required to entrain particles on the bed varies only slightly, if at all, with increasing grain size diameter.

2.6.2.1 Bedload Transport in Alluvial Channels

Whilst it has been suggested that critical bed shear stress increases with particle size (Shields, 1936), it has also been recognised that this critical value also depends upon bed roughness conditions (Richards, 1982). As such, a dimensionless critical shear stress (τ_*) is employed in which

(2.4) $\tau_* = \rho_w g d S/(\rho_w-\rho_s)gD$,

where ρ_w is the density of water (1000 kgm^{-3}), ρ_s is the density of sediment (2700 kgm^{-3}), and D is the grain size. Studies have shown that bed shear stresses in gravel-bed rivers are at critical values for entrainment (Paola and Mohrig, 1996) and that alluvial channels are characterised by a narrow range of dimensionless shear stresses, with values for gravel-bed rivers ranging from 0.02 (Dade and Friend, 1998; Charlton *et al.*, 1978) to 0.10 (Jorgensen, 1998; Dade and Friend, 1998). Buffington and

Montgomery (1997) found that the critical value of τ_c required to move the median grain size (τ_{*c50}) varied from 0.03 to 0.073, whilst Andrews (1984) found that τ_* would only reach 0.08 along the Colorado River during an extreme 100 year flood. These studies indicate that along gravel-bed rivers τ_* only slightly exceeds τ_{*c50} even during flood conditions. Channels dominated by sand-bed channels have higher characteristic dimensionless shear stresses than their gravel-bed counterparts, with values in the range 0.5 to 5 (Parker *et al.*, 1998).

2.6.2.2 Sand-Bed Alluvial Channels

By contrast to gravel-bed alluvial channels, sand-bed channels have been shown to have higher dimensionless shear stresses (for example, Parker *et al.*, 1998; Dade and Friend, 1998), with values ranging from 0.5 to 5, which are higher than the mean values of 0.02 to 0.1 documented as existing in many gravel-bed channels (Dade and Friend, 1998).

2.6.3 Grain Size Variations Along Channels

The mean size of gravel-bed material decreases downstream along channel networks. This phenomenon has been attributed to abrasion of particles during transport (Kodema, 1994), variations in the amount and size of material supplied to the channel from upstream and hillslopes, and selective entrainment, transport and deposition (for example, Paola *et al.*, 1992; Rice, 1998). Whilst abrasion does affect both the depositional and erosional parts of river systems, it results in a relatively slow decrease in grain size (Powell *et al.*, 1998). Research by Pizzuto (1995; 1992) indicates that of the possible explanations proposed, variations in the size of gravel supplied to the channel from the hillslopes is of the most significance, and suggests that where resistant lithologies outcrop, higher mean grain sizes will result. Given equation 2.4, whereby the critical dimensionless shear stress (τ_*) needed to move the median grain size (D_{50}) is proportional to the ratio of the threshold bed shear stress (τ_c) to the median grain size. It has been shown above that for gravel-bed rivers, the dimensionless shear stress is essentially constant along channels, thus variations in the threshold bed shear stress are proposed to be a function of median grain size along the channel network (Talling, in review). A better understanding of how channel bed characteristics, shear stress and grain size are linked is critical to both improve our

understanding of current sediment transport in rivers, as well as to enhance our interpretations of how ancient river deposits were formed. Links between flow characteristics and grain size are now examined using the example of the Enza River in the Northern Apennines, where a combination of topographic map and digital terrain model data, together with detailed grain size and field observations allow such calculations to be made.

2.6.4 Case Study: The Enza River, Northern Apennines, Italy

Field observations in the Northern Apennines indicate that the Enza River demonstrates an 'alluvial-veneer' bedrock channel for much of its course through the mountain belt (Talling, in review). The channel comprises small outcrops of bedrock which are overlain by deposits of gravel of up to 5 metres thickness. Bedrock outcrops consist of Miocene turbidite deposits of the Tuscan Sequence (Section 5.5.3) in the uppermost reaches of the river, and Pliocene marine mud and sandstones in the lower parts of the basin. In places where the marine muds are exposed, fieldwork has determined that pressure from a finger can remove material.

'Alluvial-veneer' bedrock or 'mixed bedrock-alluvial' channels (Howard, 1998; Howard *et al.*, 1994) have been observed in a number of field locations in northern California (Seidl and Dietrich, 1992), the Appalachian Mountains (Brush, 1961) and Indiana (Miller, 1991). Such channels can occur under conditions where the episodic delivery of sediment and discharge to the channel network, for example from debris flows in the former's case (for example, Dietrich and Dunne, 1997), results in alternating alluvial and bedrock flooring of channels during periods of high and low yield respectively. Alluvial-veneer channels can also occur where resistant lithologies outcrop, such that the channel's potential energy is greater than the rate of regional uplift. At present, one of the unresolved issues concerning such channel types is whether alluvial-veneer channel morphologies are governed by the processes of bedrock erosion or instead by those applying to gravel-bed alluvial channels (Howard, 1998; Talling, in review). In the simplest case, the bedrock form ceases to be eroded by the conventional processes of bedrock erosion, such as plucking, solution, abrasion by sediment particles and weathering (Howard *et al.*, 1994), once the channel is covered by sediment, or if the sediment transport capacity is reached (Howard *et al.*, 1998). However, events such as episodic scour and fill mean that bedrock reaches are

exposed and the processes of bedrock erosion can occur. Furthermore, the upper reaches of such alluvial veneer channels are commonly mantled by coarse boulders delivered from the surrounding hillslopes. Field observations show that the upper Enza River is mantled with such boulders (size of up to 3 m diameter), especially where the river valley narrows into a gorge. Such material must be denuded *in situ* and can thus be viewed as a special type of bedrock channel (Howard, 1998).

In order to assess the nature of bed shear stress, grain size and sediment transport along the Enza River, the following measurements were required: channel slope (S), channel depth (d), grain size (D) and the empirical constants of gravitational acceleration (g) and the density of water (ρ_w).

2.6.4.1 Channel Slope

Channel slope measurements used were the same as those used previously in section 2.3.1, calculated as the average among 3 points along the channel long profile derived from detailed 1:10,000 topographic maps.

2.6.4.2 Channel Depth

Channel depth measurements were not available for the entire Enza channel network, and hence calculations were made using empirical relationships between channel depth and area (or mean annual discharge).

2.6.4.3 Mean Annual Discharge, Channel Cross-Sectional Area and Flow Velocity

Previous studies (Leopold and Maddock, 1953; Leopold and Miller, 1956; Carlston, 1969) have shown that adjustments in a number of channel cross-sectional parameters occur to accommodate changing discharge (Q in $m^3\ s^{-1}$) along a river. Leopold and Maddock (1953) showed that

(2.5) $w = {}_aQ^b$,

(2.6) $d = {}_cQ^f$ and

(2.7) $v = {}_kQ^m$,

where w is channel width (in m), d is channel depth (in m) and v is channel flow velocity (in m/s). Leopold and Maddock (1953) showed that as wdv = Q, b+f+m = 1 (Talling and Sowter, 1998). It has subsequently been shown that a number of power

functions may be used to describe trends in dependent variables with discharge. Talling and Sowter (1998) show that for the Po Basin, increases in channel discharge are primarily accommodated by variations in channel width and depth, with exponents of b, f and m being 0.49, 0.46 and 0.02 respectively (Figures 2.30, 2.31 and 2.32). Other researchers have found values of b to be around 0.5 (Carlston, 1969; Leopold and Miller, 1956) and f around 0.3 (Leopold and Maddock, 1953). Values of m are cited as varying from 0.1 (Leopold and Maddock, 1953) to 0.2 (Leopold and Miller, 1956).

2.6.4.4 Mean Annual Discharge and Basin Area

Previous workers (Brush, 1961; Knighton, 1987) have demonstrated a strong linear dependence of discharge on drainage area (A in km^2) along a channel network, such that as drainage area (A) increases downstream so does discharge. This relationship takes the form

(2.8) $Q = k_a A^{\alpha}$,

where k is a constant. For 30 stations located in the Po Basin of northern Italy, K_a has been calculated as 0.049 and α as 0.96 (Figure 2.33) (Talling and Sowter, 1998). Similar values have been found in other studies, with exponents ranging from 0.7 to 0.9 (e.g. Slingerland *et al.*, 1994, p.47; Nixon, 1959).

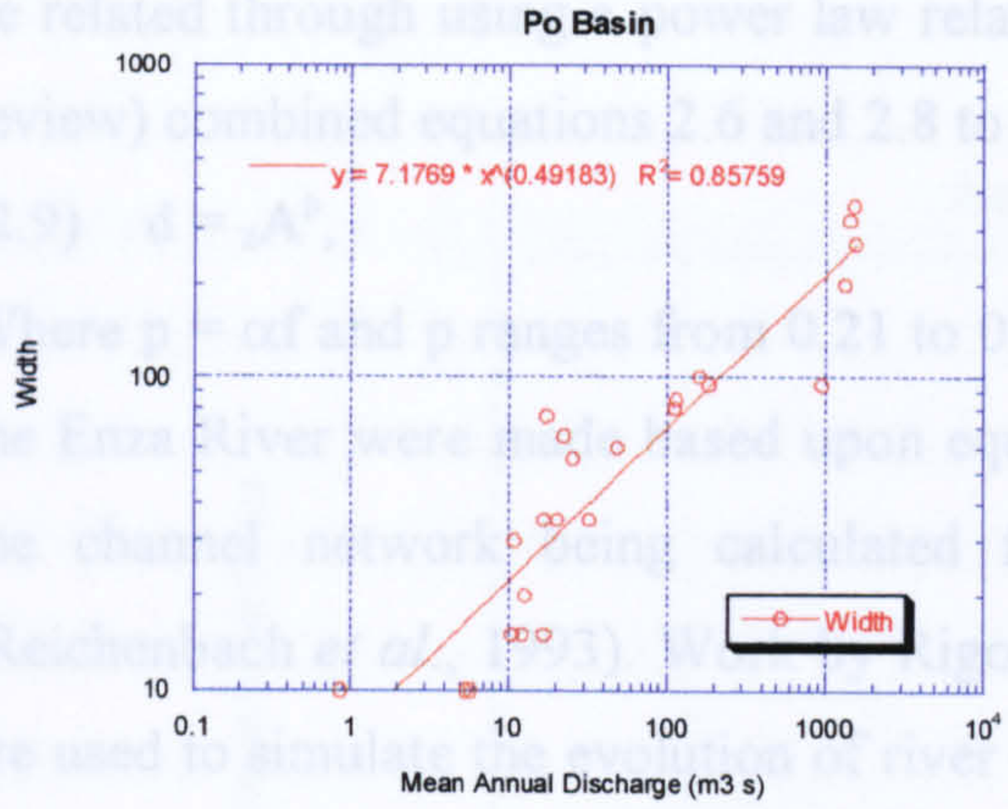

Figure 2.30 Mean Annual Discharge Versus Width, Italian Basins (after Cati, 1983)

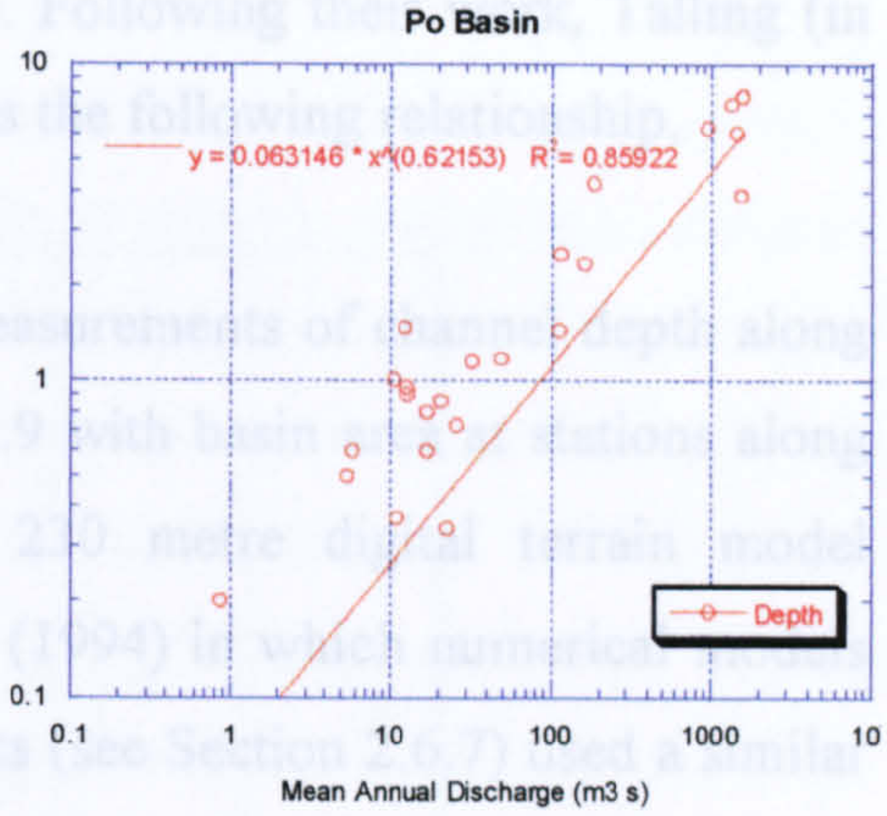

Figure 2.31 Mean Annual Discharge Versus Depth, Italian Basins (after Cati, 1983)

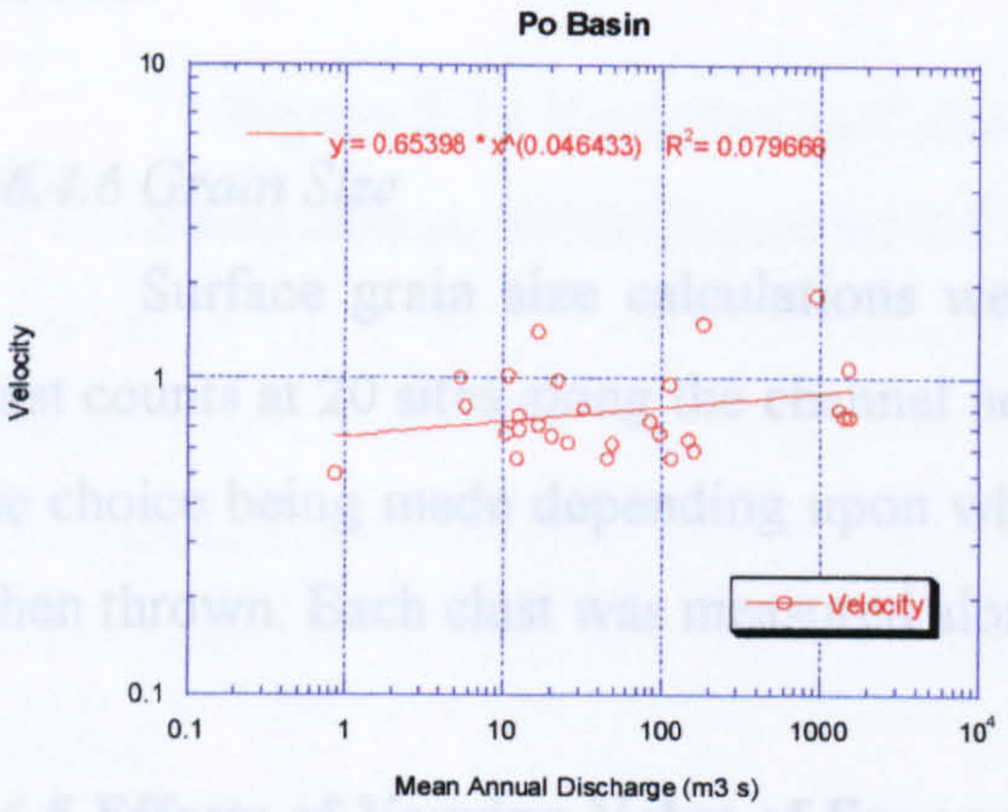

Figure 2.32 Mean Annual Discharge Versus Velocity, Italian Basins (after Cati, 1983)

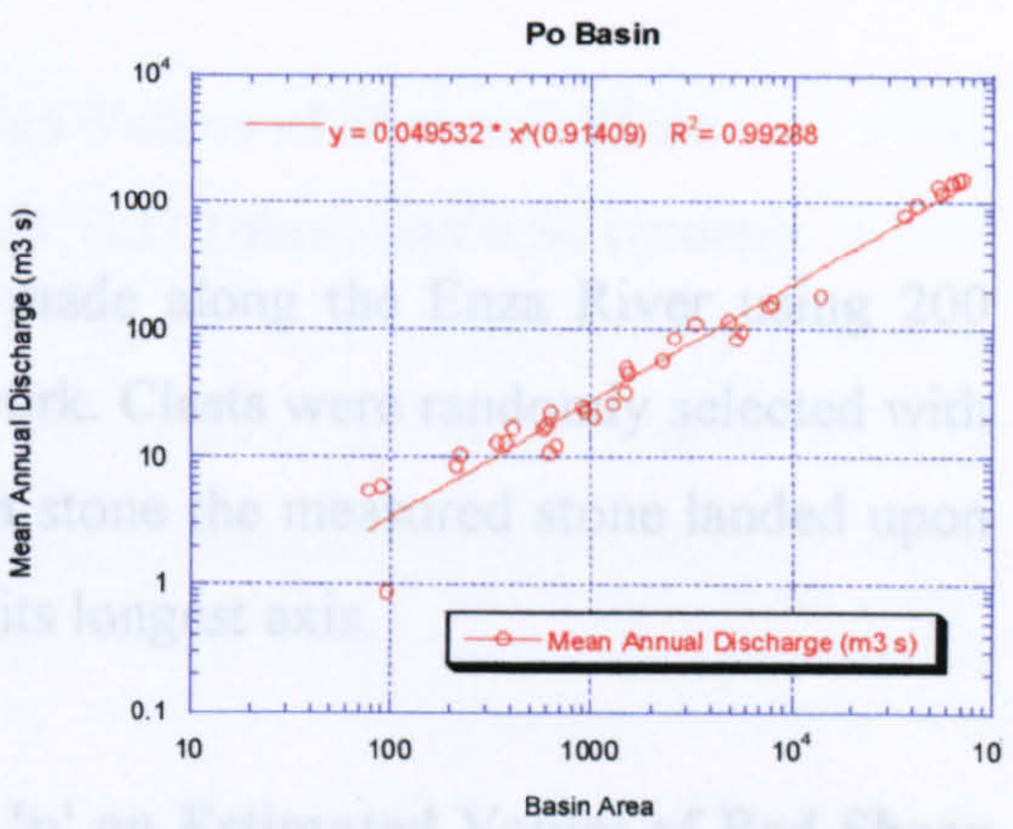

Figure 2.33 Basin Area Versus Mean Annual Discharge (after Cati, 1983)

2.6.4.5 *Basin Area and Channel Depth*

Leopold and Maddock (1953) showed that basin area and channel depth can be related through using a power law relationship. Following their work, Talling (in review) combined equations 2.6 and 2.8 to provides the following relationship,

(2.9) $d = {}_zA^p$,

Where $p = \alpha f$ and p ranges from 0.21 to 0.36. Measurements of channel depth along the Enza River were made based upon equation 2.9 with basin area at stations along the channel network being calculated from a 230 metre digital terrain model (Reichenbach *et al.*, 1993). Work by Rigon *et al.* (1994) in which numerical models are used to simulate the evolution of river networks (see Section 2.6.7) used a similar power law relationship between channel depth and basin area, with the exponent p having the value 0.5. This value is somewhat lower than those estimated from other data (for example, Leopold and Maddock, 1953), and hence this study will both use Rigon *et al.*'s (1994) exponent of 0.5, as well as test the outcome of varying values of p on bed shear stress calculations and the critical dimensionless shear stress values it predicts.

2.6.4.6 Grain Size

Surface grain size calculations were made along the Enza River using 200 clast counts at 20 sites along the channel network. Clasts were randomly selected with the choice being made depending upon which stone the measured stone landed upon when thrown. Each clast was measured along its longest axis.

2.6.5 Effects of Varying Value of Exponent 'p' on Estimated Values of Bed Shear Stress and Dimensionless Critical Shear Stress

Bed shear stress and the dimensionless critical shear stress were calculated as outlined in equations 2.3 and 2.4. Results shown in Figure 2.34 indicate that variations in the value of the exponent p used to calculate channel depth from basin area along the Enza has a significant effect on estimated values of τ_*, such that the higher exponent of 0.5 used by Rigon *et al* . (1994) produces values of τ_* of between 0.073 in the headwaters and 2.15 in the lower parts of the Enza. By comparison, using an exponent of 0.21 produces corresponding values of 0.04 and 0.36. Whilst the value of τ_* of 0.073 calculated for the upper Enza is within the range of values previously

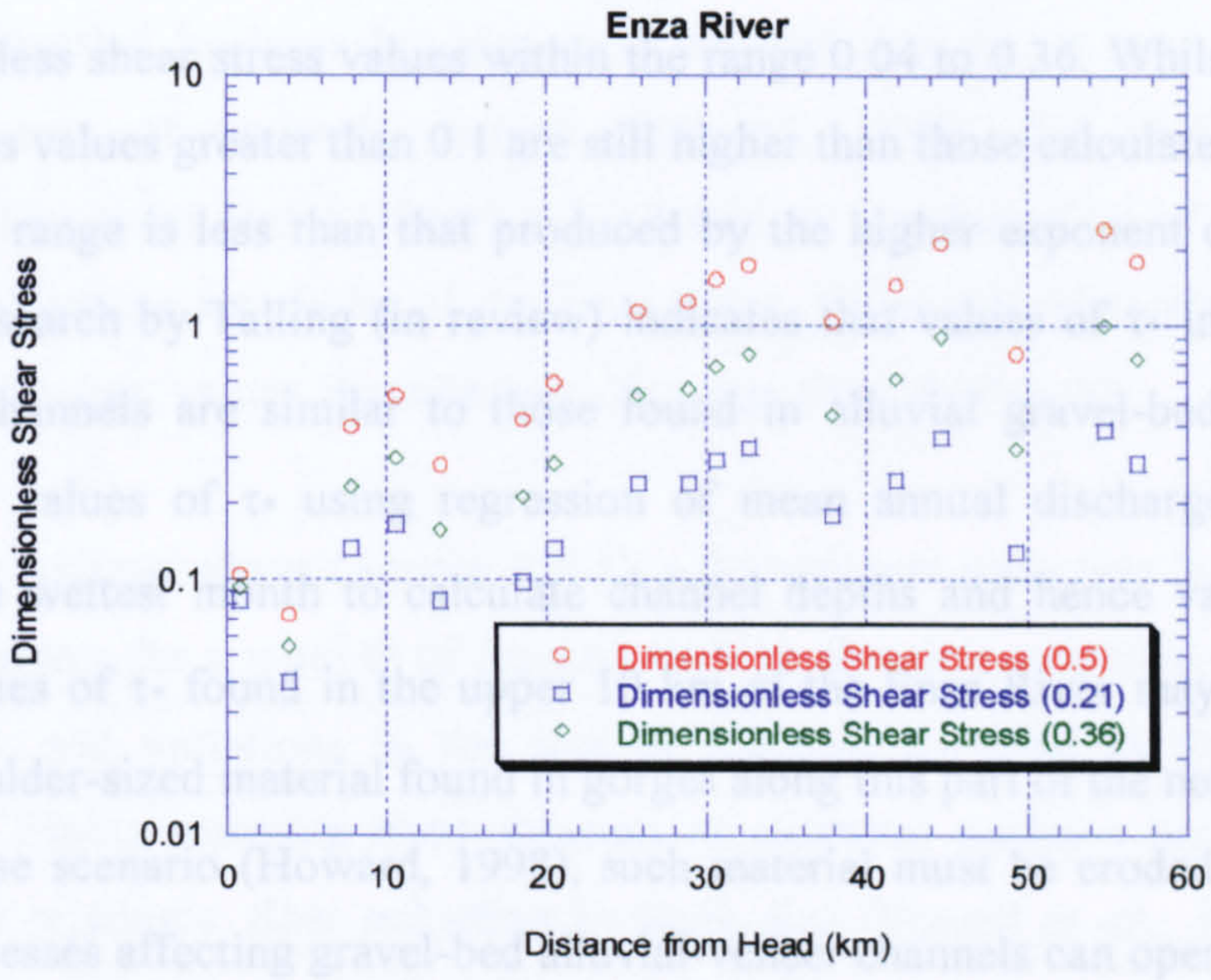

Figure 2.34 Variation in Calculated Values of Dimensionless Shear Stress, With Exponent 0.5 (red), 0.21 (blue) and 0.36 (green)

documented as existing for gravel-bed alluvial channels (for example, Dade and Friend, 1998), values further downstream increase quickly such that less than 7 km from the headwaters, dimensionless shear stresses are at values of 0.3 and above. By comparison, calculated values of $\tau*$ based on an exponent value of 0.21 produce dimensionless shear stress values within the range 0.04 to 0.36. Whilst dimensionless shear stress values greater than 0.1 are still higher than those calculated for gravel-bed rivers, the range is less than that produced by the higher exponent of Rigon (*et al.*, 1994). Research by Talling (in review) indicates that values of $\tau*$ in alluvial-veneer bedrock channels are similar to those found in alluvial gravel-bed rivers. Talling calculated values of $\tau*$ using regression of mean annual discharge and discharge during the wettest month to calculate channel depths and hence values of τ_o. The lower values of $\tau*$ found in the upper 10 km of the Enza River may result from the coarse boulder-sized material found in gorges along this part of the network. Seen as a special case scenario (Howard, 1998), such material must be eroded in place before those processes affecting gravel-bed alluvial-veneer channels can operate

These results indicate that using DTM-derived basin area calculations along the Enza River to establish estimates of bed shear stress and dimensionless critical shear stress may result in over-estimates of both values. It is suggested that the lower exponent provided by empirical studies of 0.21 or an even lower value be used in future studies. However, despite this observation, general downstream trends in values of the both bed shear stress and dimensionless shear stress parameter can still be assessed.

2.6.6 Downstream Trends in Bed Shear Stress and Dimensionless Shear Stress

Figure 2.35 shows that bed shear stresses along the Enza River generally have higher values in the uppermost basin (< 10 km from headwaters) than further downstream. This is characterised by values of around 100 N/m^2 (assuming p = 0.21) in the uppermost basin and values closer to 50 N/m^2 for the majority of the channel downstream. Grain size measurements along the Enza (Figure 2.36) show that variations in bed shear stress are mirrored by variations in grain size. Whilst the middle to lower reaches of the Enza are characterised by near constant grain size values of around 60-70 mm, the upper 6 km of the Enza River is characterised by a

much larger mean grain size of around 1000 mm. A sharp decrease of an order of magnitude in grain size is thus observed at a distance of around 6-7 km from the Enza's headwaters. Larger mean grain sizes in the uppermost Enza River are accompanied by decreased values of dimensionless shear stress. As outlined above, channels mantled by large boulder-sized material may be in need of treatment as 'special' cases of bedrock channel (Howard, 1998). By contrast, values of dimensionless shear stress (Figure 2.37) based on a value of 'p' of 0.21 show little variation along the remainder of the Enza River. Given the relatively high degree of scatter in the data, values characteristically range from 0.08 to 0.3.

As outlined above (Section 2.6.3), a downstream reduction in mean grain size occurs in rivers for a number of reasons such as abrasion, selective entrainment and deposition, and variations in the size of material supplied to the channel from hillslopes. Fining resulting from abrasion of sediment particles has been shown to result in a relatively slow reduction in grain size (Powell *et al.*, 1998), whilst the transition seen in the upper Enza occurs rapidly. Results of modelling by Pizzuto (1995; 1992), which explored the nature of controls on downstream fining of river sediment, indicated that variations in grain size are most likely to occur as a result of changes in bedrock lithology surrounding the channel, with the exposure of more resistant lithologies resulting in higher mean grain sizes. Examination of lithological patterns and field observations along the Enza River indicate that the upper 7-8 km of the basin is dominated by outcrops of Miocene turbidites of the Tuscan formation, whilst the middle to lower basin demonstrates outcrops of Pliocene mudstones and sandstones. The latter are much more erodible than the former, as demonstrated by both the morphology of the hillslopes (see Chapter 5) and the mean grain size of sediment along the channel network. Thus field observations made in the Northern Apennines support Pizzuto's (1995; 1992) view that grain size variations are largely controlled by changes in bedrock lithology.

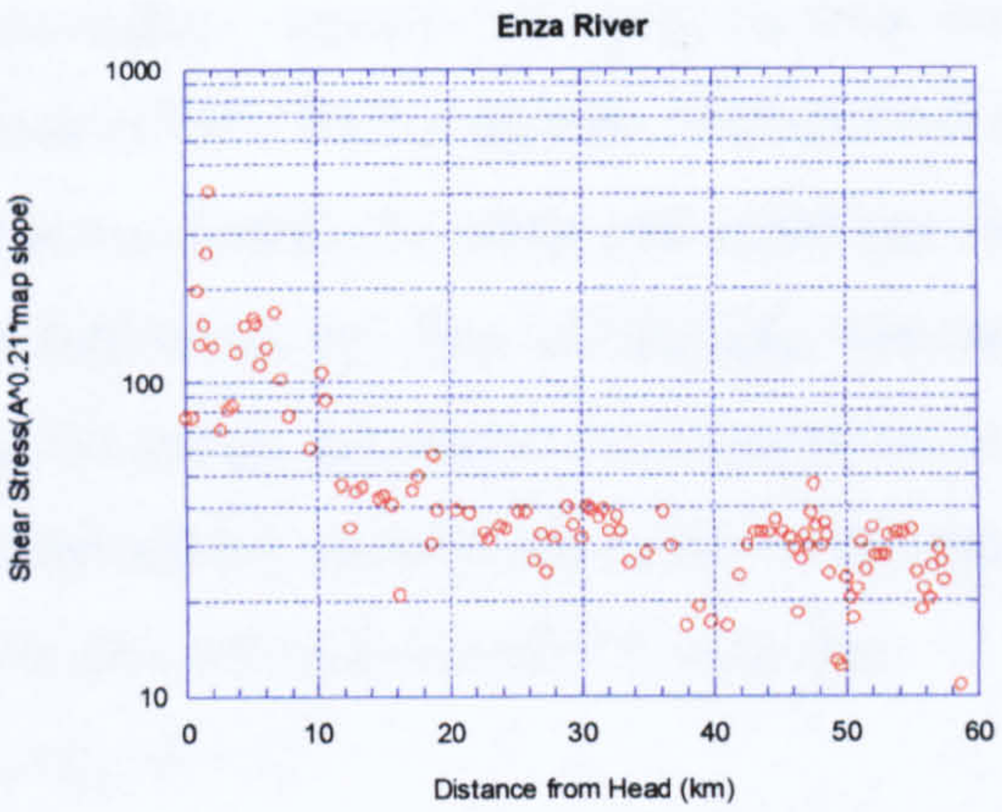

Figure 2.35 Distribution of Bed Shear Stress Along the Enza River

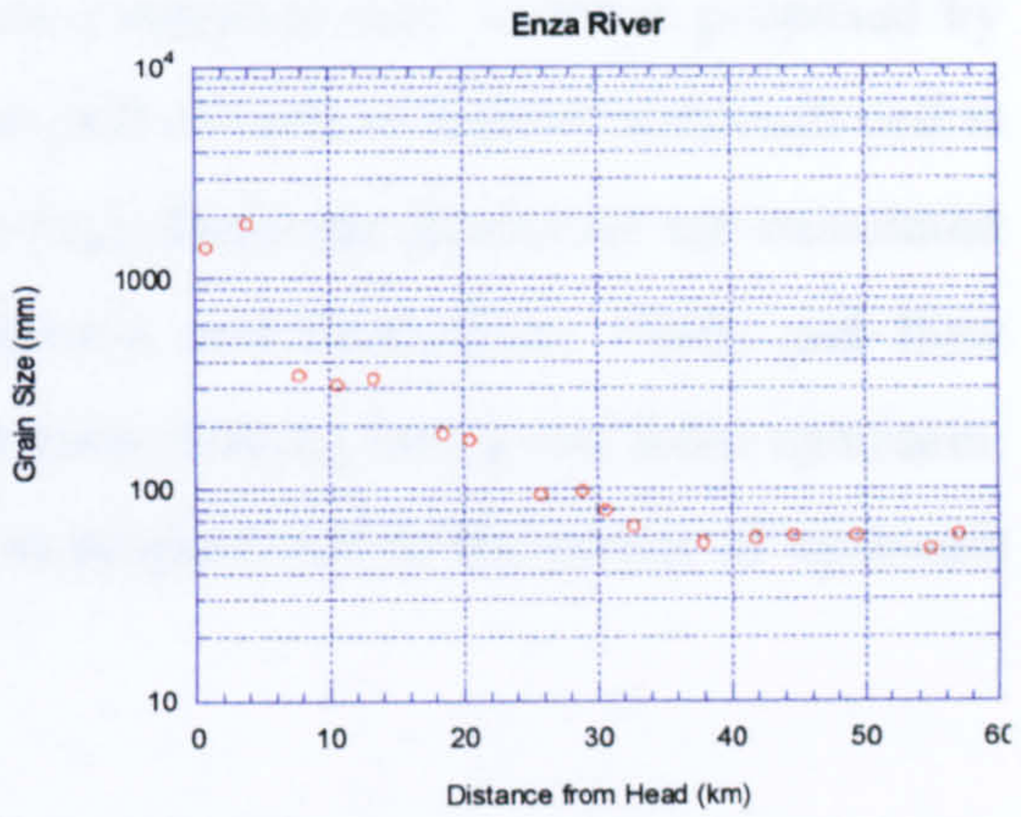

Figure 2.36 Grain Size Variation Along the Enza River, Italy

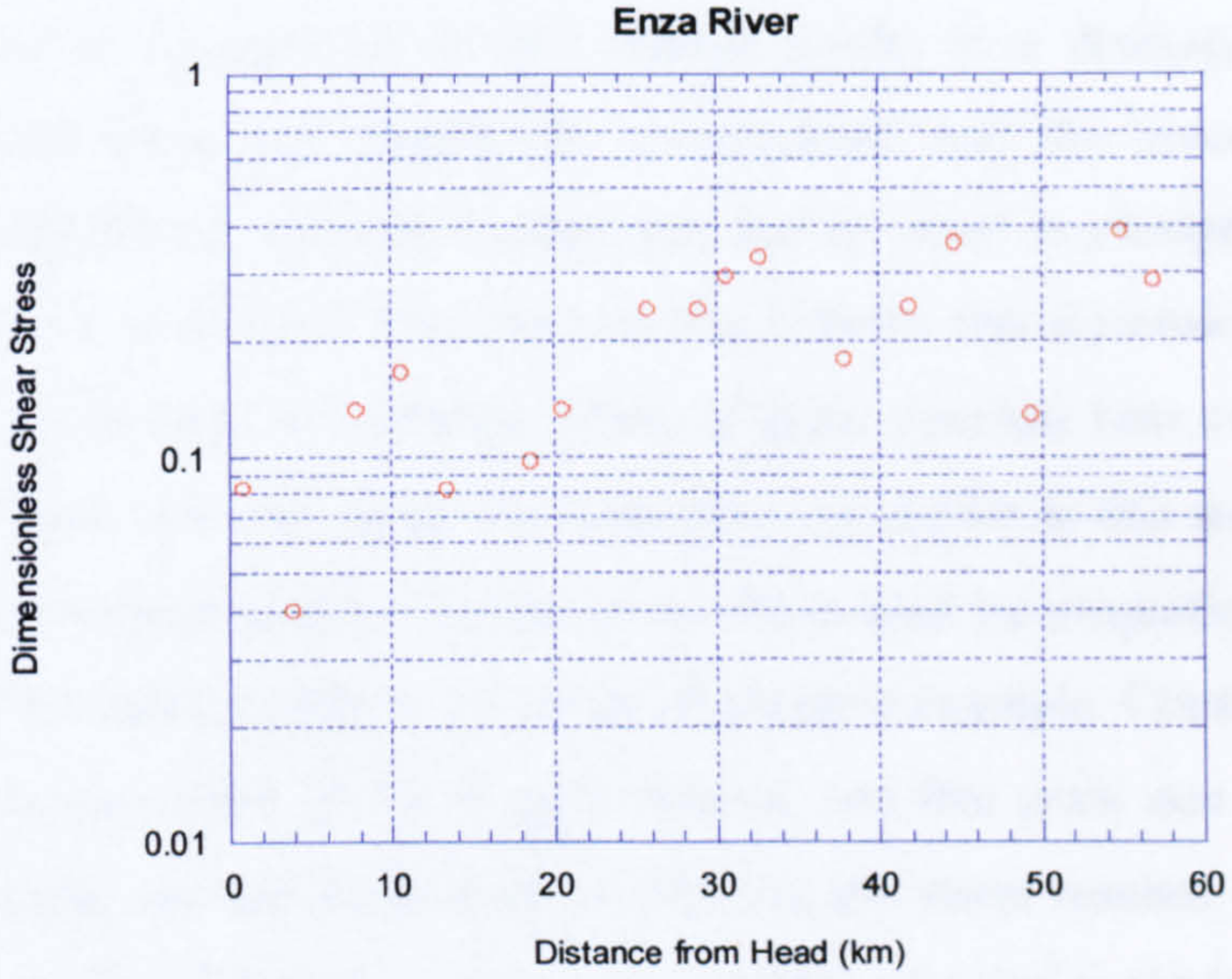

Figure 2.37 Distribution of Dimensionless Shear Stress Along the Enza River, Italy

2.6.7 Implications for Modelling of Channel Networks

A recent numerical model (Rigon *et al.*, 1994) has been developed which successfully reproduces many channel network properties such as those proposed by Hack (1957). In this model, a two dimensional grid of cells is defined and each cell is given an initial elevation and threshold value (τ_{th}). Drainage directions are calculated as following the line of steepest descent (Jensen and Domingue, 1988) and flow accumulation calculated as proportional to all cells flowing into a cell from upstream. In the model, channel depth (d) is calculated as proportional to the power of upstream area (A) with a value of 0.5, such that

(2.10) $d = A^{0.5}$.

Shear stress (τ) is calculated as the product of local slope and channel depth in each cell, such that

(2.11) $\tau = Sd = SA^{05}$.

If the value of τ_{th} exceeds that of τ, the elevation of that cell is reduced until the values are equal. Once all cells are at this critical stage, the system is peturbed by adding elevation to one cell. If this change results in a drainage diversion, flow directions and areas and depths are re-calculated and the process repeats. This continues until further changes in elevation fail to result in changes in shear stress, such that $\tau_{th} = \tau$ in all cells. Previous work has shown that dimensionless shear stress (calculated as the ratio of bed shear stress to grain size) has near constant values for gravel-bed rivers and also along the Enza River as shown in this study. Thus, if $\tau*$ is constant, downstream changes in bed shear stress must be proportional to changes in grain size. This can be outlined by means of a simple example. Consider that values of $\tau*$ have a constant value of 0.2 along a channel, and that grain size varies from 1000 mm in the upper reaches of the river to 10mm in the lower reaches. Calculated values of τ thus vary from 200 N/m^2 in the upper reaches to 2 N/m^2 in the lower reaches.

Thus, whilst Rigon *et al.*'s (1994) model successfully reproduces the fundamental character of fluvial systems (Talling, in review) as indicated by near constant values of $\tau*$ calculated for natural systems, work presented here indicates that threshold values of τ_{th} used by Rigon *et al.* (1994) should be adapted to take account of bed grain size variations which are shown to strongly influence bed shear stress along the Enza River. Additionally, values of τ_{th} need to take account of the 'special'

case scenario in which the channel bed is mantled with large boulder-sized material. Under such conditions, dimensionless shear stress values are lower than those found in both gravel-bed and sand-bed alluvial channels. Lower values of the exponent p are required to reduce the shear stress values estimated in channels where boulder-mantling exists. Changes in lithology therefore directly affect the size of material supplied to the channel, which, in turn, affects the processes operating on the channel. Rigon *et al.*'s (1994) model must therefore be adapted to incorporate the effects of lithological variation on bed grain size and shear stress, especially in areas mantled by large boulder-sized material.

CHAPTER 3

MODELLING THE SPATIAL DISTRIBUTION OF EROSIONAL PROCESSES WITHIN OROGENIC MOUNTAIN BELTS

3.1 INTRODUCTION

It has long been known that the morphology of mountains represents the interplay of geomorphic and crustal processes (e.g. Arrowsmith *et al.*, 1996; Strahler, 1950), and that their development is influenced by the interactions of climate, tectonics, isostasy, and erosion and deposition (Masek *et al.*, 1994). Upland mountain belts consist of an interlinked series of ridges, valleys and, sometimes, plateaus. Of these features, it is the hillslopes extending from the drainage divide to the stream channels which are of interest in this and the following two chapters. Prior to the 1950s, studies of slope form and process tended to focus on attempting to develop ways of reconstructing the history of mountain belts based on the slope forms it currently exhibited (for example, Davis, 1892). Only in the last three decades has research placed more emphasis on the processes operating upon slopes and how these affect form (Summerfield, 1991). This increased awareness has resulted not only from a general post-war interest in process studies and from work carried out by engineers concerned with slope stability analyses, but also from a revised interest in the interactions of tectonics and topography (for example, Basin Research, vol. 11; Journal of Geophysical Research, vol. 99). Research has indicated that the spatial distribution of erosional processes within orogens affects the large scale distribution of crustal stresses beneath the belts as the mass flux of material exiting the uplands and being deposited at lower elevations unloads and loads the crust (Koons, 1995). Broad scale variations in erosional processes are also believed to impact upon global climatic trends, influencing events such as the yearly Indian Monsoon (Raymo and Ruddiman, 1992). This chapter provides an outline of how hillslopes evolve and by what processes they are affected. The role of intrinsic, for example lithology, and extrinsic controls on hillslope form are also examined. Finally, a brief assessment of the implications of large scale process studies such as those in this thesis are outlined.

3.2 MODELLING THE EVOLUTION OF MOUNTAINOUS REGIONS

3.2.1 Mountain Belt Erosion

Recently, there has been increasing acknowledgment of the importance of surficial erosion and topographic development in the dynamic evolution of mountain belts (Zhou and Stuwe, 1994; Masek *et al.*, 1994) and of the strong coupling between tectonic and geomorphic processes (Howard *et al.*, 1994). As this awareness has grown, it has become apparent that a knowledge of the factors determining the spatial distribution of erosional processes, and thus the supply of sediment to basins from orogens, is fundamental if we are to better comprehend the ways mountains grow and evolve (Montgomery, 1994; Summerfield and Hulton, 1994).

The spatial distribution of erosional processes within an orogen has a number of implications for studies at large spatial and temporal scales. The importance of erosion in orogenic evolution has been highlighted by Koons (1989), who developed ideas of coupling between tectonics and topography in fold-thrust belt mechanics (see also Kooi and Beaumont, 1994). The style of deformation adopted by a mountain belt, the spatial distribution of stresses in orogens, uplift patterns and even climate, have been suggested to be affected by erosional process variability. Deformation within orogens is controlled by a number of factors, amongst them large-scale process variability (Dahlen and Suppe, 1988; Mather, 1992). By changing the gravitational component of stress within a mountain, uplift trajectories are drawn towards the areas of maximum denudational unloading (Beaumont *et al.*, 1992; Hoffman and Grotzinger, 1993).

The role of surficial denudation in the complex feedbacks between erosion, uplift and climatic change has received considerable attention over the last decade (Montgomery, 1994; Molnar and England, 1990). As erosion of bedrock incises valleys, increasing local relief, the resulting isostatic rebound uplifts local mountain peaks, and has been suggested to result in climatic changes associated with the Indian Monsoon (Molnar *et al.*, 1993). The increased relief in such areas is believed to increase rates of chemical denudation, drawing atmospheric carbon dioxide into the sedimentary system, reducing global levels of the atmospheric gas and cooling global climates (Raymo and Ruddiman, 1992).

The role played by the spatial arrangement of erosion in the emplacement and morphology of orogens is, however, only one part of a much larger picture. Denudation of mountains involves the total removal of material from the mountain system to the sedimentary system. Thus the factors controlling erosion within mountains not only control their morphology (Braun and Sambridge, 1997), and, to a lesser extent, their tectonic development (Koons, 1989; Chase, 1992), but also the input of material to the sediment routing system (Hovius, 1995).

3.2.2 Sediment Routing in Orogens

Many factors affect the sediment supply out of mountains, including lithology, drainage basin size and characteristics, tectonic structures and erosional process variation (Tucker and Slingerland, 1996). Recent research suggests that deep, bedrock-involved (Hovius *et al.*, 1997; Densmore *et al.*, 1998a, 1998b) and shallow, regolith landsliding (Seidl and Dietrich, 1992) mechanisms may dominate sediment transport in steep, mountainous areas, with the sediment efflux from such areas being largely proportional to such activity. These mass movement processes not only determine where material enters the sediment system, but their magnitude and frequency also determines the rate and amount of material too (e.g. Allen and Hovius, 1998). Additionally, the removal of material by landsliding processes exerts a strong influence on the topography of the area through the feedbacks and links suggested above. The following chapter examines whether such changes in topographic form resulting from dominant hillslope processes can be determined from large scale DTM analyses, thus providing a broad scale picture of process dominance across orogens. Such macro-scale process variability mapping thus has implications for both the evolution of the actual orogenic belts, and also for the sediment flux out of such systems. The flux of sediment from mountain regions is often reflected in the gross morphology of an area. Areas of net accumulation exist where large, upland plateaus, such as the Andean Altiplano (Masek *et al.*, 1994), exist. Whilst where steady-state ranges are believed to be in existence, for example in the New Zealand Southern Alps (Hovius *et al.*, 1997), the fluxes in and out are roughly equal.

The sediment supply from hillslope and fluvial channel incision exerts a first order control on sedimentary facies distributions within alluvial fill basins (Hovius

and Leeder, 1998). As discussed above, the sediment supplied to a fluvial network depends upon a large number of factors, including uplift and precipitation rates, lithological and structural variability, and the morphological nature of the drainage basin. Whilst many studies have tended to focus on the correlations between the determinant variables and denudation rates (for example Summerfield and Hulton, 1994), there is a real need to understand sediment flux variation in terms of the tectonic, climatic and lithological controls. By improving our comprehension of the roles these variables play, and how they interact, we can better interpret sedimentary sequences of past environments with more certainty (van der Beek and Braun, 1998).

3.3 MORPHOLOGY OF HILLSLOPES AND PROCESSES OF HILLSLOPE EROSION

A variety of classification systems exists concerned with the nature of erosional processes. Generally, however, hillslopes are affected by two types of erosional process: mass movement processes and those involving water in the transport of material (Summerfield, 1991). Mass movement processes are those involving the downslope movement of material under the influence of gravity without the assistance of moving water, air or ice (Summerfield, 1991), whilst processes such as rainsplash erosion are directly influenced by the action of flowing water. The former group includes a huge range of processes (see, for example, Varnes, 1958 for an extensive review), including creep, flow (solifluction, debris flows), slides (translational and rotational), heave, fall and subsidence. Many mountainous regions in the USA (e.g. Schmidt and Montgomery, 1995) and Italy (e.g. Sowter and Talling, 1998) exhibit steep ridge and valley topography with planar rectilinear hillslopes. Such planar slopes have also been noted by Howard (1997) in his study of badlands, where such topography was defined as 'ridge and gully'. Despite being observed in a variety of locations throughout the Apennines (field observations, 1996, 1997) and the USA (Densmore *et al.*, 1998; Anderson, 1994), there are no studies which systematically determine the controls on such hillslope form or what controls their spatial distribution. Studies also differ in their interpretations of what types of erosional process affect such hillslopes. Proposed mechanisms include diffusional processes (e.g. Roering *et al.*, 1999, 1998; Rosenbloom and Anderson, 1994), shallow regolith landsliding (e.g. Dietrich *et al.*, 1993) and bedrock landsliding (e.g. Densmore *et al.*, 1998a).

3.3.1 Slope Diffusion

Hillslopes can be affected by a number of diffusional processes, including rainsplash, animal burrowing, cyclical wetting and drying of soil, freeze/thaw cycles and tree throw (Roering *et al.*, 1999; Carson and Kirkby, 1972). These processes act to detach and mobilise the uppermost layers of soil regolith, which then move the soil downslope (Heimsath *et al.*, 1997). One of the first studies of the effects of diffusional processes on hillslope morphology was that of Gilbert (1909). In this study, Gilbert asserted that for the interfluves between ridges to be lowered, transport rates must increase with distance from the divide. In order to accomplish increased transport downslope, slope gradients were required to increase, resulting in convex slope profiles (Figure 3.1) (Summerfield, 1991; Roering *et al.*, 1999). On soil-mantled hillslopes, energy supplied by disturbances such as rainsplash and animal burrowing is dissipated by the frictional and gravitational forces acting on the load (e.g. Jaeger and Nagel, 1992). In general, diffusive processes tend to smooth the landscape upon which they act (Montgomery and Dietrich, 1989).

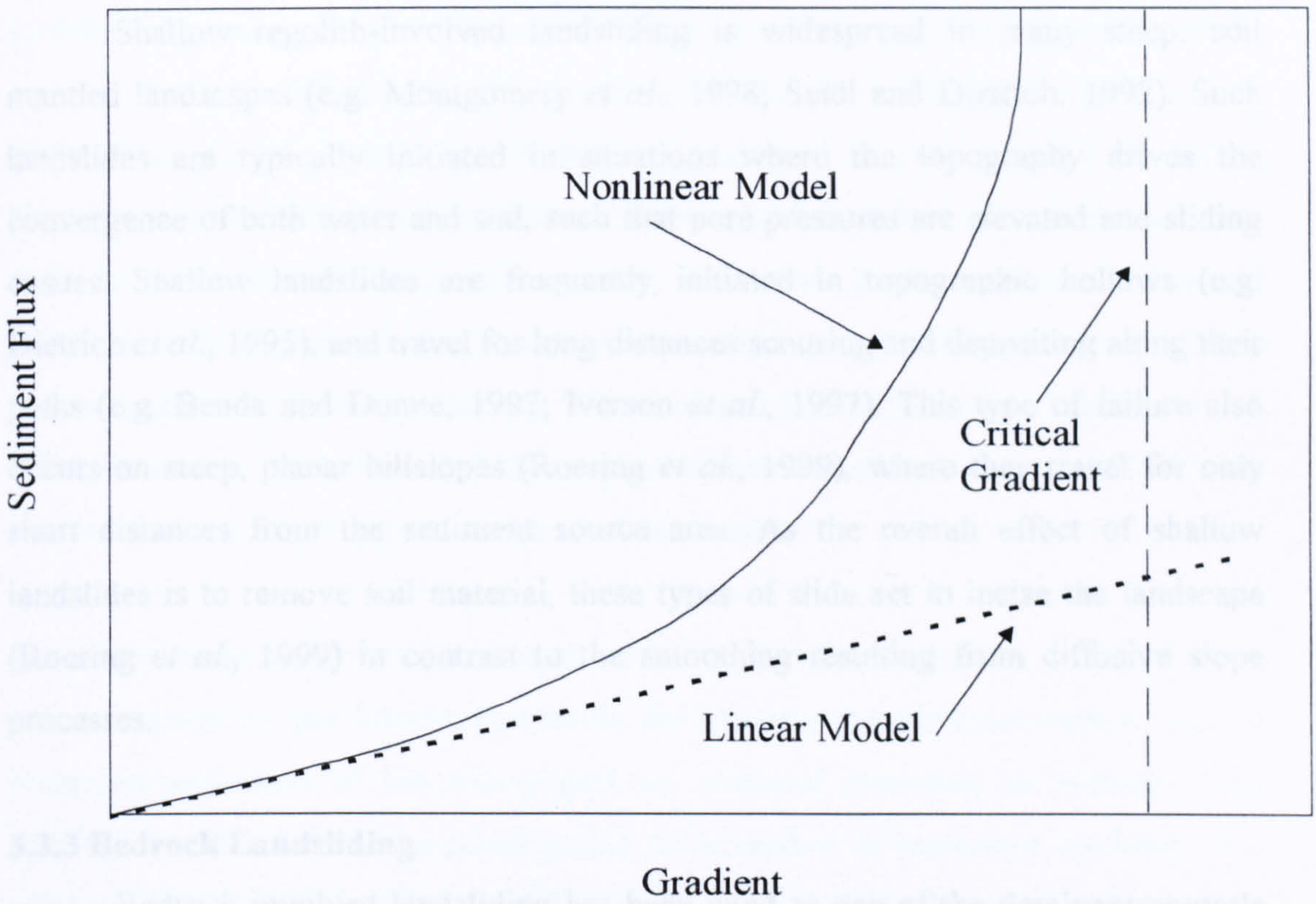

Figure 3.1 Linear Slope Diffusion and its Relationship to Sediment Flux
(After Roering *et al.*, 1999)

3.3.2 Regolith Landsliding

Shallow regolith-involved landsliding is widespread in many steep, soil mantled landscapes (e.g. Montgomery *et al.*, 1998; Seidl and Dietrich, 1992). Such landslides are typically initiated in situations where the topography drives the convergence of both water and soil, such that pore pressures are elevated and sliding ensues. Shallow landslides are frequently initiated in topographic hollows (e.g. Dietrich *et al.*, 1995), and travel for long distances scouring and depositing along their paths (e.g. Benda and Dunne, 1997; Iverson *et al.*, 1997). This type of failure also occurs on steep, planar hillslopes (Roering *et al.*, 1999), where they travel for only short distances from the sediment source area. As the overall effect of shallow landslides is to remove soil material, these types of slide act to incise the landscape (Roering *et al.*, 1999) in contrast to the smoothing resulting from diffusive slope processes.

3.3.3 Bedrock Landsliding

Bedrock involved landsliding has been cited as one of the dominant controls on landscape evolution in the north-western Himalayas (Burbank *et al.*, 1998), the Basin and Range province (Densmore *et al,* 1997; 1998a, 1998b), the Southern Alps (Hovius *et al.*, 1997) and the Santa Cruz Mountains (Anderson, 1994; Schmidt and Montgomery, 1995). Erosion rates are typically high for areas experiencing bedrock sliding, with those in the Southern Alps ranging from 5-12 mm/a (Hovius *et al,* 1997), whilst in the Bolivian Andes rates range from 10-14 mm/a (Blodgett *et al.*, 1996). Despite widespread agreement on the importance of bedrock slides in sediment mass transfer and landscape evolution in mountainous regions, there appears to be confusion as to what 'bedrock sliding' actually involves and what forms of mass movement it incorporates.

This study adopts the terminology of Densmore *et al.* (1998a, p.15207), who defines bedrock sliding as "... a mass movement that involves intact or unweathered bedrock rather than being confined to a mobile regolith layer". Bedrock slides therefore differ from shallow slides of soil (e.g. Dietrich *et al.*, 1992; 1993), and debris flows (e.g. Seidl and Dietrich, 1992). The form of terrain affected by bedrock slides would also seem to be a matter of confusion. Whilst Densmore *et al.* (1997) cite evidence of sliding of competent sandstones in the Van Duzen Basin (see Kelsey,

1980), the large-scale form of topography in the area is largely smoothed by earthflow-type processes, which largely affect the surface layers of soil and rock. In contrast, bedrock slide topography is affected at deeper levels, resulting in largely linear hillslopes (e.g. Anderson, 1994), such as those seen in parts of the Italian Apennines around Bologna (Sowter *et al.*, 1997). Although both rotational flows and slides can affect bedrock (e.g. Carrara *et al.*, 1995), here the focus in on translational slides of bedrock, transporting material downslope into the fluvial system. These slides result in prominent rectilinear hillslopes and triangular facets (e.g. Anderson, 1994; Densmore *et al.*, 1998a), forming the distinctive rectilinear topography which is examined in the following two chapters of this thesis.

3.4 MODELLING SEDIMENT TRANSPORT IN MOUNTAINOUS REGIONS

Interest in the forces responsible for shaping mountainous regions and an increased awareness of the role played by erosional processes in mountain belt development has led to the development of a number of landscape evolution and surface process models (Kooi and Beaumont, 1994, 1996; Braun and Sambridge, 1997; Densmore *et al.*, 1998a; van der Beek and Braun, 1999). These models attempt to capture the coupling between crustal and surficial processes with the interactions of fluvial and hillslope processes (for example, Willgoose *et al.*, 1991) and the development of large scale tectonic frameworks (for example, Lifton and Chase, 1992). LEMs and SPMs differ both in their level of sophistication (compare, for example Chase, 1992 and Willgoose *et al.*, 1991) and scale. Differences in the latter are apparent when comparing models such as Howard's (1994) model of drainage basin evolution with Beaumont *et al.*'s (1992) model of large scale orogenic development. Early SPMs, such as Koons' (1989) Southern Alps framework combined the effects of erosion and tectonics in a model of orogenic evolution. Subsequent research (for example Hovius and Leeder, 1998) has tended to emphasise the importance of surficial mass redistribution on mountain belt development, and, as such, later models have attempted to incorporate the effects of such movement in their simulations.

LEMs combining the effects of both fluvial and hillslope processes frequently employ transport laws relating the former to a slope-discharge product (see chapter 2), whilst the latter are often modelled as proportional to slope gradient (for example

Willgoose *et al.*, 1991; Kooi and Beaumont, 1994). Diffusion and mass wasting processes, such as creep, flow, fall and sliding are incorporated into equations in which transport is proportional to changes in slope gradient (for example Koons, 1989; Howard, 1994). The way in which these processes are incorporated in such simulations is crucially important if they are to accurately model how orogens evolve. As outlined above, it has been proposed that linear ridge-type topography results from a variety of diffusive and mass wasting processes (for example Roering *et al.*, 1999; Sowter and Talling, 1998). However, it is not just agreement on linear ridge process which is lacking at present. The transport laws operating in areas of such steep, planar terrain also vary as a function of the erosional processes proposed to be operating. As such, a variety of linear and nonlinear transport functions have been proposed to simulate how sediment moves on such planar hillslopes. Previous studies utilising hillslope gradient analyses have shown how both linear and nonlinear functions of slope gradient describe hillslope evolution in different field settings (Gilbert, 1909; Burbank *et al.*, 1996; Roering *et al.*, 1999). Chapter 4 provides such an analysis of the Santa Cruz Mountains in California, allowing for an assessment of both types of transport function in defining sediment transport in an area dominated by linear hillslopes.

3.4.1 Linear Sediment Transport

Early workers such as Gilbert (1909) tended to emphasise the role played by hillslope gradient in sediment transport on slopes in mountainous regions. Subsequently, a number of researchers have related the rate of hillslope sediment transport to slope gradient through the diffusion equation (see Nash, 1980 for examples) shown below

(3.1) $\delta h/\delta t = k\,[\delta^2 h/\delta x^2 + \delta^2 h/\delta y^2]$

where h is height (m), t is time, k is a diffusion coefficient (L^2T^{-1}), and x and y are space dimensions (Martin and Church, 1997). The diffusion equation assumes transport-limited conditions such that there is infinite weathering of regolith and bedrock on upper hillslopes which, given sufficient hillslope gradients, will be transported downslope. Research in certain areas, for example the coastal marine terraces of the Santa Cruz Mountains (Chapter 4) (Rosenbloom and Anderson, 1994), indicate that linear diffusion laws accurately represent the relationship between

hillslope gradient and sediment transport. Thus SPMs and LEMs adopting the linear diffusion equation (for example Willgoose *et al.*, 1991; Kooi and Beaumont, 1994) may adequately simulate landform development in certain situations.

3.4.2 Nonlinear Sediment Transport

Recognition from field studies in scarp environments (Andrews and Bucknam, 1987), the Oregon Coast Ranges (Roering *et al.*, 1999), and the Queen Victoria Islands of British Columbia (Martin and Church, 1997) indicate that nonlinear relationships may exist between slope gradient and sediment transport rates. Hillslope evolution in the Oregon Coast Ranges by deep-seated mass movements is proposed to result from nonlinear threshold limited instabilities (Roering *et al.*, 1997), which imply nonlinear transport mechanisms. Under such conditions, the linear diffusion equation and models simulating hillslope evolution based upon it are seen as inadequate and in need of adjustment.

A number of models do, however, attempt to incorporate nonlinear transport laws in their hillslope evolution algorithms (for example, Anderson, 1994; Howard, 1997). Models such as Anderson's (1994) of the Santa Cruz Mountains simulates hillslope evolution as occurring by linear diffusion below a critical threshold angle, with rapid slope lowering occurring by landsliding once this threshold is breached (Figure 3.2). Upon breaching the slope limit, sediment transport ensues and slopes are reduced to stable values lower than the threshold value (see also Arrowsmith *et al.*, 1996). These models produce the distinctive rectilinear hillslopes observed in the Northern Apennines (Chapter 5). Nonlinear transport mechanisms have been proposed to be valid for a variety of process conditions, from creep and shallow landsliding dominated (Roering *et al.*, 1999; Martin and Church, 1997) to deeper, bedrock-involved landsliding (Hovius *et al.*, 1998; Densmore *et al.*, 1998b).

Thus whilst a number of SPMs and LEMs may be capable of producing realistic-looking topography (for example Willgoose *et al.*, 1991), they are frequently based upon poorly defined and validated transport laws and oversimplified algorithms (van der Beek and Braun, 1998). By better understanding the interactions of topography and the processes of erosion which act upon it, we may be able to derive more accurate simulation models with which to evaluate flux variation and landform

evolution in orogens. Data from real world examples, such as those presented in Chapters 4 and 5, are vital is computer simulations of such processes are to be improved in the future.

Having outlined the various mechanisms proposed to be operating in mountainous terrain around the world, the following two chapters examine two case studies of areas in which steep, linear hillslopes are present. In the first, Chapter 4 looks at terrain variation in the Santa Cruz Mountains of California, USA, and provides an insight into 'topographically fingerprinting' linear hillslopes using a 30 metre digital terrain model (DTM). In the second study, the work in Chapter 5 looks at the interactions of erosional processes and terrain form in the Italian Apennines, and how these are influenced by the external lithological and tectonic regimes operating in the Northern Apennines. As outlined above, the spatial distribution of erosional processes within orogens has implications for its long term growth and development (Zhou and Stuwe, 1988). As rectilinear hillslopes dominate landscapes in a variety of mountainous settings , determining the long term processes responsible for their development and mapping their spatial distribution may allow for a large scale process mapping within orogens. At present, however, such predictions are hindered by two main factors. Firstly, as outlined above, there is little agreement on which processes are responsible for the development of such slopes. Secondly, despite their widespread occurrence, no previous studies have attempted to map their large scale spatial distribution. This thesis thus addresses both these issues, with Chapter 4 examining the latter issue and Chapter 5 looking at both terrain variation and the processes responsible for such differences across the Northern Apennines.

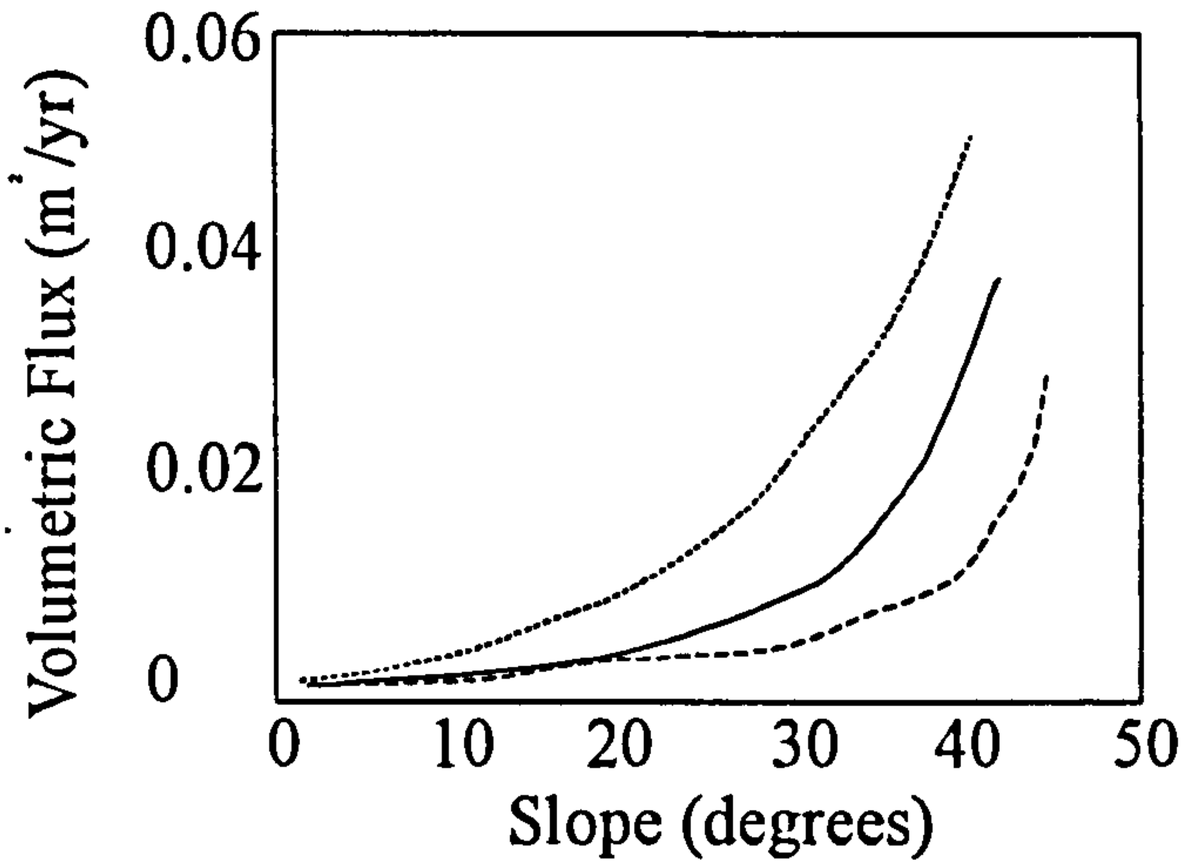

Figure 3.2 Critical Threshold Sliding (after Anderson, 1994). Solid and Dashed Lines Indicate Model Output After Simulating Diffusion at Low Slopes Angles and Nonlinear Landsliding Above Critical Threshold

CHAPTER 4

CHARACTERISING THE NATURE OF STEEP, LINEAR-RIDGE TERRAIN, SANTA CRUZ MOUNTAINS, CALIFORNIA, USA

4.1 INTRODUCTION

Strong links exist between erosional hillslope processes and the landscapes which result from them (e.g. Keller and Pinter, 1996). In areas where tectonic uplift rates are matched by rates of fluvial and hillslope erosion, hillslopes adjust rapidly to changes in rates of downcutting (Ellis *et al.*, 1999; Burbank *et al.*, 1996). Studies from tectonically active mountainous regions around the world indicate the widespread existence of steep, threshold linear hillslope terrain in areas such as the Basin and Range Province of Nevada, USA (Densmore *et al.*, 1997) and the Olympic Peninsula of Washington State, USA (Schmidt and Montgomery, 1995). Despite widespread agreement on the importance of surficial process distributions on mountain belt development (Section 3.2.1), at present there is both a lack of agreement on which processes are responsible for linear hillslopes and also what controls their distribution at large spatial scales. In the past, variations in factors such as bedrock lithology have been dismissed as of little importance to the gross scale morphology of orogens (e.g. Ahnert, 1970). However, more recent research has indicated the importance of such factors in controlling many aspects of terrain form (e.g. Meigs *et al.*, 1999). More large scale process studies are thus required, in order that these issues be better resolved at relevant scales of examination.

Surface process models (e.g. Tucker and Slingerland, 1996; Braun and Sambridge, 1998) provide a way of increasing our understanding of the ways in which surface and crustal processes interact. By simulating how landscapes evolve under changing conditions of factors such as water discharge, erosional process and sediment flux, they allow for an assessment of how these variables affect topographic evolution and the spatial distribution of erosion and deposition (Burbank and Pinter, 1999). However, despite growing acknowledgment of the importance of bedrock landsliding in the development of many upland areas (Densmore *et al.*, 1998a; Ellis *et al.*, 1999), few surface process models attempt to incorporate the mechanism into their algorithms (Densmore *et al.*, 1997). Previous models have attempted to incorporate

landsliding mechanisms into their simulations by applying artificially high diffusivity coefficients in modelling hillslope erosion (e.g. Koons, 1989). More recently, field observations (e.g. Martin and Church, 1997) have shown bedrock mass wasting to be a nonlinear function of slope gradient, implying that models utilising simple linear functions of slope gradient to model landsliding are inadequate. In response to such observations, some SPMs (e.g. Anderson, 1994; Tucker and Slingerland, 1996) have incorporated nonlinear slope sliding into their hillslope evolution parameters. Such models frequently apply a critical threshold slope angle, beyond which hillslopes fail and lower than which they remain stable. The values used in such modelling, however, remain largely without an empirically observed basis, and need to be better constrained by measurement and quantification of natural processes (Burbank and Pinter, 1999).

This study attempts to address the two main issues raised above, namely to determine the relevant threshold values to be used in SPMs looking at bedrock sliding mechanisms, and to assess the influence of bedrock variability on landscape scale morphology. This chapter thus addresses these issues by focusing on three primary aims:

1) To identify terrain parameters which are capable capturing the characteristic nature of linear ridge terrain.
2) To identify threshold values of slope and relief, characteristic of hillslopes dominated by bedrock sliding, suitable for constraining threshold sliding algorithms used in SPMs.
3) To assess the role played by bedrock variability in large scale terrain development.

The Santa Cruz Mountains in California were chosen to address these issues for a number of reasons. Firstly, independent field observations (Anderson, 1994; Schmidt and Montgomery, 1995) indicate the widespread occurrence of threshold linear ridge slope forms in many areas of the mountain belt. Secondly, field observations made in these studies have shown bedrock landsliding mechanisms to dominate slope evolution in the area. Thirdly, as with many other areas of the USA, a high resolution (30 metre spatial resolution) digital terrain model (DTM) of the Santa Cruz Mountains was freely available over the internet. In the future, 30 metre models

may be available for a large proportion of the globe resulting from current NASA missions (E. Fielding, pers. comm.), thus enabling this type of analysis to be performed across the World's larger orogens, such as the Himalayas and Andes. At present, however, the 30 metre DTMs available for the USA are of much higher resolution that those available for other countries such as the 230 metre model of Italy (Chapter 5; Reichenbach *et al.*, 1993). Finally, access to digital geological databases of the Santa Cruz Mountains provided by the USGS enabled an assessment of the role played by variations in bedrock lithology on large scale terrain form.

By applying a suite of terrain analysis algorithms (Appendix 2) to the Santa Cruz area, hillslopes should demonstrate at what values sliding appears to occur, thus enabling the identification of relevant slope and relief values to be used as critical input values to SPMs. In addition, by studying the nature of landscape properties which dominate areas of linear ridge terrain, predictions made by SPMS may also be tested using the same suite of parameters. In other words, SPMs should be capable of replicating the characteristic nature of landscape observed from DTM analysis. Finally, by examining the role played by bedrock variation on terrain form, an assessment of one of the factors controlling gross scale landscape form may be enabled. By improving surface process models in this way, we can gain a better understanding of the roles played by different surface processes in large scale mountain belt development. Thus by determining what processes controls the distribution of linear slopes within orogens, large scale process maps may eventually be derived from DTMs using terrain analysis.

4.2 TOPOGRAPHY AND TECTONIC SETTING OF THE SANTA CRUZ MOUNTAINS

4.2.1 Geography and Climate

The Santa Cruz Mountains form the California Coast Ranges from the Golden Gate on the northwest to the Pajaro River in the south-west, lying between the San Francisco Bay and Santa Clara Valley to the east and the Pacific Ocean to the west (Figure 4.1). The crest of Ben Lomond Mountain forms the high point in the west. This flat-topped mountain forms a natural drainage divide, to the east of which the San Lorenzo River and its tributaries dissect the topography (Anderson, 1994). The San Lorenzo River traces the Ben Lomond Fault, whilst the southwards flowing tributaries tend to traverse the northwest-southeast structural trend of the region. To the west of the Ben Lomond divide, drainages flow southward into the Pacific, cutting a series of steep sided canyons into the terraced southwestern slope of the mountain. The region generally has a cool-summer Mediterranean climate with moderately heavy rainfall in the winter months, and coastal fogs during the summer months (Clarke, 1981). Rainfall in the area varies considerably, from an average of 50-76 cm/a on the coast to greater than 150 cm/a on the slopes of Ben Lomond (Rantz, 1968).

4.2.2 Topography of the Study Areas

Inspection of the shaded relief map (Figure 4.1) portrays distinctive differences in the topographic characteristics of the Santa Cruz Mountains. To the west, the Pacific coastline runs south into Monterey Bay in the south-west of the image. Running in a north-west south-east direction, the San Andreas Fault system bisects the Santa Cruz Range. Anderson (1994 and Rosenbloom and Anderson, 1994) defines the area to the west of the fault as the 'northern mountains', and those to the east as the 'southern range'. For the purpose of this study, the mountains to the west will be defined as the Coastal Range, and those further east as the Central Range. The Coastal Range drains through several marine cut terraces (Rosenbloom and Anderson, 1994) before entering the Pacific Ocean, whilst those drainages flowing from the Central Range tend to terminate in large east-facing alluvial fans (Anderson, 1994).

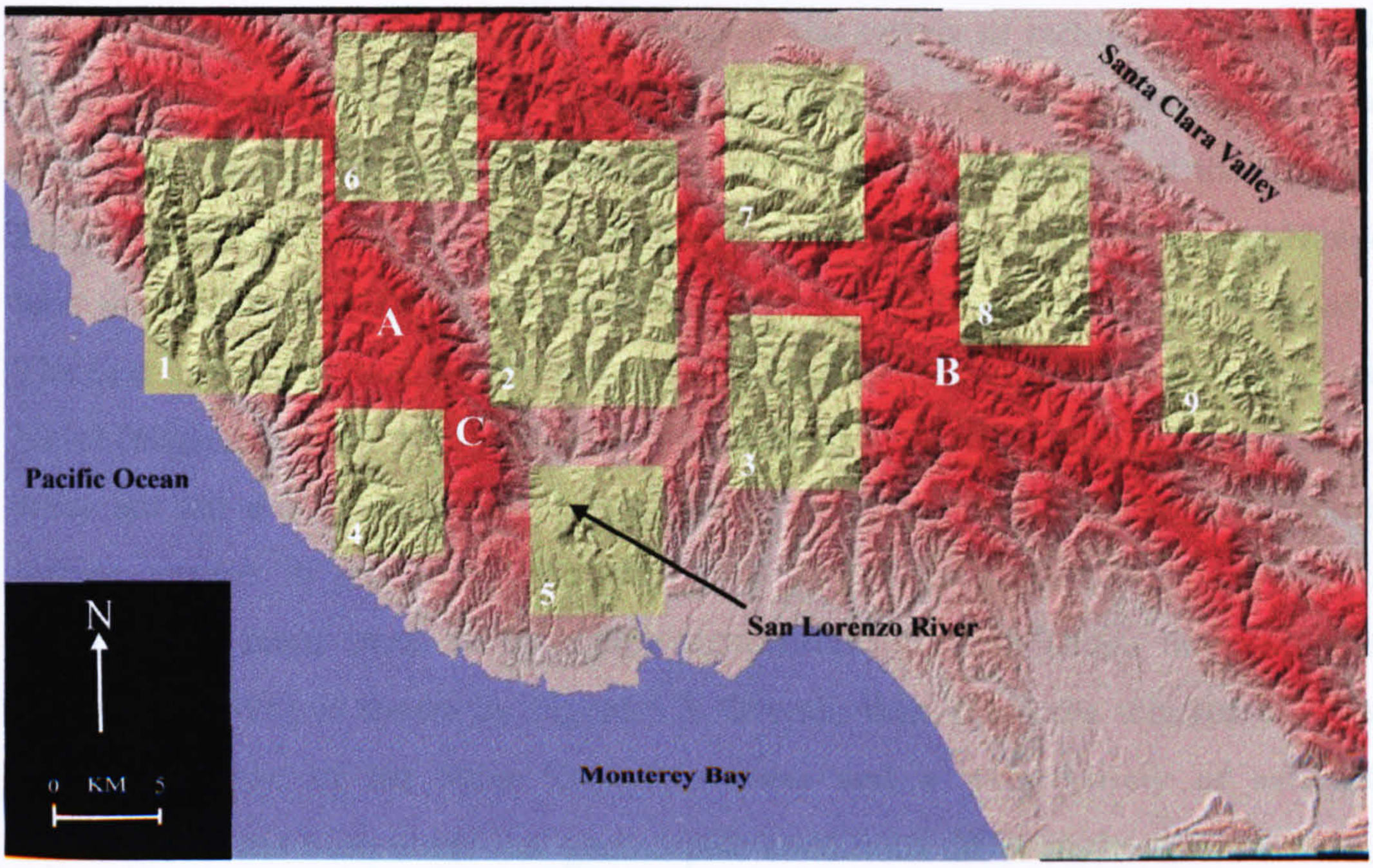

Figure 4.1 Shaded Relief Map of the Santa Cruz Mountains, California

(Study Areas in Yellow and Darker Red Indicating Areas of Higher Topography)

1- Coastal Basin, 2- Mid Basin, 3- New Basin, 4- New2 Basin, 5-New3 Basin

6- New4 Basin, 7- New5 Basin, 8- New6 Basin, 9- New7 Basin

A- Coastal Range, B- Central Range, C- Ben Lomond Mountain

Figure 4.2 Slope Map, Santa Cruz Mountains.

Shading Indicates Slope Angles: Mauve < 10°, Green 10-19°, Red 20-24°, White > 24°

The nine areas are selected to represent the variety of tectonic, climatic and lithologic settings possible in the Santa Cruz Mountains. Figure 4.1 shows how the more elevated parts of the mountain range are found near the coast in the Coastal Range and further inland in the Central Range. Of the areas chosen, New5 and New6 have the highest mean elevations (c. 500 m), in parts reaching more than 1000 m asl. The next highest mean elevations are found in the Coastal Range around Coastal and New2 (mean c. 300 m), with maximum elevations of around 700 m. The lowest of the areas studied are found at New3 and New7, the former representing a dissected marine terrace in the south and the latter an alluvial piedmont to the east. Additionally, many parts of the range demonstrate linear hillslope morphologies (Anderson, 1994) as shown by Figure 4.3. Overall, then, the areas selected cover a large percentage of the Santa Cruz Mountains and a wide variety of external conditions. It has been noted that geomorphic conditions differ in the east and west, and these characteristics are largely reflected in elevation characteristics.

Coastal Ranges

The areas within the Santa Cruz Coastal Ranges (Coastal, New2, New3, New4 and Mid) occupy both the low elevation marine cut terraces (Rosenbloom and Anderson, 1994) and the higher elevation mountains. Moving inland of the coastal terraces, Coastal, New4 and Mid all demonstrate linear ridge topography seen elsewhere. The shaded relief map (Figure 4.1) indicates that New2 appears to represent what will from this point onwards be called 'mixed topography' with linear ridge morphology to the south and west, and a relatively smooth area to the north and east. New3 represents the now-incised remains of a marine terrace in the south, having little apparent relief and no linear ridge type terrain.

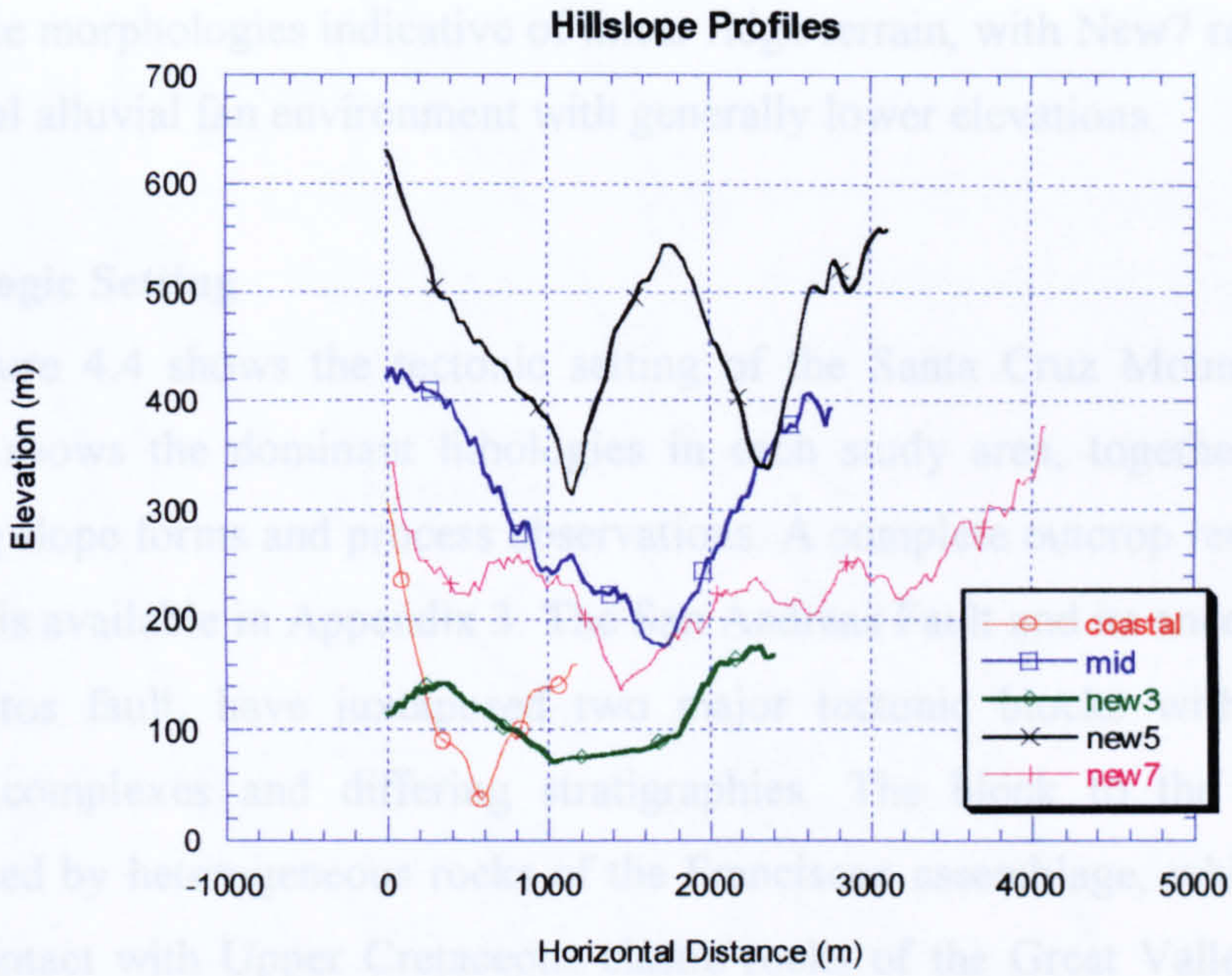

Figure 4.3 Hillslope Profiles of Mountains in the Santa Cruz Mountains Sampled from 30 Metre Digital Terrain Model

Central Ranges

Further to the east of the Coastal Ranges, New5, New, New6 and New7 are included in the Central Ranges of the Santa Cruz Mountains. The first three areas all demonstrate morphologies indicative of linear ridge terrain, with New7 representing a depositional alluvial fan environment with generally lower elevations.

4.2.3 Geologic Setting

Figure 4.4 shows the tectonic setting of the Santa Cruz Mountains, whilst Table 4.1 shows the dominant lithologies in each study area, together with notes concerning slope forms and process observations. A complete outcrop record for each study area is available in Appendix 3. The San Andreas Fault and its ancestral branch, the Pilarcitos fault, have juxtaposed two major tectonic blocks with contrasting basement complexes and differing stratigraphies. The block to the northeast is characterised by heterogeneous rocks of the Franciscan assemblage, which in turn is in fault contact with Upper Cretaceous clastic rocks of the Great Valley Sequence, with Cenozoic clastics overlaying this sequence. Southwest of these fault systems, and northwest of the San Gregorio fault, the basement consists of crystalline Salinian rocks, with Cenozoic clastics and volcanics resting upon the basement. Southwest of the San Gregorio fault, the Upper Cretaceous clastic sedimentary rocks outcrop along the coast (Clarke, 1981).

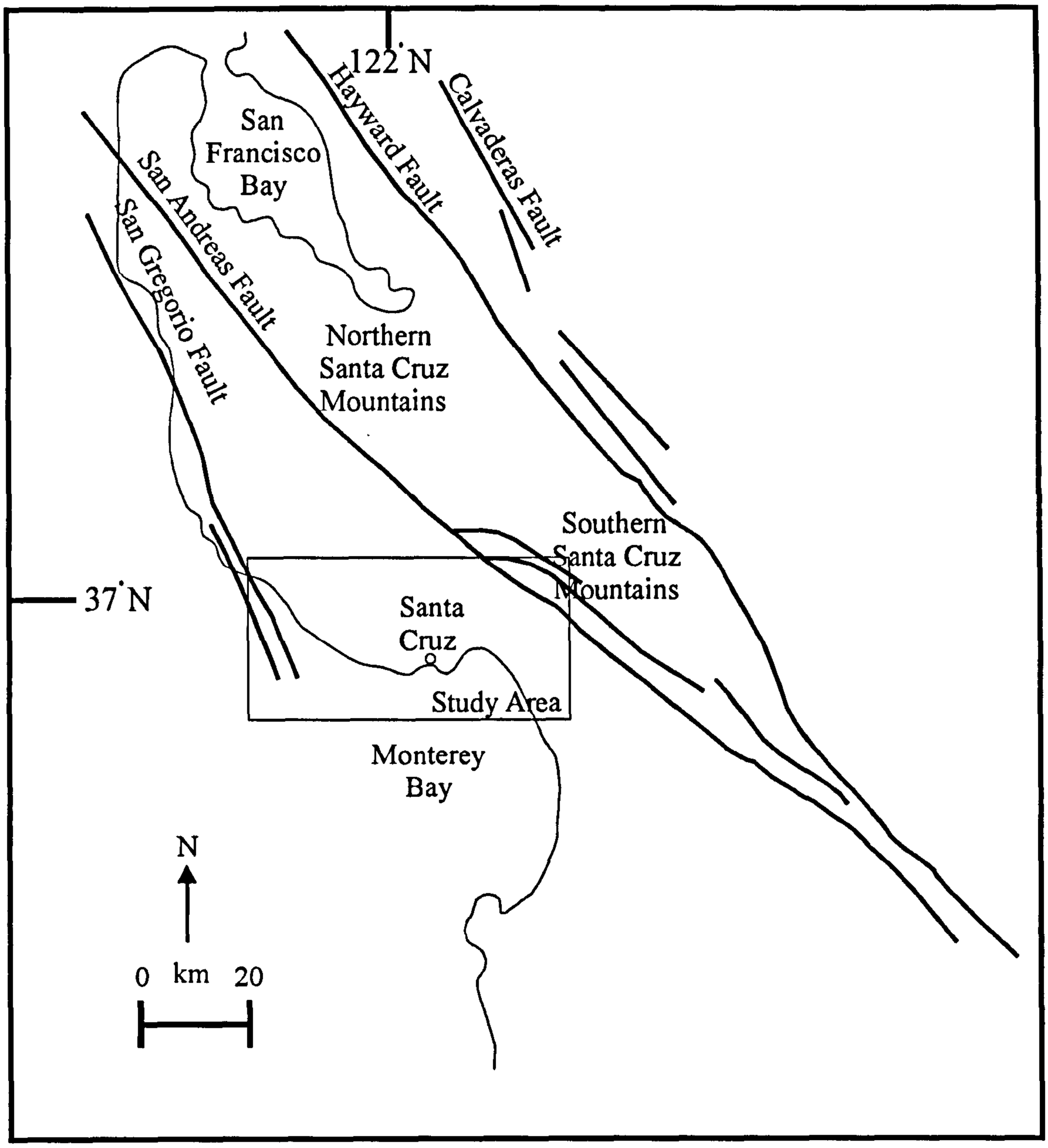

Figure 4.4 Fault Map of the Santa Cruz Mountains

Basin	Lithological Patterns	Notes (After Anderson, 1994; Schmidt and Montgomery, 1995; Rosenbloom and Anderson, 1994)
Coastal	Butano Sandstone Santa Cruz Mudstone Vaqueros Sandstone	• Coastal areas affected by landsliding of material into channels • Short, linear slopes present on DTM
Mid	Vaqueros Sandstone Butano Sandstone Monterey Formation	• Mountainous centre affected by Loma Prieta Earthquake (LPE) • Widespread linear hillslopes
New	Purisima Formation Butano Sandstone Vaqueros Sandstone	• Mountainous centre affected by LPE • Linear slopes longer than those along coast
New2	Quaternary Deposits Santa Cruz Mudstone Santa Margarita Sandstone	• Mixed smooth and linear-type topography • Landsliding occurs along coastal stretch
New3	Quaternary Deposits Santa Margarita Sandstone Purisima Formation	• Smooth diffuse topography (Quaternary deposits) • Little/no landsliding
New4	Vaqueros Sandstone Rices Mudstone Butano Sandstone	• Central area affected by LPE • Linear slopes dominate area
New5	Franciscan Complex Quaternary Deposits Monterey Formation	• Central area affected by LPE • Long linear hillslopes
New6	Franciscan Complex Quaternary Deposits Great Valley Sequence	• Further from LPE focus • Fewer linear slopes. Long hillslope lengths

Table 4.1 General Lithological Trends and Notes for Study Areas, Santa Cruz Mountains (Outcrop types determined from USGS Digitised Geological Maps)

The Santa Cruz Mountains experienced widespread landsliding during the Loma Prieta earthquake of 1989 (Magnitude 7.1), with sliding concentrated in the mountainous area surrounding the earthquake epicentre, as well as the coastal cliffs of Monterey Bay (Figure 4.1) (Schmidt and Montgomery, 1995). The area north of Monterey Bay contains at least five emergent marine terraces, which have been studied in detail by Rosenbloom and Anderson (1994). The Santa Cruz mountains are being uplifted and deformed as the result of advection of crust around a left bend in the San Andreas Fault to the northeast (Anderson, 1994; Burgmann *et al.*, 1994). Uplift rates vary from 0.16 to 0.48 m/ka (Bradley and Griggs, 1976). The area around Ben Lomond Mountain consists of a SW tilted block, where erosion has exposed a crystalline Palaeozoic core of metasedimentary and Mesozoic plutonic rocks (James, 1992). This complex is unconformably overlain by gently southwest dipping Tertiary marine sediments (Clarke, 1981). The terraces are primarily cut into the Santa Cruz Mudstone of the sequence. The Santa Cruz Mudstone is a highly jointed siliceous mudstone of late Miocene age of high durability. This formation is underlain by the friable thickly-bedded Santa Margarita Mudstone, which in turn is underlain by the sandy siltstone and siliceous mudstone of the Monterey Formation (Rosenbloom and Anderson, 1994).

Whilst the northern mountains on the southwest side of the San Andreas Fault system are characterised by broad warping and folding, the southern Santa Cruz Mountains are formed by a long-lived, deep rooted reverse fault system forming a well defined, elongate uplift zone (Burgmann *et al.*, 1994).

4.3 TERRAIN VARIATION WITHIN THE SANTA CRUZ MOUNTAINS

As noted above, the nine study areas chosen represent a variety of bedrock lithologies and terrain forms. Differences in these forms are now examined using a variety of morphometric variables to test their ability to discriminate linear ridge terrain.

4.3.1 Data and Methods

GRID elevation data upon which the morphometric calculations were performed were obtained from the California DEM data repository at the University of Southern California. The data files were tiled together producing a coverage of the Santa Cruz Mountains with a horizontal resolution of 30 metre and a vertical resolution accurate to the nearest metre. The data were entered as raster lattice format into Arc/Info and geometrically transformed to conform to a UTM projection system (Zone 33). The geological data sets were obtained from the USGS at Menlo Park, having the same spatial resolution as the elevation data. These data were also projected to a UTM system, in order that spatial correlations and analysis could be performed.

4.3.1.1 Slope

Slope (S) analyses were performed upon the DTM sets within Arc/Info, which involves calculation of the slope gradient in the steepest descent path for the nine cells neighbouring the central calculation pixel. For each area analysed, the total number of cell calculations (>10,000) were collected into histograms (in a similar fashion to Burbank *et al.*, 1996). The distributions were then sorted into 1° bins and normalised by area in order that comparisons between study sites with different spatial areas be possible.

4.3.1.2 Local Relief

Relief calculations in the Santa Cruz Mountains involved several different techniques and the testing of several relief parameters previously outlined by other researchers. The parameters calculated were determined over varying spatial scales, from single cell calculations to those carried out over much larger window sizes of up to 200 pixels. The calculations were performed within Arc/Info. Windows of varying

sizes were used to test both how window size affects the overall distribution of relief parameters and what the most appropriate size for calculation would appear to be. As with slope analyses, the distributions were sorted into 1 m bins and normalised by area to permit inter-basin comparisons.

Local relief (R) is defined as the difference between the maximum and minimum elevation within a window (Gilchrist *et al.*, 1994; Summerfield, 1991) or drainage basin (Strahler, 1952). For this study, local relief was derived within nested circular windows with a radius (r) of 3, 5, 20 and 50 pixels, and was calculated as :

(4.1) $R = (Z_{max} - Z_{min})_r$

Where Z_{max} is the maximum elevation within the window, and Z_{min} is the minimum elevation within the same window.

4.3.1.3 Dispersion of Altitude

Ohmori and Sugai (1995) proposed that relief variation within terrain in Japan is better defined by the standard deviation of elevation within a moving window than as defined by local relief variations. This results from the ways the two parameters are calculated: the former placing less reliance on the range of the window than the latter, thus reducing the effects of potentially spurious data points. The dispersion of altitude in a moving window (DA) is thus calculated within Arc/Info using the standard deviation of the values within windows of 3, 5, 20 and 50 pixel radius.

4.3.1.4 ZR Ratio

The ZR ratio is "...a relief morphometric parameter designed to capture the local ruggedness of a landscape" (Formento-Triglio and Pazzaglia, 1998, p.445). Its calculation is based on mean elevation (Z) and mean local relief (R) within a circular window of radius r. Local relief, R, has been derived above, thus:

(4.2) $ZR = Z / R$

In this example, calculations were made within a 3 pixel radius window.

4.3.1.5 Elevation-Relief Ratio / Hypsometric Integral

The third measure of relief calculated within the Santa Cruz study areas is the elevation-relief ratio (or hypsometric curve). Mathematically identical to the hypsometric curve (Strahler, 1952; Zavoianu, 1985), the elevation-relief ratio was proposed by Pike and Wilson (1971), whilst the hypsometric curve was formally defined by Strahler (1952). The elevation-relief ratio represents the land mass within a drainage basin above a specified datum (generally sea-level). It therefore shows the degree of dissection of a landscape, or level of 'opening-up' by erosion of the basin (Keller and Pinter, 1996). Highly dissected, young terrains have high hypsometric integrals, whilst older, more eroded landscapes characteristically have lower integrals as more of their land mass has been denuded (Ciccacci *et al.*, 1992).

Whilst the hypsometric integral may only be derived at a drainage basin scale, the elevation-relief ratio may also be derived on a point measure basis by examining the relationship between a central cell and its neighbours. The former is a dimensionless measure of a basin's dissection (Keller and Pinter, 1996). Evans (1972) proposes that the frequency distribution of elevation may be used as a surrogate for the hypsometric curve. Other workers to use the hypsometric curve include Warren (1976) who used the technique to derive sand dune volumes, and Wilkin (1996) who derived volume of bedrock eroded from basins in the US in a similar manner. Elevation-relief ratios were derived in each study areas within 3 and 5 pixel radius windows. The method thus deviates from the initial method and usage proposed by Strahler (1952) and Pike and Wilson (1971) who calculated the index within drainage basins rather than moving windows. The elevation-relief ratio (ER) was calculated, and the output data binned into single value categories before being normalised by area. ER is thus calculated as:

(4.3) $ER = (E_{mean} - E_{min} / E_{max} - E_{min})_r$

Initial calculations of ER in the form defined above indicated that a high range of values existed within a small range (< 0.01) of values, thus ER values were multiplied by 100 to allow for easier examination of the data.

(4.4) $ER = (E_{mean} - E_{min} / E_{max} - E_{min})_r * 100$

4.3.1.6 Dissection Index

The dissection index (ϕ) has been proposed to indicate the level of local relief occupied by valleys, and was initially tested in the Alps and Himalayas (Gilchrist *et al.*, 1994). The index is once again based on calculations of elevation within a circular window of 3 pixel radius, with output binned into single value levels and normalised by area. ϕ is thus derived:

(4.5) $\phi = (E_{max}\text{-}E_{mean})_r / (E_{max} - E_{min})_r$

As with the ER index, the range of values created by sampling the Santa Cruz areas with ϕ was relatively small, thus the index was finally multiplied by 100.

(4.6) $\phi = ((E_{max}\text{-}E_{mean})_r / (E_{max} - E_{min})_r)*100$

4.3.1.7 Nogami Index

The next measure of relief and dissection calculated within the Santa Cruz Mountains is the Nogami Index (NI)(after Nogami, 1995). Calculation of the Nogami Index involved examining the range of elevation values within a given window shape and size.

(4.7) $NI = (E_{max} - E_{min})$

The calculation of this index was once again performed within Arc/Info using 3 pixel radius moving windows, binned into single value bins and normalised by area. Calculation of NI showed a wide range of values, and it was thus decided that in order for analysis and comparison to be enabled, cumulative plots of the NI index were derived.

4.3.1.8 Slope Variability Index

Slope variability (V) within pre-defined windows (radius, r) was analysed within the nine study areas. The calculations were carried out using AML macros written for use within Arc/Info. S is slope gradient of the central calculation pixel in degrees, F_{mean} is the mean value of slope gradient within a circular window of radius, r, and F_{sum} is the sum of $(S - F_{mean})$ within a circular window of radius, r. V is calculated thus:

(4.8) $V = F_{sum} / S$

4.3.2 Bedrock Lithology and Terrain Form

Having derived lithological maps for each of the study areas, and projecting them to the same UTM coordinate system, slope analyses were performed upon each area within each lithological type. For each lithology, mean, standard deviation and range of slope values were calculated within single calculation pixels. Having obtained these statistics and following examination of the lithological maps for the study areas it became apparent that both inter- and intra-basin variations in outcrop areas existed, with some outcrop areas cumulatively covering more than 50 km^2, with others covered less than 0.5 km^2. Thus whilst it is recognised that at local scales such small variations may have direct influences on small scale hillslope form and process, it was decided that for the purpose of this study only outcrops with cumulative areas greater than 6 km^2 would be examined between basins to reduce the impact of variations in outcrop sizes on slope statistics. Such calculations and assumptions will more accurately reflect large scale morphological trends and the influences lithological variations have upon them.

4.4 RESULTS

4.4.1 Slope Analysis

An examination of hillslope gradient statistics (Table 4.2) for the Santa Cruz Mountains demonstrates several noticeable trends. Given that the Central Range has higher elevations than the Coastal Range generally, it might be expected that the former would have the higher slope values. The range of slope values for each area indicates that the Central Range's slope are generally at 50° or less, whilst the Coast Range (Coastal and New2 in particular) have slopes as high as 62°. However, despite this trend, the Central Range's New5 and New6 have a higher proportion of hillslopes at greater values than in the Coast Ranges, giving them the highest mean slope values. Those characteristics may be explained in terms of hillslope length variations existing in the two areas. Longer apparent hillslope lengths in the Central Range mean that despite their higher mean elevations, the slopes are longer in length, accommodating the lower slope values. The two areas of lower elevation in the study, New3 and New7, have lower mean slope values as expected from largely depositional environments.

Moving away from individual statistics to look at the frequency distributions of slope by area (Figure 4.5), several trends emerge from the data. The Coastal Ranges show overall characteristics towards having a broader range of slope values as shown in the plots, where values of 10° to 25° occupy some 3 % of the area. Conversely, those areas in the Central Range, such as New5 and New6, show higher proportions of land at higher slope values (greater than 20°). Away from the coastline itself, the inland study areas of Mid and New4 have slope frequencies showing characteristics of near-normal distributions about mean value of 18°- 20°. The differences between those areas with linear ridge morphologies and those without is demonstrated well by New2 and New3 respectively. New2's mixed topography is picked up by the slope distribution of the area which shows a bi-modal character, with one peak around 5° and another around 17°- 18°. By comparison, New3 shows only one peak around 5° as it lacks the steeper linear ridge terrain

Area	Slope	Relief	Standard Deviation of Elevation	Dissection Index	Elevation – Relief Ratio	Nogami Index
Coastal	20.474 (10.249)	63.688 (29.194)	17.108 (8.203)	50.927 (9.566)	49.073 (9.566)	492.403 (169.696)
Mid	19.054 (7.866)	58.087 (20.282)	15.595 (5.599)	51.276 (8.503)	48.724 (8.503)	490.004 (162.673)
New	17.926 (7.352)	54.240 (18.438)	14.557 (5.141)	50.563 (8.360)	49.437 (8.360)	494.041 (159.924)
New2	15.711 (9.925)	47.317 (25.805)	12.903 (7.346)	49.236 (10.398)	50.764 (10.398)	501.906 (188.254)
New3	10.449 (8.006)	31.036 (21.125)	8.498 (6.014)	51.498 (11.865)	48.502 (11.865)	485.271 (205.825)
New4	18.748 (7.287)	57.097 (19.331)	15.291 (5.267)	51.164 (7.747)	48.836 (7.747)	491.408 (153.309)
New5	21.696 (9.052)	67.708 (26.869)	17.978 (7.217)	49.697 (7.713)	50.303 (7.713)	501.248 (150.5)
New6	21.182 (8.318)	65.541 (23.332)	17.423 (6.234)	51.130 (8.576)	48.870 (8.576)	492.266 (156.472)
New7	13.988 (9.875)	42.238 (27.492)	11.271 (7.378)	54.534 (11.269)	45.466 (11.269)	471.8 (204.18)

Table 4.2 Descriptive Statistics for Study Areas in Santa Cruz Mountains

(N.B. Mean and Standard Deviation (in Brackets)

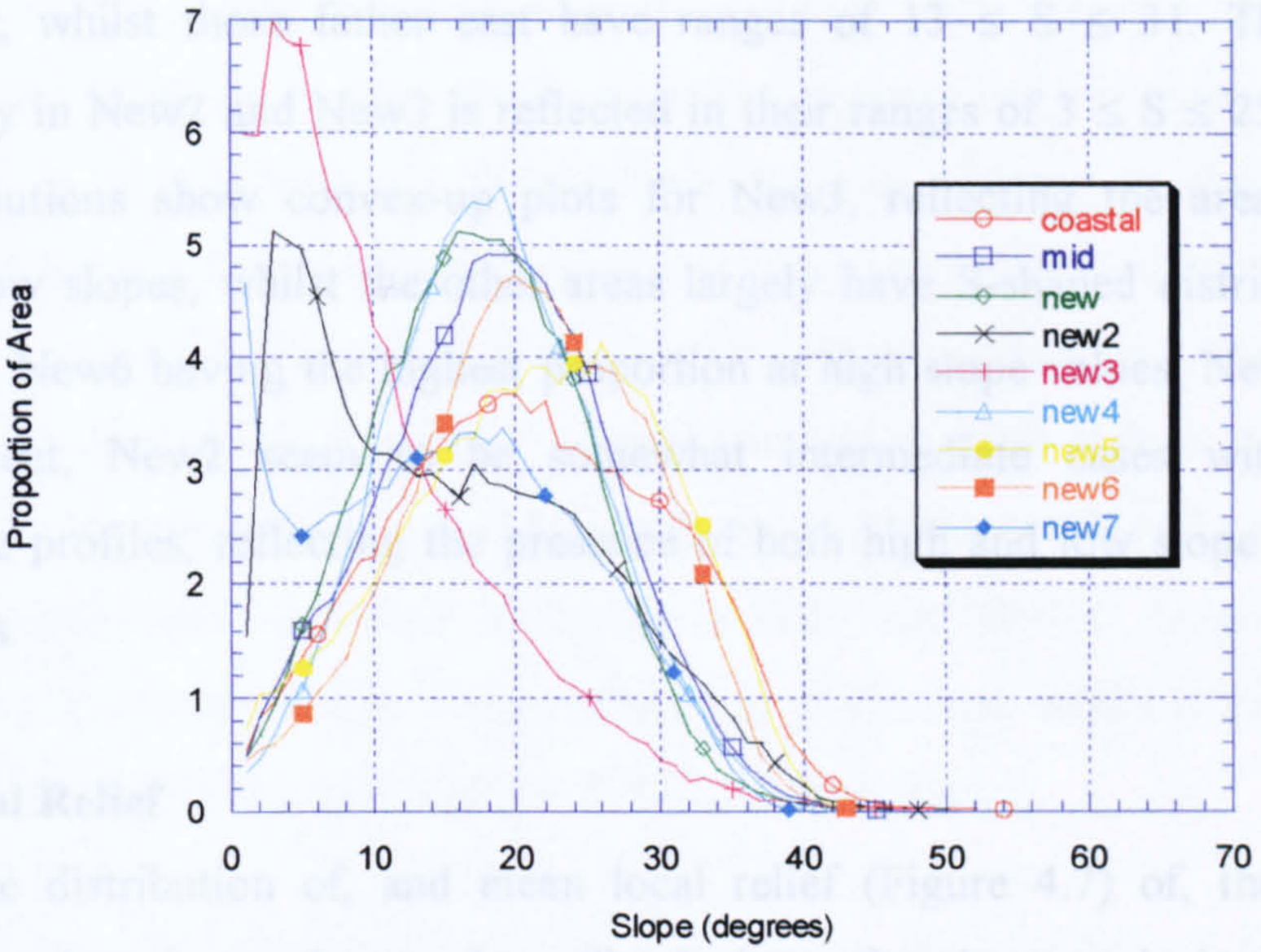

Figure 4.5 Slope Distribution Plots

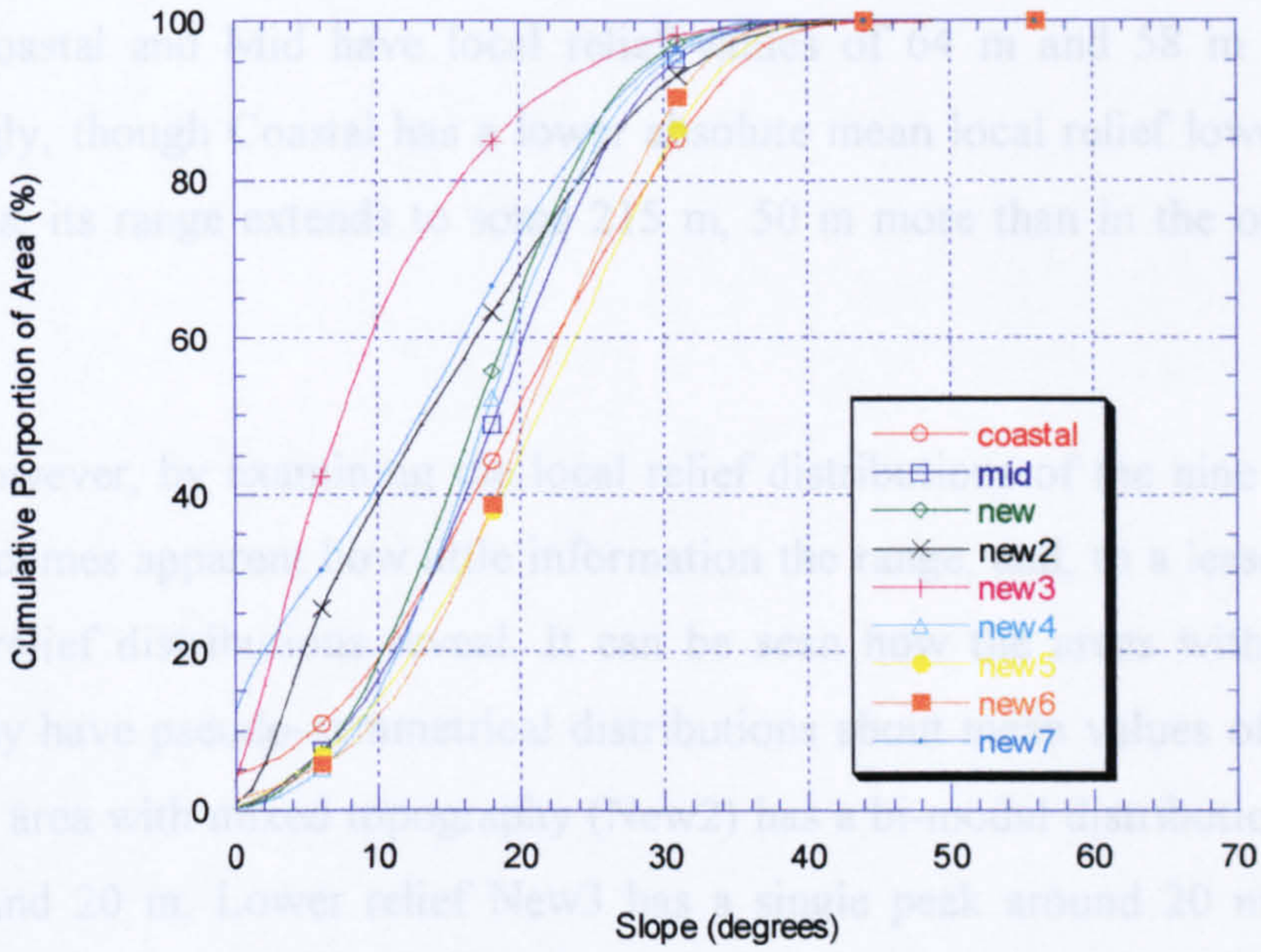

Figure 4.6 Cumulative Slope Distribution Plots

Figure 4.6 shows the cumulative frequency plots of slope for the nine study areas. It can be seen that distinct variations in the shape of these distributions exist, largely reflecting the trends outlined above. Examination of the range of values existing for the central 60 % of the plots show that the Coastal linear ridge areas have ranges of $11 \leq S \leq 29$, whilst those father east have ranges of $13 \leq S \leq 31$. The smoother topography in New2 and New3 is reflected in their ranges of $3 \leq S \leq 25$. Generally, the distributions show convex-up plots for New3, reflecting the area's tendency towards low slopes, whilst the other areas largely have S-shaped distributions with New5 and New6 having the highest proportion at high slope values. New7 and, to a lesser extent, New2 seem to be somewhat intermediate cases with straighter cumulative profiles, reflecting the presence of both high and low slope gradients in these areas.

4.4.2 Local Relief

The distribution of, and mean local relief (Figure 4.7) of, the nine areas studied largely mirrors the trends outlined above for slope analysis (Figure 4.5). Despite the fact that in some areas, for example upland plateaus (e.g. Masek *et al.*, 1994), relief and elevation are not well correlated, it would appear that the two are well related within the Santa Cruz Mountains (Table 4.2). New5 and New6 in the Central Range have the highest mean local relief of around 66 m, whilst in the Coastal Range, Coastal and Mid have local relief values of 64 m and 58 m respectively. Surprisingly, though Coastal has a lower absolute mean local relief lower than some other areas, its range extends to some 215 m, 50 m more than in the other 8 basins studied.

However, by examining the local relief distributions of the nine areas (Table 4.2), it becomes apparent how little information the range, and, to a lesser extent, the mean of relief distributions reveal. It can be seen how the areas with linear ridge topography have pseudo-symmetrical distributions about mean values of 45 m-65 m, whilst the area with mixed topography (New2) has a bi-modal distribution with peaks at 50 m and 20 m. Lower relief New3 has a single peak around 20 m. The mixed terrain characteristics if New7 are reflected by the scattered distribution of local relief values ranging from $0 \leq R \leq 80$.

Having examined the local relief characteristics of each area within a 3*3 window, it was decided to perform similar analyses within larger windows of 20 and 50 pixel radii to test whether larger analysis windows were better able to differentiate linear and non-linear types of terrain. Results showed a wider range of values than resulted from the 3 pixel window analyses as larger areas were covered with each window, thus in order to plot distributions and observe any apparent trends it was necessary to plot cumulative distributions by area. Many of the study areas demonstrating linear ridge topography show 20 pixel cumulative pots with distinctive convex curves, especially at higher R-values > 150. By comparison, the lower relief areas (New2 and New3) show near-vertical cumulative plots with some 80 % of R lying within the range $80 \leq R \leq 160$. Interestingly, New5 and New7 show distinctly stepped distributions at lower R-values (R=200 and R=160 respectively). The distributions reflect the higher topography being in the east, which is mirrored in the higher R values in these study areas at 20*20 window sizes.

At windows of 50 pixel radius, the steps apparent at 20 pixel window size have disappeared; the scale of their source is thus taken to have a spatial resolution of less than 1500 m. New3 and New7 both show 100% of R at $R \leq 400$, with other study areas showing less than 5 % of their terrain having R-values less than 200 m. New5 has the most strongly concave plot with some 80 % of its distribution at $R > 400$.

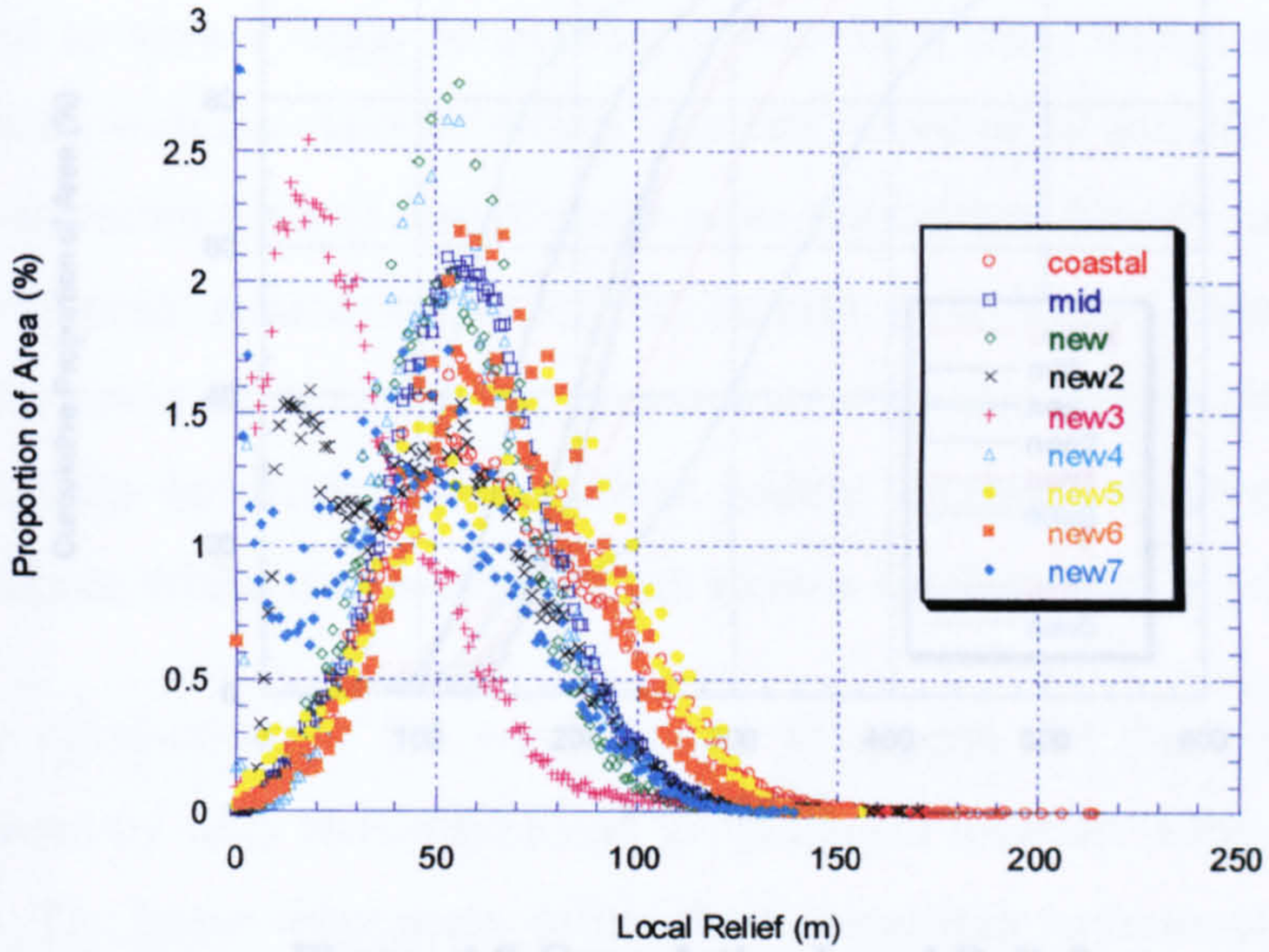

Figure 4.7 Cumulative Local Relief

(3 Pixel Radius)

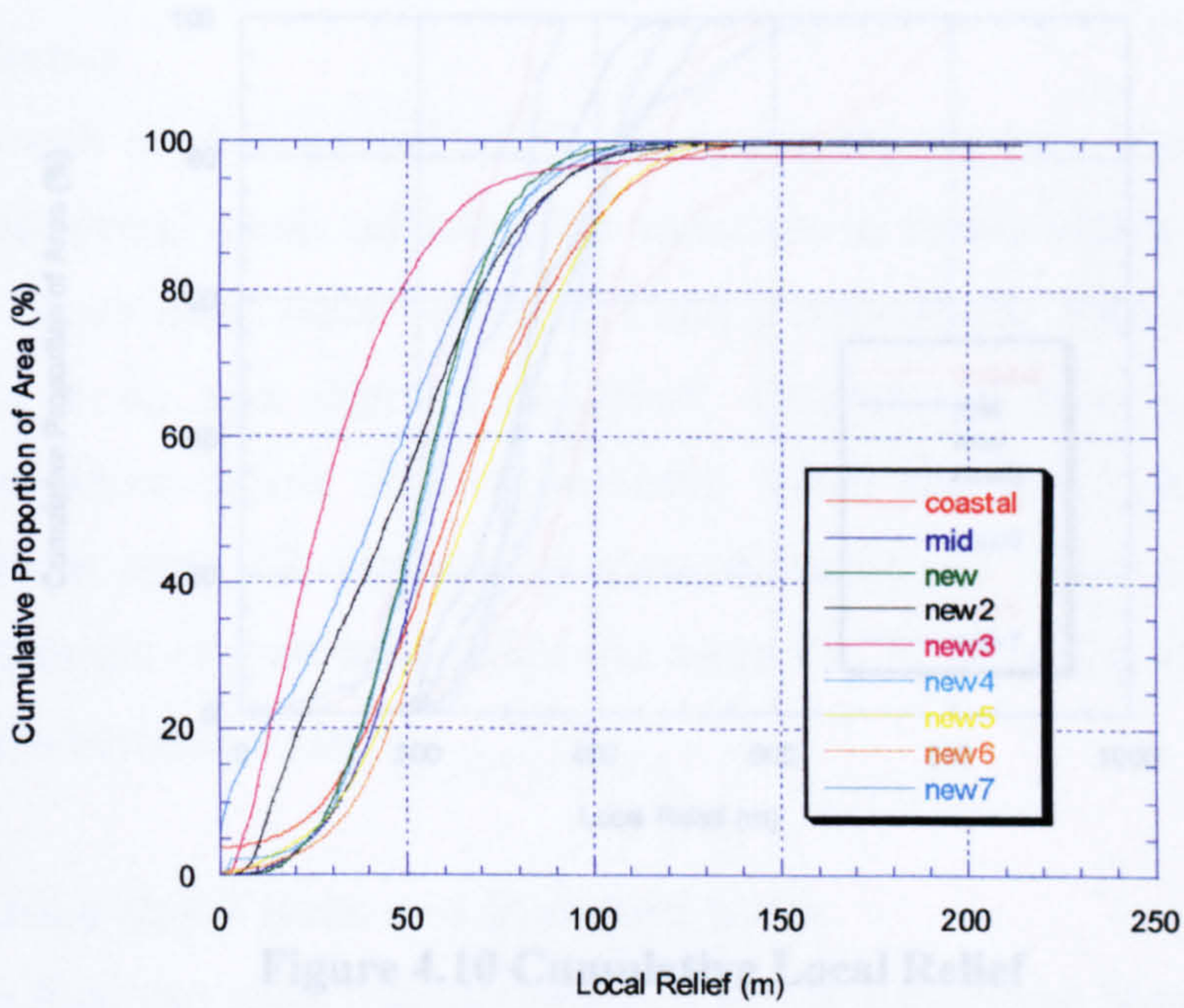

Figure 4.8 Cumulative Local Relief

(3 Pixel Radius)

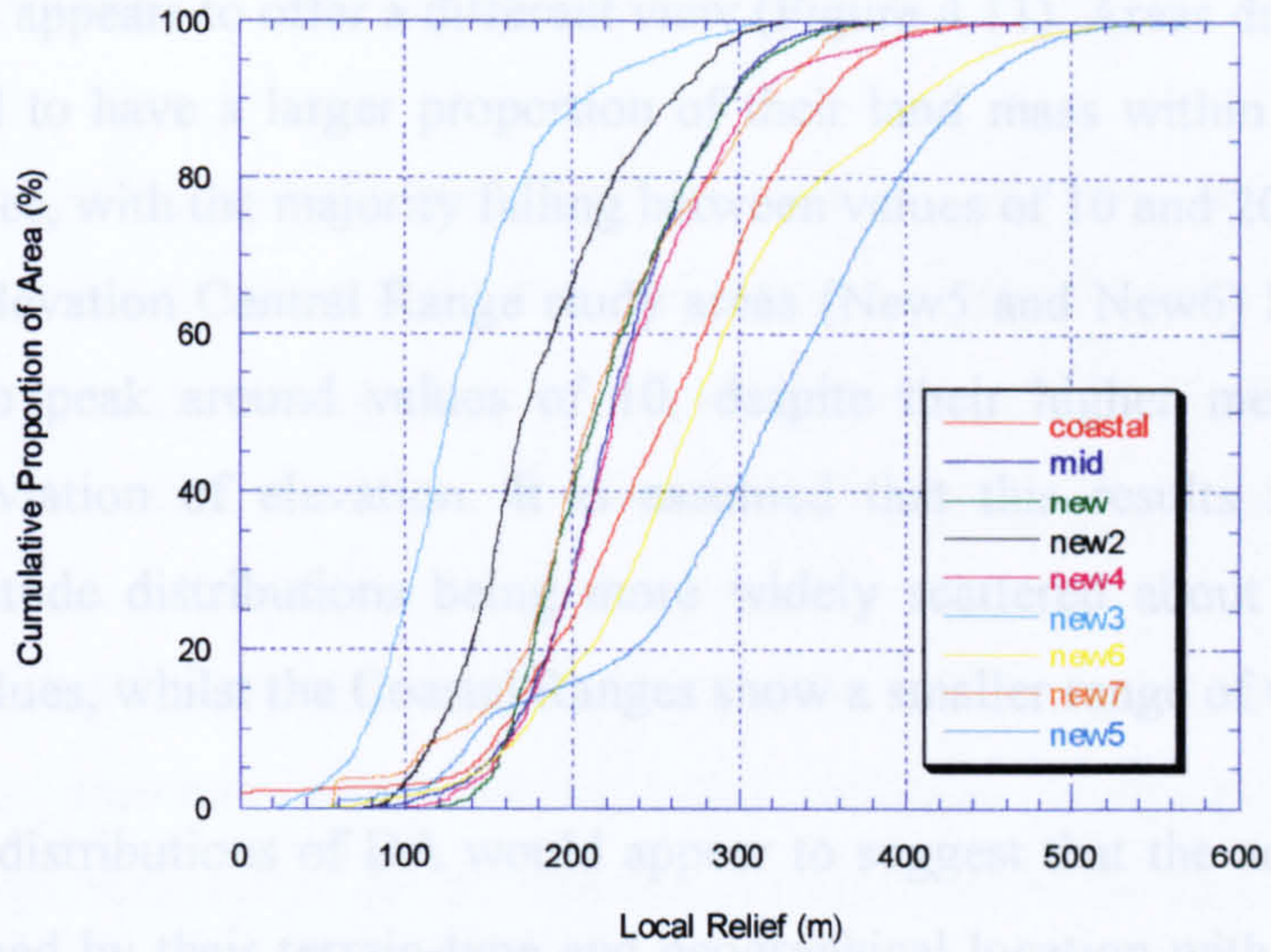

Figure 4.9 Cumulative Local Relief (20 Pixel Radius)

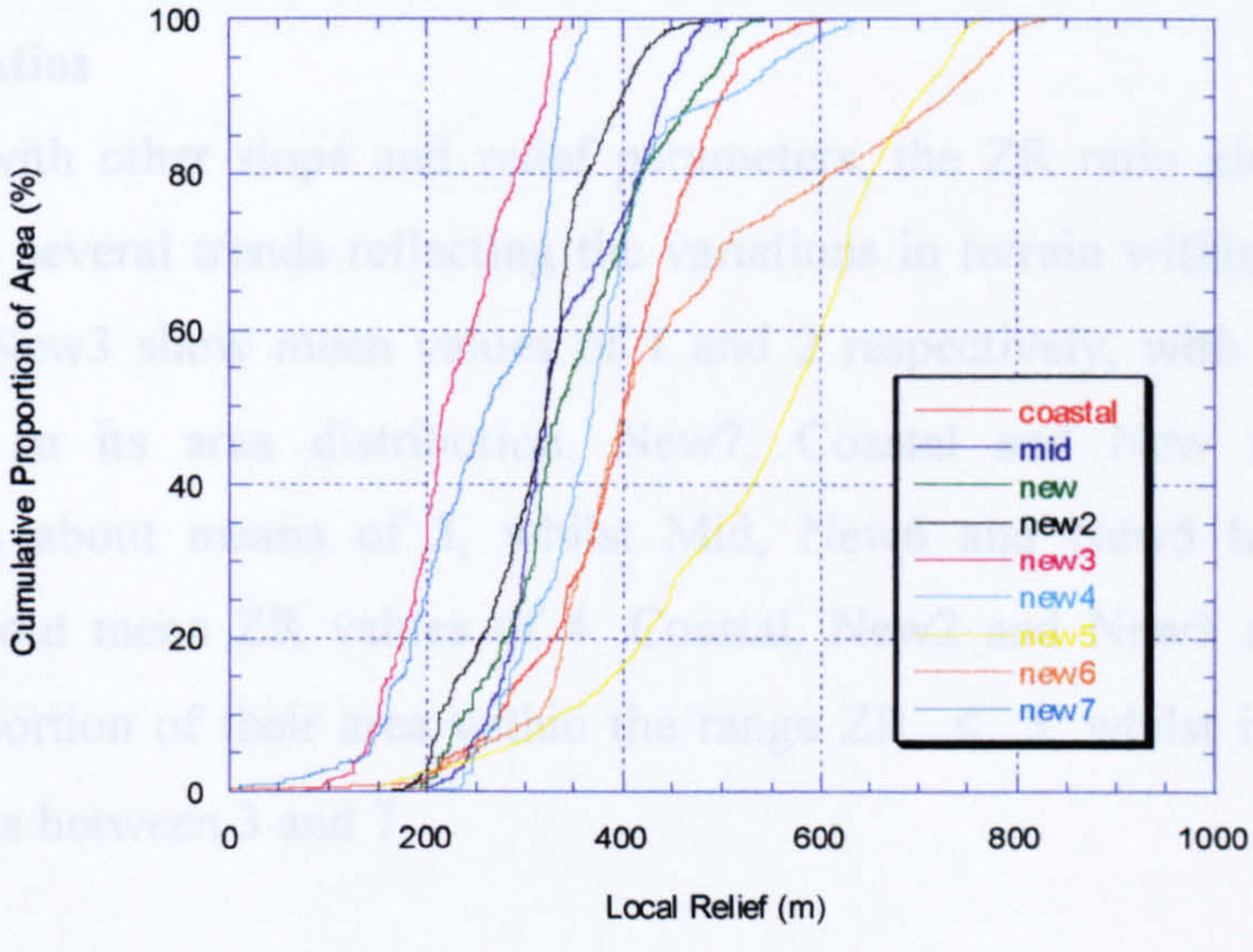

Figure 4.10 Cumulative Local Relief (50 Pixel Radius)

4.4.3 Dispersion of Altitude

Mean values of dispersion of altitude (Table 4.2) for the nine areas also reflects the trends shown by local relief, yet once again examination of the distributions appears to offer a different view (Figure 4.11). Areas draining the coastal reaches tend to have a larger proportion of their land mass within a small range of altitude values, with the majority falling between values of 10 and 20. By comparison, the higher elevation Central Range study areas (New5 and New6) have distributions appearing to peak around values of 10, despite their higher mean value for the standard deviation of elevation. It is assumed that this results from the Central Ranges' altitude distributions being more widely scattered about a large range of elevation values, whilst the Coastal Ranges show a smaller range of values.

The distributions of DA would appear to suggest that the areas' mean values are determined by their terrain-type and geographical location within the Santa Cruz Mountains. The linear ridge areas within the Coastal Belt have means of $8 \leq$ DA ≤ 10, whilst the mixed topography of New2 has mean values of 3 and 14, the former reflected by New3's mean value of 4. Low values are thus representative of smoother topography.

4.4.4 ZR Ratios

As with other slope and relief parameters, the ZR ratio plots (Figure 4.12) demonstrate several trends reflecting the variations in terrain within the study areas. New2 and New3 show mean values of 1 and 2 respectively, with the latter having dual peaks in its area distribution. New7, Coastal and New all have peaked distributions about means of 3, whilst Mid, New6 and New5 have distributions arranged about mean ZR values of 4. Coastal, New2 and New3 appear to have a greater proportion of their area within the range ZR $\leq$ 5, whilst in other areas the majority falls between 3 and 7.

4.4.5 Elevation-Relief Ratio and Dissection Index

The final two relief indices calculated for the Santa Cruz Mountains appear to offer no discrimination between the areas of linear ridge terrain and those which show no such terrain characteristics. Plots of each index by area (Figures 4.13 and 4.14) show that in all nine areas both indices have distributions with mean values of around

50. Interestingly, however, it can be seen how areas with higher mean values of the elevation-relief ratio have the lower dissection indices and vice-versa. Despite this, there would appear to be little correlation between the absolute rankings and how these relate to apparent morphology and/or process dominance in the nine areas.

Although there would appear to be a lack of clear distinction between terrain type, geographical location and values of ER and ϕ, some trends may, upon closer examination, be present. The range of values for the central 60 % of each study area's distributions show that in all cases the lower 80 % of values lie at ER $\leq$ 56, except for where smoother topography exists in New2 and New3, where the 80 % range extends to ER > 58 and ER > 59 respectively. The general uniformity of the distributions can therefore be assumed either to represent uniform topographic characteristics independent of terrain type, or the inadequacy of this particular parameter.

As with values of ER, the cumulative distribution plots of ϕ show that the central 60% of values lie in the range $40 \leq \phi \leq 60$. However, the intermediate case, New3, has a 60 % range of $43 \leq \phi \leq 57$, both of which extend beyond the range of values shown by the central 60% of linear ridge terrain areas. The smoother area (New2) shows values of $\phi \leq 43$, but not $\phi > 57$, thus the lower ϕ-values are taken to be indicative of smoother topography.

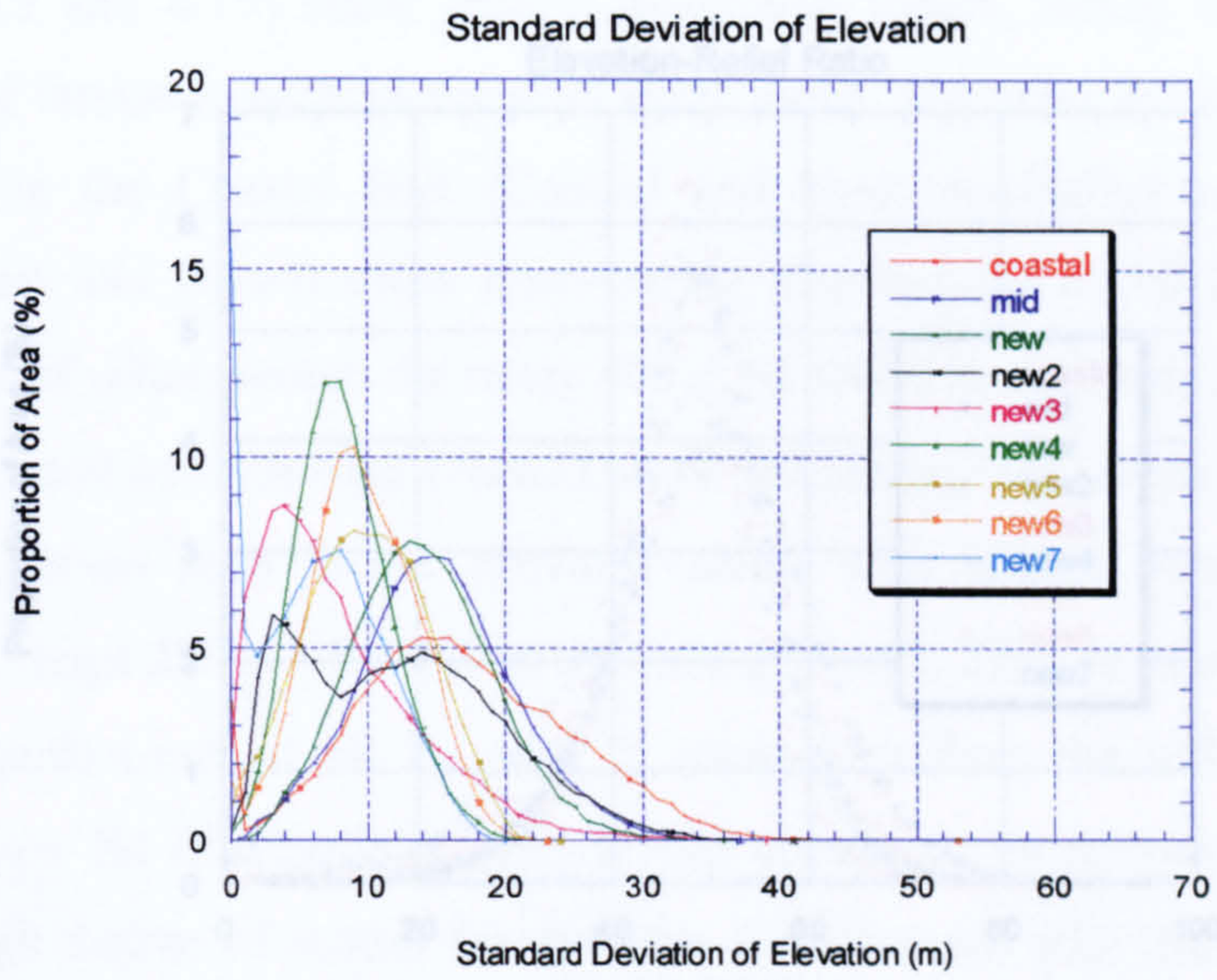

Figure 4.11 Dispersion of Altitude Plots

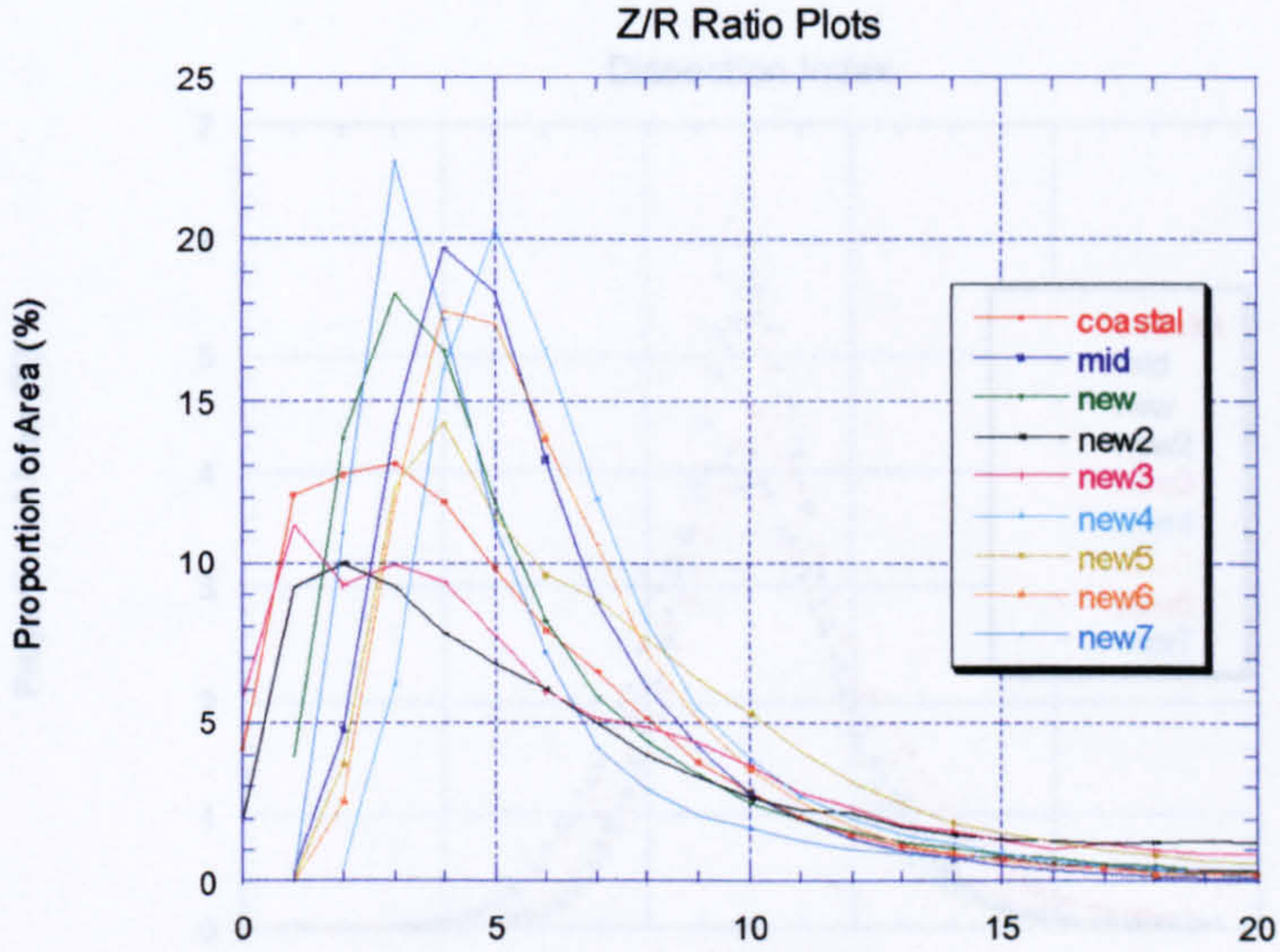

Figure 4.12 ZR Ratio Plots

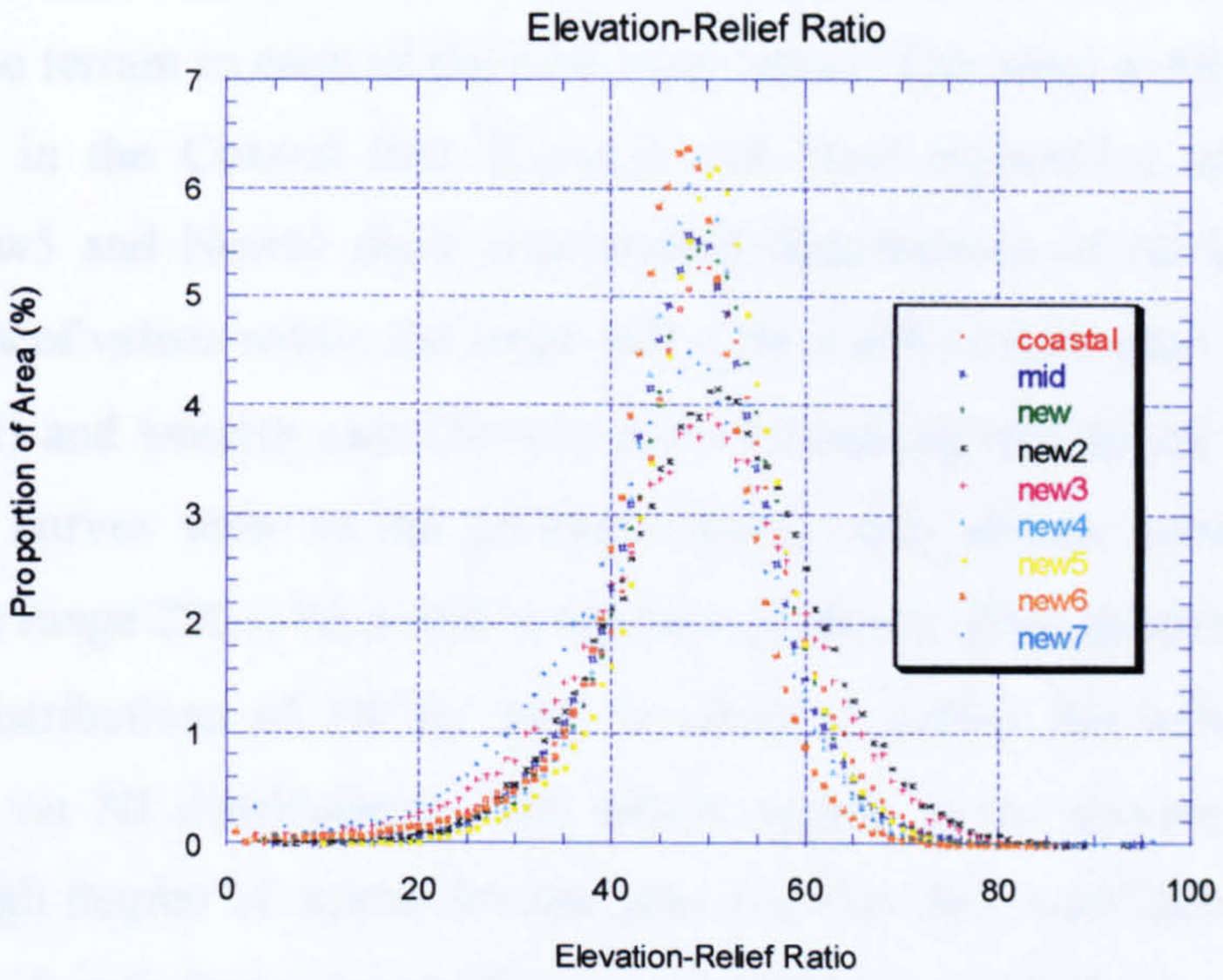

Figure 4.13 Elevation-Relief Ratio Plots

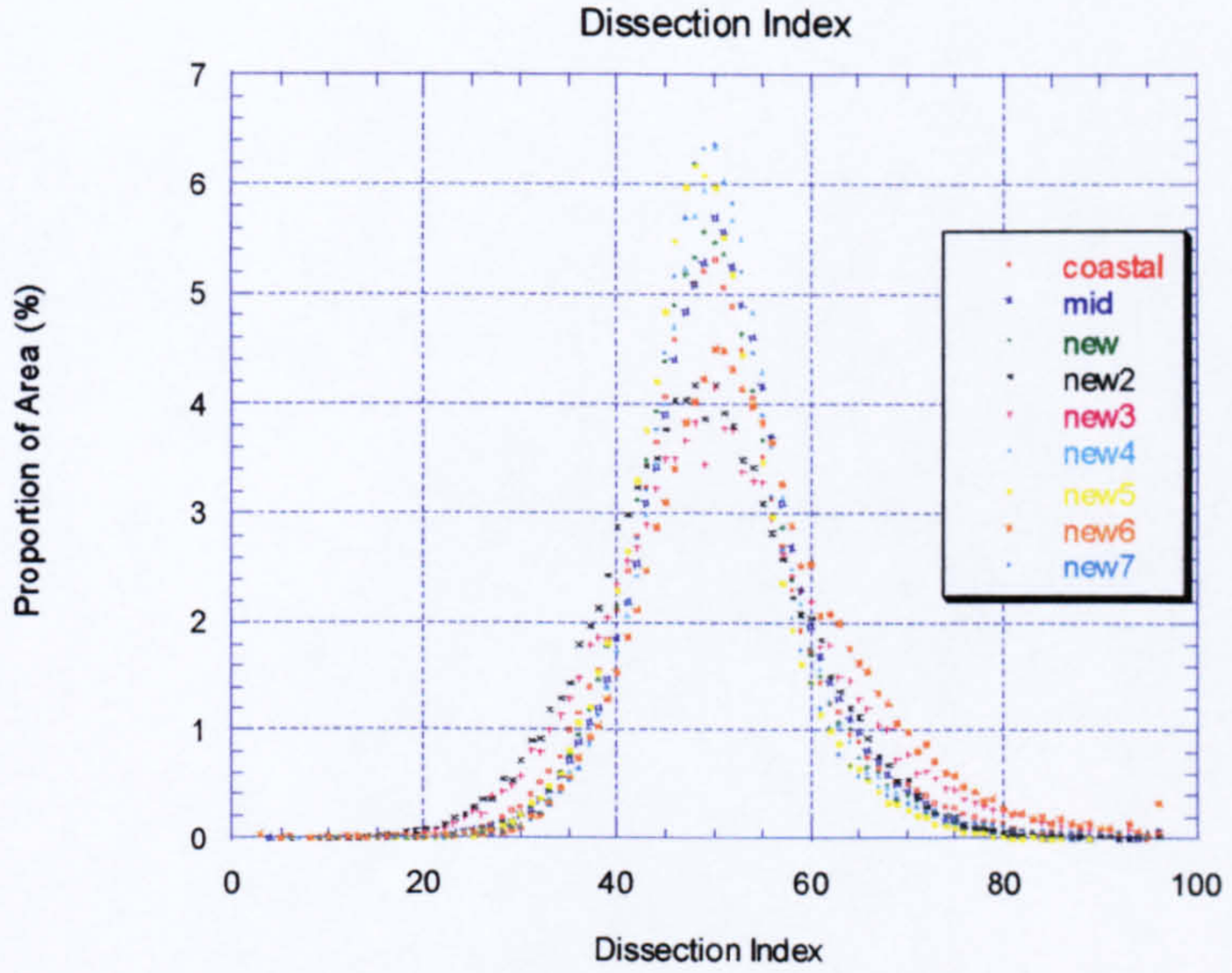

Figure 4.14 Dissection Index Plots

4.4.6 Nogami Index

Examination of the combined NI index plots by area and cumulative area (Figures 4.15 and 4.16) show several distinctive trends, which largely reflect the nature of the terrain in each of the nine study areas. The areas exhibiting linear ridge topography in the Coastal Belt (Coastal and New especially) and further inland (New4, New5 and New6) show near-normal distributions of NI by area, with the central 60 % of values within the range $400 \leq NI \leq 600$ in each case. The intermediate case (New2) and smooth case (New3) show interesting deviations from the smooth cumulative curves seen in the previous areas, with abrupt, steep linear profiles between the range $220 \leq NI \leq 460$ in the case of New2. This, in combination with the scattered distributions of NI by area, is taken to reflect the influence of smooth topography on NI distributions. Mid would appear to be somewhat idiosyncratic, having a high degree of scatter for the area distributions, with little normality to its distribution, despite its apparently linear type hillslope morphology.

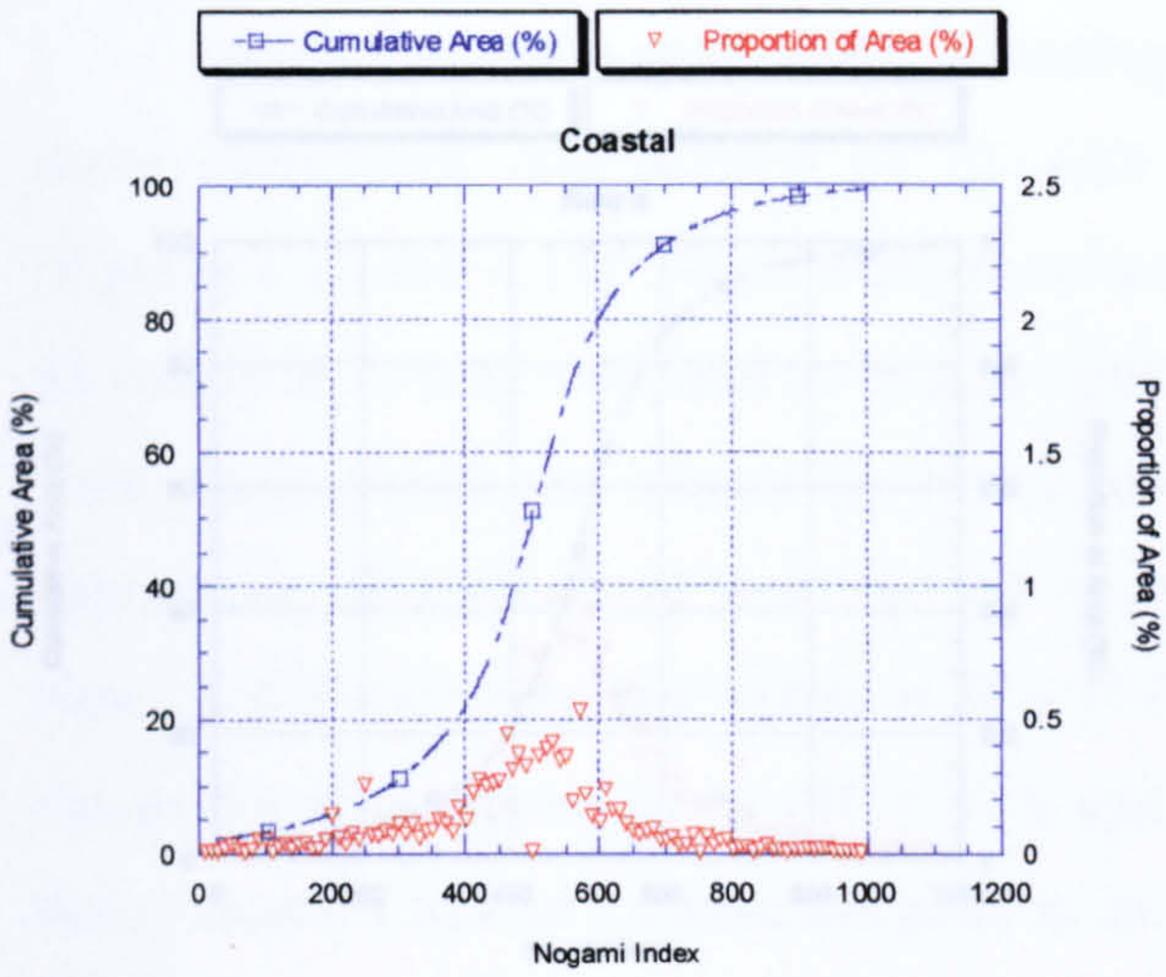

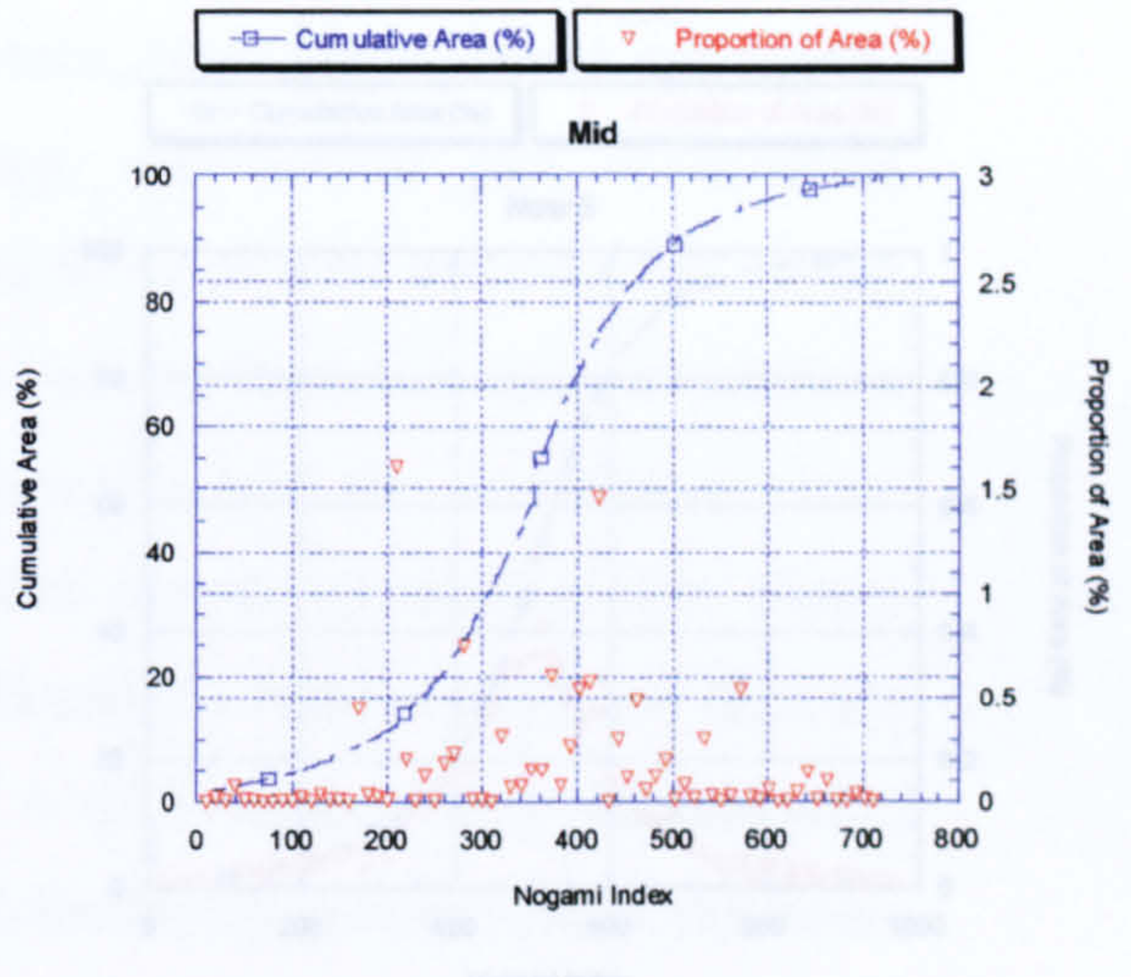

Coastal

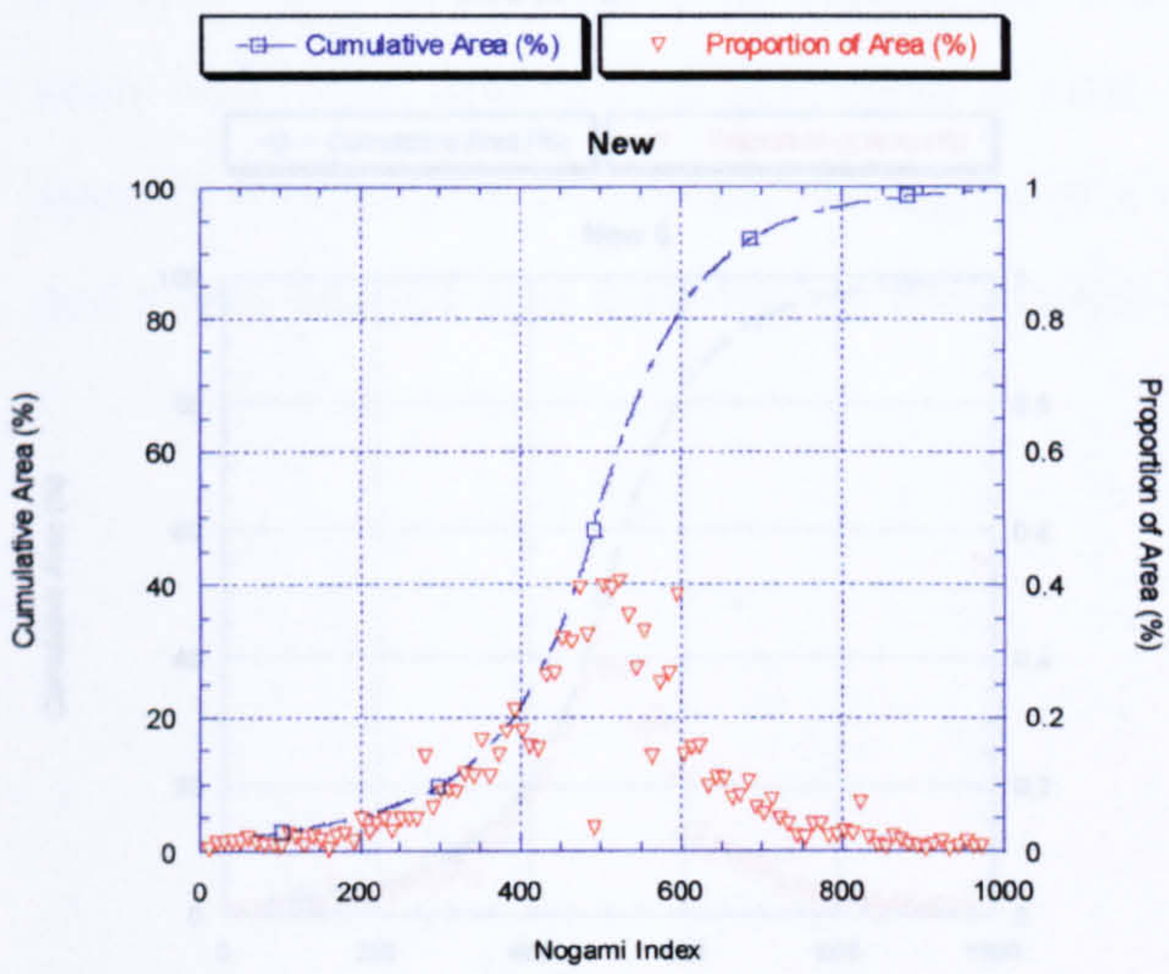

New

Mid

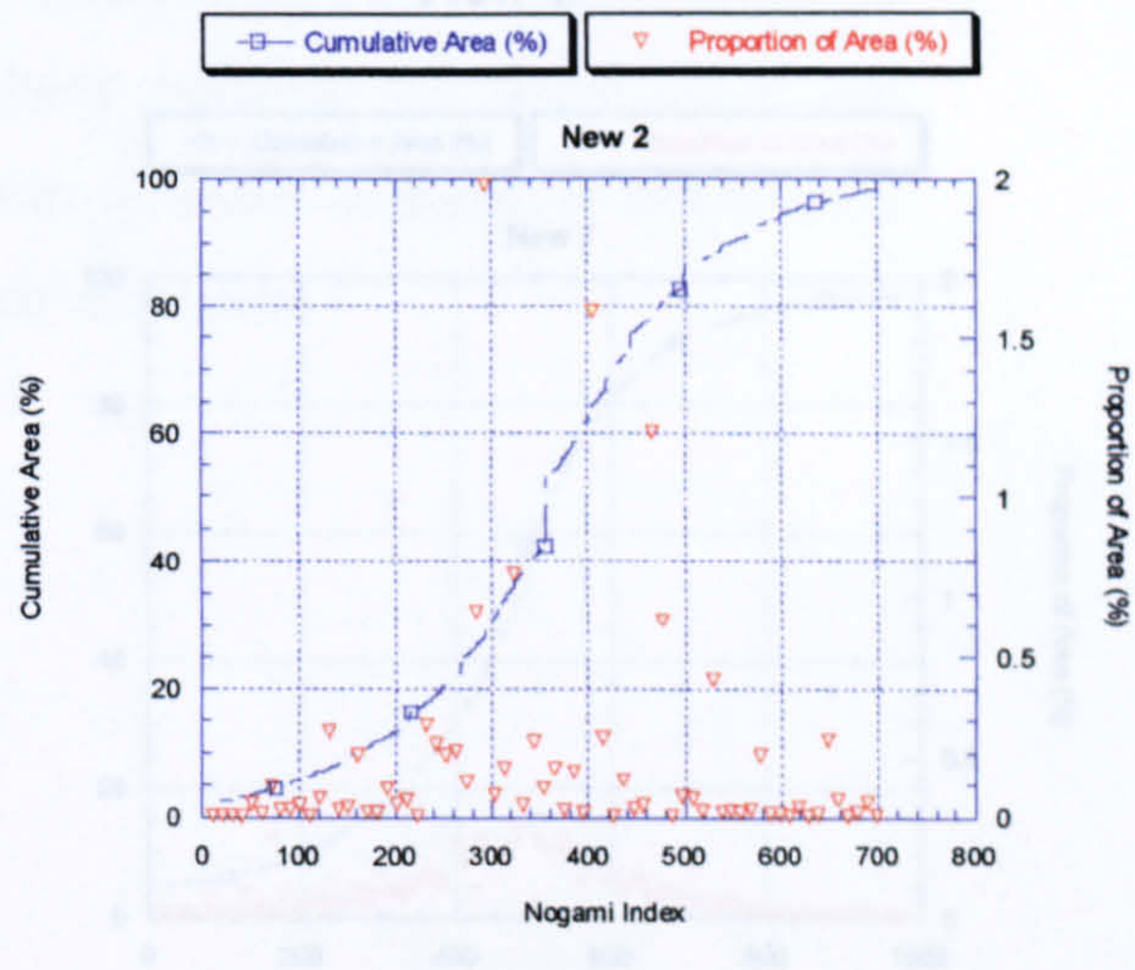

New 2

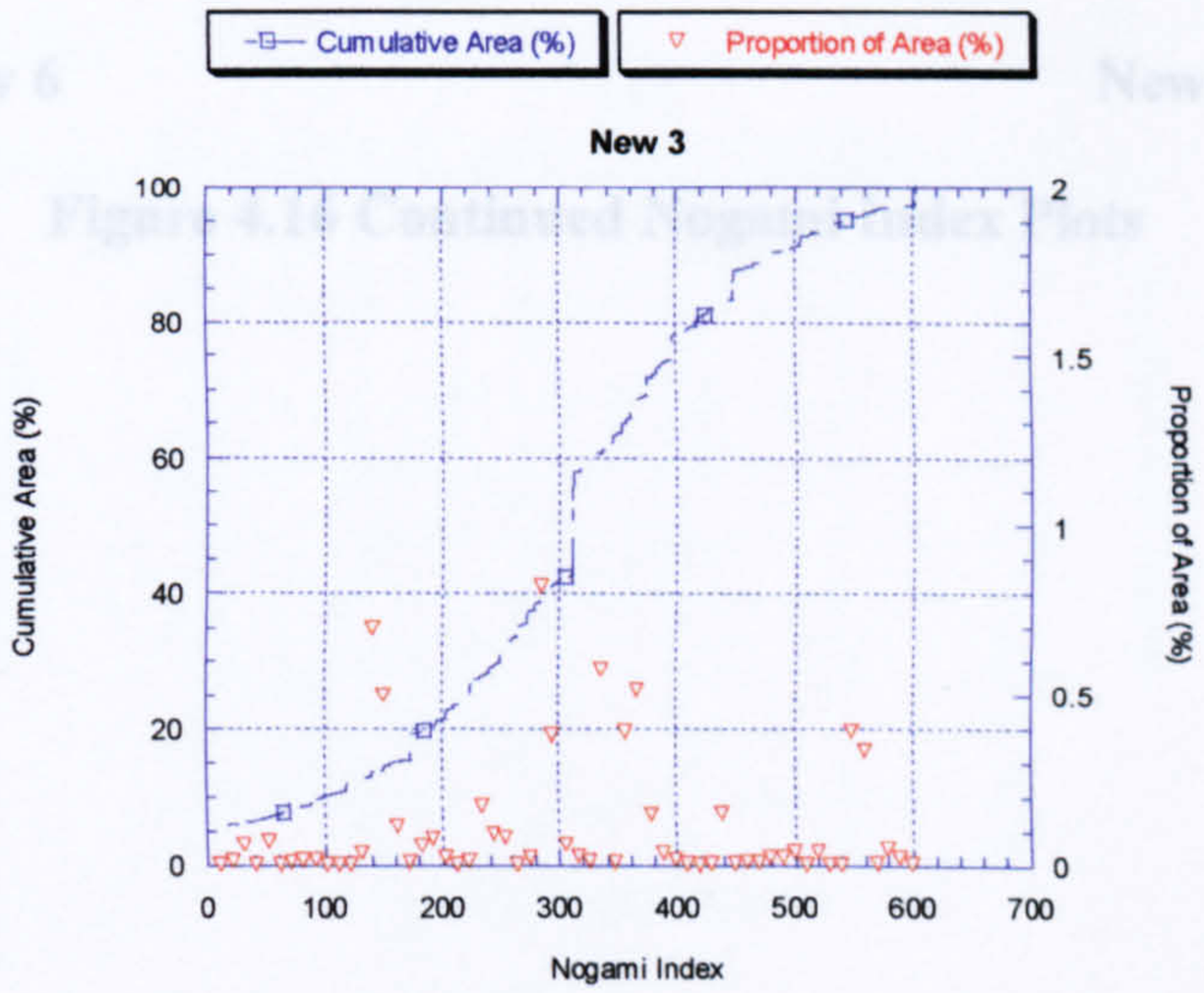

New 3

Figure 4.15 Nogami Index Plots

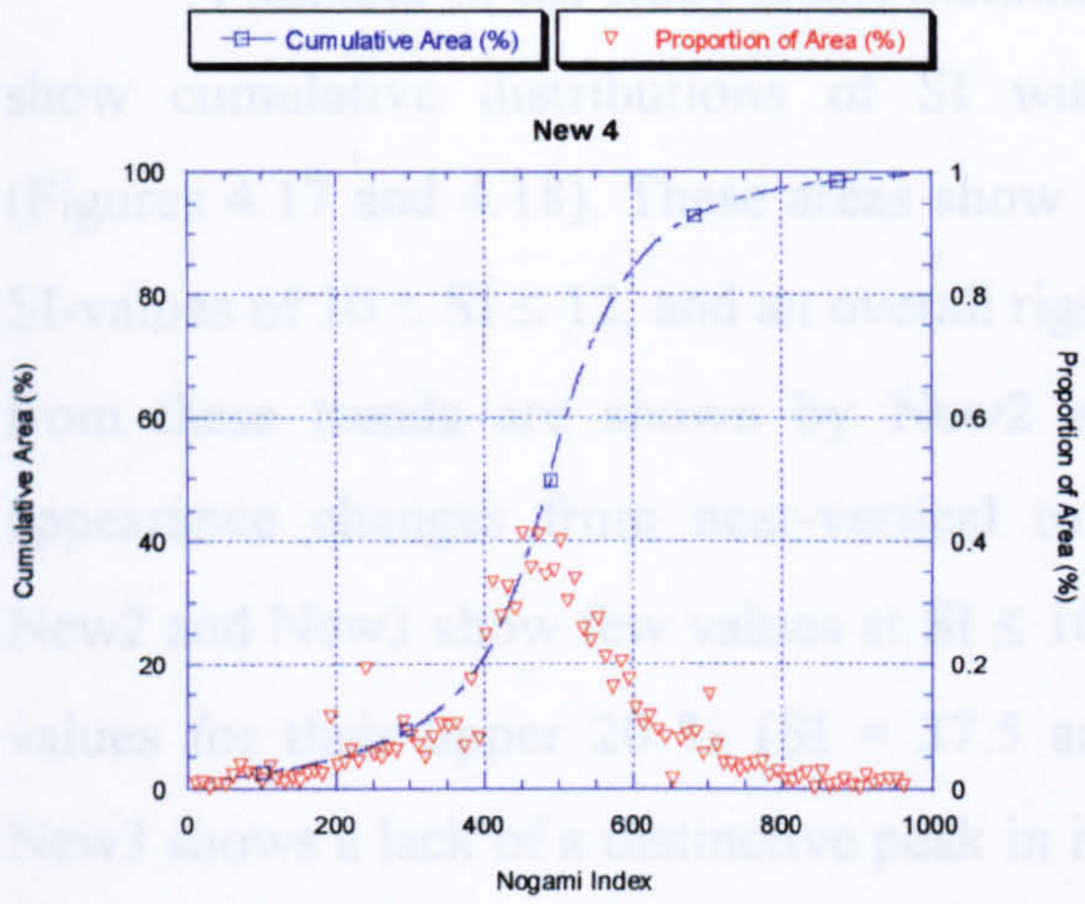

New 4

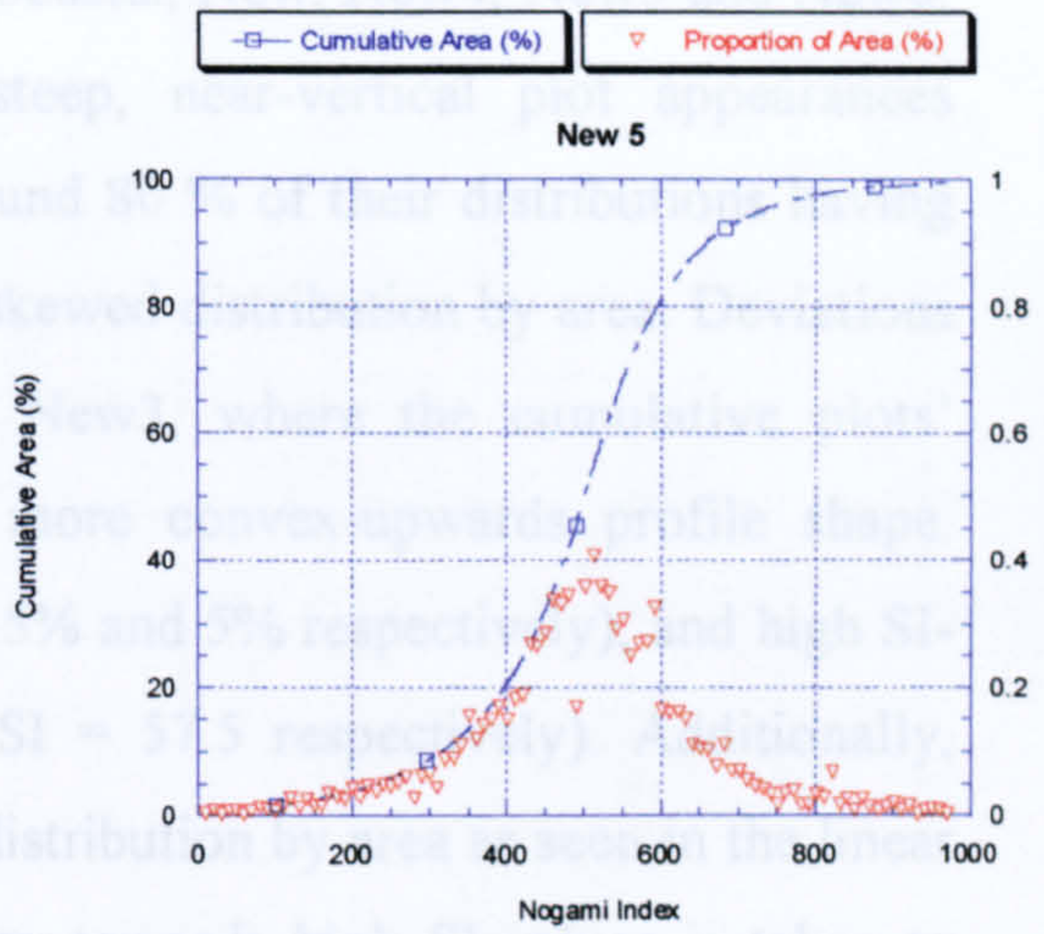

New 5

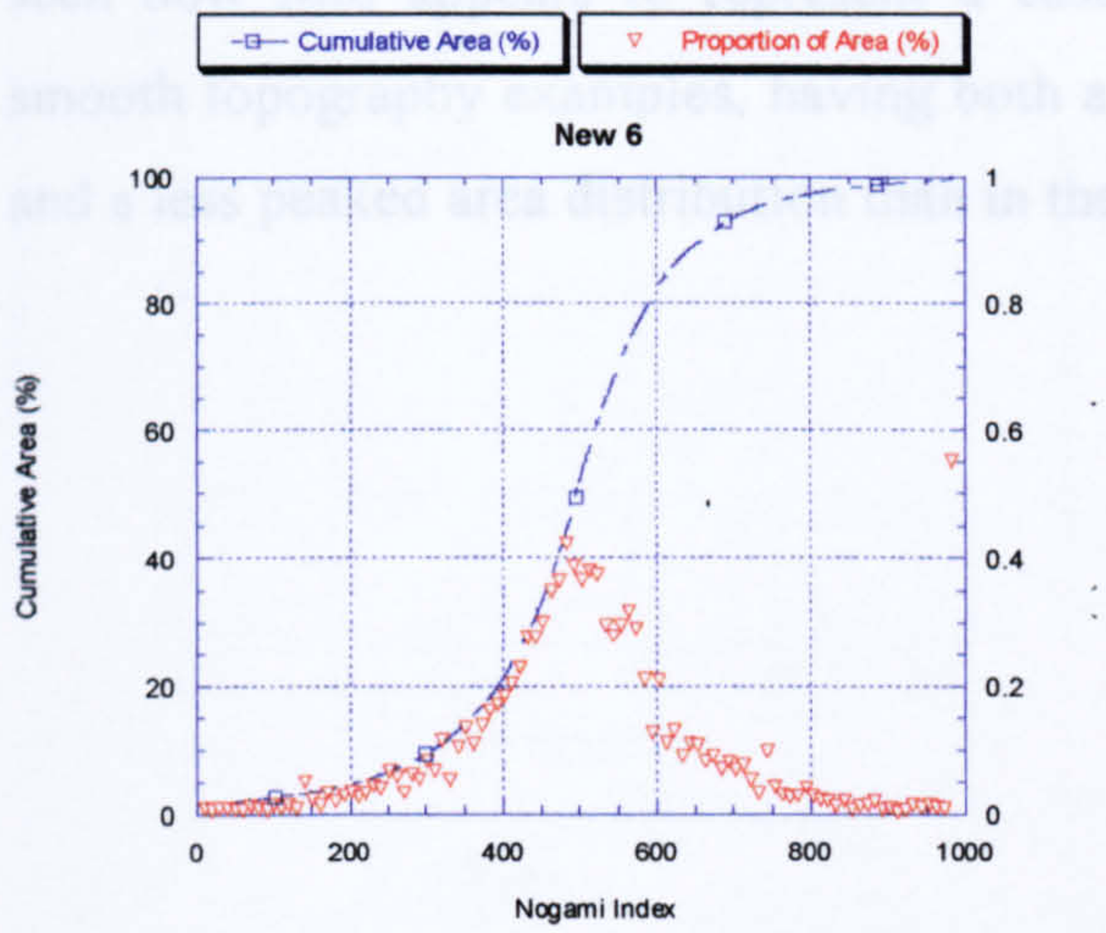

New 6

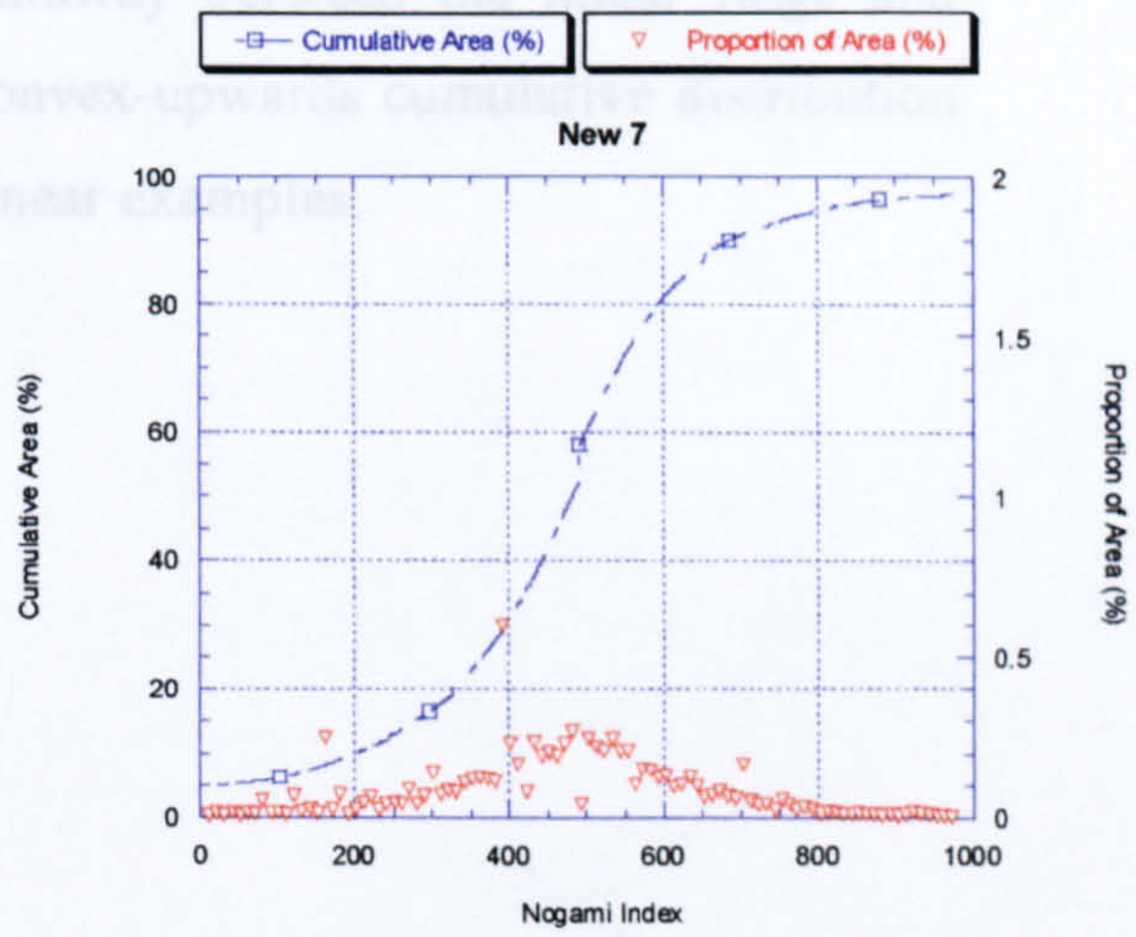

New 7

Figure 4.16 Continued Nogami Index Plots

4.4.7 Slope Variability Index

A number of the study areas, including Coastal, New, New4, New5 and New6, show cumulative distributions of SI with steep, near-vertical plot appearances (Figures 4.17 and 4.18). These areas show around 80 % of their distributions having SI-values of $10 \leq SI \leq 12$, and an overall right-skewed distribution by area. Deviations from these trends are shown by New2 and New3, where the cumulative plots' appearance changes from near-vertical to a more convex-upwards profile shape. New2 and New3 show few values at $SI \leq 10$ (15% and 5% respectively), and high SI-values for their upper 20 % (SI = 37.5 and SI = 57.5 respectively). Additionally, New3 shows a lack of a distinctive peak in its distribution by area as seen in the linear ridge examples. The lack of peak and tendency towards high SI-values is taken to represent smooth topography. Again, as with calculations of the NI-index, it can be seen how Mid appears to represent a case midway between the linear ridge and smooth topography examples, having both a convex-upwards cumulative distribution and a less peaked area distribution than in the linear examples.

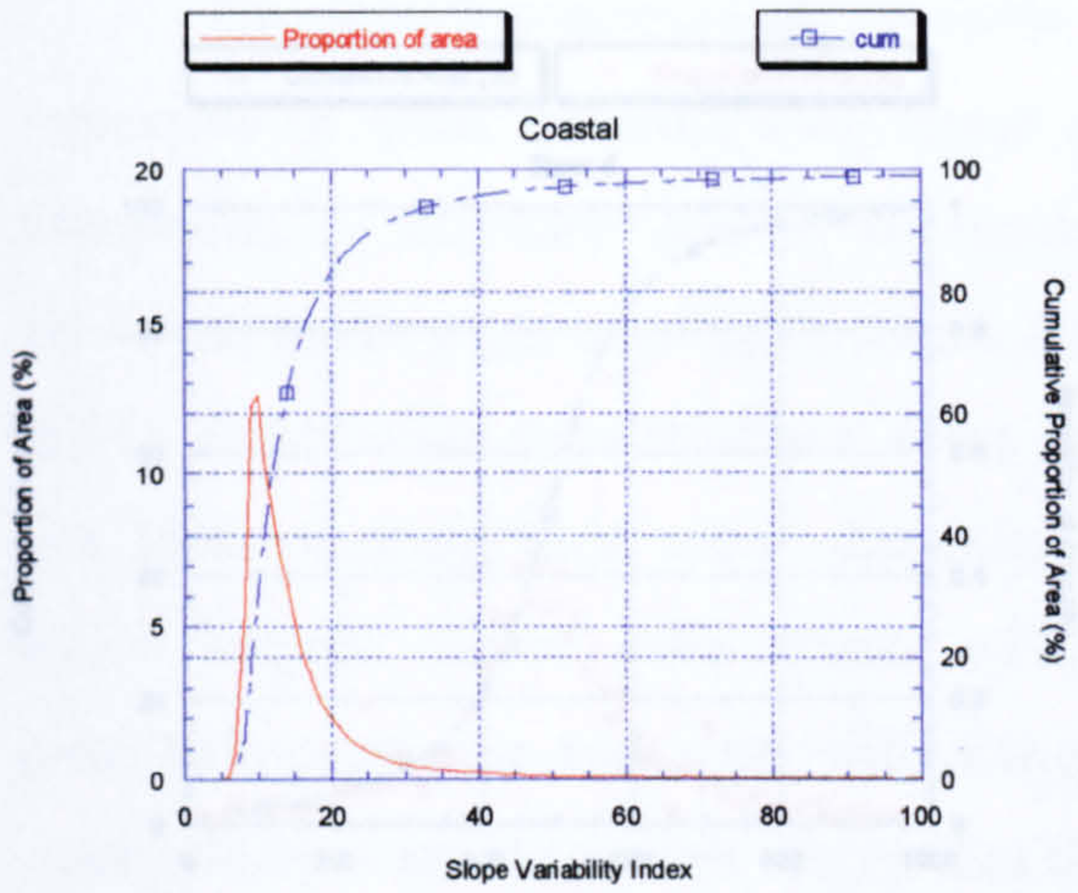

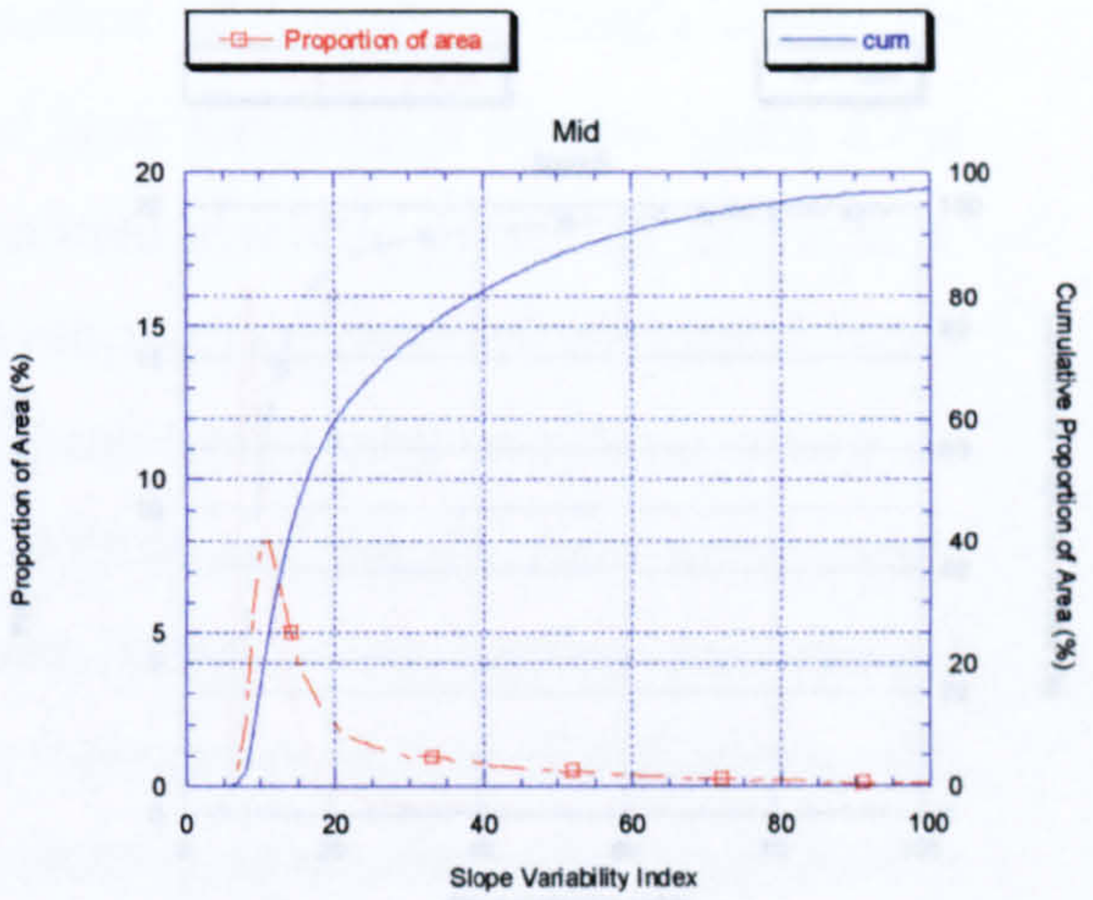

Coastal

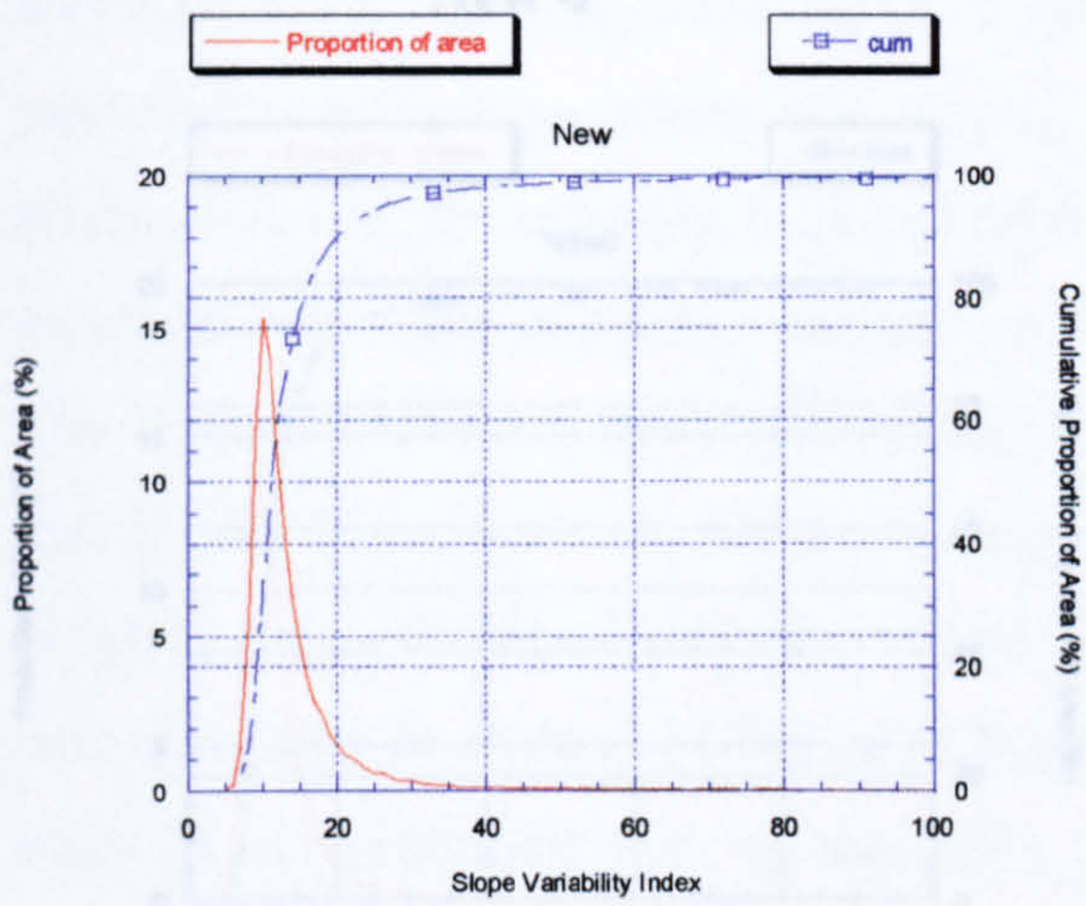

Mid

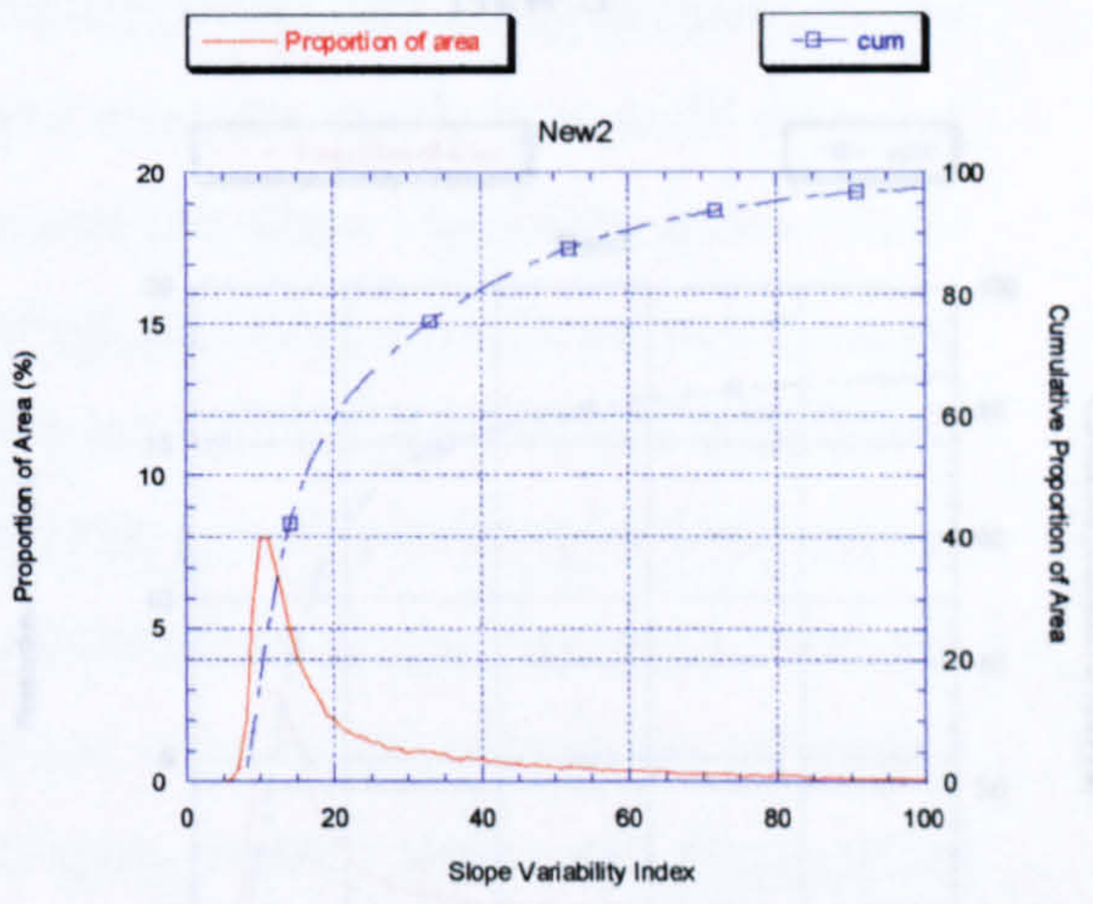

New

New 2

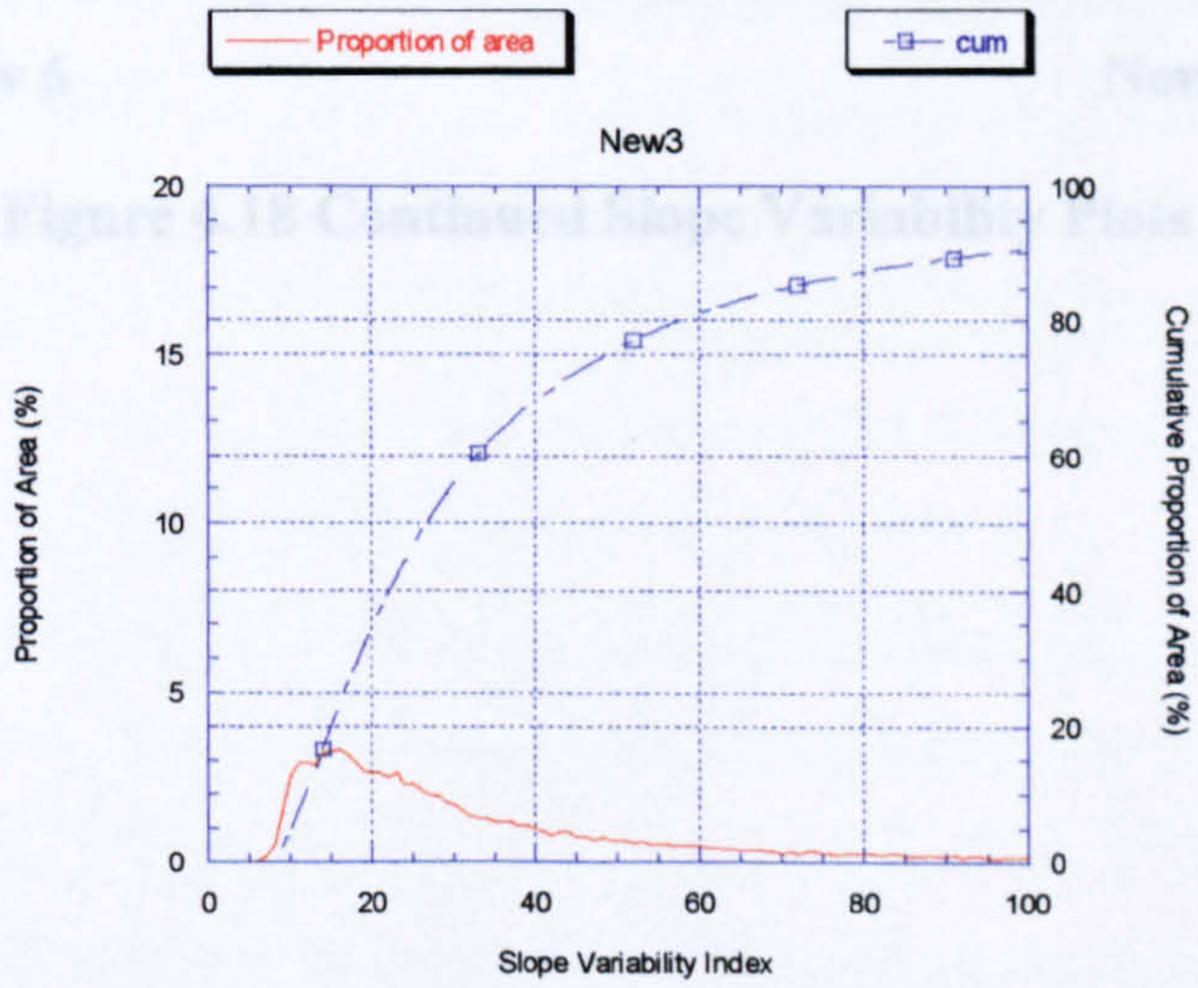

New 3

Figure 4.17 Slope Variability Plots

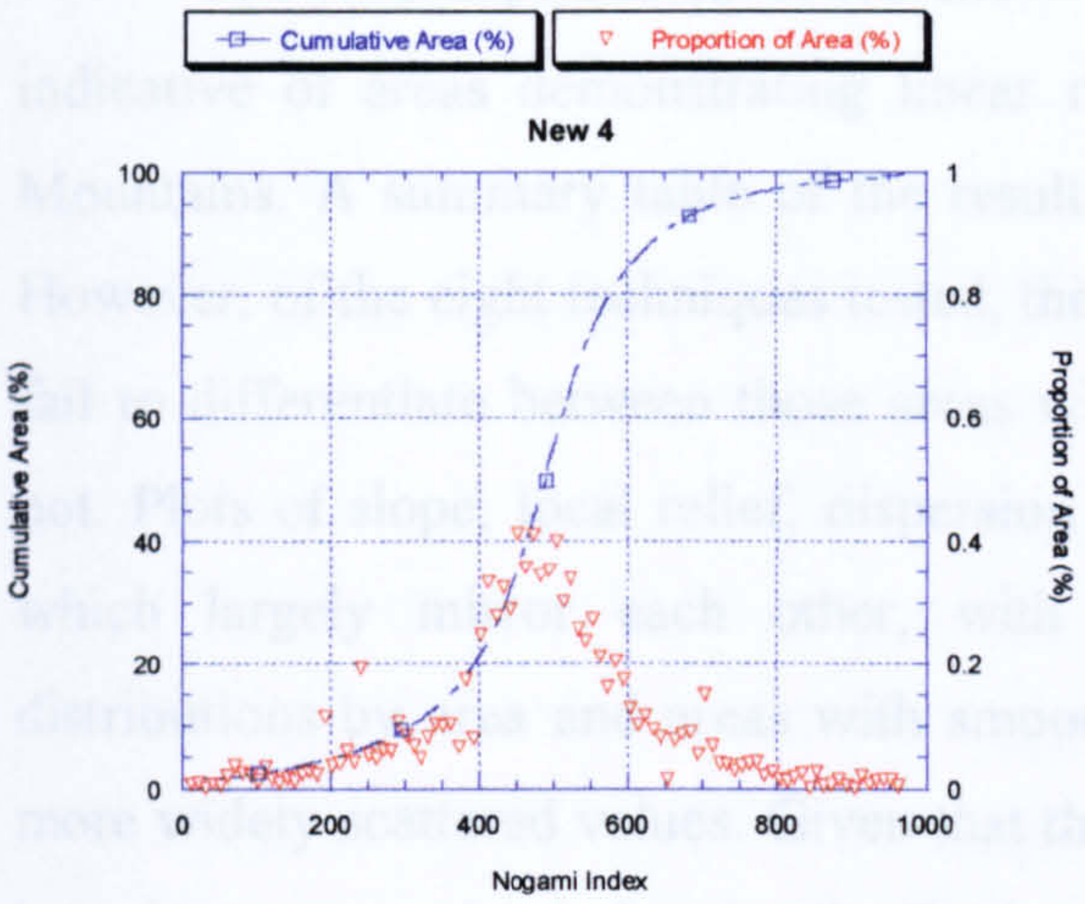

New 4

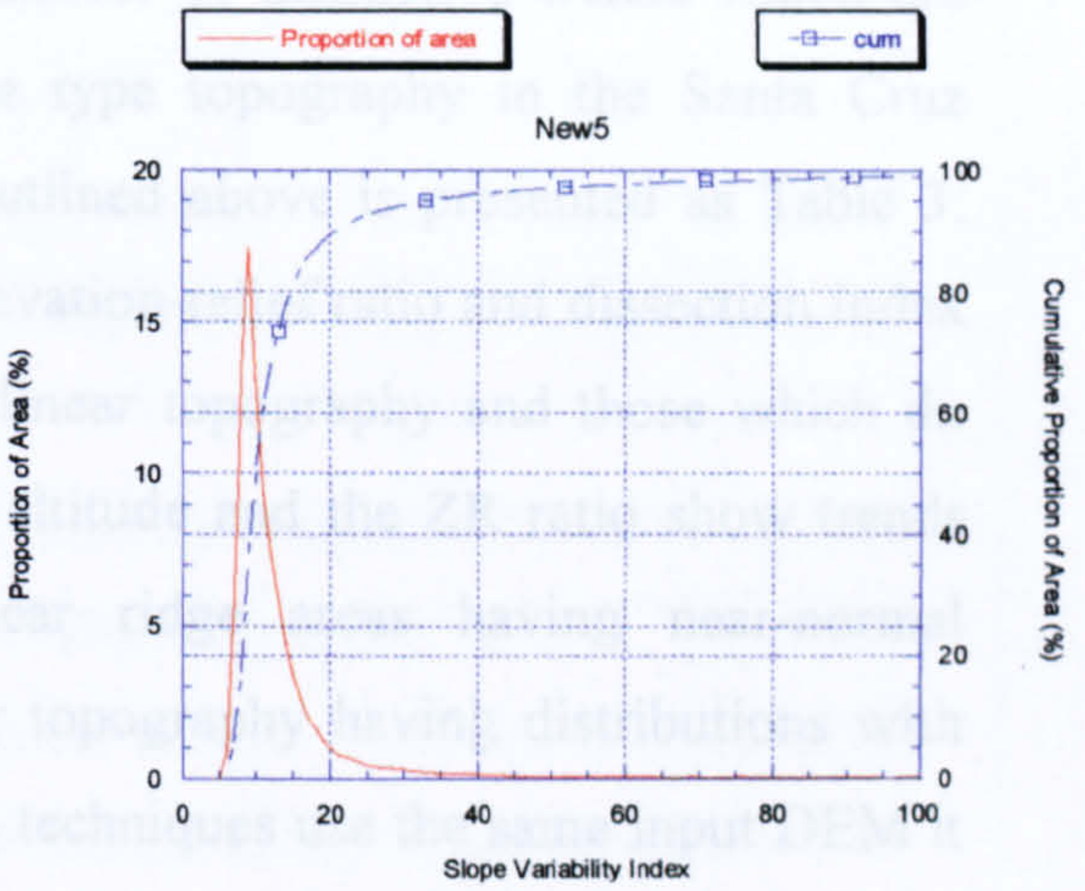

New 5

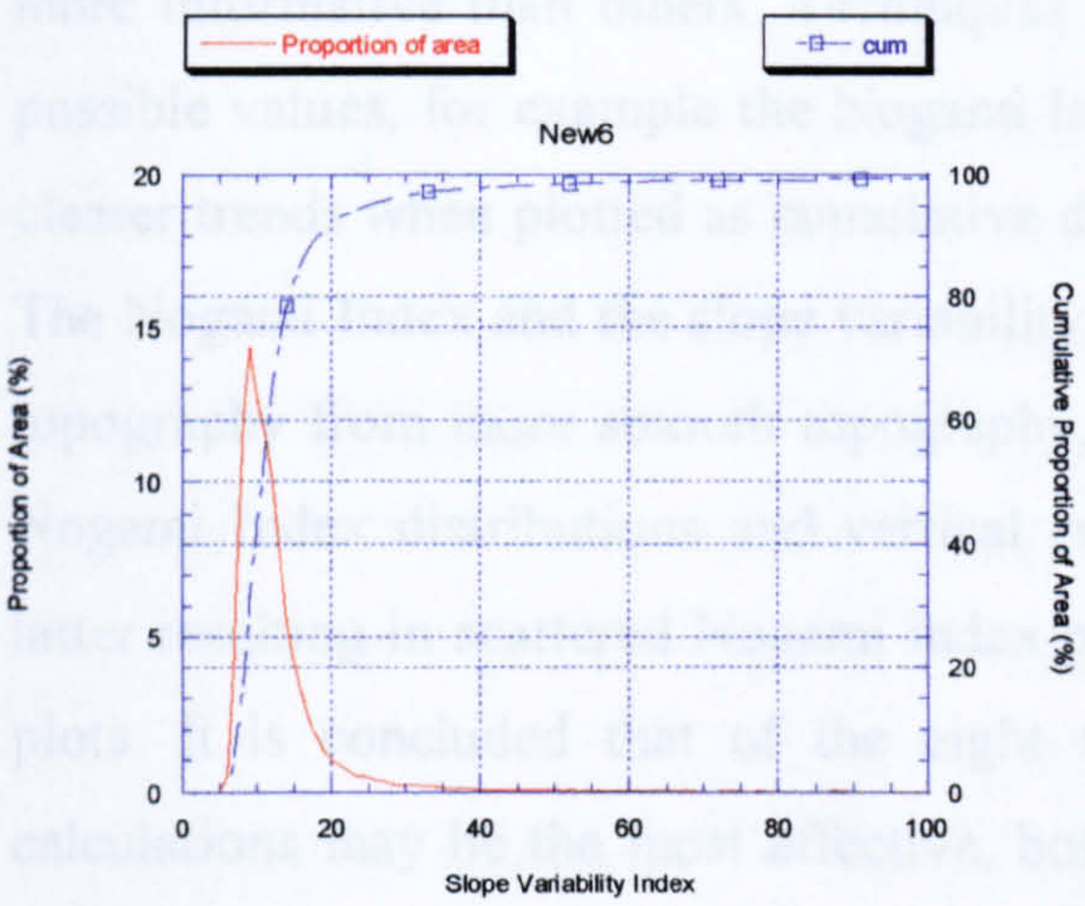

New 6

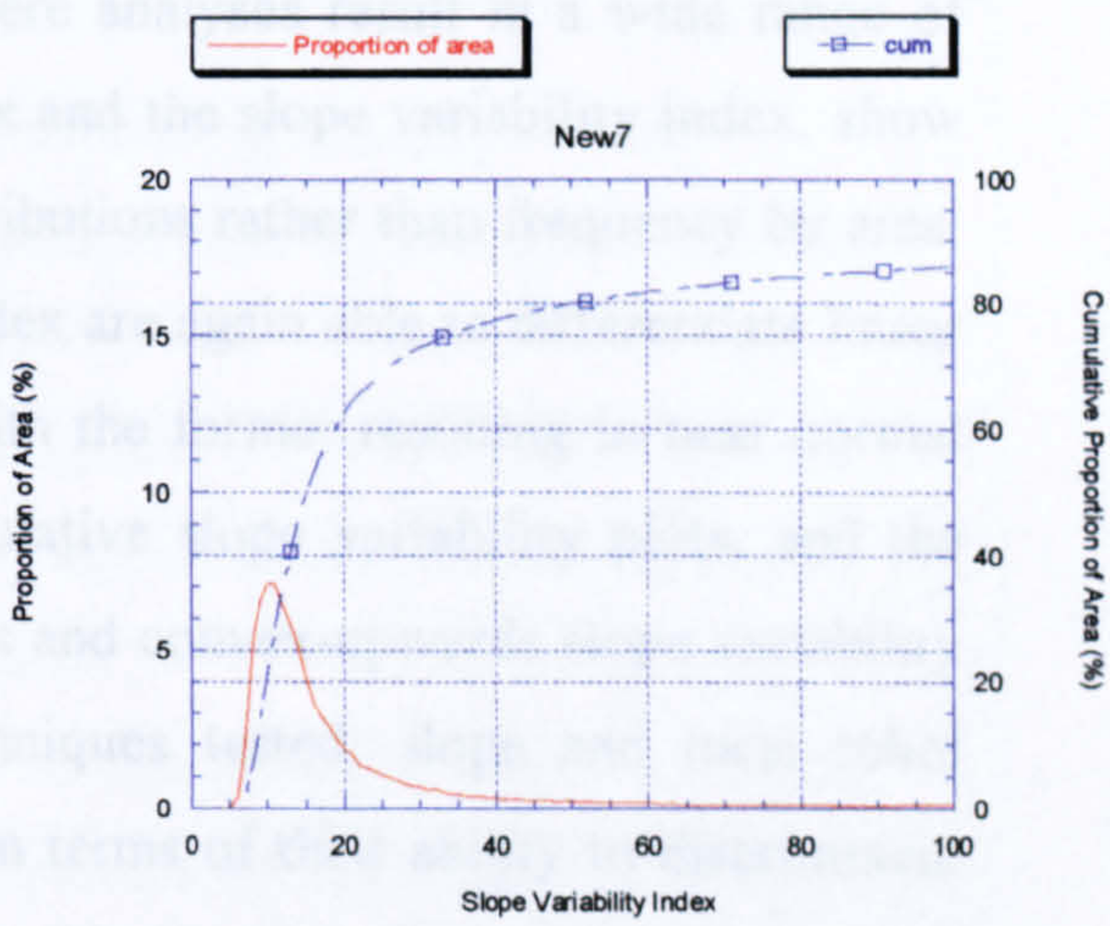

New 7

Figure 4.18 Continued Slope Variability Plots

4.5 SUMMARY OF RESULTS

The results presented above show a number of distinctive trends which are indicative of areas demonstrating linear ridge type topography in the Santa Cruz Mountains. A summary table of the results outlined above is presented as Table 3. However, of the eight techniques tested, the elevation-relief ratio and dissection index fail to differentiate between those areas with linear topography and those which do not. Plots of slope, local relief, dispersion of altitude and the ZR ratio show trends which largely mirror each other, with linear ridge areas having near-normal distributions by area and areas with smoother topography having distributions with more widely scattered values. Given that these techniques use the same input DEM it is perhaps unsurprising that the distributions show similar trends, yet the failure of the elevation-relief and dissection index to differentiate show that some techniques are more informative than others. Techniques where analyses result in a wide range of possible values, for example the Nogami Index and the slope variability index, show clearer trends when plotted as cumulative distributions rather than frequency by area. The Nogami Index and the slope variability index are again able to differentiate linear topography from more smooth topography, with the former resulting in near normal Nogami Index distributions and vertical cumulative slope variability plots, and the latter resulting in scattered Nogami index plots and convex-upwards slope variability plots. It is concluded that of the eight techniques tested, slope and local relief calculations may be the most effective, both in terms of their ability to discriminate linear topography from non-linear topography and in the ease with which they may be calculated over large areas.

Index	Notes
Slope	• Excellent ability to discriminate. Identifies clustering of threshold slope values of 16-24°
Local Relief	• Excellent capability to discriminate at 3 pixel level. • Clustering around values of 50-70 m where threshold slopes present • Higher pixel window sizes fail to reproduce clear results due to high range of values resulting
Dispersion of Altitude	• Excellent ability to differentiate linear slope areas • Threshold values in the range 10-20. • Coastal ranges have higher values than central counterparts
ZR Ratio	• Again, excellent ability to discriminate, yet smaller range of values for linear and non-linear terrain • Values of 3-5 present for linear ridge terrain
Elevation Relief Ratio	• No ability to discriminate between linear ridge and smoother types of topography
Dissection Index	• No ability to discriminate between linear ridge and smoother types of topography
Nogami Index	• Near normal cumulative distributions with values ranging from 400 to 600 for linear ridge terrain
Slope Variability Index	• Near vertical cumulative plots for linear ridge terrain, with values between 10 and 12.

Table 4.3 Summary Table of Morphometric Indices Ability to Identify Linear Ridge Topography

4.6 BEDROCK VARIATION AND HILLSLOPE FORM IN THE SANTA CRUZ MOUNTAINS

As outlined above, many current surface process models overlook variations in factors such as bedrock lithology in their simulations. This is partly due to the belief that such variation is of little significance to large scale relief development (e.g. Ahnert, 1970), and also due to the difficulty of incorporating the variability of such factors into models. More recently, research has indicated that bedrock lithology plays a key role in controlling terrain form in the Santa Monica Mountains (Meigs *et al.*, 1999). Work presented in Appendix 1 demonstrates that variations in lithology also determine which areas are affected by rotational landslide activity in Marin County in California. More studies at the scale of orogens are required if the current lack of agreement concerning the importance of bedrock variation on hillslope relief and process dominance is to be revolved. This section explores the general relationships existing between lithology and slope gradient in the Santa Cruz Mountains. Within each of the study areas, the relationship between slope form and bedrock variations are examined.

4.6.1 Slope-Lithology Interactions

Within each of the study areas there appears to be a high degree of variation in the correlations between slope characteristics and lithological type; in some cases showing clearly defined relationships and in others no such features.

Coastal shows high slope gradient values dominating in the west and centre of the study area (Figure 4.2). As shown in Figure 4.19, these high slope values (μ=23°) appear where Upper Tertiary Santa Cruz mudstones and shales dominantly outcrop. Slope values are also high in the centre of the study area where Lower Tertiary Butano sandstones outcrop (μ=22°). Towards the northeast of Coastal, Rices mudstone outcrops, and this is reflected in somewhat lower mean slope values (μ=19°). There therefore exists to be a relatively good correlation between lithology and slope within the Coastal area. Linear ridge type terrain also dominates in the south and south-west of the area, mirroring the trends shown by slope and lithology. However, locally high slope values on the lower hillslopes may reflect external influences on slope form, including fluvial undercutting of slopes and mass movements.

Mid shows a relatively complex assortment of lithologies cropping out at the surface, ranging from broad bands of Lower Tertiary Butano sandstones, Rices mudstones and Lower Tertiary Vaqueros sandstones in the north and north-east, to Santa Margarita sandstones and Monterey Formation shales in the south and south-west. Examination of the shaded relief map (Figure 4.1) shows that generally the hillslopes get more dissected, and linear ridge type morphologies dominate more, the further north-east one moves in the study area. This appears to correlate well with lithological outcrop patterns, with low slope gradient Monterey Formation shales in the south-west (μ=18°) and more resistant Butano sandstones in the north-east (μ=22°)..

New is dominated by surface outcrops of the Upper Tertiary Purisima Formation (covering some 52 % of the study area). This formation appears to show a high degree of variability in slope gradient values (ranging from 0° to 47°). Despite the appearance of variations in hillslope morphology (Figure 4.1) from smoother topography in the south-east, to linear ridge type terrain in the centre of the basin, and longer linear hillslopes in the north-east, and apparent correlations with lithological variations (Figure 4.19) from dominantly the Purisima Formation in the south-west and centre to other lithologies in the north-east, these are not mirrored by slope characteristics. High slope values are scattered widely about the study area, and appear to show little preferential siting upon particular lithologies. This is reflected in the dominant three lithologies (Purisima Formation, Butano Sandstone and the Monterey Formation) having mean slope values of 18° and 19°.

The morphology of New2 varies from smooth, diffuse topography in the north-east of the study area to more dissected, linear terrain in the south-west and north-west. These characteristics are largely reflected by slope and lithological patterns, with the higher southern slope values (μ=21°) and linear terrain dominating where Upper Tertiary Santa Cruz shales outcrop, whilst in the north-east and centre of the study area Santa Margarita sandstones and Quaternary deposits are reflected by lower slope values (μ=11° and μ=15° respectively) and diffuse topography.

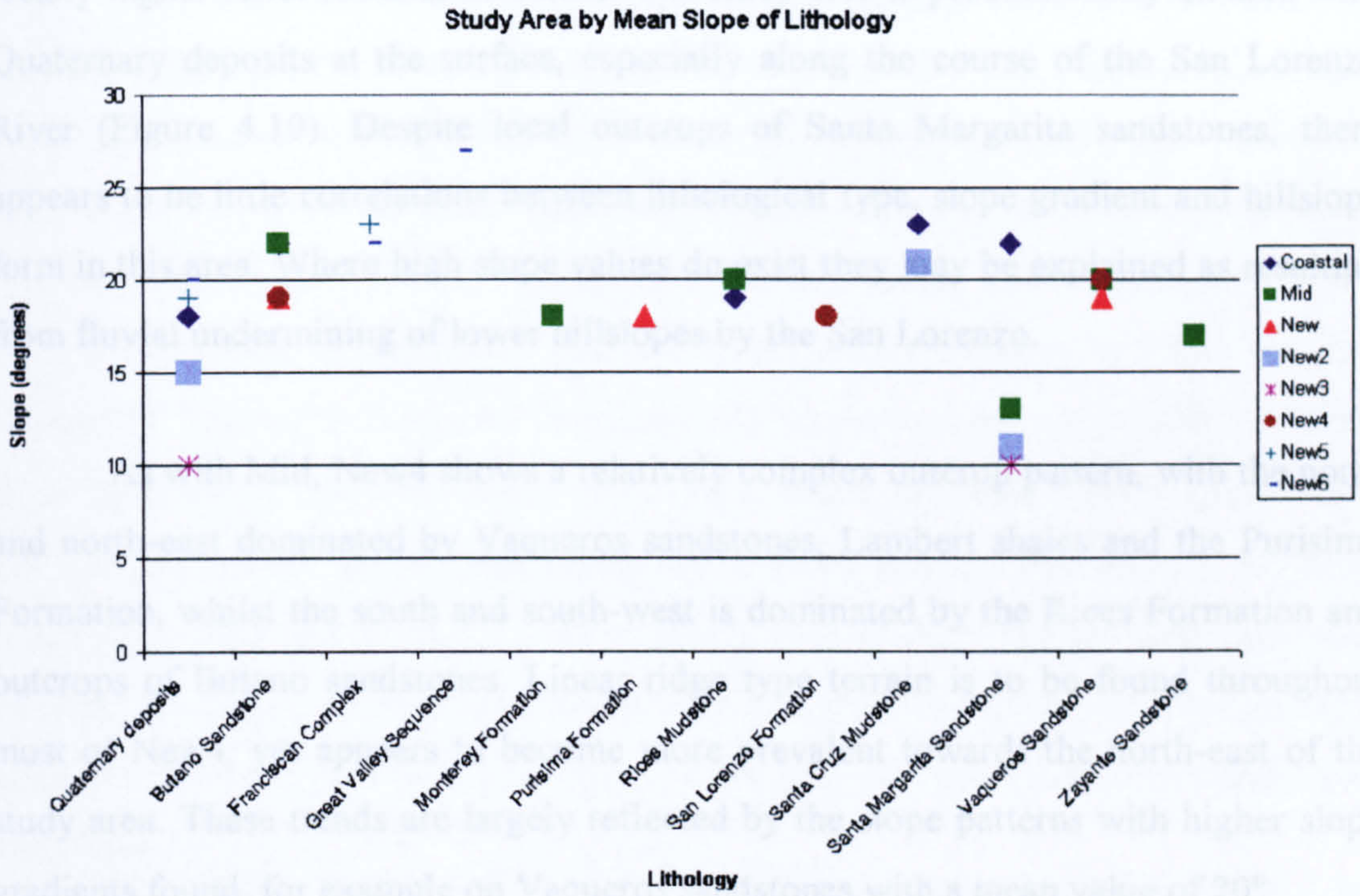

Figure 4.19 Mean Slope of Bedrock Lithologies in Santa Cruz Study Areas

New3 is an area with dominantly low topographic relief and a small area of locally higher relief towards its centre. The study area is predominantly an area with Quaternary deposits at the surface, especially along the course of the San Lorenzo River (Figure 4.19). Despite local outcrops of Santa Margarita sandstones, there appears to be little correlations between lithological type, slope gradient and hillslope form in this area. Where high slope values do exist they may be explained as resulting from fluvial undermining of lower hillslopes by the San Lorenzo.

As with Mid, New4 shows a relatively complex outcrop pattern, with the north and north-east dominated by Vaqueros sandstones, Lambert shales and the Purisima Formation, whilst the south and south-west is dominated by the Rices Formation and outcrops of Butano sandstones. Linear ridge type terrain is to be found throughout most of New4, yet appears to become more prevalent towards the north-east of the study area. These trends are largely reflected by the slope patterns with higher slope gradients found, for example on Vaqueros sandstones with a mean value of 20°.

New5 is dominated by outcrops of Mesozoic Franciscan complex sheared shale and metasandstone with hard blocks (melange), covering some 70 % of the study area. The shaded relief map indicates that as with New4, large parts of the study area show linear ridge type terrain, with only the far north showing lower relief terrain. This lower slope terrain exists where Monterey shale and Temblor sandstones outcrop (μ=14° and μ=15° respectively). By contrast, the Franciscan melange shows a higher mean slope value of 22°.

Lithological outcrops in New6 support findings from many other study areas in the Santa Cruz Mountains. The centre and east of the area is dominated by outcrops of Franciscan melange, with linear terrain and high mean slope values (μ=22°), whilst towards the south-west, the Great Valley Sequence dominates, and has the highest slope values of all outcrops in the Santa Cruz study areas (μ=27°). Interestingly, the north and north-east of the area is dominated by Quaternary deposits, as is the far south. The north shows smoother topography than the south, despite similar lithologies; this variation within a lithology is reflected by the slope range from 0° to 44°, with higher values dominance reflected by the relatively high mean value of 20°.

4.6.2 Summary of Findings

Comparing among the study areas, there are several distinctive trends which emerge. Where the Great Valley Sequence outcrops it has a much higher mean slope value than many other lithologies. The Franciscan complex and Santa Cruz mudstones also seem to demonstrate mean slope values greater than 20° within the areas where they outcrop extensively. Lithological types showing overall lower mean slope values ($\mu \leq 18°$) include the Monterey Formation, Purisima Formation and San Lorenzo Formation. The Santa Margarita Sandstone also seems to show a generally low mean slope value (< 15°), except for the case of Mid, where the mean value is greater than 20°. As suggested above, this could result from fluvial undercutting of lower hillslopes as hillslope processes yield to fluvial ones. Overall, though, where the more resistant lithologies dominantly outcrop there is a good correlation with higher slope values and the existence of linear ridge type terrains, with good examples being New5 and New6.

4.7 DISCUSSION

This chapter has demonstrated the ability of slope and relief terrain measures to distinguish linear hillslopes from DTM data. In addition, it has been shown that variations in bedrock lithology play a key controlling role in determining the distribution of hillslope gradients in the Santa Cruz Mountains. These implications of these findings for surface process models and large scale landscape analyses are now examined.

4.7.1 Linear Ridge Terrain, Bedrock Landsliding and Surface Process Modelling

Linear ridge type terrain has been widely observed in the mountainous uplands of Japan (Ohmori and Sugai, 1995), the Oregon Coast Range, California (Roering *et al.*, 1999) and in the Olympic Mountains of Washington State (Schmidt and Montgomery, 1995). Early studies of relationships between slope, relief and denudation rates found highly linear correlations between the rate of hillslope erosion and transport (e.g. Penck, 1924). These early findings have subsequently been mirrored by work in the 1960s (e.g. Ruxton and McDougall, 1967) and also in recent research examining slope-dependent erosion rates (e.g. Dietrich *et al.*, 1993).

4.7.1.1 Linear Hillslope Transport

Early work tended to emphasize the role played by hillslope gradient in sediment transport, relating the rate of transport linearly to slope gradient through the linear diffusion equation. The diffusion equation (Equation 3.1) assumes that sediment transport is transport limited, implying that there is infinite weathering of regolith and bedrock on the upper hillslopes, which can be transported downslope given sufficient hillslope gradients.

Research in the past decade has emphasized the role played by non-linear transport mechanisms in hillslope transport, and the implications such findings have for computer simulations of landscape evolution (e.g. Roering *et al.*, 1997). It has been recognised that early models (for example Koons, 1989) which simulated hillslope evolution using artificially high diffusivity coefficients may be flawed, despite their ability to reproduce realistic-looking topography (Martin and Church, 1997). Despite this recognition, several later models (e.g. Anderson, 1994; Wilgoose *et al.*, 1991; Kooi and Beaumont, 1994) have continued to adopt the linear diffusion

equation as it permits simpler modelling and seems to be able to describe the gradient-transport laws in certain field situations (e.g. Rosenbloom and Anderson, 1994).

Recognition from field studies of scarp environments (Anderson and Bucknam, 1987) and other situations (Schumm, 1964; van Asch *et al.*, 1989) of the role played by non-linear relations between slope gradient and sediment transport rates has led to the incorporation of threshold instabilities to diffusion equations in some simulations (for example Howard, 1994; Tucker and Slingerland, 1994), yet these models assume instantaneous slope lowering above a threshold slope value (Densmore *et al.*, 1997). Additionally, whilst linear diffusion has been widely adopted to simulate hillslope transport, sediment flux calculations adopting this approach tend to produce landscapes in which slopes decline and landscapes are smoothed over time. In a study of the Oregon Coast Range, Roering *et al.* (1999) provide evidence that linear hillslopes result from nonlinear slope diffusion of regolith. However, despite the ability of their model to simulate both sediment fluxes and slope forms observed in the area, they explicitly state that such findings would be invalid in areas where regolith production is outpaced by sediment transport and denudation involves bedrock sliding.

4.7.1.2 Bedrock Landsliding

Bedrock-involved landsliding (Section 3.3.3) has been shown to dominate slope evolution in many landscapes, for example in New Zealand (Hovius *et al.*, 1997). Independent field observations (Anderson, 1994) have shown bedrock sliding to dominate many parts of the Santa Cruz Mountains, whilst computer simulations (Densmore *et al.*, 1998; Densmore *et al.*, 1996) modelling bedrock landsliding have captured linear hillslopes and triangular facets observed in the field and clustering of slope values observed from DTM analysis (Figure 4.5). ZSCAPE (Ellis *et al.*, 1999; Densmore *et al.*, 1998a, 1998b) simulates bedrock landsliding occurring as a result of base level fall, creating steep lower hillslope segments which in turn trigger upper slope instability and failure. Models which simulate hillslope mass wasting as resulting from failure above an upper slope threshold (e.g. Anderson, 1994; Tucker and Slingerland, 1996) could be improved by applying results from the analyses in this chapter.

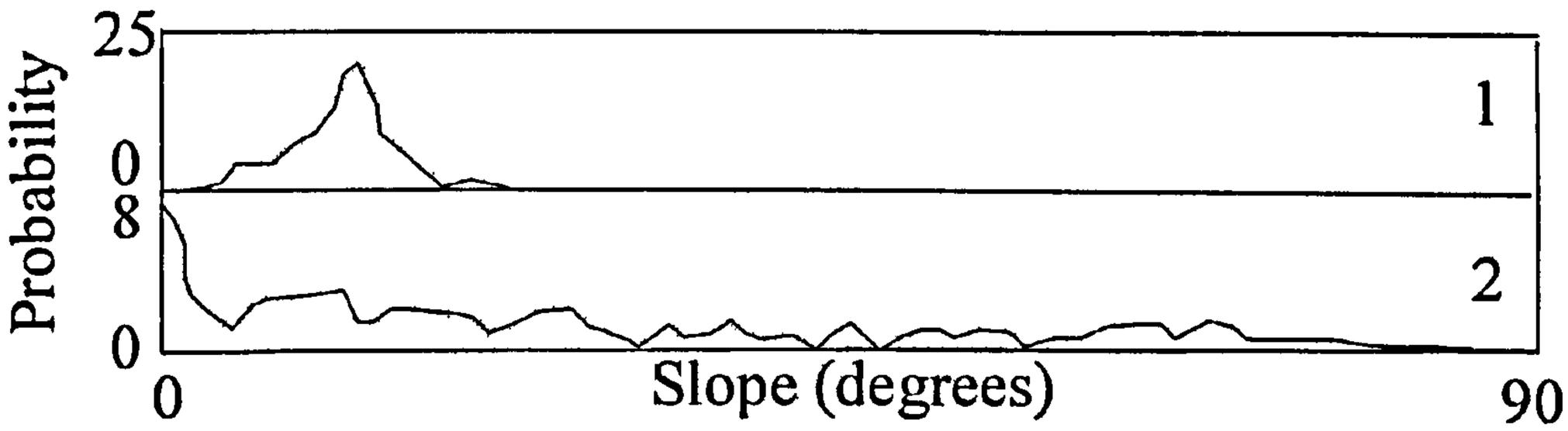

Figure 4.20 Slope Gradient Distributions Resulting from Linear Slope Diffusion (1) and Bedrock Landsliding (2) (After Densmore *et al.*, 1998). (Note Peaked Slope Distribution Resulting from Bedrock Landsliding Compared to More Widely Distributed Slope Distribution Resulting from Diffusive Processes).

Results have indicated that areas demonstrating linear ridge terrain have slope values clustering about values of 18-20°, with local relief values of 60-70 m. By applying threshold values determined from DTM analysis, criticism that SPMs lack a real world underpinning (Burbank and Pinter, 1999) can be overcome. This chapter also demonstrated the ability of slope and local relief algorithms to capture the nature of linear ridge terrain, thus by applying such algorithms to the output of SPMs, one may test their ability to replicate landscape morphology under different conditions.

4.7.2 Bedrock Controls on Relief Development

The role played by variations in bedrock lithology on terrain development has received considerable attention, yet agreement on the importance of such variability is far from lacking. Whilst many agree that bedrock lithology plays a significant role in determining landscape form at small scales (e.g. Ahnert, 1970), it is at larger scales that its role has been debated. Whilst some have argued that bedrock lithology may control sediment fluxes and denudation rates at orogenic or larger scales (Summerfield and Hulton, 1994), others (for example Ahnert, 1970) have proposed that variations in bedrock strength at such large scales will in effect balance out as resistant and weaker lithologies outcrop over similar areas. Furthermore, Hovius (1996) suggests that regular spacing of drainage outlets from mountainous regions implies that bedrock variation is unimportant. At best, the relationship between processes, bedrock lithology and terrain form is poorly constrained (Campbell, 1975).

The importance of bedrock lithology on form and process within mountains also has important implications for large scale studies of controls on relief as well as the relationships of slope and denudation. Conventionally, relief within many mountainous areas has been held to be incision limited, with the lower boundary condition driving relief formation and being determined by rates of fluvial incision into the underlying bedrock. However, studies in Washington State (Schmidt and Montgomery, 1995) and the Himalayas (Burbank *et al.*, 1996) indicate that relief development may be limited by the strength of the bedrock forming the hillslopes rather than being limited by rates of fluvial incision. In these areas, as well as in the Santa Cruz Mountains, it has been proposed that limits to relief are determined by the bedrock strength, with deep bedrock-involved landsliding occurring wherever the

critical shear strength of the bedrock material is exceeded (Schmidt and Montgomery, 1995; Densmore *et al.*, 1998).

4.8 CONCLUSIONS AND SUGGESTIONS FOR FUTURE RESEARCH

This chapter has shown evidence that linear hillslopes in the Santa Cruz Mountains are clustered at or close to critical values of slope gradient. Uplift of the mountain slopes or downcutting as a result of base level fall (Ellis *et al.*, 1999) will result in bedrock sliding of such slopes as the upper threshold for stability is breached. By applying realistic values of this slope threshold to surface process simulations, modellers can address criticism that their models lack real world underpinning (Burbank and Pinter, 1999). In addition, by comparing simulated output to that resulting from DTM analysis of areas with good process constraints, additional criticism that models are compared on a purely observational basis (Willgoose and Hancock, 1997) may also be minimalised.

The work in this chapter also supports the conclusion that variations in bedrock lithology affect orogenic scale topographic form (Meigs *et al.*, 1999; Tucker and Slingerland, 1996). This finding has a number of implications, both for our understanding of how orogens evolve and for how SPMs model their development. It had previously been suggested that bedrock variations were of little importance for large scale studies of terrain form, sediment flux and denudation (e.g. Ahnert, 1970). As a result of this, many models failed to address how variations in bedrock lithology affected these issues. Future work needs not only to examine other areas to see how changes in bedrock resistance affects terrain form and the types of processes acting upon it, but also how such variations can influence the spatial distribution of the material exiting the mountainous regions, i.e. denudation rates and resultant sediment fluxes. As with studies of terrain form, previous workers looking at denudation in mountainous regions largely overlooked bedrock variability. This issue is now addressed in the next chapter.

CHAPTER 5

HILLSLOPE EROSION, TERRAIN VARIATION AND SEDIMENT FLUX IN THE ITALIAN APENNINE MOUNTAINS

5.1 INTRODUCTION

An understanding of rates of denudation and the factors controlling them are of significance for a variety of reasons (Summerfield and Hulton, 1994). LEMs simulating the evolution of mountainous terrains (for example Kooi and Beaumont, 1994; Tucker and Slingerland, 1996) need to apply realistic rates of landscape lowering, whilst SPMs require such data to improve their ability to predict gross rates of sediment flux from upland areas to sedimentary basins (Tucker and Slingerland, 1996). The ways that mountains are eroded and the nature of removal of the resulting sediment has also been cited as significant in changing global climatic patterns (for example Raymo and Ruddiman, 1992), patterns of crustal activity beneath the mountainous terrain (Hoffman and Grotzinger, 1993), and the uplift of mountain peaks (Montgomery, 1994). Understanding how sediment is released into the sedimentary system is also important for understanding how catchment-delivery systems interact and in modelling basin stratigraphy (Allen and Hovius, 1998), and thus represent the key link between geomorphology and basin analysis (Leeder, 1997).

Despite growing acknowledgement of the importance of understanding how these processes interact, studies in the past have either tended to focus on global analyses (e.g. Summerfield and Hulton, 1994) or single drainage basin studies (e.g. Ahnert, 1970). Landscape evolution models represent a useful tool in examining the various interacting processes responsible for mountain belt development. However, as landscape evolution and surface process models frequently address process interactions at the scale of mountain belts (e.g. Tucker and Slingerland, 1996; Kooi and Beaumont, 1994), the fundamental links between denudation rates, surface morphology and erosional processes require examining at such a scale using field data and examples. In addition, despite the use of SPMs in studies predicting sediment flux from regions (e.g. Tucker and Slingerland, 1996) and in reconstructing the past morphology of areas based on flux information (Pazzaglia and Brandon, 1996), our

current understanding of how sediment flux from a region varies in terms of the climatic, tectonic and lithological characteristics of the source area remains relatively poorly constrained (van der Beek and Braun, 1998). Recently, research has indicated the importance of bedrock lithology in shaping orogenic topography (Tucker and Slingerland, 1996; van der Beek and Braun, 1999). Such studies have also suggested that previously adopted linear relief - denudation relationships may be far from the norm; lithological variations are held to affect both the relief of the landscape and rates of sediment liberated from it. At present then, relationships between both hillslope processes and bedrock lithology (Campbell, 1975), and relief and sediment fluxes are in need of better constraints (Tucker and Slingerland, 1996). Chapter 4 determined that variations in bedrock lithology play a key role in determining the macro-scale relief of the Santa Cruz Mountains, yet a more detailed study of how these variables interact and influence sediment fluxes is hindered by a lack of both detailed field observations and sediment yield data.

This study addresses many of the problems raised above by examining the nature of sediment redistribution in the Northern Apennines of Italy. Field observations have been made examining the nature of interactions between surface morphology, lithological variation and dominant erosional process. Links between sediment loads and denudation rates are then compared with variations in the terrain across the belt determined from a 230 m DTM. These observations not only allow for an assessment of the nature of orogenic scale controls on landscape morphology and sediment fluxes, but have important implications for the ways in which SPMs and LEMs simulate orogenic development. This chapter therefore has three main aims:

- To examine the relationship between landscape morphology and bedrock lithology in the Northern Apennines.
- To document quantitatively how field observations of landscape morphology and process dominance are reflected by changes in terrain parameters derived from a DTM.
- To investigate the relationship between sediment flux, denudation rate and relief in the Northern Apennines.

5.2 CONTROLS ON DENUDATION RATES AND SEDIMENT FLUXES FROM MOUNTAINOUS REGIONS

Denudation rates involve both the detachment of material by erosional processes and its transportation through a sedimentary system (Summerfield, 1991). The sediment flux exiting a mountainous system is a function of both the hillslope and fluvial characteristics of the basin, with factors such as terrain, climate, and drainage basin geometry being important (Tucker and Slingerland, 1996). Despite the large number of studies undertaken to examine these relationships, the major factors controlling the sediment flux entering sedimentary basins remains poorly constrained (Tucker and Slingerland, 1996). Within the hillslope system, denudation rates are controlled by a variety of basin characteristics such as the amount of weathering, rates and mode of mass wasting processes (Montgomery and Buffington, 1997), and drainage basin morphometry (e.g. Ahnert, 1970). Once liberated from the hillslopes, this material is transported through the sedimentary system by stream networks. The flux of material exiting the system is thus as much a function of the stream's capability to transport sediment as the efficacy of the hillslope system in producing the material originally.

5.2.1 Relief and Denudation Rates

Relief has been cited as a key control on rates of denudation in many landscapes (Ahnert, 1970). Studies around the world have found consistent trends between relief in the world's largest drainage basins and their denudation rates (Figures 5.1, 5.2 and 5.3) (Milliman and Meade, 1983; Summerfield and Hulton, 1994). Such findings support a study by Ahnert (1970), which found a strong linear relationship between denudation rates and relief measured in 400 km^2 windows within 20 mid-latitude drainage basins (Figure 5.2). Ruxton and McDougall (1967), investigating denudation on the Hydrographer's Volcano in Papua New Guinea also found a linear trend between relief and denudation (Figure 5.3). By contrast, Schumm (1963) found an exponential trend between relief and denudation rates. More recently, surface process models (Tucker and Slingerland, 1996; van der Beek and Braun, 1998; 1999) examining mountain belt scale relief - denudation interactions have shown nonlinear relationships, with simulations showing that under certain conditions relief and denudation are negatively related (Figure 5.4). The importance of variations

in bedrock lithology is held to be a key controlling factor in determining such trends, yet there are few studies which test this assumption in a natural setting.

5.2.2 Basin Topography and Denudation Rates

The relationship between basin area and denudation rates has been studied for a number of decades and remains a matter of debate (Summerfield and Hulton, 1994). Schumm (1963) and Milliman and Syvitski (1992) found strong linear relationships between basin area, denudation rate and sediment yields respectively (Figures 5.5 and 5.6). This has been postulated to be due to a number of reasons. Small drainage basins are frequently found in the uppermost areas of mountainous regions (Summerfield, 1991), and as such they are more likely to have steeper hillslopes reducing their capacity to store sediment as may occur on shallower slopes. In addition, larger basins are more likely to contain low gradient features such as floodplains and lakes, which store sediment (e.g. Trimble, 1983) and reduce sediment yields released at the system's outlet. By comparison, Summerfield and Hulton's (1994) global study found a weak negative linear relationship between basin area and denudation rates (Figure 5.6), which they attributed to factors such as storage and the effects of lithological variation. Slaymaker's (1987) study of basins in western Canada found that small basins (<100 km^2) had the lowest denudation rates, whilst intermediate-sized ones (1000-100,000 km^2) had the highest denudation rates. Trends from geographical area to area and between basins of different size are therefore far from consistent, however it is likely that variations in lithology play key roles in denudation rates (Summerfield and Hulton, 1994).

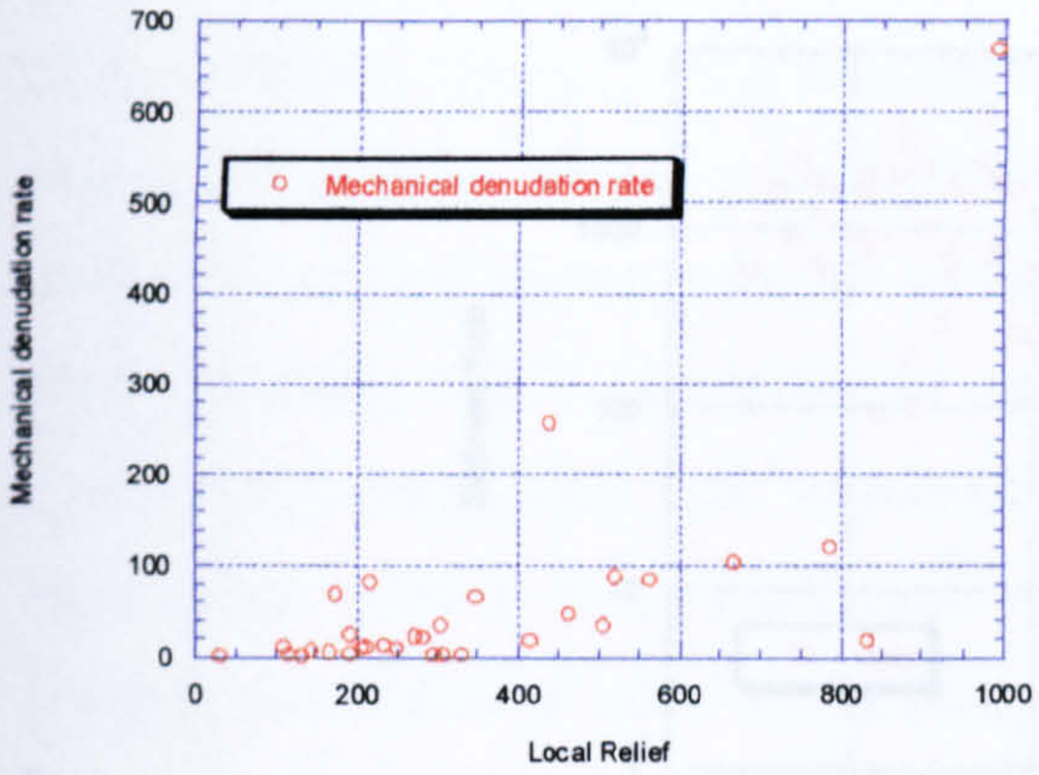

Figure 5.1 Relationship of Local Relief and Mechanical Denudation Rate (After Summerfield and Hulton, 1994)

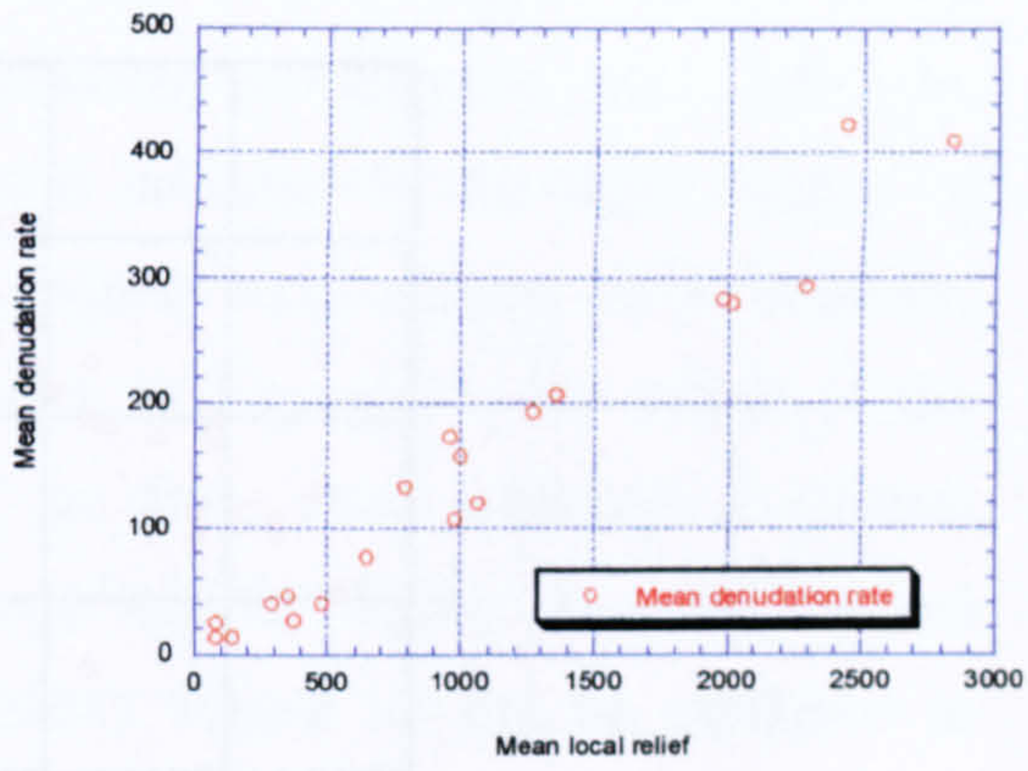

Figure 5.2 Relationship of Local Relief and Mean Denudation Rate (After Ahnert, 1970)

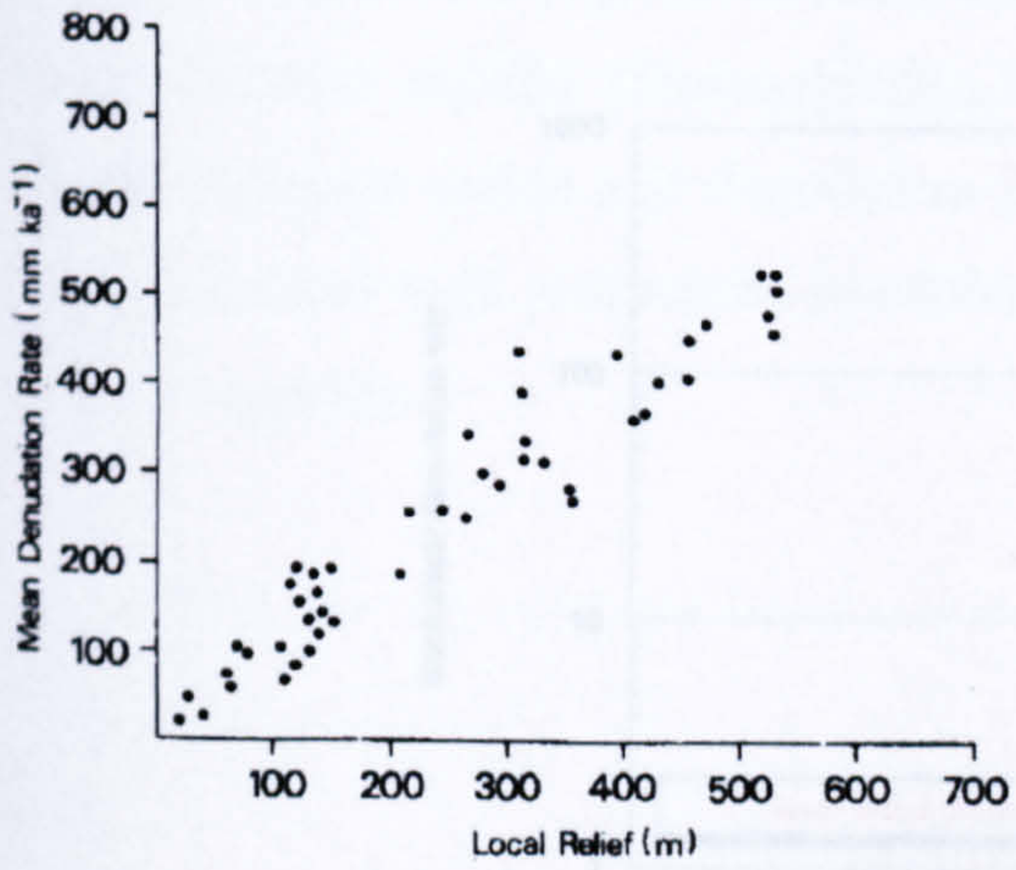

Figure 5.3 Relationship of Local Relief to Mean Denudation Rate, Hydrographer's Range, Papua New Guinea (After Ruxton and McDougall, 1967)

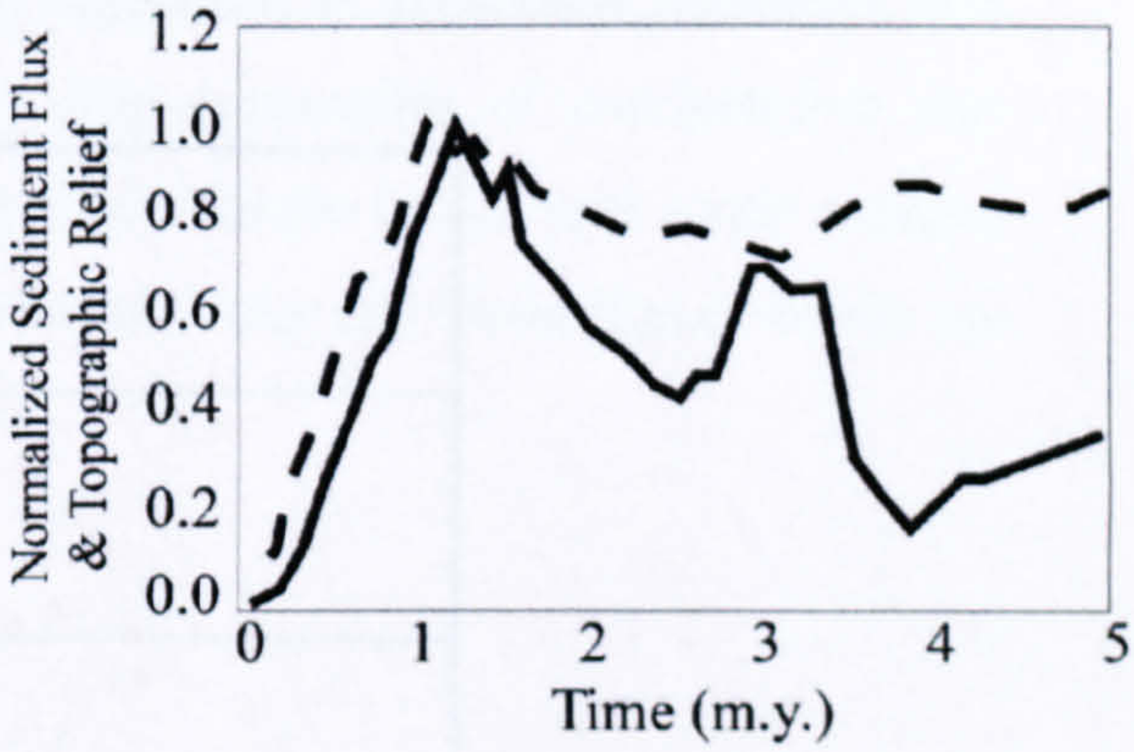

Figure 5.4 Computer Model Based Comparison of Sediment Flux Versus Mean Local Relief Through Time For the Zagros Fold Belt (After Tucker and Slingerland, 1996, Fig. 16). Note Both Positive and Negative Relationships Between Relief and Sediment Yield.

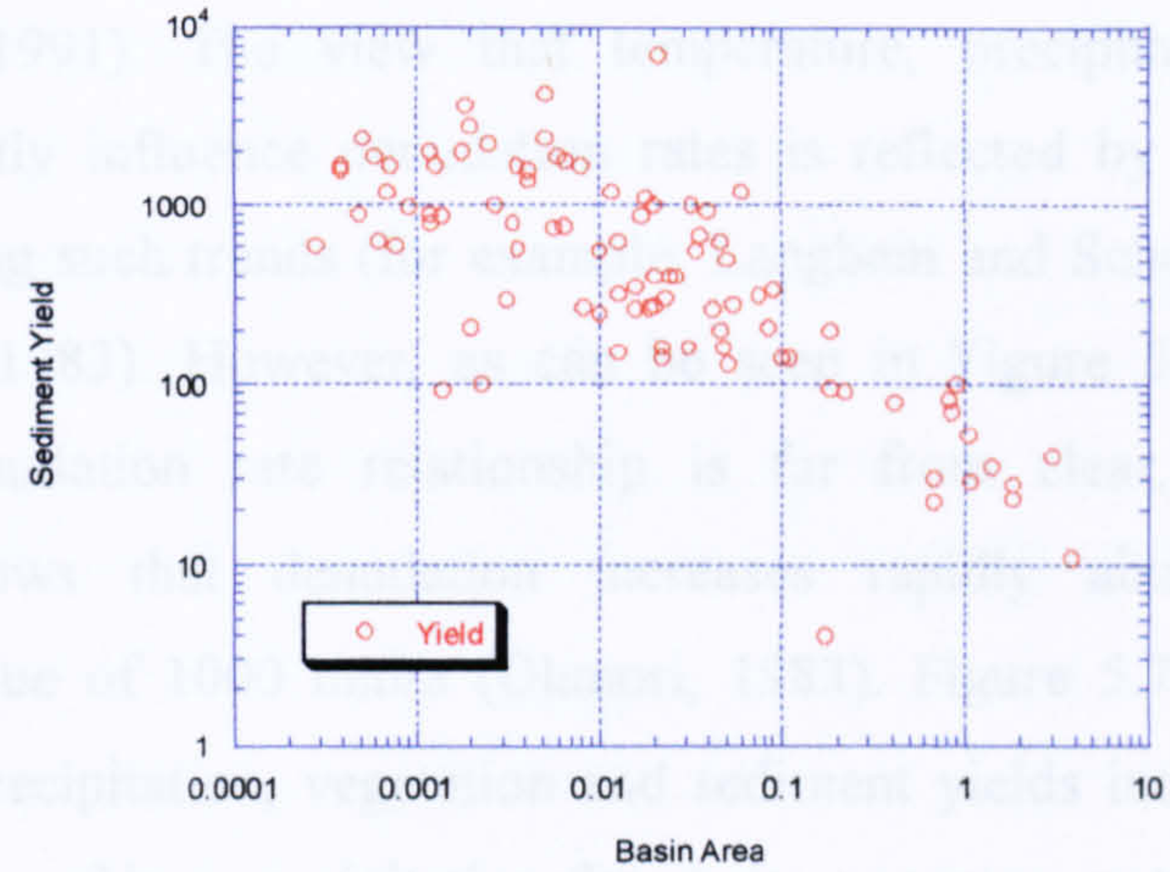

Figure 5.5 Relationship of Basin Area and Sediment Yield (After Milliman and Syvitski, 1992)

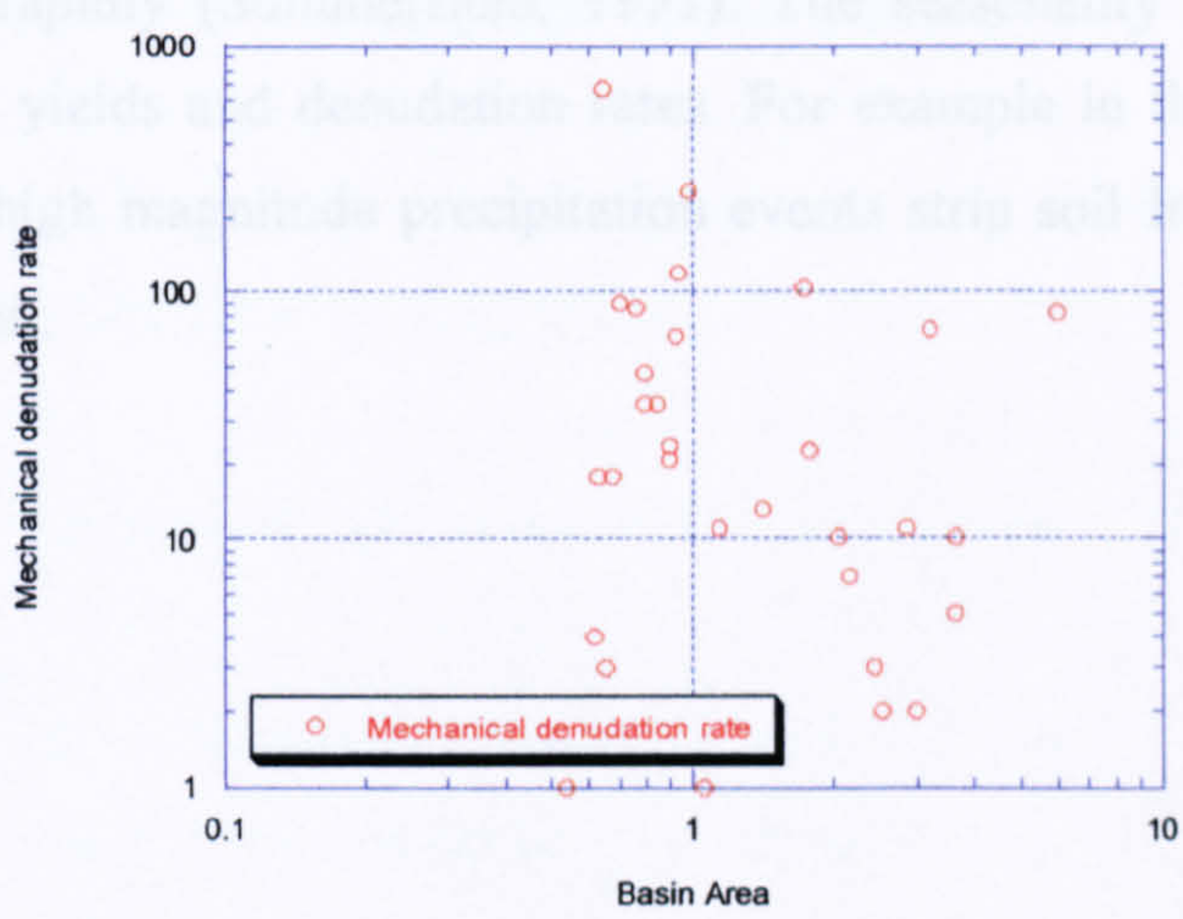

Figure 5.6 Relationship of Basin Area and Mechanical Denudation Rate (After Summerfield and Hulton, 1994)

5.2.3 Climatic Controls on Denudation Rates

In contrast to the generally accepted relationship between denudation rates and relief, the effects of climatic variables on the former are the subject of more debate (Summerfield, 1991). The view that temperature, precipitation and, indirectly, vegetation directly influence denudation rates is reflected by the large number of studies examining such trends (for example, Langbein and Schumm, 1958; Fournier, 1960; Ohmori, 1983). However, as can be seen in Figure 5.7, the nature of the precipitation-denudation rate relationship is far from clear, although a general observation shows that denudation increases rapidly above a mean annual precipitation value of 1000 mm/a (Ohmori, 1983). Figure 5.7 can be explained in terms of how precipitation, vegetation and sediment yields interact. Low yields are observed in areas of low precipitation for obvious reasons, yet yields remain low at higher precipitation values as vegetation becomes more dominant and covers hillslopes (Langbein and Schumm, 1958). However, a maximum precipitation value is reached, above which runoff is too great for vegetation to hold back sediment, and yields increase rapidly (Summerfield, 1991). The seasonality of precipitation also affects sediment yields and denudation rates. For example in the arid south-western USA, localised high magnitude precipitation events strip soil from slopes which are void of vegetation.

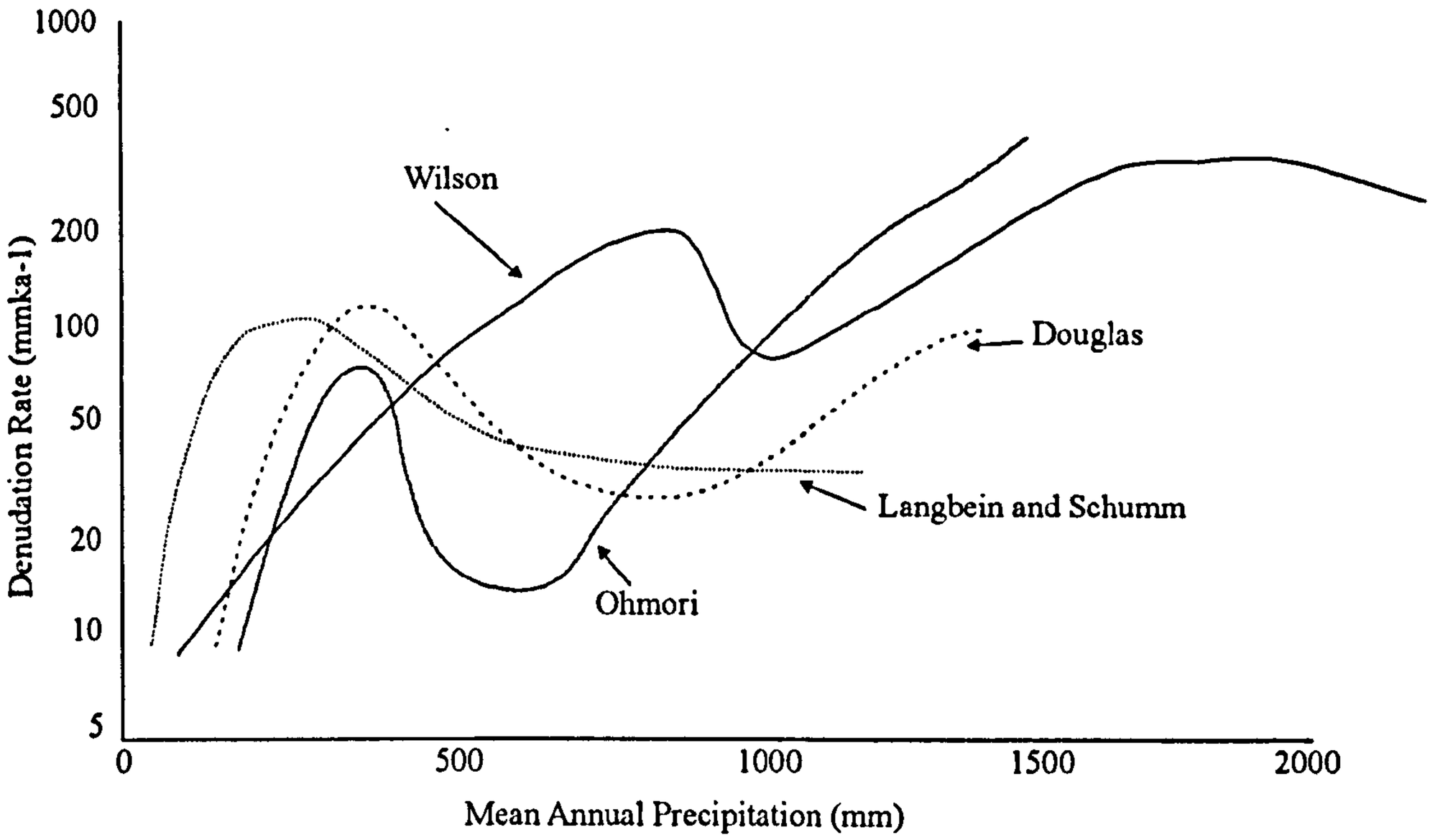

Figure 5.7 Relationship Between Precipitation Rate and Mechanical Denudation Rate (After Ohmori, 1983)

5.3 ESTIMATING DENUDATION RATES

The importance of being able to determine denudation rates has led to the proposal of a variety of techniques based on different data which vary in the resolution of their predictions. Among the techniques proposed are those based on river sediment load measurements, those based on sediment volumes in reservoirs and sedimentary basins (for example, Howell and Murray, 1986), and those directly attempting to measure rates of land surface lowering, for example, using K-Ar dating to record land surface lowering in the Hydrographers' Volcano, Papua new Guinea (Ruxton and McDougall, 1967). Additional techniques include those attempting to estimate denudation rates using radiometric and fission track dating methods (for example Brown *et al.*, 1994), and, finally, those using cosmogenic isotope analysis (for example Cockburn *et al.*, 1997; Granger *et al.*, 1996). Of these techniques, denudation rates estimated from sediment yields measured in river systems exiting upland areas are amongst the most frequently used. Sediment load data allow for back-calculation of the total volume of rock eroded, which, when divided by basin area, give crude estimates of denudation rates at the scale of individual basins (Ahnert, 1970). At more local scales, where factors such as climatic and morphometric variables may be constrained, denudation rates within individual basins may be modelled (Allen and Hovius, 1998).

5.3.1 Problems Associated with Calculating Denudation Rates from Sediment Yield Data

Despite the widespread usage of sediment yield data in determining denudation rates, there exist a number of problems and assumptions associated with such calculations. These problems include those directly associated with measurement strategy (Milliman and Meade, 1983), those associated with basin morphology (Trimble, 1977; 1983), and those resulting from the method used to calculate the denudation rates (Summerfield, 1991).

Firstly, many estimates of denudation rates based on sediment load data only use suspended sediment yields in rivers (for example, Dole and Stabler, 1909), neglecting the role of bedload in such calculations (Milliman and Meade, 1983). Whilst this may be of little significance in lowland tropical rivers, it is likely to introduce significant error in mountainous regions where bedload contribution to the

overall sediment load of rivers increases (Summerfield, 1991). For example, Peters (1978) found that bed load in the Zaire River may account for a greater proportion of transported material than solute and suspended sediment loads.

Secondly, problems are associated with the measurement process itself, including the technique used, the sampling strategy employed, and the time period over which sampling is undertaken. Measurements from some rivers were taken in the last century, for example the Irrawaddy River's calculations taken in the 1870s (Milliman and Meade, 1983), thus techniques may be variable. In addition, some gauging stations, where sediment loads are calculated, are based upstream of river mouths, and thus tend to underestimate the amount of sediment exiting the system (Milliman and Meade, 1983). Estimates taken at single periods can underestimate measurements by occurring at low sediment load periods, for example by taking measurements in the winter instead of the summer (Trimble, 1977).

A major problem associated with using sediment loads to estimate denudation rates comes from the way in which a river transports sediment fluctuates over time. Flood events are widely held to be times when most of the sediment within a system is transported, for example, Meade (1982) states that for US rivers draining into the Atlantic Ocean 50% of sediment is transported in 1% of the time available. Curtis *et al.* (1973) found that the Santa Clara River in southern California, which normally has a sediment load of some $69 * 10^3$ t a moves up to $50 * 10^6$ t a in flood events.

This type of problem is associated with the concept of unity, or steady state in drainage basins, where the amount of sediment derived from hillslopes and fluvial erosion equals that exiting the system through the river mouth (for example, Menard, 1961; Judson and Ritter, 1964). Although over long temporal periods, this must be true in order that the river system does not become choked with sediment, studies in the American Piedmont suggest that sediment delivery ratios are low (Trimble, 1977). The above observations imply that the majority of sediment spends little time in transport and most in storage (Trimble, 1975; Meade, 1982; Schumm *et al.*, 1976). This sediment has been proposed to be stored in drainage basins in a variety of ways. A reservoir or dam collecting one-tenth of the water passing through it will hold back 80-90% of the sediment reaching it (Brune, 1953). Sediment is also stored in

lowlands, deltas and alluvial plains, which tend only to exist in larger basins (Wilson, 1972). For example, of total sediment loads in the Huang He River, only around 24% reaches the ocean (Milliman and Meade, 1983).

The final problem in calculating denudation rates from sediment loads is that incurred as a result of anthropogenically induced activity. Agricultural activities in the USA by early European settlers massively increased stripping of sediment from the land (Henderson *et al.*, 1963), especially in the lower Piedmont area of South Carolina and Georgia (Meade, 1982). Despite reductions in sediment stripping resulting from improved agricultural practices in the Twentieth Century, the problem of sediment storage outlined above means that loads measured today may still be reflecting past denudational events (Meade, 1982). Trimble (1977; 1983) states that taking these problems into account, sediment loads and yield observations cannot be taken as accurately reflecting the nature of upland erosional processes or the role played by lithology, vegetation and land use in rates of denudation. Without taking account of storage effects, such measurements may be of limited use (Trimble, 1983).

5.4 INTERACTIONS OF EROSIONAL PROCESSES, LITHOLOGY, SEDIMENT FLUX AND DENUDATION RATES IN THE NORTHERN APENNINES, ITALY

Having outlined the importance of being able to estimate denudation rates and sediment fluxes from mountainous regions and problems associated with doing so, the impact of lithological and process variation on terrain form and sediment flux from orogens is now investigated by means of the case study of the Northern Apennines in Italy. The Northern Apennines represent an ideal place to study how erosional processes, sediment transport, terrain morphology, geology and tectonics interact as previous studies have documented both the nature of large scale patterns of erosion and deposition in the area (Talling and Sowter, 1998) and variations in both sediment flux (Talling, 1994) and denudation rates (Bartolini *et al.*, 1996) along the range. In addition, climate is relatively constant along the range with small variations in mean annual precipitation occurring as a function of elevation (Cati, 1983), thus problems associated with climatic controls may be avoided. The case study will begin with a brief outline of the geology, tectonics and topography of the Northern Apennines, before discussing previous work examining sediment fluxes from the range. Such observations will then be considered in the light of field observations of erosional process regimes occurring in the mountains, how these relate to the tectonics and lithological patterns of the area, and how terrain variability determined from the Italian DTM reflects not only these controls, but also how it compares with sediment yield observations. Lithological and process variability within the Apennines will also be compared with observed patterns of fluvial sediment transport and incision, to assess the role played by such variables on sediment yields and also how they interact with terrain morphology in mountainous regions. The importance of such controls on the evolution of mountainous terrains is of significant importance to geomorphologists studying both hillslope and fluvial processes and the interactions between them. The study area extends from the Trebbia Basin in the north-west of the Northern Apennines to the Foglia Basin in the south-eastern Northern Apennines (Figure 5.8).

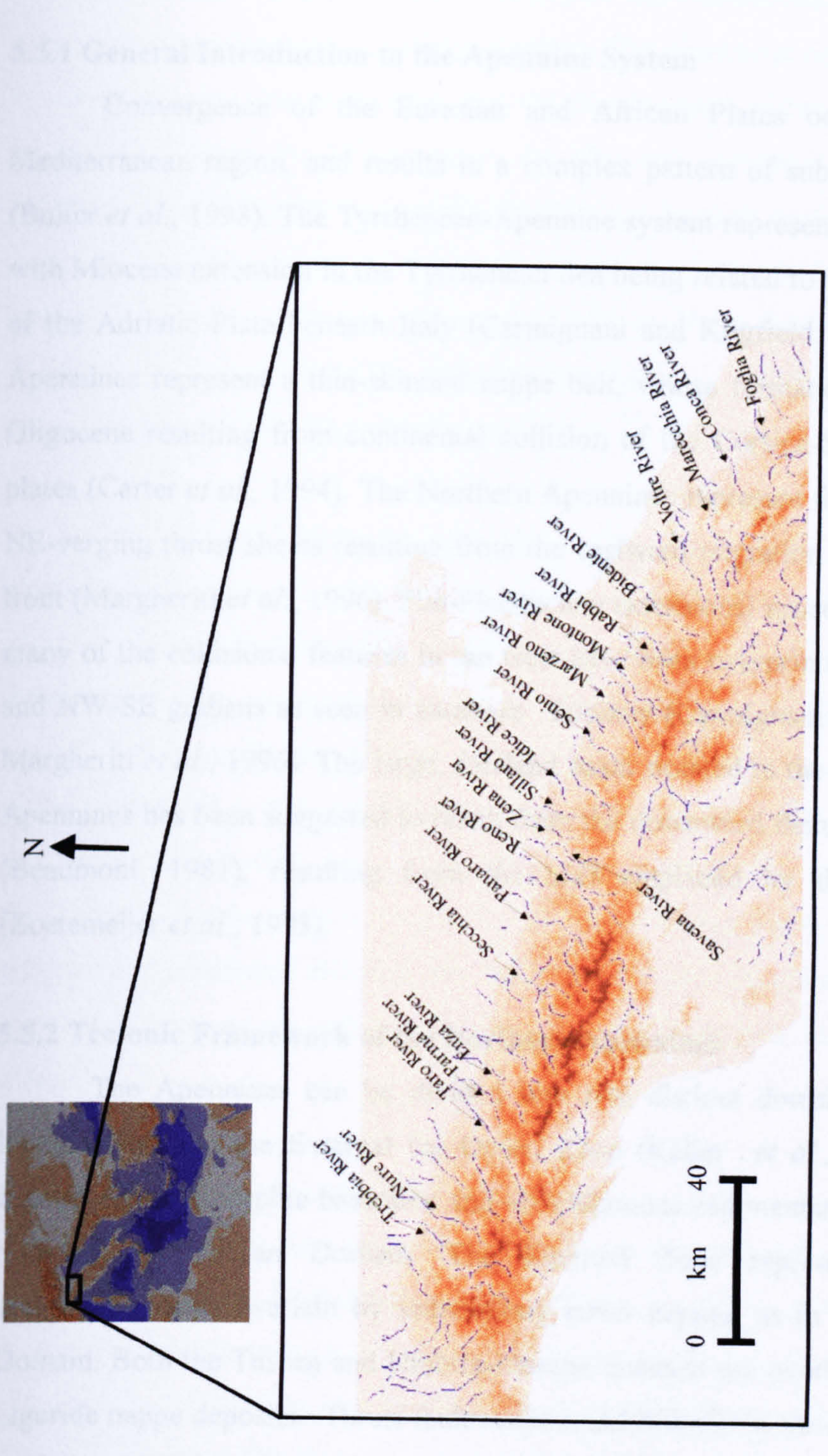

Figure 5.8 Map Showing Location of Northern Apennines in Context of Europe and Apennine Rivers Mentioned in the Text.

Darker Orange Colours Indicate Areas of Higher Elevation.

5.5 GEOLOGY, TECTONICS AND TOPOGRAPHY OF THE NORTHERN APENNINES

5.5.1 General Introduction to the Apennine System

Convergence of the Eurasian and African Plates occurs throughout the Mediterranean region, and results in a complex pattern of subduction and collision (Buiter *et al.*, 1998). The Tyrrhenean-Apennine system represents part of this system, with Miocene extension in the Tyrrhenean Sea being related to westwards subduction of the Adriatic Plate beneath Italy (Carmignani and Kligfield, 1990). The Northern Apennines represent a thin-skinned nappe belt, whose formation began in the Late Oligocene resulting from continental collision of the Corsica-Sardinia and Adriatic plates (Carter *et al.*, 1994). The Northern Apennines represent the stacking of several NE-verging thrust sheets resulting from the eastward migration of the compressional front (Margheriti *et al.*, 1996). Plio-Pleistocene extensional processes have meant that many of the collisional features in the west have been overprinted by a series of N-S and NW-SE grabens as seen in southern Tuscany (Carmignani and Kligfield, 1990; Margheriti *et al.*, 1996). The large, foreland basin situated to the north and east of the Apennines has been suggested to result from the downward flexure of the lithosphere (Beaumont, 1981), resulting from the load emplaced by the evolving orogen (Zoetemeijer *et al.*, 1993).

5.5.2 Tectonic Framework of the Northern Apennines

The Apennines can be divided into two distinct domains: the Internal (or Inner) Zone, and the External (or Outer) Zone (Keller *et al.*, 1994). The former consists of metamorphic basement and allochthonous sedimentary cover nappes, and includes the Tuscan Domain. The External Zone represents autochthonous sedimentary units overlain by sedimentary cover nappes, as in the Umbria-Marche Domain. Both the Tuscan and Umbria-Marche domains are overlain by ophiolite and Liguride nappe deposits. Thrust fault traces trend NW-SE in the northern Apennines, changing to a N-S orientation in the southern Apennines. During the Paleogene, the Tyrrhenean-Apenninic system consisted of the Corsica-Sardinian block, the Apulian microplate and the Apennine orogenic wedge, which built up during convergence, consisting of Liguride flysches and oceanic ophiolites (Keller *et al.*, 1994).

From the Mid-Cretaceous to the Late Eocene, eastwards collision of the Corsica-Sardinian block resulted in accretion and underplating of Tethyan Ocean material to the migrating accretionary prism. The eastwards compression resulted in crustal thickening and shortening, and the development of the Apennines (Keller *et al.*, 1994). During the Oligocene to the Miocene convergence continued, as the Ligurian ophiolitic nappe was overthrust onto the Apulian continental margin (Keller *et al.*, 1994). This convergence was accompanied by mantle delamination migrating eastwards being accompanied by extension in southern Tuscany. Further east, the Macigno, Marnosa-Arenecea and Marche-Adriatic foreland basins developed accompanying the migrating thrust front.

From the Mid-Miocene to the present day, the northern Apennines have been characterised by late orogenic extension in the west and continued collision in the east resulting from overthickening of the continental crust. The Pliocene saw the development of a series of extensional grabens in Tuscany and the Umbria-Marche region, for example the Gubbio graben. This late-orogenic extension was also accompanied by a N-S orientated extension in the west forming the present day Tyrrhenean Sea (Keller *et al.*, 1994). Extension has currently migrated as far east as the Umbria-Marche region, where the Perugia-Gubbio region's this-skinned NE-vergent compressional features are being overprinted by more recent extensional features (Keller *et al.*, 1994). NE-thrust sheets are currently active beneath the Po Plain.

5.5.3 Geologic Framework of the Apennines

The Northern Apennines represent the stacking of units from several palaeo-geographic domains (Carmignani *et al.*, 1994). The units outlined here are those cropping out in the area under study and are represented by the Tuscan Domain, the Umbria-Marche Domain, the Ligurian Sheet, the Sub-Ligurian deposits and the Epi-Ligurian deposits. The Tuscan and Umbria-Marche domains are of similar age, and were overthrusted by the Ligurian sheet (Figure 5.9).

Tuscan Domain (Unita Toscana)

The autochthonous Tuscan Domain consists of a series of limestones overlain by muds and flysches deposited on the Adria passive margin. During the Late

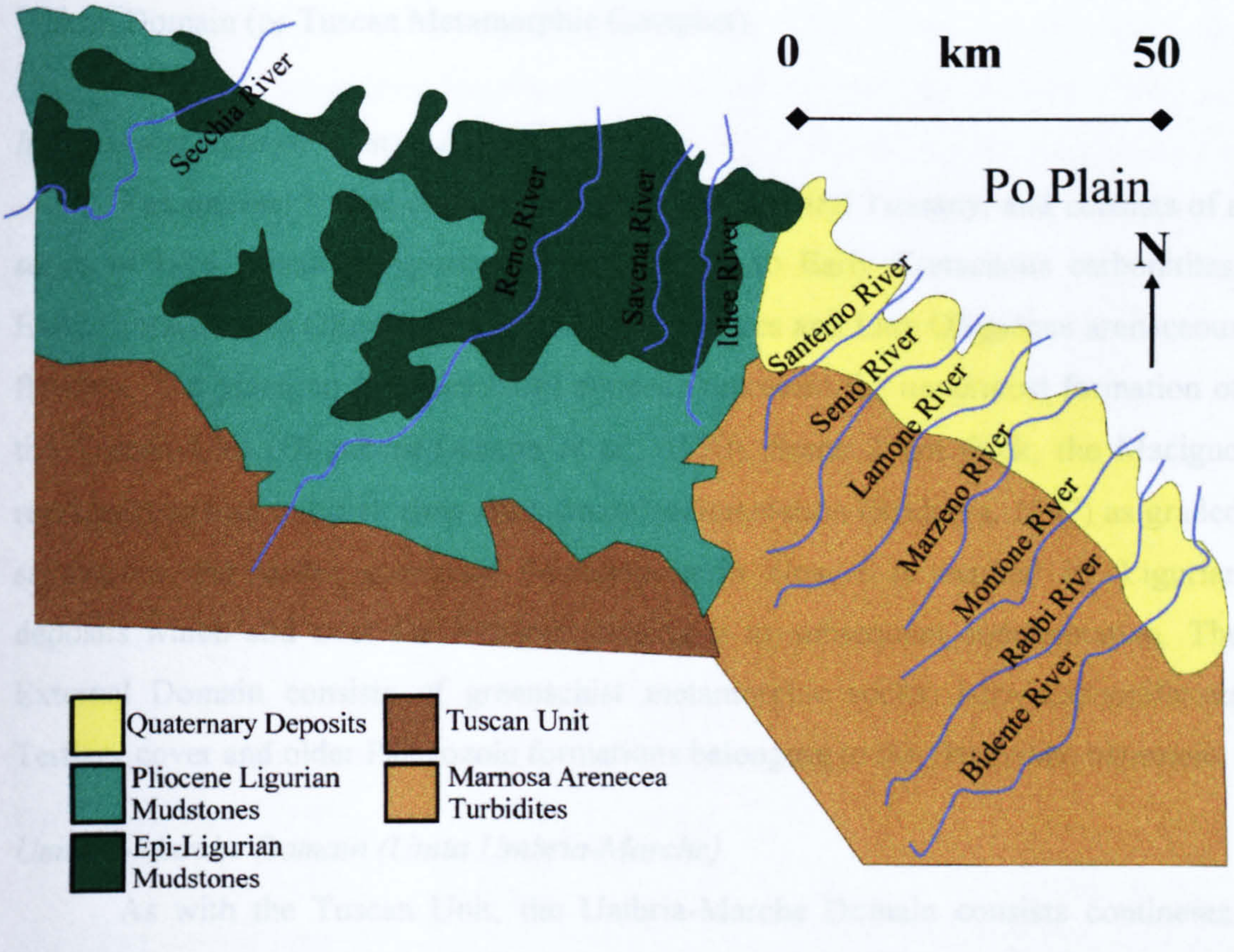

Figure 5.9 Generalised Geological Map of the Northern Apennines

Oligocene, the Tuscan sequence overthrusted the Umbria-Marche domain in the northern Apennines. The unit consists of several sedimentary sequences deformed at different structural levels including the Internal Tuscan Nappe and the External Tuscan Domain (or Tuscan Metamorphic Complex).

Internal and External Tuscan Domains

The Internal Nappe outcrops in western and central Tuscany, and consists of a series of Late Triassic evaporites, Early Jurassic to Early Cretaceous carbonitites, Early Cretaceous to Oligocene argillaceous sequences and Late Oligocene arenaceous flysches. The Macigno foredeep basin deposits represent the uppermost formation of the Tuscan Unit (Oligocene)(Abatte *et al.*, 1970). Some 2 km thick, the Macigno represents an end to quiet, slow open-ocean sedimentation (Rodgers, 1997) as graded sandstones and shales dominate. Macigno basin closure is marked by Ligurian deposits which slid over the foredeep closing it to subsequent sedimentation. The External Domain consists of greenschist metamorphic rocks, Late Carboniferous Tertiary cover and older Palaeozoic formations belonging to the Hercynian basement.

Umbria-Marche Domain (Unita Umbria-Marche)

As with the Tuscan Unit, the Umbria-Marche Domain consists continental margin deposits, and represents the External Zone of the Northern Apennines. The Domain consists of Permian-Triassic '*Verrucano*', Late Triassic evaporites, Early Jurassic to Eocene carbonates, Eocene to Miocene argillaceous sequences, and Late Miocene arenaceous flysches.

Marnosa-Arenecea Formation

The Marnosa-Arenecea formation consists of turbidites of the Mid to Lower Miocene, with calcareous sandstones and mudstone foredeep deposits having a provenance in the north-eastern Alps. The Contessa Bed is the largest marker unit in the Marnosa-Arenecea formation, and consists of carbonitic sediments with a south-eastern Apenninic provenance. The Contessa Bed outcrops throughout the Apennines from Gubbio in the south-west to Bologna. As with the Tuscan Unit, Pliocene Liguride marine deposits were thrust onto the Marnosa Arenecea formation.

· *Ligurian Sheet Facies*

The Ligurian Sheet consists of Jurassic ophiolites and related Jurassic to Early Cretaceous cover, overlain by Cretaceous to Eocene calcareous and argillaceous flysches (Van Wamel, 1987; Carmignani *et al.*, 1994). They outcrop from the Tyrrhenean coast to eastern Liguria on the Adriatic, consisting of shales, silts and sands, for example the *Argille Scagliosa* (Rodgers, 1997), and representing remnants of the Tethyan Oceanic crust and flysch sediments obducted onto the continental margin in the Eocene (Carter *et al.*, 1994).

Sub-Ligurian Sheet

This allochthonous unit represents the transition from the oceanic Ligurian Sheet to the continental crust of the Tuscan Domain. Consisting of calcareous to argillaceous sedimentary sequences of Late Cretaceous age which give way to Oligocene-Miocene turbidites, both the Ligurian and Sub-Ligurian domains were stacked within an accretionary wedge during the Late Cretaceous to Eocene (Carmignani *et al.*, 1994). They were then overthrust onto the Adria Plate during the Late Oligocene.

Epi-Ligurian Deposits

Lower Tertiary clastic facies of the Epi-Ligurian basins unconformably overlap the Cretaceous facies of the Ligurian sheet, which in turn lie over the Tuscan Sequence deposits (Rodgers, 1997). As the Ligurian Sheet deposits were being thrust onto the Tuscan Unit, piggy-back deposition of sandstones occurred forming the Epi-Ligurian units.

5.5.4 Topography of the Northern Apennine Study Area

Within the study area, the maximum elevations are found in the vicinity of the Upper Parma valley, where Mts. Bocco, Sillara and Marmagna reach 1791, 1861 and 1851 m respectively. At a more broad scale, as one moves southeast from the Trebbia Basin, maximum elevations along the range decline towards the Adriatic Coast.

5.6 OBSERVATIONS OF THE INTERACTIONS OF PROCESS, LITHOLOGY AND TERRAIN FORM IN THE NORTHERN APENNINES

5.6.1 Field Observations in the Northern Apennines

Field observations in 1996 and 1997 have determined that systematic changes in the gross morphology of the terrain of the Northern Apennines occur as one moves south-eastwards from the Trebbia basin in the north-west (Figure 5.8). At a large scale, this change is represented by an increase in the presence of rectilinear hillslopes with straight slopes and triangular faceted fronts in the upper reaches of many drainage basins (Plate 5.1). Such terrain features have been observed in a variety of geomorphic and tectonic settings in the USA (Chapter 4, Ellis *et al.*, 1999; Densmore *et al.*, 1998a) and the Southern Alps (Hovius, 1995). Field observations in the Apennines suggest strong links between terrain form, the dominant erosional processes operating and the nature of the underlying bedrock. For example, field observations in the Enza and Parma River basins have shown these basins to be dominated by low relief, relatively rounded hillslopes from the mountain front to the Apennine Divide (Figure 5.2). These basins are largely underlain by soft, Ligurian marine sediments (Section 5.5.3), which result in mass movements such as the Corniglio landslide (Plate 5.3) in the upper Parma Basin (Figure 5.8). This slide occurred in July and August 1996, and involved the movement of flysch deposits above Ligurian muds, with a slip depth of around 120 m following 400 mm of rainfall. Badland type terrain (Howard, 1997; Howard and Kerby, 1983) is also apparent in the Enza Basin around Ciano d'Enza and in the Sabia Basin, again resulting from erosion of Ligurian mudstones.

Plate 5.1 Linear Ridge Topography (A), near Santa Sofia, Bidente River Basin, Italy. Marnosa Arenecea Deposits Cropping out at the Surface

Plate 5.2 Rounded Hillslope Forms in the Trebbia Valley. Ligurian Sheet Deposits Overthrusting Tuscan Unit Deposits

Plate 5.3 Landslide (A), Corniglio, Parma Valley. 1200 m^3 of Flysch Deposits Moved on Top of Ligurian Sediments

Further south-eastwards, the soft, Ligurian sediments are largely replaced by outcrops of the Marnosa-Arenecea formation (Section 5.5.3). Southeast of the Reno River and Bologna (Figure 5.8), the Apennine mountain belt becomes more tectonically active, with a number of thrust faults extending both beneath the mountain belt (di Dio *et al.*, 1997). In combination, the different lithologies and tectonic regime operating in this area compared to those occurring further northwest result in distinctive differences in both terrain form and processes operating. Field observations in the Bidente and Rabbi River basins (Figure 5.8) has shown the widespread presence of linear ridge terrain, which occur where the Marnosa Arenecea Formation outcrops. Such trends are also seen in the terrain around the headwaters of the Lamone River (Figure 5.8) around Marradi, where outcrops of Marnosa Arenecea turbidites also outcrop. This type of transition from rolling topography to linear ridge topography is also seen as one moves across the Northern Apennine drainage divide moving from Emilia Romagna into Tuscany, for example around Collina, Tuscany (Plate 5.4) in the vicinity of the upper Enza Basin. Here, Ligurian muds are replaced by surface outcrops of Tuscan Unit rocks. Observations made along the Apennine chain suggest that Ligurian marine sediments tend to be dominated by badland type erosion and widespread mass movements (such as the Corniglio landslide). By contrast, hillslopes in areas of more resistant Tuscan (for example the Collina area (Plate 5.4) and Marnosa Arenecea outcrops appear to be both steeper and lacking evidence of widespread mass movements. It is suggested that bedrock type controls slope stability at a gross scale, which not only influences the morphology of the terrain, but also affects the types of processes operating upon them.

The role of lithology on terrain form is further supported where changes in bedrock type occur within basins. For example downstream of Cuzercole in the Bidente Basin (Figure 5.8), surface bedrock changes from Marnosa Arenecea to Messinian evaporites. The terrain in this area is seen to change from dominantly linear ridge type to a more gently rolling type (Figure 5.8). This trend has also been observed in the Marecchia Basin (Plate 5.5), again as evaporitic sediments begin to outcrop.

Plate 5.4 Triangular Facets (A), Collina, Tuscany. Tuscan Unit Rocks Cropping out

5.6.2 Comparison of Field Observations With Surface Process Modelling

There would therefore appear to be strong evidence of the relationship between the occurrence of linear ridge topography and changes in bedrock lithology in the Northern Apennines. Surface process models have simulated landscape development under conditions of both regolith and bedrock landsliding (Ellis *et al.*, 1999; Densmore *et al.*, 1998). Whilst many other modelling approaches (e.g. Tucker and Bras, 1998; Roering *et al.*, 1999) have produced planar hillslopes resulting from diffusive hillslope transport (Sections 3.3.1 and 3.4.1), predicted features such as convex hilltops (Roering *et al.*, 1999) are lacking from terrain in the Apennines (Plate 5.1), where ridge tops are sharp and angular. Of the models proposed, it would appear that only ZSCAPE (Ellis *et al.*, 1999), produces the suite of features observed in the Northern Apennines, such as linear hillslopes and triangular facets (Plates 5.6 and 5.7) (Ellis *et al.*, 1999). Conditions of both regolith and bedrock involved landsliding were simulated and compared to terrain features in the Basin and Range province, USA (Densmore *et al.*, 1998a). Results indicate that triangular facets and planar slopes are only produced by bedrock involved landsliding. In addition, the shape of such features is suggested to result not from exposure of fault surfaces, but rather from the efficiency with which bedrock landslides remove sediment from the areas they affect (Densmore *et al.*, 1997). These conclusions support many of the observations made in the Northern Apennines concerning processes operating in areas of resistant bedrock outcrops and linear hillslopes.

It has already been determined that linear ridge type terrain in the Santa Cruz Mountains in California correlates well with changes in bedrock lithology (Chapter 4), thus general relationships would appear to exist in areas other than the Apennines. Given this observation, it was decided to test whether the morphology of the Northern Apennines determined from large scale DTM analysis reflects the morphological changes seen in the field. If changes in terrain determined from field observations can be detected by DTM analysis, it may thus be possible to infer broad scale changes in lithology, and thus process dominance, across orogens such as the Apennines.

Plate 5.5 Linear Hillslopes (A), Trebbia River Valley. Tuscan Unit Rocks Cropping out at the Surface

Plate 5.6 Linear Hillslopes and Triangular Front Facets, Upper Marecchia Valley. Resistant Marnosa Arenecea Outcrops Dominate. Note Difference in Hillslope Morphology from Rounded Forms in Plate 5.2

5.6.3 DTM Analysis of the Northern Apennines

A digital terrain model (DTM) was obtained for the whole of Italy with a ground resolution of 230 m and a vertical resolution of around 1 m (Reichenbach *et al.*, 1993). The model was compiled from mean elevation values based on 1:25,000 scale topographic map data. Whilst the northern part of the model resulted largely from computer-aided data analysis, the central and southern parts were entered manually (Reichenbach *et al.*, 1993). The individual grid cell *tiles* were then joined together, and geo-referenced to the Universal Mercator projection system within the Erdas Imagine software package at Bristol University. It has previously been determined (Chapter 4) that of the various measures of relief and slope available to the geomorphologist, slope and local relief were best able to distinguish between areas exhibiting linear ridge type terrain and those which do not. As such, Arc Macro Language (AML) scripts used in Chapter 4 (Appendix 2) were run on the Italian DTM and the necessary data extracted.

Table 5.1 and Figure 5.10 show results obtained from terrain analysis of drainage basins in the Northern Apennines. Systematic trends in mean slope and local relief are observed. In basins where field observations show badland and more widespread forms of mass movement, such as the Taro, Parma and Enza basins (Figure 5.8), mean local relief values of around 200 m within a 230 m radius window are found and associated mean slope values are generally between 9° and 10° across 230 m grid cells. Basins where linear ridge type terrain dominates in the upper basin, such as in the Panaro and Reno basins, show mean local relief values around 225 m and slopes averaging 11°. Observed differences between slope and relief values for basins demonstrating linear ridge terrain and those without appear low (1° and 25 m difference for slope and local relief respectively). A higher resolution DTM would afford more detailed terrain analysis of the type undertaken in this study, with differences between terrain type becoming more apparent as the resolution of the data improves. Further to the south-east, where Marnosa Arenecea turbidites crop out, for example in the Bidente Basin, mean local relief values are shown to increase to around 250 m, with slopes increasing to values around 11-12°. The increasing presence of rolling topography seen in the far south-eastern basins, such as the Conca basin, is again reflected by lower mean local relief and slope values. Apparent

anomalies exist in basins to the east of the Reno Basin, for example in the Savena, Zena and Idice basins. In these basins, field observations show that the uppermost basins exhibit linear ridge type terrain, believed to reflect Marnosa Arenecea lithologies, whilst terrain data show relatively low mean values of both relief and slope. Such trends are believed to result from a combination of bedrock variation and also the way in which Arc/Info delineates drainage basins. These basins are dominated by surface outcrops of weak Pliocene marine deposits (Section 5.5.3) near the mountain front (Figure 5.1), which lacks linear ridge terrain (field observations, 1997) and results in a more rolling type of topography than that found in the basins' upper reaches where Marnosa Arenecea outcrops dominate. It may also be the case that some of the upper basin area of the Savena, Idice and Zena's basins is attributed to larger basins, such as the Reno Basin as a result of the flow accumulation algorithms used by Arc/Info.

Whilst the variations in terrain parameters may seem small, being only of the order of one or two degrees in the case of mean slope, it must be remembered that the DTM used is of relatively low spatial resolution (230 m), and that should higher resolution data be available, slope and relief values would more accurately represent variation in hillslope form in the Apennines. The observed differences in slope and relief are consistent across the orogen and have been shown to relate to both lithological variation and process dominance across the mountain belt. Future availability of models such as the global 30 metre DTM would allow for higher resolution process mapping of the type demonstrated here, allowing for the calculation of threshold slope angles as shown in Chapter 4.

Basin	Mean Basin Slope	Mean Basin Local Relief
Trebbia	11.99	258.1
Nure	9.29	195.6
Taro	9.75	216.8
Parma	9.52	198.88
Enza	8.65	187.13
Secchia	10.13	221.069
Panaro	10.814	230.51
Reno	10.46	228.8
Savena	7.85	154.11
Zena	6.29	120.4
Idice	8.02	154.78
Sillaro	7.58	147.80
Santerno	9.98	203.76
Senio	9.78	190.76
Lamone	10.70	210.58
Marzeno	9.35	180.93
Rabbi	10.418	198.95
Bidente	11.58	236.82
Voltre	9.42	200.13
Marecchia	8.57	184.51
Conca	7.43	158.087
Foglia	9.32	202.99

Table 5.1 Mean Slope and Local Relief Measurements for Northern Apennine

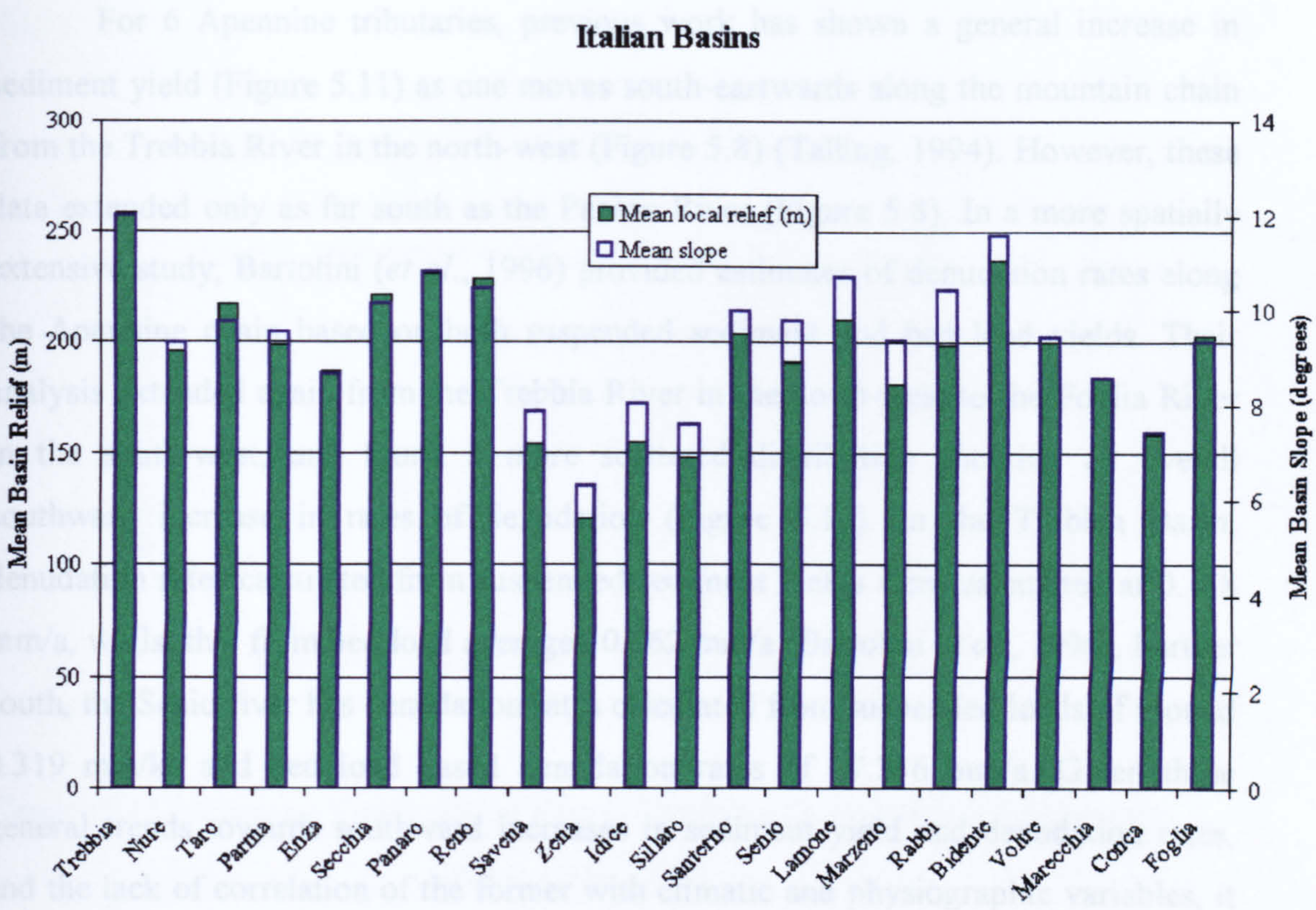

Figure 5.10 Mean Slope (Blue) and Local Relief (Green) Values Calculated for Basins Draining the Northern Apennines, Italy

5.7 SEDIMENT FLUX FROM THE NORTHERN APENNINES

For 6 Apennine tributaries, previous work has shown a general increase in sediment yield (Figure 5.11) as one moves south-eastwards along the mountain chain from the Trebbia River in the north-west (Figure 5.8) (Talling, 1994). However, these data extended only as far south as the Panaro River (Figure 5.8). In a more spatially extensive study, Bartolini (*et al.*, 1996) provided estimates of denudation rates along the Apennine chain based on both suspended sediment and bed load yields. Their analysis extended again from the Trebbia River in the north-west to the Foglia River in the south-west, and found a more scattered distribution showing an overall southward increase in rates of denudation (Figure 5.12). In the Trebbia Basin, denudation rates calculated from suspended sediment yields were calculated at 0.118 mm/a, whilst that from bed load averaged 0.262 mm/a (Bartolini *et al.*, 1996). Further south, the Senio river has denudation rates calculated from suspended loads of around 0.319 mm/ka and bed load based denudation rates of 27.336 mm/a. Given these general trends towards southward increases in sediment yield and denudation rates, and the lack of correlation of the former with climatic and physiographic variables, it has been suggested that bedrock lithology may play a key role in determining both sediment yields and denudation rates in the Northern Apennines (Talling, 1994). Canali and Allodi (1963) attempted to draw correlations between the two, and found the yields may well be correlated with changes in bedrock lithology, with more erodible evaporitic rocks in the Umbria and Marche Apennines to the southeast creating both higher denudation rates and sediment yields. Bearing this observation in mind, this study now examines how these trends compare with those seen in the field, and how they are reflected in the terrain morphology of the Apennines.

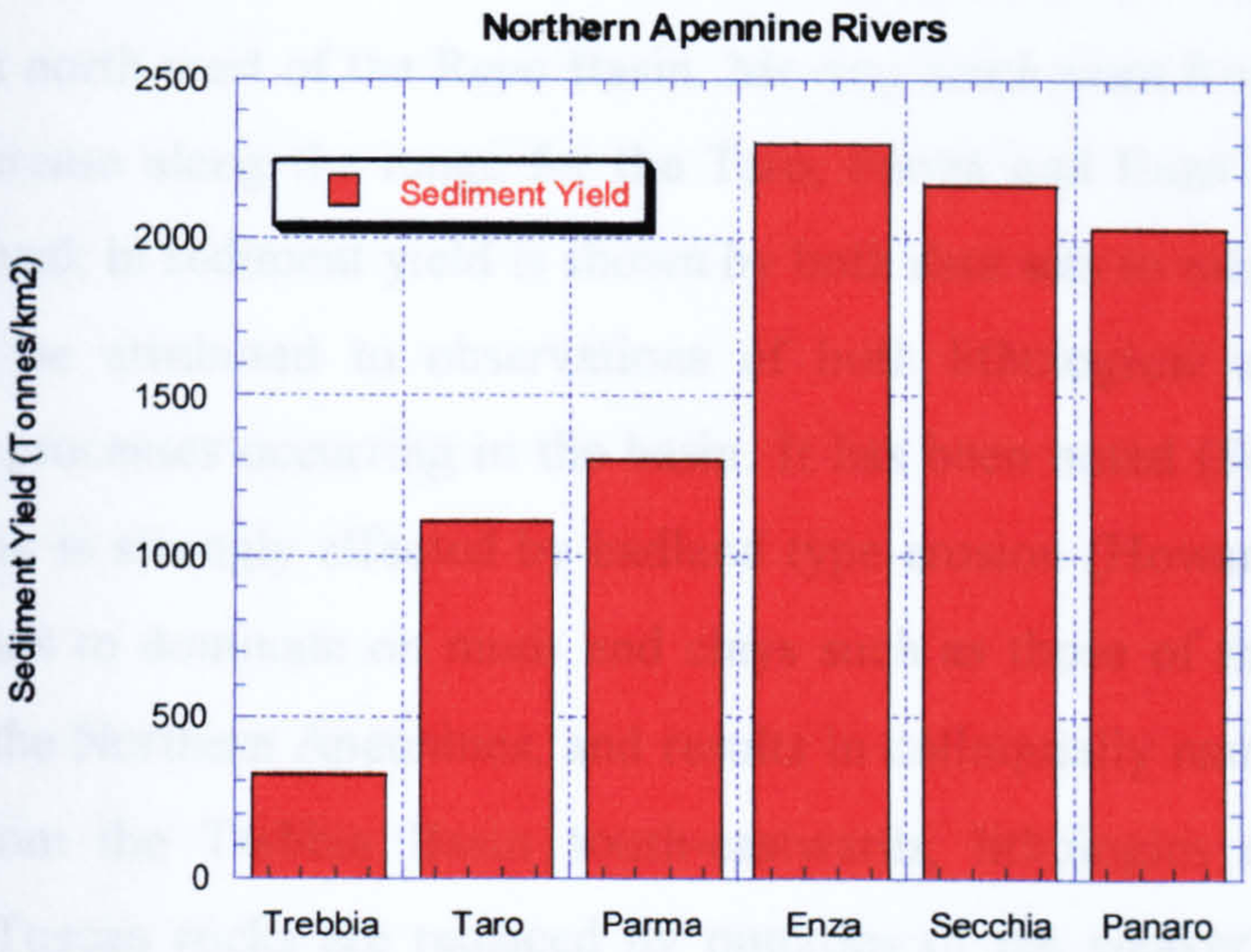

Figure 5.11 Sediment Yields Along Rivers Draining the Northern Apennines (After Cati, 1983)

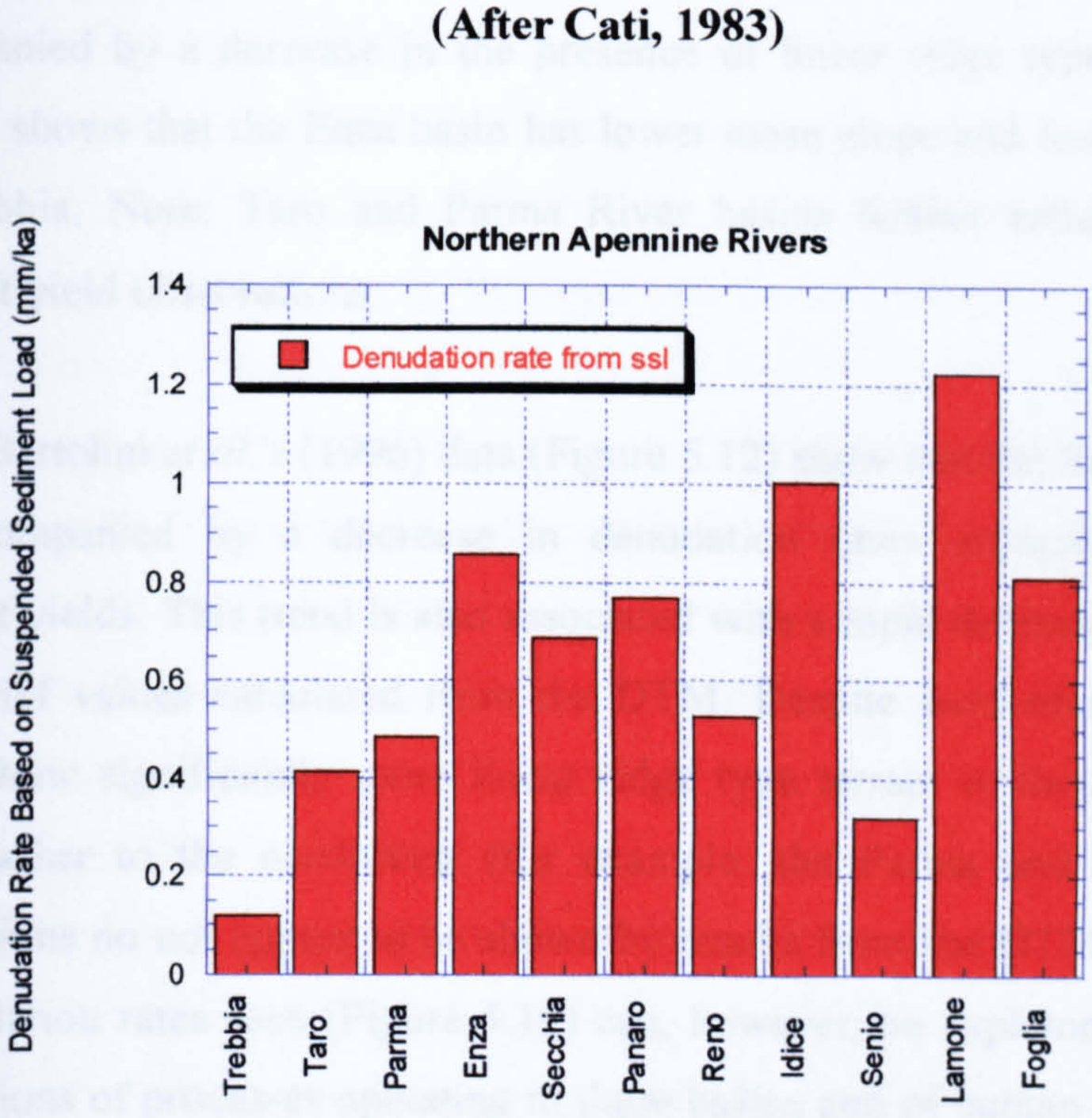

Figure 5.12 Denudation Rates Along Rivers Draining the Northern Apennines (After Bartolini *et al.*, 1996)

5.8 COMPARISON OF OBSERVED TRENDS WITH SEDIMENT YIELD AND DENUDATION RATE DATA

Estimates of denudation rates from Bartolini *et al.* (1996) show distinct trends for basins north-west of the Reno Basin. Moving south-west from the Trebbia Basin, yields increase along the range for the Taro, Parma and Enza River basins (Figure 5.11). A peak in sediment yield is shown by both data sets to exist on the Enza River. This can be attributed to observations of both lithological outcrop patterns and erosional processes occurring in the basin. It has been noted (Section 5.6.1) that the Enza Basin is strongly affected by badland type erosion (Howard and Kerby, 1983), which tends to dominate on muds and clays such as those of the Ligurian sequence found in the Northern Apennines, and results in colloquially named *calanchi*. As one moves from the Trebbia Basin south-eastwards, lithologies change as relatively resistant Tuscan rocks are replaced by outcrops of the weaker, Ligurian sequence. This trend is observed in the morphology of the terrain both in the field and on the DTM. Field observations show that the southward increase in Ligurian rocks is accompanied by a decrease in the presence of linear ridge type topography. DTM analysis shows that the Enza basin has lower mean slope and local relief values than the Trebbia, Nure, Taro and Parma River basins further reflecting the field and sediment yield observations.

Bartolini *et al.*'s (1996) data (Figure 5.12) show that the Reno and Idice basins are accompanied by a decrease in denudation rates estimated from suspended sediment yields. This trend is also associated with a rapid decrease in mean slope and local relief values calculated from the DTM. Despite field observations that these basins show significantly more linear ridge type terrain in their upper basins than those further to the north-west (for example, the Parma and Enza basins), such observations do not appear to be shown by results from the DTM analysis. The drop in denudation rates seen (Figure 5.12) can, however, be explained as resulting from observations of processes operating in these basins and of human activity in the Reno Basin. Field observations support the causal linkage between lithological variation and process dominance in the Northern Apennines, such that Ligurian outcrops are associated with widespread slope failures and sediment influx to fluvial systems. Where outcrops of more resistant Tuscan and Marnosa Arenecea turbidites crop out, linear ridge terrain dominates and mass movement processes appear to be relatively

inactive given the lack of slope failures seen in such basins (field observations, 1996; 1997). Using these observations, one can infer that low denudation rates in the Reno and Idice basins reflect the stronger lithologies cropping out in the upper basins, which are associated with less active slope failure and reduced input of sediment to the fluvial system. The Reno Basin has a number of dams and reservoirs along its course (field observations, 1996; 1997), thus the assumption of unity adopted in determining denudation rates (Section 5.3.1) from sediment loads data may be in error. Storage may be resulting in reduced yields reaching the gauging stations, which in turn, are reflected by reduced denudation rates.

The above trends appear to be in contrast to those seen for the Lamone Basin (Figure 5.8). Field observations again show linear ridge type topography in the upper basin, and outcrop patterns show that most of the basin is underlain by Marnosa Arenecea turbidites. DTM analysis confirms these observations, with high mean slope and local relief values. However, where in the Reno and Idice basins such lithologies and terrain forms were associated with low denudation rates and sediment yields, in the Lamone Basin, very high denudation rates are inferred from sediment yield data (Bartolini *et al.*, 1996). This may, at first glance, appear to contradict the above conclusions. However, towards the south-east in the Northern Apennines, activity on faults within the mountain range increases. Such activity may contribute to heightened slope failure as uplift increases hillslope and channel gradients. As hillslopes steepen, the potential for failure increases and sediment is released from the slopes which tend to be more stable further north-west. Furthermore, as river channels also steepen they have increased transport capacities and remove are able to remove more of the sediment supplied into them. This type of tectonic input to the hillslope-channel system is supported by observations which show the Lamone River to have a bedrock channel morphology as far south as Fognano (Plate 5.7 and Figure 5.8). Bedrock channels can exist where either supply-limited or transport-excess (Howard, 1994) situations occur. High denudation rates calculated for the Lamone Basin suggest the latter scenario is more likely as the former would be accompanied by lower yields and estimated rates of denudation. In addition, the bedrock channel is accompanied by widespread terrace incision, indicative of increased rates of incision. This trend compares well with field observations for the Northern Apennines belt as a whole, which has shown that, generally, rivers north of the Enza River tend to be aggrading

and braided in nature (Plate 5.8), whilst those rivers south of the Reno tend to be incising past the mountain front into the Po Plain (field observations, 1996; 1997).

Plate 5.7 Bedrock Channel (A) in the Lamone Basin, near Fognano

Plate 5.8 Braided River Channel (A), Taro River

5.9 RELIEF AND DENUDATION RATES IN THE NORTHERN APENNINES

5.9.1 Introduction

As outlined in section 5.2.1, a number of previous studies (e.g. Ahnert, 1970; Summerfield and Hulton, 1994; Milliman and Syvitski, 1992) have determined strong positive correlations between local relief and denudation rates. Tucker and Slingerland (1996) simulated landscape evolution using their model, GOLEM, which indicated that relief and denudation will not follow a simple, monotonic relationship in areas where terrain form and hillslope processes are strongly influenced by lithological variation. Gunnell (1998) employed Ahnert's (1970) relationship between relief and denudation in a study of erosional rates in the Dharwar Craton of South India. Ahnert (1970) proposed that

(5.1) $D_r = 0.1535h$

where D_r is the denudation rate and h is local relief (Figure 5.2). He determined that trends predicted by Ahnert's law correlated well with both present and past rates of denudation determined from sediment load and apatite fission track dating respectively. This chapter has shown how both terrain form and the types of erosional processes operating in the Northern Apennines are strongly influenced by changes in bedrock lithology. In combination with the availability of DTM and denudation rate information, these data allow for an examination of both the trends between relief and denudation and the potential influence of bedrock lithology on such trends.

5.9.2 Relief - Denudation Rate Relationships in the Apennines

For the 13 basins examined by Bartolini *et al.* (1996), values of local relief within the individual basins were calculated. Actual values of denudation rates are those shown in Figure 5.12. Using Equation 5.1, estimates of denudation rate are given based on Ahnert's (1970) work. These two estimates of denudation rate are shown in Figure 5.13, with values based on sediment load shown in red and those based on Ahnert's (1970) empirical relationship in blue. It is immediately apparent that the two data sets show distinctly different trends. Whilst Ahnert's relationship predicts that relief and denudation rate will be positively related, the data based on sediment load shows a negative correlation between the two of the form

(5.2) $D_r = 2.207 - 0.0072h$

Despite the high degree of scatter in the relationship based on sediment load data, it can clearly be seen that differences exist between denudation rates predicted and those observed (Figure 5.14). This finding clearly contrasts with that of Ahnert (1970). It is proposed that the negative relationship results from the way in which lithological patterns vary across the Apennine orogen, and the impact this has on both topographic form (section 5.6.3) and the processes dominating the hillslopes (section 5.6.1). These findings are now explored below.

5.9.3 Relief, Denudation Rate and Bedrock Lithology

Previous studies have found strong linear correlations between local relief and rates of denudation at both global (e.g. Summerfield and Hulton, 1994; Milliman and Syvitski, 1992) and more local scales (Ahnert, 1970). Despite this widespread agreement, it also acknowledged that scatter in such trends are both apparent (Summerfield and Hulton, 1994) and of significance. Indeed it has been suggested that deviations from strong positive linear relationships between relief and denudation rates may be indicative of lithological variation (Summerfield and Hulton, 1994). Indeed, surface process modelling by Tucker and Slingerland (1996) has shown that relief - denudation rate interactions are largely controlled by variations in bedrock lithology. Areas with relatively consistent climatic and lithological regimes are predicted to show linear relationships, with bedrock variations being responsible for deviations from such trends (see also van der Beek and Braun, 1998).

Data presented here based on DTM analysis and denudation rate calculations based on sediment loads (after Bartolini *et al.*, 1996) show both scatter and an unusual negative correlation between local relief and denudation rates. This contrasts with previous studies based on sediment load data. This chapter has already demonstrated the importance of variations in bedrock lithology on both terrain form, for example in the Rabbi Basin where resistant Marnosa Arenecea outcrops result in linear ridge terrain and high relief values. Indeed, it is suggested that resistant lithologies are capable of supporting steeper slopes and hillslope relief. These slopes fail less frequently than those consisting on weaker lithologies, such as Miocene Ligurian mudstones in the Enza Basin, resulting in low sediment yields despite their high mean relief values. Whilst weaker rocks are dominated by badland type topography and rill type incision, more resistant outcrops demonstrate linear ridge slopes and triangular

facets indicative of bedrock landsliding (Ellis *et al.*, 1999). The Northern Apennines thus support evidence provided by Tucker and Slingerland (1996) which suggests that lithological variation influences both the rate and type of process operating on hillslopes and well as the sediment yield liberated from them. By contrast, Pazzaglia and Brandon's (1997) study, in which rock type variation is concluded to be of secondary importance in determining sediment yields, is not supported by this study.

Naturally, due to the limited nature of sediment load sampling, observed trends could also be due to problems inherent in basing denudation rates on sediment data. As outlined previously, in mountainous areas, bedload can be a significant proportion of the total load exiting a basin (Summerfield, 1991). Although Bartolini *et al.* (1996) do provide some bedload measurements for the Northern Apennines, they are too few to base subsequent calculations upon. Secondly, storage of sediment in lakes and reservoirs and on alluvial plains can also lead to under-estimates of denudation rates based on sediment load values. In larger Northern Apennine basins, such as the Taro, Secchia, Reno and Trebbia, such effects could help explain the low denudation rates provided by Bartolini *et al.* (1996). Field observations have demonstrated that dams and reservoirs do exist on the Reno and Secchia rivers, supporting this theory.

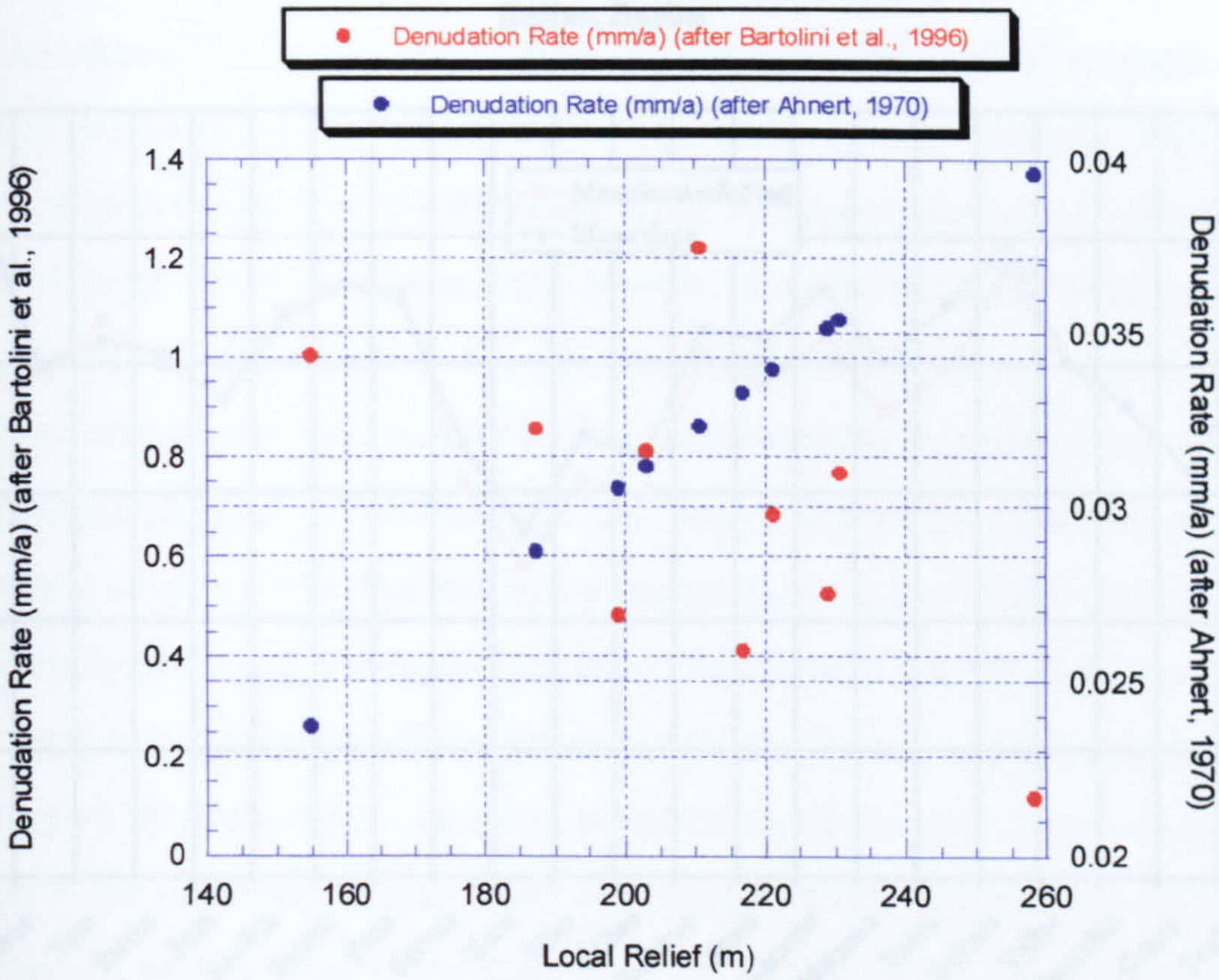

Figure 5.13

Relationship Between Local Relief and Mechanical Denudation Rate, Northern Apennines. Based on 1) Ahnert's Law (Blue) and 2) Sediment Load Data (Red)

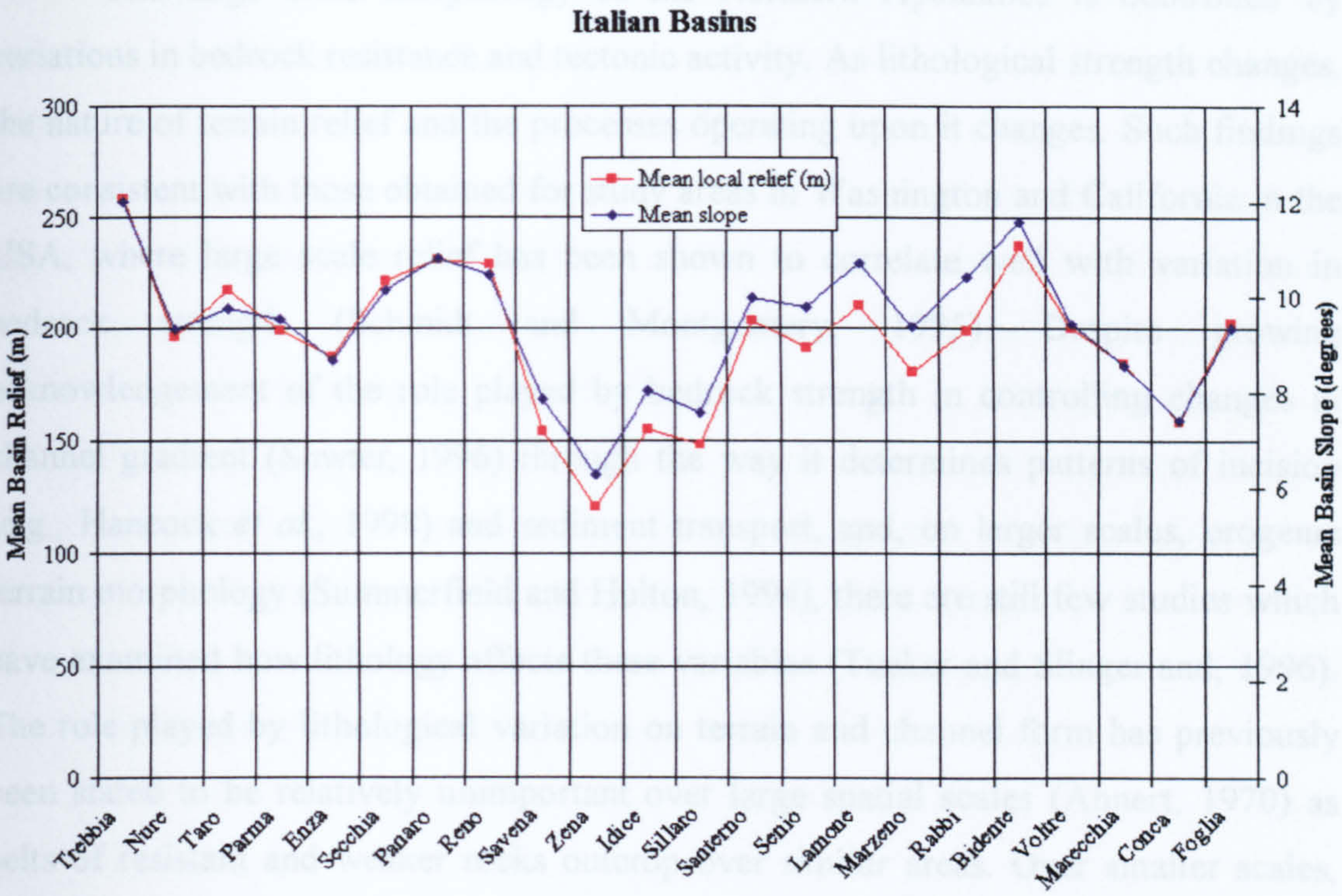

Figure 5.14

Rates of Denudation in the Northern Apennines Based on Ahnert's (1970) Empirical Relationship in Blue, and Based on Sediment Load Data (After Bartolini *et al.*, 1996) in Red. Ahnert (1970) Predicts a Positive Linear Relationship Between Relief and Denudation, Whilst Bartolini *et al.*'s (1996) Data Predicts a Negative Correlation

5.10 CONCLUSIONS.

The large scale morphology of the Northern Apennines is controlled by variations in bedrock resistance and tectonic activity. As lithological strength changes, the nature of terrain relief and the processes operating upon it changes. Such findings are consistent with those obtained for study areas in Washington and California in the USA, where large scale relief has been shown to correlate well with variation in bedrock strength (Schmidt and Montgomery, 1995). Despite growing acknowledgement of the role played by bedrock strength in controlling changes in channel gradient (Sowter, 1996) through the way it determines patterns of incision (e.g., Hancock *et al.*, 1998) and sediment transport, and, on larger scales, orogenic terrain morphology (Summerfield and Hulton, 1994), there are still few studies which have examined how lithology affects these variables (Tucker and Slingerland, 1996). The role played by lithological variation on terrain and channel form has previously been stated to be relatively unimportant over large spatial scales (Ahnert, 1970) as belts of resistant and weaker rocks outcrop over similar areas. Over smaller scales, variations in the relationship between relief, sediment yield (Tucker and Slingerland, 1996) and denudation rates (Summerfield and Hulton, 1994) may be attributable to bedrock lithological variation.

Studies such as this, which has examined the role played by lithological controls on terrain form and sediment transport thus has important implications for the ways in which SPMs and LEMs simulate both hillslope erosion and sediment transport in channels. By using simple linear relationships between variables such as relief and denudation (Ahnert, 1970), and holding lithology as constant (e.g., Howard, 1994) such models may be inadequate (Tucker and Slingerland, 1996). By addressing the lack of large scale lithological studies, this research indicates that future research should continue to examine the role played by lithological and tectonic variation on landscape form, erosional process and denudation rates in mountainous regions. Bedrock controls on relief - denudation rate interactions suggested by the process simulations of van der Beek and Braun (1999), Meigs *et al.* (1999) and Tucker and Slingerland (1996) are supported. It is thus suggested that models which assume bedrock strength to be constant over model space should be able to account for variations if they are to simulate areas where significant bedrock variation is known to exist.

An additional avenue of future research is that of the interactions between relief and denudation over large spatial scales. This chapter has indicated that in the Northern Apennines relief and denudation are largely inversely correlated, contrasting with studies carried out at both small and global scales. Further calculations of sediment loads in Apennines rivers and/or rates of denudation in the Apennine mountain belt would allow for better constraints on the correlation between the relief and denudation than has been carried out in this study. Again, the inverse relationship between the two is potentially attributable to variations in lithology and rates of tectonic activity along the Apennines, with more resistant lithologies resulting in higher relief and lower denudation rates. Such findings contrast with empirical laws employed by simulations in which relief and denudation are positively correlated. Thus this type of work has implications for areas other than the Apennines, and should be addressed by future work.

CHAPTER 6

LANDSLIDING AND HILLSLOPE FORM, MARIN COUNTY, CALIFORNIA, USA

6.1 INTRODUCTION

Previous work (e.g. Kelsey, 1978; 1980; Ellen *et al.*, 1997; Pike, 1997) has established that strong process-form links exist in the San Francisco Bay area. Rounded and fluted landforms co-exist in the area, and are believed to be the result of earthflow/slide and debris flow type activity respectively (e.g. Ellen *et al.*, 1988). Pike (1987; 1988) used a computer program initially developed for analysis of lunar terrain to derive 'geometric signatures' of 'hard' and 'soft' terrain in California, based on the analysis of terrain variables within windows of digital topography. This work develops the idea of 'topographic fingerprinting' of different erosional processes. Similar to the geometric signature of Pike (1988; 1987), and pattern analysis (e.g. Argialas, 1995), fingerprinting involves an assessment of the morphometric variables which appear to best constrain topographic form under given erosional processes. The terrain parameters employed will be used in analyses which attempt discriminate areas affected by earthflow-type mass movements at a scale larger that the single drainage basin studies carried out previously (for example, Gao, 1993). By discriminating between areas affected by landslide processes and those which are not, large scale DTMs may be employed in deriving erosional process maps for use in sediment flux, denudation and hazard type analyses. This work begins with an introduction to the study area in California, before moving on to look at the methods used. Results of the terrain analyses are then presented and are compared with previous studies. Finally, the implications of the study are outlined.

The work presented here was initially an investigation of the type carried out in Chapter 4, examining how terrain form changes under conditions of mass movement and identifying those parts of the terrain affected by such movements. However, subsequent to the analyses and following a field visit, it was found that hillslopes in Marin County are affected by earthflow type mass movements and not

the deeper bedrock-involved landslides upon which the latter parts of this thesis have concentrated.

6.2 SLOPE PROCESSES OPERATING IN THE MARIN COUNTY AREA

Previous workers have determined that hillslopes in the Marin County area of California (Figure 1.1) are dominated by earthflow/earthslide and debris flow type processes.

6.2.1 Earthflows and Earthslides

Earthflows and slides are common phenomena in mountainous regions, identifiable by dish-shaped scars, lobate forms and bulging toes (Keefer and Johnson, 1978). Such forms of mass movement have been recognised for most of the 20th Century (e.g. Howe, 1909), with work in the San Francisco area being undertaken for at least 50 years (e.g. Krauskopf *et al.*, 1939). In this work, 'earthflow' is taken to include both 'earthflows' and 'mudflows' as defined by Skempton and Hutchinson (1969). Slides represent the slow moving, deep seated gravitational slope deformations including sackungs, lateral spreading, slumps and translational slides. These types of movement pose serious danger to property, but little to life as they involve slow deformation of the ground surface. Earthflows involve flows of clayey earth (Wentworth *et al.*, 1997), deforming the surface upon which they flow, and remaining in the landscape as recognisable units. Generally, earthflows have a steep head scarp, separating the crown from the body of the slide. The actual body is sinusoidal in long profile, with material bulging at the toe into a convex-upward shaped body. These types of mass movement thus differ from the deeper, bedrock-involved landslides discussed in Chapters 3, 4 and 5.

6.2.2 Debris Flows

In contrast to earthflows and slides which can affect large areas of land, debris flows tend to be concentrated in pre-existing hollows and channels. Debris flows are amongst the most potentially damaging types of mountain hazard, involving rapidly moving mixtures of soil and water (Pike, 1997). Also known as debris avalanches (Sharpe, 1938), and soil-slip flows (Campbell, 1975), debris flows are suddenly mobilised in heavy rains, flowing rapidly downslope and leaving thin deposits in the landscape. Debris flows are largely granular soils, which become mixed with small

amounts of clay, water and air during mobilisation (Keefer and Johnson, 1983). The development of debris flows begins with water movement to the failure site, followed by failure of the soil mantle and its subsequent movement downslope (Ellen *et al.*, 1988). Unlike slides and earthflows, debris flows pose potential harm to property and life, their rapid nature means evacuation is frequently impossible. Only through an examination of conditioning and triggering mechanisms can such flows be potentially avoided.

6.3 STUDY AREA

The California Coast Ranges, including the Marin County area, consist of topography ranging from gentle hillslopes to steep-sided ridge and valley formations. The San Francisco area experiences a Mediterranean climate with warm dry summers and cool, rainy winters (Keefer and Johnson, 1983; Dietrich *et al.*, 1993). Landslide processes occur widely in the Marin County area of California, where weak rock lithologies and heavy rainfalls frequently conspire to cause large mass movements, such as those which occurred following the storms of January 3-5, 1982 (Ellen *et al.*, 1988). During the 1990s, the USGS initiated a program to assess the potential influence of El Niño on natural hazard occurrence in California (San Francisco Bay Mapping Team, 1997). This work resulted in the landslide maps used as base maps in this work. From the DEM data set, six drainage basins were identified to form the areas under examination. The six areas cover a large proportion of southern Marin County and drain both into the San Francisco Bay to the east and into the Pacific Ocean to the west.

The Marin County area is in the Central Belt of the Franciscan Complex. Active during the Late Jurassic to Early Tertiary, this formation developed as part of an accretionary wedge on the ancient convergent plate margin of North America (Hagstrum and Murchey, 1993). The Franciscan Complex consists of a series of clastic sedimentary rocks, greenstones, radiolarian cherts and shales, and a series of metamorphic and sheared rocks (Schlocker, 1974). In southern Marin County, Franciscan greenstones (altered basaltic rock consisting of pillow lavas, tuff brecchias and related intrusive rocks), Franciscan cherts and shales dominate the area studied, with unsheared graywackes and shales dominating much of the coastal regions.

Further to the north and east in Marin, variably sheared or brecchiated Franciscan sandstones and shales give way to smaller amounts of unsheared Franciscan sandstones and shales in the upper basins (Ellen and Wentworth, 1983).

6.3.1 Tennessee Basin

The Tennessee Basin area (Figure 6.1) covers some 6.2 km^2 of moderately low relief land (mean relief 49.93 m) of the southern Marin Peninsula. The basin delineated includes Tennessee Basin to the north-west and the land surrounding Pirate's Cove and the Marin Headlands State Park on the coast, draining into the Pacific Ocean at Tennessee Point. The geology of the area is divided to the north/west and south/east by a southwest-north-east trending fault, forming the central axis of the basin. To the north of the fault, variably sheared greywacke sandstones and shales, found abundantly in Marin County, outcrop. To the south of the fault, the basin's geology consists largely of Franciscan cherts, with a prominent outcrop of Franciscan sandstones and shales. The southern part of the basin displays greenstone bodies, which form some of the more elevated parts of the basin. As can be seen in Figure 6.1, approximately 16 % of the basin consists of earthflow deposits.

The elevation distribution in the Tennessee Basin area range from sea level to 320 m a.s.l. on the ridge crests. The locality map shows that the elevated parts of the basin are towards the north-western and southern boundaries - the latter being the area of prominent greenstone outcrops. The distribution of slopes in the basin is slightly left-skewed, with a mean value of 17.95°, ranging from 0° on the valley floor to 41.75° on steeper slopes. The slope map demonstrates that high slopes exist along the southern perimeter hillsides and in the north-west, both areas of high elevation, whilst other high slopes exist at lower elevations, possible due to fluvial incision of banks. As might be expected from the general topography of the basin, the majority of slopes are orientated towards the north-west (16%), south (14%), and south-west (16%), with the fewest slopes facing the northern aspects.

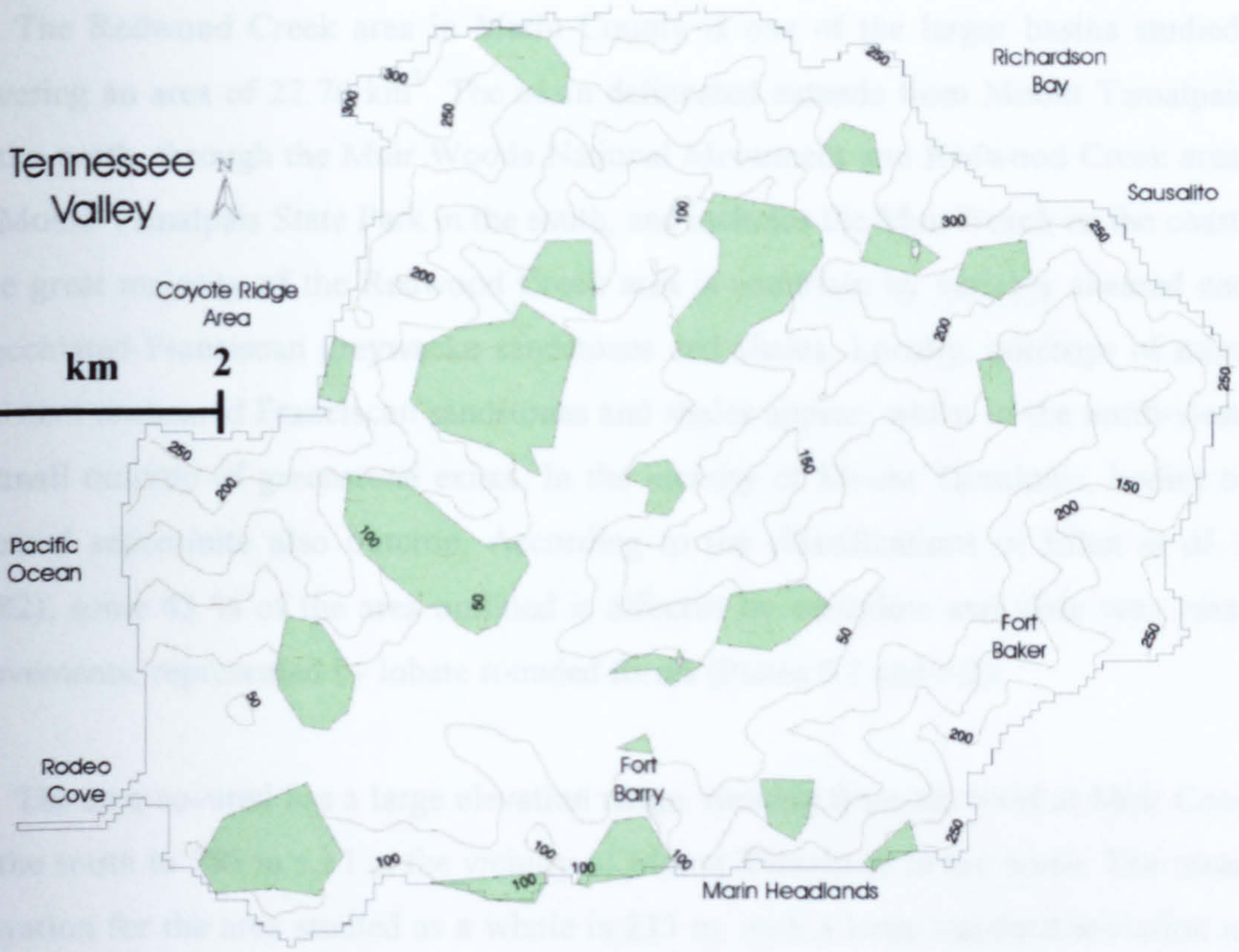

Figure 6.1 Location Map of Tennessee Basin, Marin County

(Green areas indicate those affected by earthflow activity)

6.3.2 Redwood Creek

The Redwood Creek area in Marin County is one of the larger basins studied, covering an area of 22.76 km^2. The basin delineated extends from Mount Tamalpais in the north, through the Muir Woods National Monument and Redwood Creek area, to Mount Tamalpais State Park in the south, and includes the Muir Beach on the coast. The great majority of the Redwood Creek area is underlain by variably sheared and brecchiated Franciscan greywacke sandstones and shales. Locally, outcrops of more resistant unsheared Franciscan sandstones and shales appear, whilst in the north-west, a small outcrop of greenstone exists. In the vicinity of Mount Tamalpais, bodies of sheared sepentinite also outcrop. According to the classifications of Ellen *et al.* (1982), some 43 % of the area outlined is affected by earthflow and slide type mass movements, represented by lobate rounded forms (Plates 6.1 and 6.2).

The area covered has a large elevation range, running from sea level at Muir Cove in the south to 785 m a.s.l in the vicinity of Mount Tamalpais to the north. The mean elevation for the area studied as a whole is 233 m, with a large standard deviation of 180 m, reflecting the broad contrasts between the northern uplands and south-eastern lowland areas. Generally, the south of the basin is lower than the north, with locally high ridge crests forming prominent features in the south. The slope distribution of the area shows a range from 0° in the valley bottoms to 45.87° on the steeper ridges, with a mean of 19.48°, moderately higher than in Coyote Basin. The slope map of the area shows the highest slopes to be in the low-order sub-basins, especially in the south-east and west, with a large proportion of high slopes on the eastern ridges. Somewhat surprisingly, the high areas surrounding Mount Tamalpais do not display particularly high slopes. The hillslopes in Redwood Creek face east (16 %), south-west (15.7 %), south-east (15.5 %), and south (14.8 %) most frequently, with fewer slopes facing aspects with a northern orientation. Mean local relief in the area is distributed symmetrically about a mean value of 53.99 m, higher than in the Tennessee Basin area.

Figure 6.2 Location Map of Redwood Creek, Marin County

(Green areas indicate those affected by earthflow activity)

Plate 6.1 Rounded Earthflow Topography (B), Redwood Creek, East of Shoreline Highway.

Plate 6.2 Rounded Earthflow Topography (B), Redwood Creek, East of Shoreline Highway

6.3.3 Rodeo Basin

The area delineated as Rodeo Basin (Figure 6.3) covers some 10.37 km^2 of the southern Marin Peninsula. Draining through Rodeo Cove into the Pacific Ocean, Tennessee Valley covers Fort Barry and Fort Baker in the south, and extends eastwards towards Richardson Bay. The area is underlain by a mixture of Franciscan cherts and greenstones in the south-east, south-west and centre of the basin, whilst in the north-west and north-east, outcrops of Franciscan cherts interspersed with bodies of unsheared sandstones and shales appear. Towards the east of the basin, near Richardson Bay at Sausalito, a large body of greenstone, consisting of altered basaltic rocks and related intrusive rocks, outcrop. Ellen *et al.*, (1982) classified approximately 14 % of the basin as mostly earthflow and slide bodies.

Rodeo Basin's elevation distribution is strongly left-skewed about a mean of 119.52 m, ranging from sea level at Rodeo Cove to 343 m a.s.l on the elevated ridge crests in the north-west of the basin. The slope distribution and statistics show the area to consist of lower slopes than the Tennessee Basin and Redwood Creek areas, ranging from 0° to 38.76°, with a mean of 16.33°. Mean local relief is also lower than elsewhere, with a mean value of 45.41 m. The slope map shows higher slopes to exist along ridges to the west, north-west and centre of the basin, and also in the vicinity of Fort Baker in the Sausalito area. As with elsewhere in the Marin Peninsula, slopes tend to be favorably orientated in southerly and westerly directions, with fewer facing northern and eastern aspects.

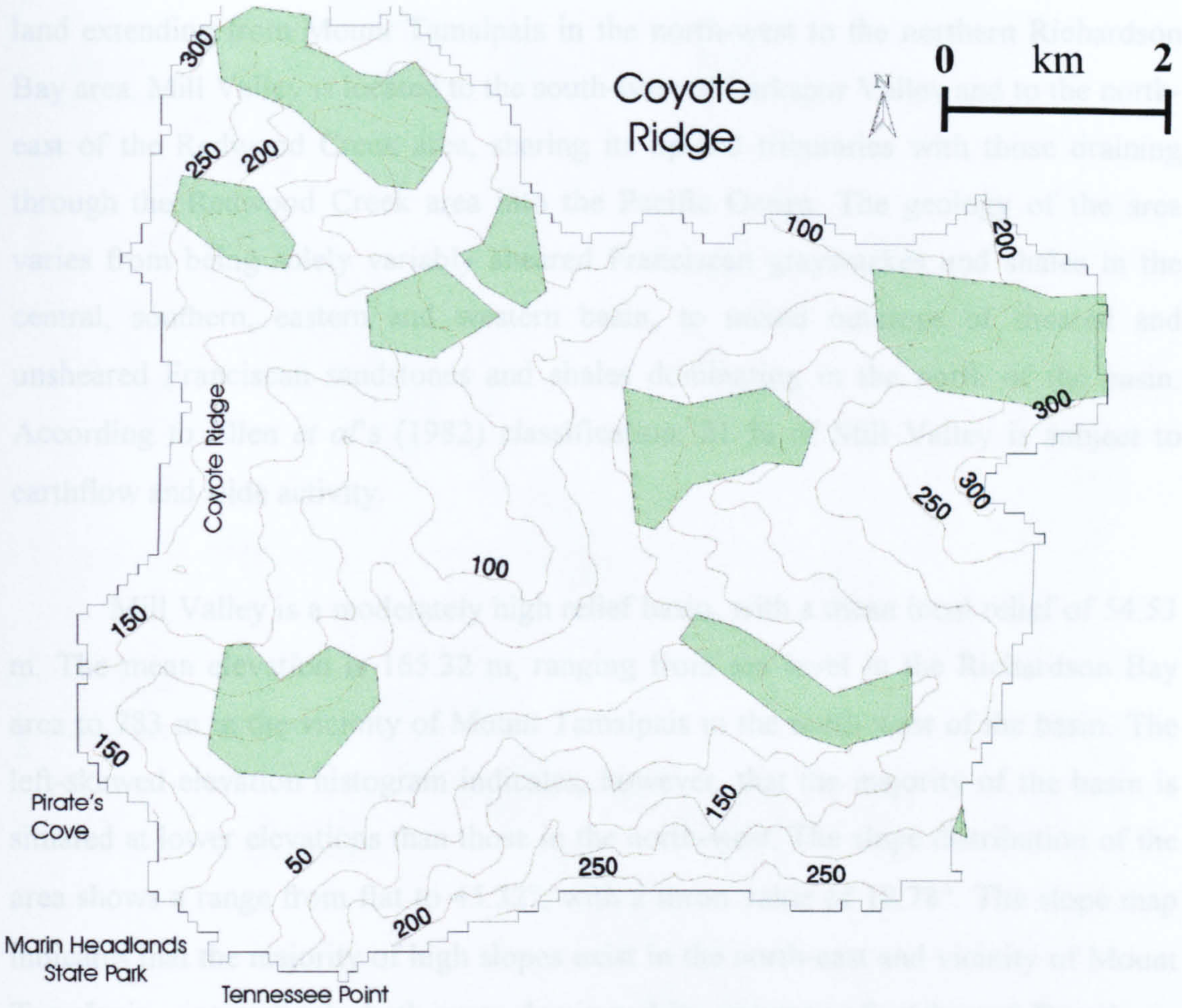

Figure 6.3 Location Map of Rodeo Basin, Marin County
(Green areas indicate those affected by earthflow activity)

6.3.4 Mill Valley

Covering an area of 14.75 km^2 in Marin County, the Mill Valley area drains land extending from Mount Tamalpais in the north-west to the northern Richardson Bay area. Mill Valley is located to the south-west of Larkspur Valley and to the north-east of the Redwood Creek area, sharing its upland tributaries with those draining through the Redwood Creek area into the Pacific Ocean. The geology of the area varies from being solely variably sheared Franciscan graywackes and shales in the central, southern, eastern and western basin, to mixed outcrops of sheared and unsheared Franciscan sandstones and shales dominating in the north of the basin. According to Ellen *et al*'s (1982) classification, 21 % of Mill Valley is subject to earthflow and slide activity.

Mill Valley is a moderately high relief basin, with a mean local relief of 54.53 m. The mean elevation is 165.32 m, ranging from sea level in the Richardson Bay area to 783 m in the vicinity of Mount Tamalpais in the north-west of the basin. The left-skewed elevation histogram indicates, however, that the majority of the basin is situated at lower elevations than those in the north-west. The slope distribution of the area shows a range from flat to 45.32°, with a mean value of 18.78°. The slope map indicates that the majority of high slopes exist in the north-east and vicinity of Mount Tamalpais - interestingly both areas dominated by outcrops of unsheared Franciscan material, contrasting with the low slopes found in Redwood Creek around Mount Tamalpais. Slopes in the area are generally orientated perpendicular to the northwest-southeast trending basin axis, with the majority facing east (20 %), north-east (17 %), south (17 %) and south-west (13 %).

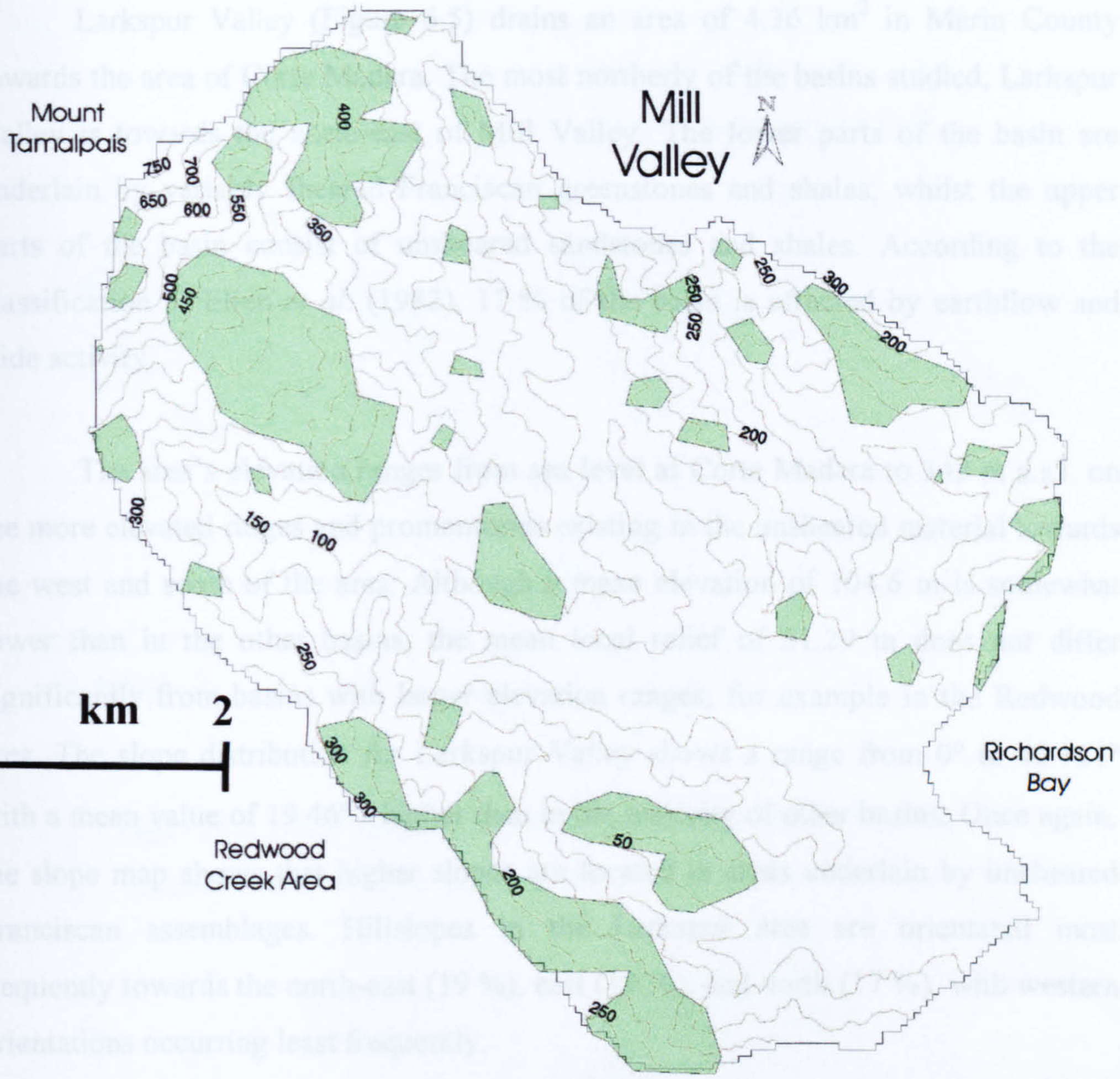

Figure 6.4 Location Map of Mill Valley, Marin County
(Green areas indicate those affected by earthflow activity)

6.3.5 Larkspur Valley

Larkspur Valley (Figure 6.5) drains an area of 4.36 km^2 in Marin County towards the area of Corte Madera. The most northerly of the basins studied, Larkspur Valley is towards the north-east of Mill Valley. The lower parts of the basin are underlain by variably sheared Franciscan greenstones and shales, whilst the upper parts of the basin consist of unsheared sandstones and shales. According to the classification of Ellen *et al.* (1982), 17 % of the basin is affected by earthflow and slide activity.

The area's elevation ranges from sea level at Corte Madera to 342 m a.s.l. on the more elevated ridges and promontories existing in the unsheared material towards the west and south of the area. Although a mean elevation of 104.6 m is somewhat lower than in the other basins, the mean local relief of 51.29 m does not differ significantly from basins with larger elevation ranges, for example in the Redwood area. The slope distribution for Larkspur Valley shows a range from 0° to 46.121° with a mean value of 19.46° - higher than in the majority of other basins. Once again, the slope map shows that higher slopes are located in areas underlain by unsheared Franciscan assemblages. Hillslopes in the Larkspur area are orientated most frequently towards the north-east (19 %), east (19 %), and north (17 %), with western orientations occurring least frequently.

6.3.6 Webb Creek

Webb Creek (Figure 6.6) covers 2.07 km^2 at the north-western end of the Marin Peninsula. Draining into the Pacific Ocean, the basin is to the north-west of the Redwood Creek area, with the eastern part covering part of Mount Tamalpais State Park. The geology of the area is relatively simple, consisting largely of the same sheared Franciscan sandstones and shales seen elsewhere in Redwood Creek, Mill Valley and Larkspur Valley. A small body of unsheared material exists in the south-east of the area. In contrast to the other five areas, 84% of Webb Creek is classed as affected by earthflow and slide activity (Ellen *et al.*, 1982).

The elevation distribution of Webb Creek shows a range from sea level to 490 m a.s.l.. The mean value is the highest of those for all six areas at 251.71 m. Slopes

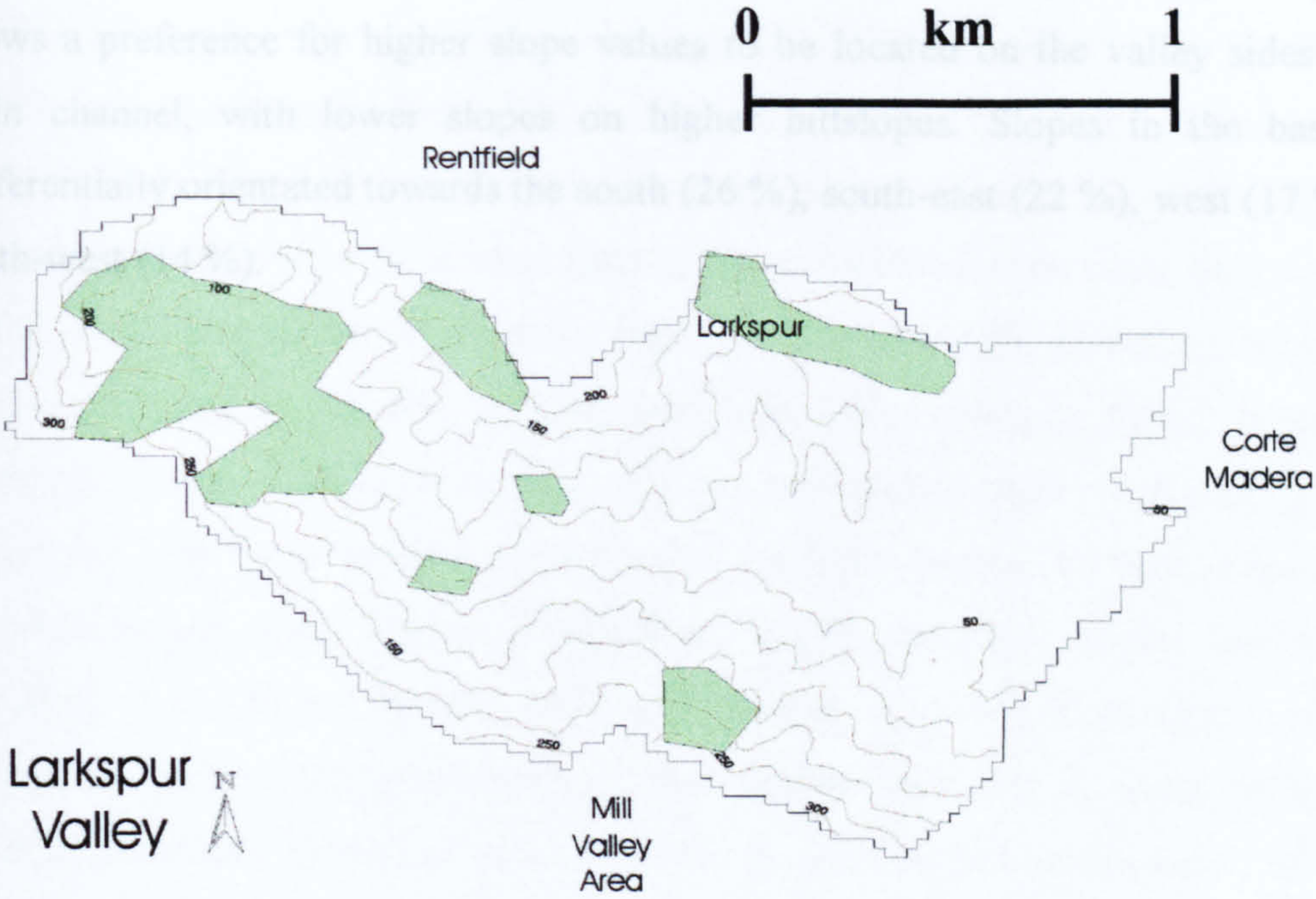

Figure 6.5 Location Map of Larkspur Creek, Marin County
(Green areas indicate those affected by earthflow activity)

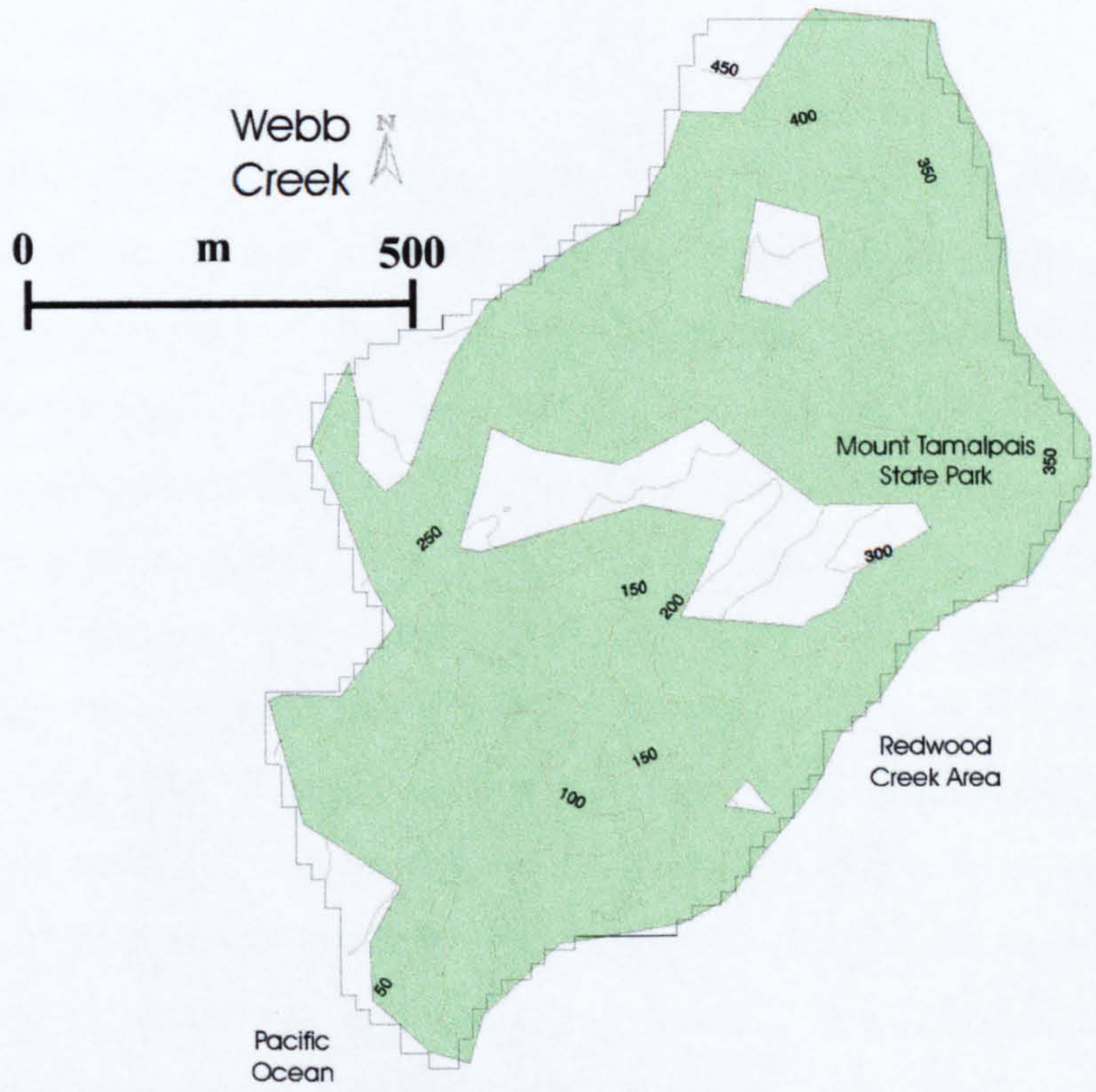

Figure 6.6 Location Map of Webb Creek, Marin County

(Green areas indicate those affected by earthflow activity)

in the area range from flat to 40.54°, lower than in other basins, such as Redwood Creek, yet the mean slope value is the highest of all the areas covered. The slope map shows a preference for higher slope values to be located on the valley sides of the main channel, with lower slopes on higher hillslopes. Slopes in the basin are preferentially orientated towards the south (26 %), south-east (22 %), west (17 %) and south-west (14 %).

6.4 DATA AND METHODS

The DEM file for Marin County was obtained from California State University and the mass movement coverages were downloaded from the USGS at Menlo Park. Both have a spatial resolution of 30 metres and a vertical resolution of 1 metre. The DEM file was then converted into a lattice for usage in Arc/Info and the coverages were likewise converted from vectorised polygons to lattice-type raster data files. The earthflow coverages contained several types of information (bodies of water, surficial deposits, and areas with few or many landslide bodies covering them). It was thus necessary to derive grids containing only the information required for the analyses carried out here. Separate grids were derived for water bodies, surficial deposits, few landslide bodies, many landslide bodies and mostly landslide bodies (terminology according to Nilsen and Wright, 1979 and Ellen *et al.*, 1997). Construction of these grids then enabled the assessment of topographic variables in areas affected by different processes within an area. In order to achieve fast computation and limit resource usage, the Marin area was divided into a number of large drainage basins within Arc/Info. Six of these basins were then chosen covering all areas and a range of lithologies.

6.4.1 Terrain Variables

Having delineated the study areas, it was decided that eight topographic variables would be selected to assess their importance on landslide distribution in Marin County. A review of the literature showed little correspondence between the suite of variables used, with different workers using different parameters for different reasons. The variables used here: elevation (Guzzetti and Reichenbach, 1994; Evans, 1972), slope gradient (Giles, 1998, Carrara *et al.*, 1995; Park, 1995), slope aspect (Atkinson and Massari, 1998; Carrara *et al.*, 1991), cell centre, profile and planform curvature (Zevenbergen and Thorne, 1987), slope shape (Gao, 1993; Dikau, 1989) and local relief (Pike, 1988; Guzzetti and Reichenbach, 1994) cover a large proportion of those methods used in previous morphometric studies. Within each study area, the distribution of each terrain variable is calculated for the basin as a whole, and for areas affected by earthflows and slides, both using grid cell and moving window techniques where appropriate (see below).

Working within Arc/Info's GRID module on the DEM and coverages outlined above, elevation distributions are calculated directly from the DEM, whilst slope gradient is calculated as the maximum change in Z-value (or elevation) for each pixel. Aspect is calculated as the down-slope direction of the maximum rate of change in value from each cell to its neighbours, and can take one of nine values: flat (no aspect), north (0° to +45°), north-east (+45° to +90°), east (+90° to +135°), south-east (+135° to +180°), south-west (+180° to +225°), west (+225° to +270°), and north-west (+270° to +360°). Cell centre curvature is the first derivative of slope for a pixel, planform curvature is curvature perpendicular to the direction of slope, and profile curvature is curvature in the direction of slope. Slope shape is a combined parameter, which classes slopes according to their profile and planform curvature (into a combination of 9 slope shapes). Finally, local relief is calculated in a window of 9 pixels as (mean value - minimum value) - (maximum value - minimum value).

Adopting the method outlined by Gao (1993), coverages of each terrain variable's distribution were calculated in each basin for the entire basin, and for the area affected by landslides. Each distribution was then divided into a number of range slices. For example, within slope calculations, the range may be from 0° to 45°, thus the slices are calculated in 2° slice intervals. For each interval, the total number of cells per slice was calculated, as were the number of landslide cells (affected cells), and number of unaffected cells (total - affected cells). These distributions were calculated using the AML's shown in Appendix 2. These values are then entered into a chi-square statistic to test for significance. In such tests, two outcomes are possible. H_o states that there appears to be a relation between the terrain variable under examination and landslide occurrence in the area examined, whilst H_1 states that there appears to be no evidence of such a relationship (Shaw and Wheeler, 1994). The number of affected cells are entered into the test for each variable as 'observed frequencies', and the number of 'expected frequencies' calculated using the method below (Section 1.4.2). The chi-square result is then assessed for statistical significance at the relevant level and for a given number of degrees of freedom. If significant, H_0 is accepted, otherwise H_0 is rejected and H_1 accepted.

6.4.2 Calculation of 'Landslide Potentials'

As outlined by Gao (1993), a great number of researchers undertake investigations into the possible causes of landslides without taking into account the general characteristics of the terrain under examination. This could result in a highly misleading interpretation of the type of terrain most vulnerable to mass movement activity. This will be outlined by means of the example below.

Elevation	Landslide Pixels	Total Pixels	Landslide Potential
0-50	45	60	75
50-100	80	100	80
100-150	100	150	66
150-200	30	50	60
200-250	18	20	90

Table 6.1 Example Data Set Used to Illustrate Calculation of 'Landslide Potentials'

Examination of Table 6.1 might initially suggest that land in the elevation range 100-150 m has the highest potential for landsliding as out of the five categories it has the highest number of affected cells. However, by taking into account the general nature of the terrain in the area, and the properties of land in each slice, it can be seen that the 200-250 m interval actually has the highest 'landslide potential' even though the total number of affected cells is less that in other slices.

6.5 RESULTS

6.5.1 Elevation

Within the Rodeo Basin area, earthflows occur most frequently at elevations of around 110 m and 250 m a.s.l., with fewer slides between these elevations. In Redwood Creek, such flows occur throughout the basin, regardless of elevation, although at lower elevations they have a slightly greater landslide potential. Rodeo Basin Valley's earthflows occur more frequently at lower elevations (<125 m) and also between 225 m and 275 m. In the Mill Valley area, the landslide bodies are distributed more preferentially at elevations between 300 m and 500 m a.s.l.. As in the Redwood Creek area, earthflows in the Larkspur Valley are distributed at all elevations, showing little preference for high or low elevations. Webb Creek's earthflows are distributed more preferentially at elevations of less than 150 m and between 300 m and 400 m. Although chi-square results for earthflow occurrence with elevation are significant for all six basins at the 99 % level, results here suggest that elevation is a relatively poor discriminator for determining landslide prone topography on scales greater than that of individual drainage basins.

6.5.2 Gradient

Earthflows in the Tennessee Basin area occur with a mean slope gradient of 20.45°, higher than the basin's mean value, whilst in Redwood Creek, the mean value is 19.48°. In both cases, the landslide potential distribution of gradients within landslide bodies is symmetrical about the means. In Rodeo Basin, the mean earthflow body gradient is 15.37°, and landslide potentials drop considerably at gradients of greater than 20°. In the Mill Valley area, earthflow gradients have a mean of 20.9° and potentials drop considerably at gradients of lower than 10°. Larkspur Valley's earthflow gradients show a general increased potential with increasing gradient, whilst in Webb Creek, landslide potentials are at 70-80 % at all gradients greater than 5°. Again, although gradient is significant in chi-square tests for the six basins, indicating a relationship between landslide occurrence and slope, the variability in mean slope values indicates that local factors largely control the slope angles present. Generally, however, we see an increase in landslide potential with increasing gradient.

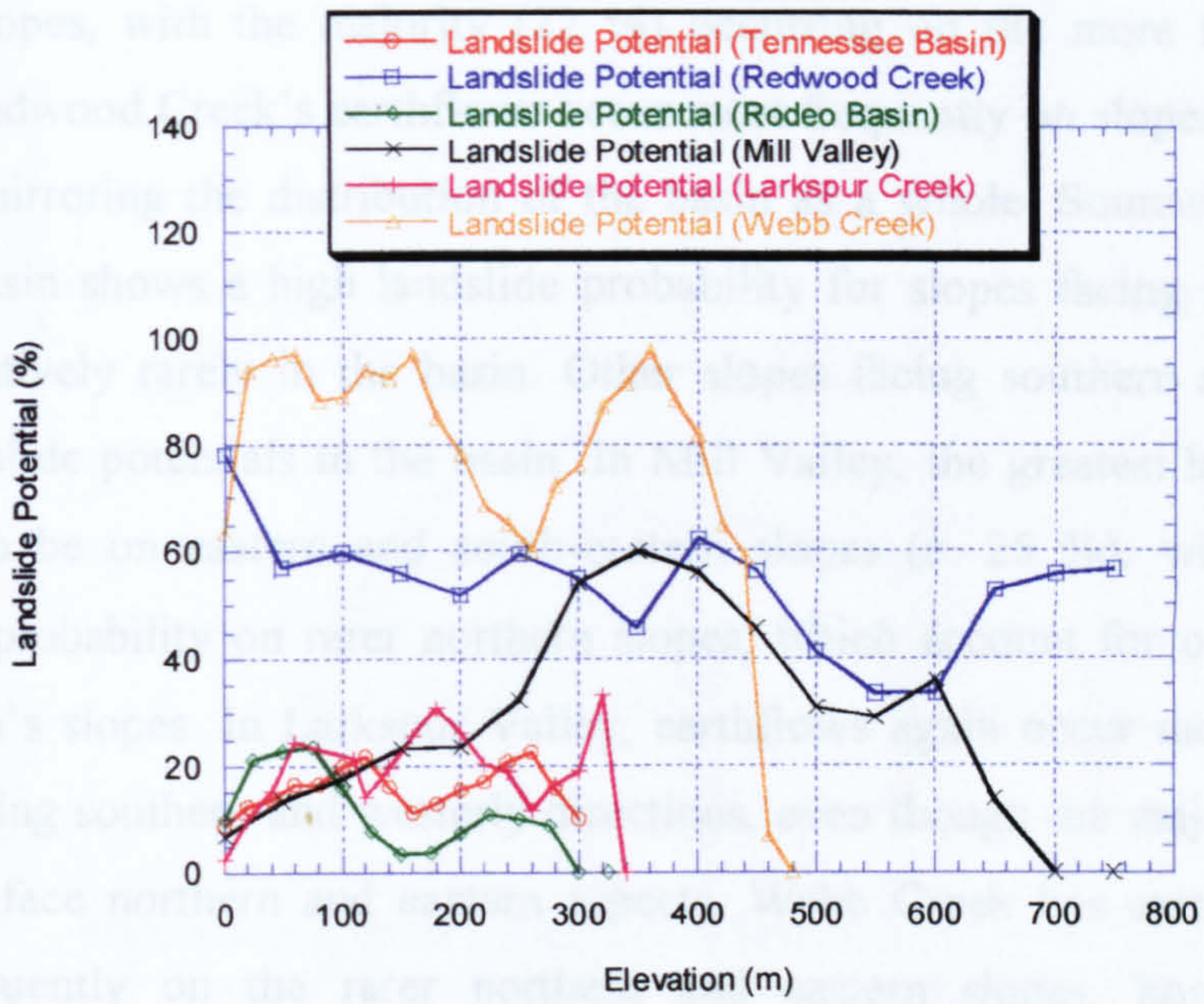

Figure 6.7 Elevation Landslide Potentials, Marin County

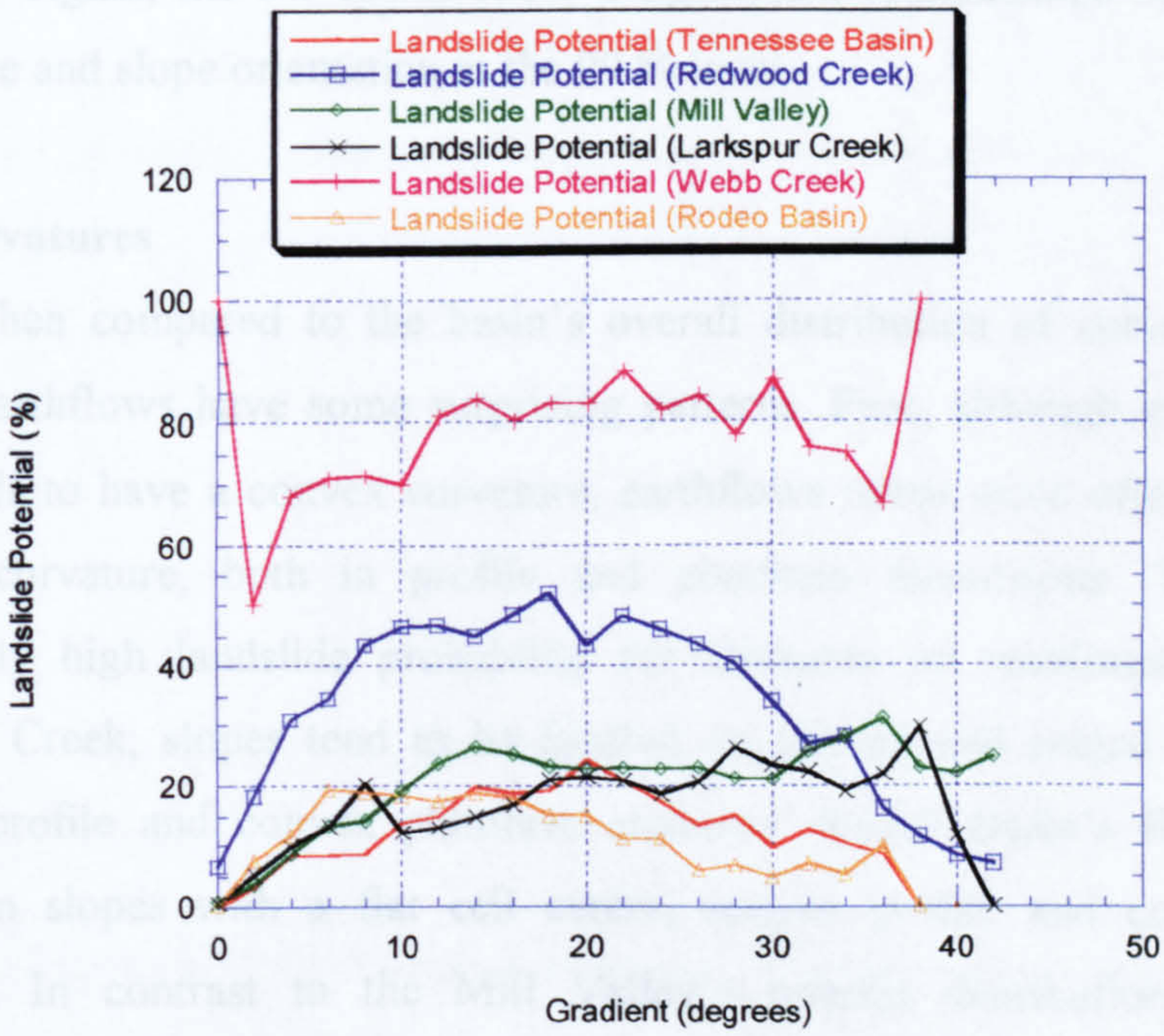

Figure 6.8 Gradient Landslide Potentials, Marin County

6.5.3 Aspect

Partially in contrast to Tennessee Basin's basin-wide aspect distribution, earthflows seem to be more prevalent on less frequently occurring west and south-eastern slopes, with the majority (22 %) occurring on the more frequent southern slopes. Redwood Creek's earthflows occur most frequently on slopes facing southerly aspects, mirroring the distribution of the basin as a whole. Somewhat anomalously, Rodeo Basin shows a high landslide probability for slopes facing north-east, which occur relatively rarely in the basin. Other slopes facing southern aspects also have high landslide potentials in the basin. In Mill Valley, the greatest landslide potential appears to be on eastern and south-eastern slopes (c. 25 %), with a higher than expected probability on rarer northern slopes, which account for only 8.9 % of the total basin's slopes. In Larkspur Valley, earthflows again occur more frequently on slopes facing southern and westerly directions, even though the majority of slopes in the basin face northern and eastern aspects. Webb Creek has earthflows occurring most frequently on the rarer northern and eastern slopes, however, the more frequently occurring southern and western slopes also have relatively high landslide potentials. Again, the six basins show a significant relationships between earthflow occurrence and slope orientation at the 99 % level.

6.5.4 Curvatures

When compared to the basin's overall distribution of curvature, Tennessee Basin's earthflows have some surprising patterns. First, although on the whole, the basin tends to have a convex curvature, earthflows occur more often in cells with a concave curvature, both in profile and planform dimensions. There is also a surprisingly high landslide probability for elements on rectilinear curvatures. In Redwood Creek, slopes tend to be located on convex cell centre curvatures, with concave profile and convex planform elements. Rodeo Basin's flows tend to be located on slopes with a flat cell centre, convex profile and concave planform curvature. In contrast to the Mill Valley's general distribution of curvatures, earthflows tend to locate at sites with concave profile and planform elements, rather than favouring the more frequently occurring convex elements. Cell centre curvature elements follow a similar trend to the basin as a whole. In Larkspur Valley , earthflows favour sites with concave cell centres, convex profile and concave planform curvatures. Finally, in Webb Creek, it is somewhat surprising to find that

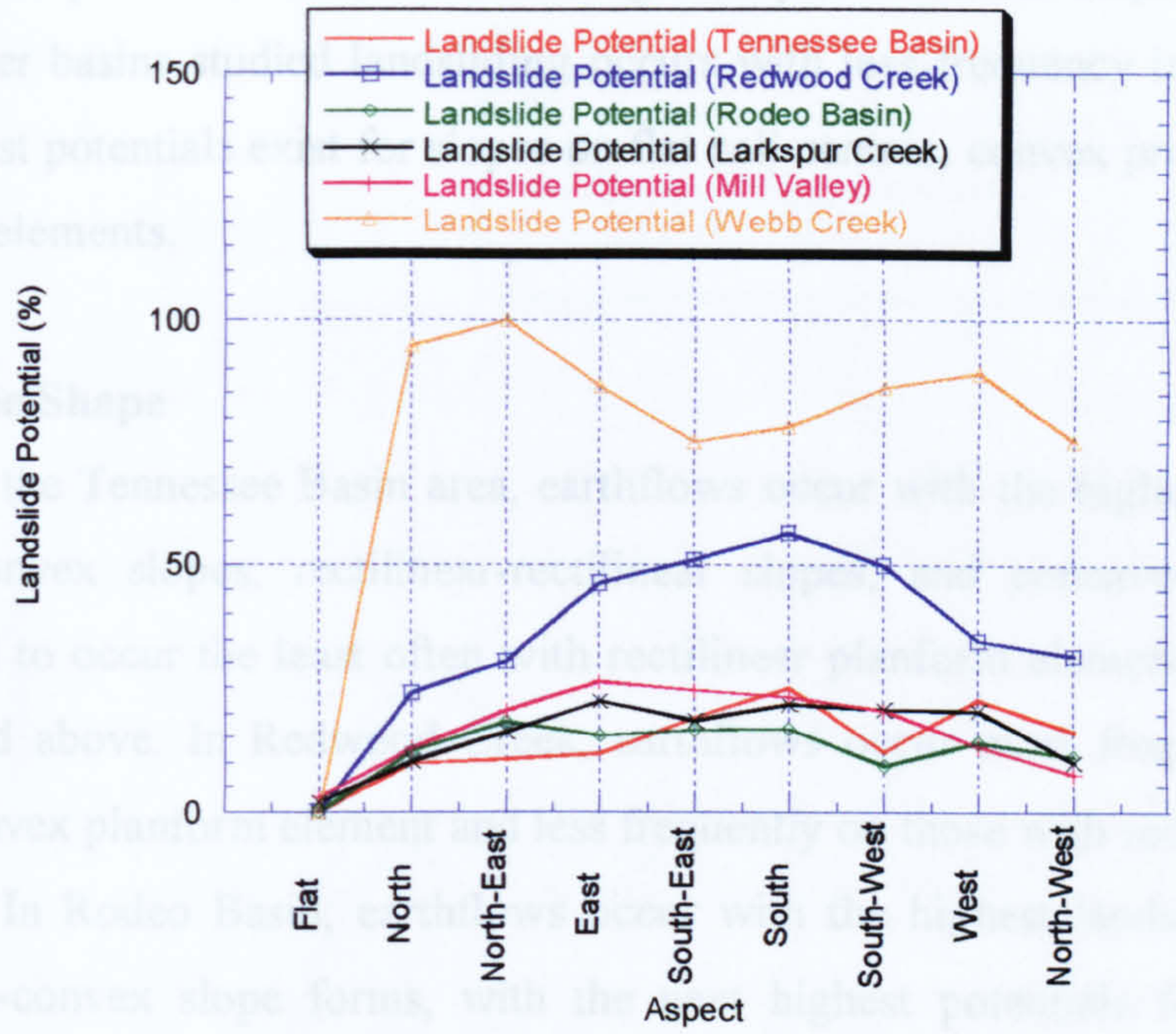

Figure 6.9 Aspect Landslide Potentials, Marin County

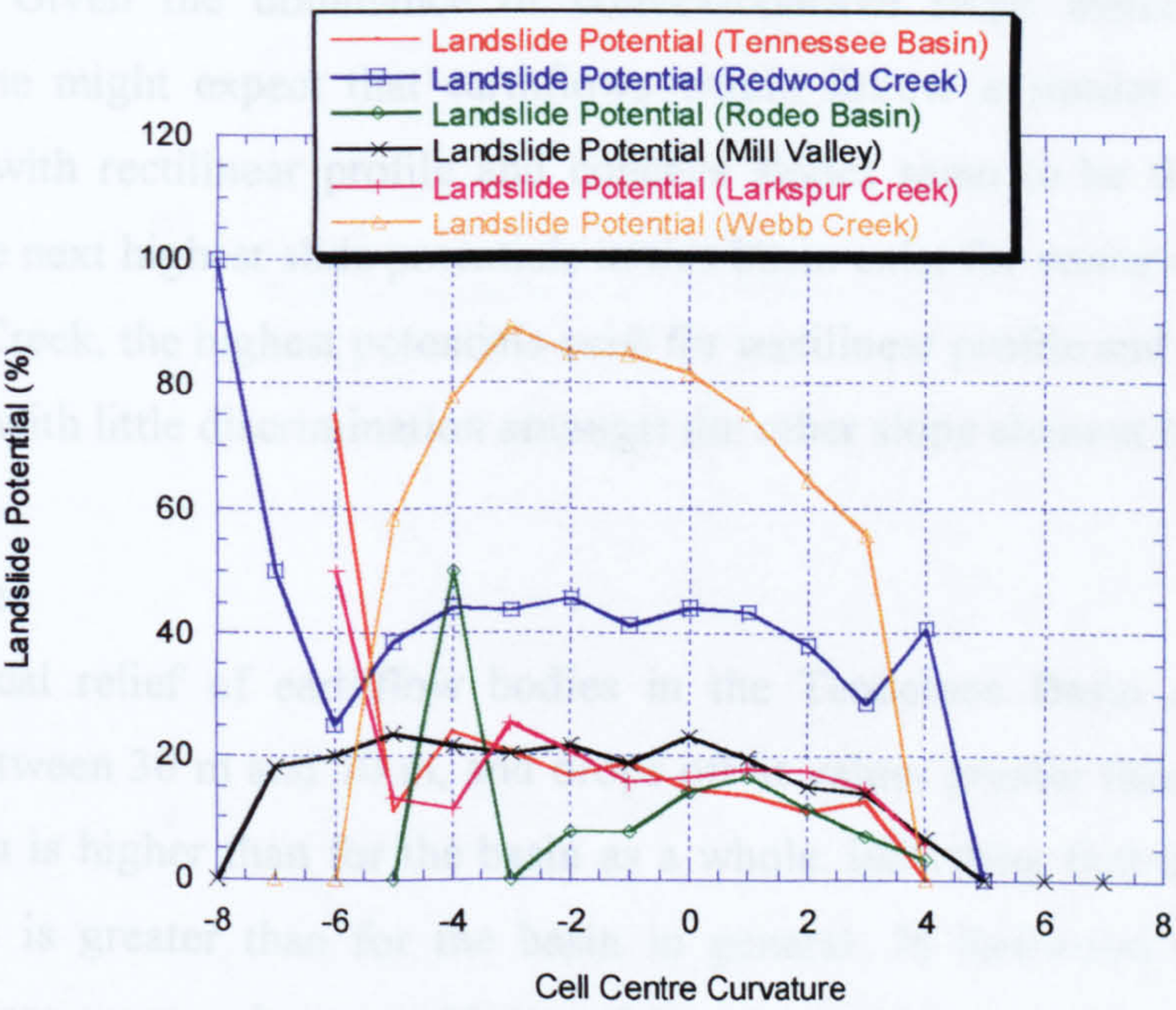

Figure 6.10 Curvature Landslide Potentials, Marin County

rectilinear slopes' landslide potential is high compared to other slope types, given that in the other basins studied landsliding occurs with less frequency in such situations. The highest potentials exist for slopes on flat cell centres, convex profile and concave planform elements.

6.5.5 Slope Shape

In the Tennessee Basin area, earthflows occur with the highest probability on convex-convex slopes, rectilinear-rectilinear slopes, and concave-concave slopes. They tend to occur the least often with rectilinear planform elements, except for the case noted above. In Redwood Creek, earthflows occur most frequently on slopes with a convex planform element and less frequently on those with rectilinear planform elements. In Rodeo Basin, earthflows occur with the highest landslide potential on rectilinear-convex slope forms, with the next highest potentials for slopes in the concave profile group, with rectilinear profile elements ranking lowly. Mill Valley's earthflows occur most frequently on slopes with convex planform and profile elements. Given the dominance of convex-concave slope elements in Larkspur Valley, one might expect that earthflows would follow a similar trend, However, elements with rectilinear profile and concave slopes seem to be the most prone to slides. The next highest slide potentials in this basin exist for concave slope elements. In Webb Creek, the highest potentials exist for rectilinear profile and convex planform elements, with little discrimination amongst the other slope element types.

6.5.6 Relief

Local relief of earthflow bodies in the Tennessee Basin area tends to be highest between 30 m and 70 m, and drops off at values greater than 80m. The mean of 56.89 m is higher than for the basin as a whole, indicating that the mean relief of earthflows is greater than for the basin in general. In Redwood Creek, earthflow potentials are greatest between 30 m and 80 m, drop between 80 m and 100 m and increase > 100 m. In Rodeo Basin, the highest potential exists at 30 m relief, with a general decrease in landslide potential with increases in local relief values. In contrast, Mill Valley shows an increase in landslide potential with increasing local relief. Finally, in Webb Creek, landslide potential increases with relief to 60 m, after which as relief increases potentials decrease.

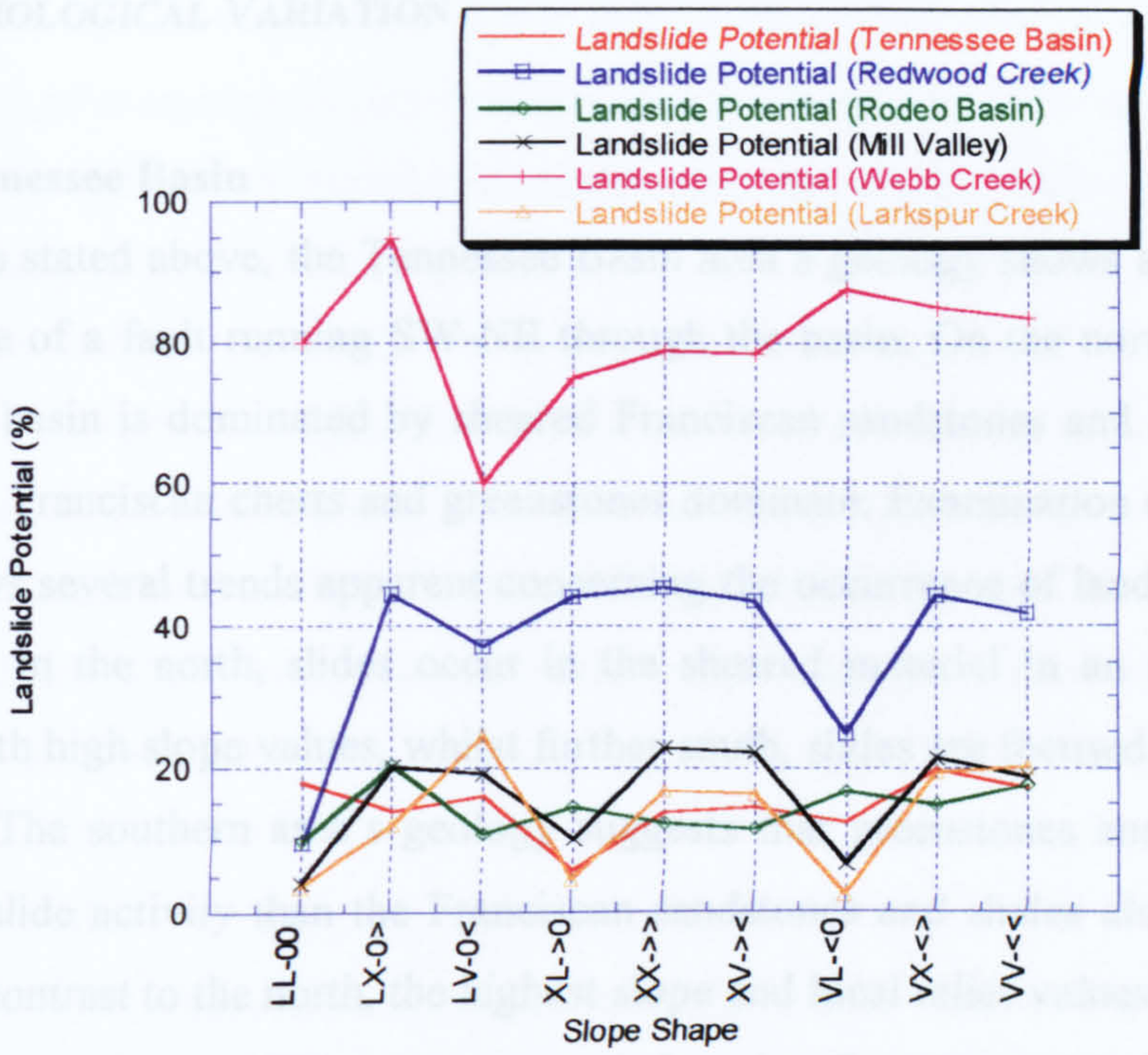

Figure 6.11 Slope Shape Landslide Potentials, Marin County

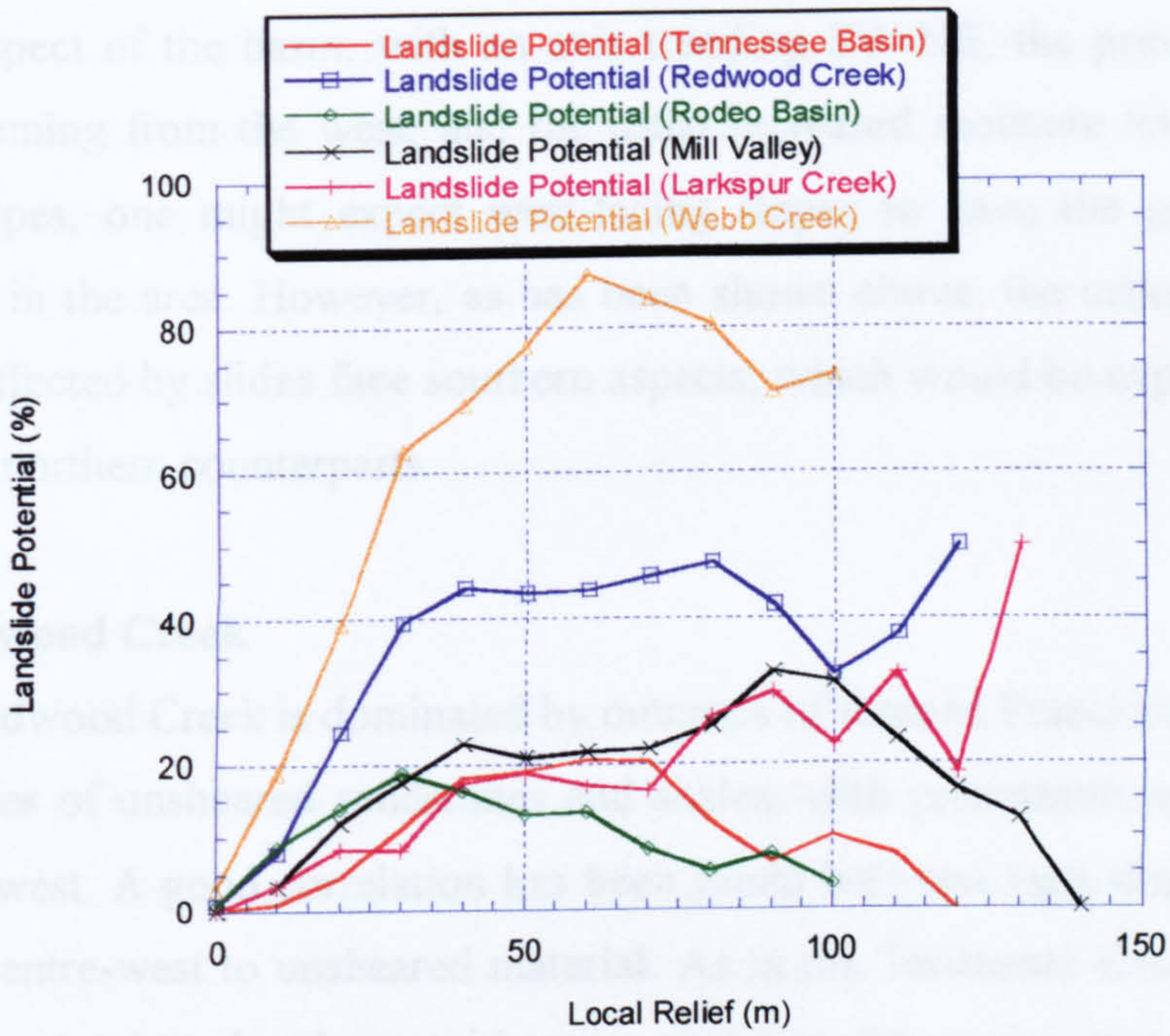

Figure 6.12 Local Relief Landslide Potentials, Marin County

6.6 INVESTIGATING THE RELATIONSHIP BETWEEN LANDSLIDING, TERRAIN FORM AND LITHOLOGICAL VARIATION

6.6.1 Tennessee Basin

As stated above, the Tennessee Basin area's geology shows an abrupt change either side of a fault running SW-NE through the basin. On the northern side of the fault, the basin is dominated by sheared Franciscan sandstones and shales, whilst in the south, Franciscan cherts and greenstones dominate. Examination of the geological map shows several trends apparent concerning the occurrence of landslide bodies and lithology. In the north, slides occur in the sheared material in an area of elevated terrain with high slope values, whilst further south, slides are focused along the valley bottoms. The southern area's geology suggests that greenstones and cherts are less prone to slide activity than the Franciscan sandstones and shales also present to the south. In contrast to the north, the highest slope and local relief values in the south are along the higher ridges. This area consists of a mix of greenstone and chert outcrops, and generally shows little evidence of landslide activity. Taking into account the general aspect of the basin, with an axis trending SW-NE, the prevailing wind and rainfall coming from the west, and the usual increased moisture levels in northern-facing slopes, one might expect west-facing slopes to have the greatest landslide potentials in the area. However, as has been shown above, the majority of slopes in the area affected by slides face southern aspects, which would be expected to be drier than their northern counterparts.

6.6.2 Redwood Creek

Redwood Creek is dominated by outcrops of sheared Franciscan material, with local bodies of unsheared sandstones and shales, with greenstone and sepentinite in the north-west. A good correlation has been found between high slopes in the north-east and centre-west to unsheared material. As in the Tennessee Basin area, areas of high slopes tend to be those with more resistant lithologies and fewer landslide bodies, with the majority of landslide bodies in this area being on sheared material. Also mirroring trends set by Tennessee Basin, those areas with highest relief (and high slope) are less affected by slides - this is seen in the area's plot of landslide potentials against relief. As the sheared material is distributed at all elevations within the basin, little correlation is found between landslide occurrence and elevation.

6.6.3 Rodeo Basin

Lithological variation is again shown to control the nature of terrain and distribution of mass movements in Rodeo Basin. The area is underlain by a mixture of greenstones, cherts and Franciscan sandstones and shales, with the more elevated areas tending to be cherts and greenstones. The area's slope map has demonstrated that higher slopes exist on the more resistant ridges and slopes formed of greenstone/chert assemblages, mirrored in the fact that the highest slide potentials in the area are at lower elevations. As slopes decline in the basin, so does the amount of chert and greenstone, yet slide activity increases. This trend is also apparent in the relief landslide potentials, with increasing relief being associated with higher slopes and lower landslide activity.

6.6.4 Mill Valley

The Mill Valley area shows a number of trends distinct from those outlined above. Consisting of sheared and unsheared Franciscan sandstones and shales, the basin has areas of high slope in the vicinity of Mount Tamalpais in the north-east. The other areas indicated that lower landslide potentials were associated with higher slopes, yet in this area the opposite seems to be true. This association is also apparent in the distribution of landslide potential with relief, which demonstrates that increasing relief is associated with increased activity. However, the general relationship between lithology and slope seems to be consistent, with lower slopes tending to occur on the sheared material compared to unsheared rock types.

6.6.5 Larkspur Creek

The Larkspur Valley area shows two lithological types, with a divide running NW-SE. To the north-east, outcrops of sheared Franciscan rocks dominate, whilst to the south-west, unsheared lithologies are present. Strong correlations exist between the higher slope values and the unsheared material, with few slides occurring on the steeper southern ridge. The distribution of the two types at all elevations in the basin seems to be reflected in the lack of preference shown by landslide potential with elevation, and this is also present in plots of landslide potentials for gradient in the area.

6.6.6 Webb Creek

Webb Creek is an area largely affected by earthflow and slide activity. The basin is predominantly underlain by sheared Franciscan assemblages. The wide distribution of landslides in the basin might expect one to assume that their would be no correlation between elevation, slope and relief in the area, with aspect mirroring the basin's general distributions. The slope map indicates that higher slopes are located towards the valley bottoms, which could be the result of fluvial incision of hillslopes. Elevation landslide potentials are higher for lower elevations, indicating that fluvial undercutting may be responsible for high slopes and instability, creating mass movements at such elevations. As expected, mass movement is shown to be independent of slopes in the basin (due to the widespread distribution of activity), whilst relief shows an increased potential up to 60 m, which then declines.

6.7. DISCUSSION

Previous work in the field has determined that certain forms of terrain may be more vulnerable to earthflow type mass movements than others (e.g. Gao, 1993), and that it may be possible to discriminate at more general scales between land affected by two types of process (e.g. Pike, 1988). However, such work has either been limited in its spatial scale (e.g. Gao, 1993), attempting to make no broad scale correlations between terrain position and mass movement, or has not attempted to assess terrain variable variation in actual landslide bodies focusing instead on the general area affected by certain processes (e.g. Pike, 1988). Having assessed the ability of terrain variables to discriminate between land affected and unaffected by landslides, the work presented here will conclude by comparing the findings to those published previously.

The results outlined above indicate that little overall relationship exists between topographic position and mass movement at intra-basin scales. Instead, lithological controls are believed to be the key determinants in mass movement activity. The patterns emerging may be the result of complex process-form links in which lithological variations result in terrain variability, which in turn conspires to make certain locations more prone to sliding than others. Lithologies such as Franciscan greenstones and greywacke sandstones demonstrate high hillslope angles and little slide movement, whilst weaker sheared lithologies frequently have lower slope angles and more movements present.

6.7.1 Topographic Variability and the Occurrence of Mass Movement

A number of workers have attempted to correlate mass movement with topographic variables over the past three decades. Prior to the widespread use of DTMs, such relationships were constrained by time to single parameter studies, such as those of slope angle (e.g. Hansen, 1984). Using DTM data, correlations have been found between terrain position and landslides using single pixel approximations of landslide bodies (Atkinson & Massari, 1998) using broad-scale process constraints (Pike, 1988), and at the single basin level (Gao, 1993). What these studies lack is either a limit to their spatial extent, or a coarse approximation of the characteristics of landslide areas.

6.7.1.1 Elevation

In his study of mass movements in Virginia, Gao (1993) came to several conclusions concerning the terrain setting vulnerable to mass movement activity. Gao (1993) found a bell shaped curve of landslide potential with elevation, indicating that more slides occur at mid-elevations. He attributed reduced activity at high elevations to convex curvature, limited infiltration and runoff. At mid-elevations, increased slide activity was attributed to increased percolation levels decreasing shear strength in slopes and leading to mass failure, whilst at low elevations low landslide potentials were seen as being due to gentler slopes existing in such locations.

A comparison of the work presented here and the findings of Gao (1993) suggests a number of conflicts. Results of this work suggest that landslide potentials vary considerably from location to location with elevation, rather than following the bell-shaped curve of Gao (1993). Mill Valley best follows such a trend, but even this is disrupted by an increase at higher elevations. Some basins, for example Rodeo Basin and Webb Creek, actually have very high landslide potentials at low elevations and lower potentials at mid-elevations, thus conclusions such as mid-elevations being more prone due to increased infiltration reducing shear strength appear not to be supported.

Broad scale patterns observed in Marin County in general appear instead to suggest that variations in landslide occurrence are determined more by the distribution of lithologies in an area with elevation than by elevation alone, thus weak rocks, such as sheared Franciscan sandstones and shales, slide frequently at all elevations, whereas stronger lithologies on ridge crests fail less frequently. It is concluded that elevation distributions may be of assistance in some aspects of general geomorphometry depending on the aim of the work being undertaken, for example in categorising landforms over the broad scales of mountain belts (e.g. Cendrero and Dramis, 1996) and countries (e.g. Guzzetti and Reichenbach, 1994). However, in attempting to correlate landslide occurrence and elevation at scales greater than individual basins, the effectiveness of elevation as a terrain parameter becomes limited.

6.7.1.2 Gradient

Previous work suggests that the relationship between slope angle and mass movement follows a distinctly non-linear trend (Carrara *et al.*, 1991). A second argument, proposed by Atkinson and Massari (1998), is that the relationship follows a linear trend, with an increase in sliding accompanying increases in slope gradient. Cendrero and Dramis (1994) argue along different lines, supporting Francis' (1987) theory of threshold slopes, whereby breaching of a critical slope gradient initiates mass movement. Jibson and Keefer (1983) also support the idea of threshold slopes, arguing that below a critical threshold slopes will remain stable and will slide above it.

Gao (1993) found that landslide potentials in Virginia varied with gradient of the slope under consideration, suggesting that the higher the gradient, the higher the landslide potential. He attributed this to a number of factors, including reduced mechanical stability on steep slopes. Given that areas with gentle gradients have less potential energy available for mass movements, one might expect that Gao's (1993) findings would apply to situations outside of Virginia.

Patterns of landslide potential with gradient in Marin County presented here display a range of trends. Some, for example the Tennessee Basin area, and, to a lesser extent, the Redwood Creek area, display bell-shaped curves, with potentials decreasing away from mean values. In other cases, such as Larkspur Creek and Mill Valley, potentials generally increase with gradient, as in Gao (1993), whilst in Rodeo Basin potentials decrease with gradient, and in Webb Creek potentials appear to be largely independent of gradient.

The trends seen in Marin County thus seem to show little consistency, yet each basin appears to provide support for the different slope angle-mass movement proposals outlined above. Larkspur and Mill Valleys show a somewhat linear trend, lending support for Gao (1993) and Atkinson and Massari's (1998) works. In other basins, such as in the Tennessee and Redwood areas, bell-shaped curves of slope angle landslide potentials may provide limited support for theories of threshold slope activity, with less movement away from a mean value. In these examples, it would seem that sliding occurs once a critical angle is reached, but once a higher threshold is

reached, slide activity ceases again. This could be due to the higher slope stability of greenstone lithologies in the Tennessee area and unsheared sandstones in the Redwood area. Webb Creek would appear to be best explained as a case of slope instability being independent of slope angle, as in the Jibson and Keefer (1983) model. As briefly mentioned above, many of these trends are best explained by lithological variation.

It has been suggested that such variation between basins is largely due to lithological variation, with higher gradient slopes existing on unsheared Franciscan rocks, and more sliding on lower gradient sheared material. Surprisingly, in a number of basins, such as Larkspur Creek and Rodeo Basin, large portions of high gradient land appear to be unaffected by earthflow and slide activity - again contrasting with Gao's (1993) findings. Although it is acknowledged that the gradient of hillslopes will ultimately affect their stability, other factors such as lithology appear to be more important in the first instance, primarily determining slope stability, which in turn determines where will slide and where will remain at a high slope, yet stable.

6.7.1.3 Aspect

The importance of slope aspect (or azimuth) as a factor in slope instability appears to be unresolved. Jacobsen *et al.* (1989) found slope morphology and aspect to be an important control on landslide activity levels, whilst Carrara *et al.* (1991) stated that no such relationship existed (see also Rice (*et al.*, 1969). Atkinson and Massari (1998) found that newer slides tended to orientate randomly, whilst older slides tended to face aspects determined largely by the tectonic and structural arrangement of the area under consideration. Gao (1993) gave possible explanations for landslide activity on certain slope aspects in Virginia, stating that those facing eastern and southern aspects are less likely to be affected by landslide activity for a number of reasons. Firstly, southern slopes tend to receive more solar radiation, and are thus drier. It therefore takes more rainfall (or a more intense period of rainfall) to saturate the drier south-facing land compared to moister northern facing slopes, they thus have lower shear stresses and lower potentials. Secondly, less moisture in the rock means that when slides do occur they will be transferred downslope less than in over-saturated northern slopes, reducing the resulting landslide paths on southern slopes.

Webb Creek seems to conform to Gao's (1993) conclusions, having a greater potential on northern and western slopes, yet this basin appears to be anomalous when compared to the Marin County's general trends. In the majority of other basins, and in particular in the Redwood Creek area and Larkspur Creek, those slopes facing southern aspects appear to have the highest potentials. This is clearly in contrast to Gao's findings, suggesting that even though south-facing slopes are drier, they still slide more frequently than northern slopes. This could, at least in part, be due to the prevailing rainfall direction from the west.

In basins such as Mill Valley, large aspect landslide potentials were found on the less frequently occurring northern slopes, whilst in Tennessee and Rodeo Basins, landslides are orientated in-line with the basins' overall slope aspect distributions. These findings may provide support for Atkinson and Massari's (1998) work, by indicating that a correlation between a basin's aspect and landslide potential distributions exist where the slides consist mainly of older slides - orientated in the direction of the basin's general topography. In comparison, basins with less agreement between the two distributions may indicate more recent slide activity.

6.7.1.4 Curvature and Slope Shape

Although undoubtedly important, the relationships between slope form and mass movement appear to have received a more limited research interest than many other parameters. In part this could have been due to difficulties associated with such analyses prior to the availability of DTMs in earlier years. In his analysis of slope form, Gao (1993) found that the concave suite of slopes in cross-section were those to have the highest landslide potentials, and slopes with concave aspects in both profile and cross-sectional (or planform) dimensions to have the greatest potential of all. This was attributed to the effects of surface curvature on the collection, transport and infiltration on water. Concave hillslope elements are sites of water convergence, whilst sites of convex topography tend to be sites of water divergence. Thus sites with convex topography in 2 dimensions tend to be those with the highest water concentrations, which leads to reduced shear strength and heightened landslide activity.

In comparison, the work presented here suggests that slope form variations have little direct impact on the distribution of landslides in Marin County. As has been shown, for five of the basins studies, the slope form with the highest landslide potential varies from basin to basin, ranging from rectilinear-convex in Rodeo Basin, to concave-convex in Redwood Creek. There does not even appear to be any particular group of elements in either the profile or planform dimension that has a higher landslide potentials consistently between basins. Again, as with the terrain variables discussed above, it is proposed that slope form is highly dependent on the lithological variations existing within each basin, which in turn affects landslide potentials to a greater extent than slope form alone.

6.7.1.5 Local Relief

As with the other terrain parameters examined in this work, local relief calculated within a 3*3 window demonstrates few consistent intra-basin trends. Basins such as Larkspur Creek and Mill Valley show general increased landslide potentials with increasing local relief, whilst the Tennessee Basin area and Rodeo Basin show increased landslide potentials initially with increasing relief, followed by a decrease. This lack of coherent trends again suggests that other factors may be responsible for actual variations in terrain and also the distribution of landslides within each basin.

6.7.1.6 Summary

Terrain variables appear to show little correlation with earthflow distributions in the basins studied. Previous work suggesting relationships between denudational process and parameters such as the hypsometric integral (e.g. Ciccacci *et al.*, 1992) and drainage density (e.g. Oguchi, 1997), which were not studied here, remain unexplored. Such general, broad scale characteristics allow for more variation in terrain topography than this study, which may help explain why apparently more significant relationships were discovered. However, such work only allows for broad-scale relationships to be examined and general trends to be explored. At the smaller intra-basin scales explored here, trends between mass movement and morphometric parameters appears best explained as the result of lithological variation.

6.7.2 Lithological Variation, Terrain Parameters and the Occurrence of Mass Movement in Marin County

Strong links exist between erosional processes and the form of the landscape which results. Although relationships of this kind have been cited for many years (e.g. Gilbert, 1877), few have attempted to infer process based on topographic form alone. Ellen *et al.* (1982) determined relationships between landscape form and the dominant type of erosion in the San Francisco Bay Area, although the terminology used suffered from an inadequacy seen in many geomorphic analyses, using 'hard' and 'soft' to distinguish between terrain types. Ellen *et al.* (1988) stated that soft terrain results from the action of earthflows and slides, and hard terrain from debris flow type activity.

Having determined that little broad-scale correlation exists between terrain variables and mass movement, and that lithological controls appear to dominate landslide distributions in Marin County, the implications will now be examined. A number of researchers have determined that variations in lithology can result in increased landslide activity (e.g. Cardinali *et al.*, 1994; Carrara *et al.*, 1995), yet their studies were carried out over somewhat limited spatial scales. This work extends these conclusions, and has determined that large-scale variations in lithology play a key role in the spatial distribution of terrain morphology and earthflow activity in Marin County.

The results presented here indicate that Ellen (1998) and Pike's (1988) classifications are inadequate. For soft terrain-earthflow and hard terrain-debris flow type relationships to be valid, correlations between gradient, terrain slope form and elevations would have been expected to have been found. Pike's (1988) findings suggested that soft melange-type rocks are strongly affected by earthflows, resulting in lower slope angles and low curvatures. Under such circumstances, the landslide distributions expected would show a peak at lower gradients and decreases with increased gradient. The landslide potential distributions of basins such as Webb Creek and Larkspur Valley are clearly in contrast to this. It is thus concluded that landslide activity is largely governed by lithological variation, and as such classifying terrain within a binary system of soft and hard terrain types based on terrain variable distributions is inadequate. Lithological variation within Marin County means that

high relief areas with slopes in excess of 20° and resistant beds frequently lack earthflow and slide activity, thus models based on linear trends between slope angle and mass movement are flawed. Future models may have to incorporate lithology as a factor in mass movement assessments, whilst a better understanding of the relationships between lithology and terrain morphometry may enable large-scale lithological mapping based on DTM analyses. In turn, such mapping may lead the way for an assessment of the spatial distribution of erosion at large scales based on remotely sensed lithological changes.

CHAPTER 7

CONCLUSIONS AND SUGGESTIONS FOR FUTURE RESEARCH

The work presented in this thesis has examined some of the ways in which sediment is liberated from, and transported through, macro-scale process systems around the world. The previous chapters outlined in detail the techniques employed, data gathered, and conclusions drawn. In this chapter, the key conclusions from each of the previous chapters are outlined and drawn together showing how they improve our understanding of the processes of sediment erosion and transport. Suggestions are also presented for future research which could develop further the work presented.

In Chapter 2, data are presented which demonstrate that downstream changes in channel slope gradient, invoked by the channel flowing across active faults, results in transitions from zones of long-term erosion to deposition. This conclusion was previously made by Yatsu (1955), who found the erosion-deposition transition in Japanese rivers was marked by a sharp reduction in channel gradient. Data from the Northern Apennines in Italy, and Death Valley and the Wheeler Ridge in California, U.S.A. support Yatsu's (1955) finding, and demonstrate it to be a general phenomenon of rivers as they switch between areas of erosion and deposition. Changes in channel slope also strongly influence parameters such as stream power and bed shear stress, which have previously been documented to correlate with sediment transport regimes.

Chapter 2 also provides a comparison of river long profiles derived from 1:10,000 scale topographic maps and a 230 metre scale DTM of Italy. Work in this chapter has shown that changes in channel slope reflect the erosion-deposition transition, influenced by tectonic activity. Long profiles derived from DTMs are much quicker to obtain than those from conventional maps, and thus offer the potential for time and energy saving in data collection. However, despite this potential, the author is not aware of any other studies which have attempted to assess the accuracy of such DTM-derived profiles. Data presented in Chapter 2 demonstrate that although profiles derived from the two sources have a grossly comparable morphology, upon more

detailed examination, for example slope analysis, data obtained from the DTM-derived profile fail to portray the details obtained from the map-derived profiles. Profiles derived from the DTM data set are shown to be around 50 metres higher than those derived from conventional 1:10,000 scale maps, with this being particularly evident in areas of high curvature, for example gorges. Possible future research could focus on investigating the accuracy of both the DTM and the 1:10,000 scale topographic maps used in this thesis. Although a comparison between the two is presented in Chapter 2, neither have been compared to profile data derived from field observations. By taking systematic measurements of elevation using an altimeter along channels in the Apennines, a third control could be obtained upon which to test the accuracy of both the map and DTM-based profiles.

Despite the above findings, contributing areas and distances along channel networks from DTM data compare well to those derived from maps, and, as such, were used to determine how values of bed shear stress vary along the Enza River. Calculations show that bed shear stress varies significantly along the channel, and field observations show similar trends for mean grain size. However, estimates of dimensionless shear stress, which takes account of grain size in calculating shear stress, is shown to be relatively constant along the channel network. This finding supports previous studies which have documented that dimensionless shear stress remains constant along sand and gravel-bed rivers. Downstream changes in grain size along the Enza River are concluded to result not from abrasion and selective entrainment mechanisms, but from broad scale changes in lithology along the Enza River from resistant Tuscan turbidites (large grain size) to weak erodible Pliocene mudstones (small grainsize). Future research could focus on investigating the actual strength of the lithologies cropping out in the Apennines, such that differences in rock strength among the Tuscan, Marnosa Arenecea Formation, and Miocene mudstones be determined.

In the next four chapters, data are presented which examine not the way in which sediment is transported via river networks, but rather the erosional processes which liberate the sediment from hillslopes and the morphology of the hillslopes which result from this erosive activity.

Fieldwork in the Northern Apennines has documented the existence of distinctive linear ridge terrain. Such terrain forms have also been documented as existing in parts of California, Japan, and the Southern Alps. Despite being relatively widespread in some areas, little previous work has been carried out to determine how such hillslope forms result. Work by Anderson (1994) and Schmidt and Montgomery (1995) has documented that such linear slopes exist in the Santa Cruz Mountains of California. Morphometric analyses presented in Chapter 4 from a 30 metre resolution DTM of the mountain belt shows that hillslope gradient and local relief parameters are best able to distinguish linear ridge terrain areas. Linear hillslopes are shown to cluster about threshold slope and relief values. Such hillslope forms are also demonstrated to occur more often, and with higher mean slope angles, on certain lithological types, for example the Great Valley Sequence, Franciscan Complex and Santa Cruz Mudstone. Modelling work carried out by Ellis *et al.*, (1999) has reproduced linear slope forms, which are believed by Ellis *et al.*, (1999) to represent pre-failure hillslopes controlled by large-scale bedrock landslides. Results presented in Chapter 4 demonstrate clustering of hillslope gradients about critical values of 18° - 20°, which are believed to represent Ellis *et al.* (199)'s pre-failure hillslopes. These threshold slopes, controlled by bedrock landslide activity, have also been documented as existing in the northwestern Himalayas (Burbank *et al.*, 1996).

Links between hillslope form, erosional process and bedrock lithology are also examined in Chapter 5 in the context of the Northern Apennines study area. Fieldwork in the area has documented that linear ridge terrain occurs in areas where resistant Tuscan and Marnosa Arenecea formations crop out. Areas in the Apennines where surface lithologies consist of weaker Miocene mudstone formations lack linear ridge terrain and demonstrate rounded hillslope morphologies. DTM analysis of the 230 metre Italian DTM in Chapter 5 shows that drainage basins with linear ridge terrain have higher mean slope and local relief values than those with rounded topography. A strong correlation is also drawn between denudation rate, surface morphology, lithology and dominant erosional processes acting in basins across the Apennines. Those basins with rounded topography are dominated by weak Miocene

mudstones, and have low mean slope and relief values and higher sediment yield and denudation rates than those basins exhibiting linear ridge terrain. The basins with rounded topography, for example the Enza Basin, also show more active landslide processes, as with the Corniglio landslide in the Parma Valley. By contrast, basins with linear ridge terrain have lower denudation rates. Threshold hillslopes in these basins cluster at critical values on resistant Tuscan and Marnosa Arenecea formations, and fail less frequently than hillslopes on mudstone formations. Threshold linear slopes represent the pre-failure forms simulated by Ellis *et al.*'s (1999) model, and result in less material exiting the hillslope system than in basins where weaker mudstones dominate, which fail more frequently - resulting in observed variations in sediment yield and denudation rate. These findings contrast with Ahnert's (1970) conclusion that local relief and denudation rate are positively correlated, and suggests that such relationships may be invalid in areas where bedrock lithology and landslides dominate the region's topography and evolution. Future research could focus on taking field measurements of hillslope angles using a clinometer, both in the Northern Apennines and Santa Cruz study areas. Such measurements could then be used to determine the accuracy of hillslope gradient calculations made from the corresponding 230 metre and 30 metre DTMs, and may be used to suggest how studies using DTMs need to adjust their values in order to have hillslope gradients comparable to those observed in the field.

Links between topographic form and erosional process are examined in Chapter 6 in a case study of Marin County in California. In this area, the topography is dominated by rounded slope forms and subject to earthflow-type landslide processes. Previous studies, for example Gao (1993), have suggested that linking variations in terrain parameters, such as slope and relief, to landslide activity can be used to predict which areas will be affected by future landslides. Results presented in Chapter 6 contrast with those of Gao (1993) and Pike (1988), and suggest that little or no correlation exists between hillslope parameters and areas of terrain affected by landslide activity. However, as in Chapters 4 and 5, earthflow-type activity is shown to occur more frequently on hillslopes where sheared Franciscan melange crops out, and activity is more limited on hillslopes dominated by chert and greenstone lithologies.

These findings have implications for the ways in which mountain belt evolution is simulated. Models which adopt simple linear relationships between local relief and denudation rate, for example, are believed to be inadequate for areas such as the Northern Apennines. Another general problem with many SPMs and LEMs at present is their failure to address the impact of surface variations in lithology on terrain morphology, dominant erosional processes and the resulting flux of material from the hillslopes. Only when such issues have been resolved by modellers can their simulations accurately portray the macro-scale evolution of mountainous areas.

REFERENCES

- Abatte, E., Bortolotti, V., Passerini, P., and Sagri, M., 1970, Introduction to the Geology of the Northern Apennines: *Sedimentary Geology*, v. 4, p. 207-249.
- Ahnert, F., 1970, Functional relationships between denudation, relief and uplift in large mid-latitude drainage basins: *American Journal of Science*, v. 268, p. 243-263..
- Allen, P.A., and Hovius, N., 1998, Sediment supply from landslide-dominated catchments: implications for basin-margin fans: *Basin Research*, v. 10, p. 19-35.
- Amorosi, A., Farina, M., Severi, P., Preti, D., Caporale, L., and Di Dio, G., 1996, Genetically related alluvial deposits across active fault zones: an example of alluvial fan-terrace correlation from the upper Quaternary of the southern Po Basin, Italy: *Sedimentary Geology*, v. 101.
- Anderson, R.S., and Bucknam, R.C., 1987, Fitting degradation of shoreline scarps by a nonlinear diffusion model: *Journal of Geophysical Research*, v. 92, p. 12857-12867.
- Anderson, R.S., 1994, Evolution of the Santa Cruz Mountains, California, through tectonic growth and geomorphic decay: *Journal of Geophysical Research*, v. 99(B10), p. 20161-20179.
- Andrews, E., 1984, Bed material entrainment and hydraulic geometry of gravel-bed rivers in Colorado: Geological Society of America Bulletin, v. 95, p. 371-378.
- Andrews, D.J., and Bucknam, R.C., 1987, Fitting degradation of shoreline scarps by a nonlinear diffusion model: *Journal of Geophysical Research*, v. 92, p. 12857-12867.
- Arrowsmith, J.R., Pollard, D.D., and Rhodes, D.D., 1996, Hillslope development in areas of active tectonics: *Journal of Geophysical Research*, v. 101(B3), p. 6255-6275.
- Ashworth, P., and Ferguson, R., 1989, Size-selective entrainment of bed load in gravel-bed streams: Water Resources Research, v. 25, p. 627-634.
- Atkinson, P.M., and Massari, R., 1998, Generalised linear modelling of susceptibility to landsliding in the Central Apennines, Italy: *Computers and Geosciences*, v. 24(4), p. 373-385.
- Bagnold, R., 1980, An empirical correlation of bedload transport rates in flumes and natural rivers: *Proceedings of the Royal Society*, v. 372A, p. 453-473.
- Band, L.E., 1986, Topographic partition of watersheds with digital elevation models: *Water Resources Research*, v. 22, p. 15-24.
- Bartolini, C., Caputo, R., and Pieri, M., 1996, Pliocene-Quaternary sedimentation in the Northern Apennine foredeep and related denudation: *Geological Magazine*, v. 133(3), p. 255-273.
- Beaumont, C., 1981, Foreland basins: *Geophysical Journal of the Royal Astronomical Society*, v. 65, p. 291-329.
- Beaumont, C., Fullsack, P., and Hamilton, J., 1992, Erosional control of active compressional orogens, *in* McClay, K.R., ed., *Thrust Tectonics*, p. 1-18.
- Benda, L., and Dunne, T., 1997, Stochastic forcing of sediment supply to channel networks from landsliding and debris flows: *Water Resources Research*, v. 33, p. 2849-2863.
- Blodgett, T.A., Isacks, B.L., Fielding, E.J., Masek, J.G., and Warner, A.S., 1996, Erosion attributed to landslides in the Cordillera Real, Bolivia: *Eos Transactions, AGU*, v. 17(17), p. S261.

- Bonneau, P., and Snow, R., 1992, Character of headwater adjustment to base level drop, investigated by digital modelling: *Geomorphology*, v. 5, p. 475-487.
- Bradley, W.C., and Griggs, G.B., 1976, Form, genesis and deformation of the central California wave-cut platforms: *Geological Society of America Bulletin*, v. 104, p. 433-449.
- Braun, J., and Sambridge, M., 1997, Modelling landscape evolution on geological time scales: a new method based on irregular spatial discretization: *Basin Research*, v. 9, p. 27-52.
- Brown, R., Summerfield, M., and Gleadow, A., 1994, Apatite fission track analysis: its potential for the estimation of denudation rates and implications for models of long-term landscape evolution, *in* Kirkby, M., ed., *Process Models and Theoretical Geomorphology*: London, John Wiley & Sons, p. 23-53.
- Brune, G., 1953, Trap efficiency in reservoirs: *Transactions American Geophysical Union*, v. 34, p. 407-418.
- Buffington, J., and Montgomery, D., 1997, A systematic analysis of eight decades of incipient motion studies, with special reference to gravel=bedded rivers: Water Recources Research, v. 33, p. 1993-2029.
- Buiter, S.J.H., Worter, M.J.R., and Grovers, R., 1998, The role of subduction in the evolution of the Apennines foreland basin: *Tectonophysics*, v. 296, p. 249-268.
- Bull, W.M., 1979, Threshold of critical power in streams: *Geological Society of America Bulletin*, v. 90, p. 453-464.
- Burbank, D.W., Leland, J., Fielding, E., Anderson, R.S., Brozovic, N., Reid, M.R., and Duncan, C., 1996, Bedrock incision, rock uplift and threshold hillslopes in the northwestern Himalayas: *Nature*, v. 379, p. 505-510.
- Burbank, D.W., Law, J., Meigs, A.J., Fielding, E.J., and Blythe, A.E., 1998, Consistent long and short term denudation patterns in the San Gabriel and Himalayan mountains (abstract): *Eos Transactions*, AGU, v. 79 (45), p. F338.
- Burbank, D., and Pinter, N., 1999, Landscape evolution: the interactions of tectonics and surface processes: Basin Research, v. 11, p. 1-6.
- Burgmann, R., Arrowsmith, R., Dunitru, T., and McLaughlin, R., 1994, Rise and fall of the Santa Cruz Mountains, California, from fission tracks, *Geomorphology*, and *Geology*: *Journal of Geophysical Research*, v. 99, p. 20181-20202.
- Campbell, R.H., 1975, Soil slips, debris flows, and rainstorms in the Santa Monica Mountains and vicinity, southern California: *U.S. Geological Survey Professional Paper*, v. 851.
- Canali, L., and Allodi, G., 1963, Contributo di studio sul transporto solido in sospensione die corsi d'acqua padani e sulla degradazioni del suolo nel bacino del Po: *Giorno Genio Civile*, v. 101, p. 252-271.
- Cardinali, M., Galli, M., Guzzetti, F., Reichenbach, P., and Borri, G., 1994, Relationships between mass movements and tectonic setting in the Carpina Basin (northern Umbria): *Geografiska Fisica e Dinamica Quaternaria*, v. 17, p. 3-17.
- Carmignani, L., and Kligfield, R., 1990, Crustal extension in the Northern Apennines: The transition from compression to extension in the Alpi-Apuane core complex: *Tectonics*, v. 9(6), p. 1275-1303.
- Carrara, A., 1988, Drainage and divide networks derived from high fidelity digital terrain models, *in* Chung, C.F., ed., *Quantitative analysis of mineral and energy resources*, D.Reidel, p. 581-597.
- Carrara, A., Cardinali, M., Detti, R., Guzzetti, F., Pasqui, V., and Reichenbach, P., 1991, GIS techniques and statistical models in evaluating landslide hazard: *Earth Surface Processes and Landforms*, v. 16, p. 427-445.

- Carrara, A., Cardinali, M., Guzzetti, F., and Reichenbach, P., 1995, GIS technology in mapping landslide hazard, *in* Carrara, A., and Guzzetti, F., eds., *Geographical Information Systems in Assessing Natural Hazards*: Netherlands, Kluwer Academic, p. 135-175.
- Carson, M., and Kirkby, M., 1972, *Hillslope form and process*: New York, Cambridge University Press, 475 p.
- Carter, K.E., Dworkin, S.I., Carmignani, L., Mecchen, M., and Fantozzi, P., 1994, Dating thrust events using $^{87}Sr/^{86}Sr$. An example from the northern Apennines, Italy: *Journal of Geology*, v. 102(3), p. 297-305.
- Castaldini, D., and Panizza, 1988, Geomorphological features of the central sector of the Po Valley, Joint meeting on Geomorphological hazards, International Geographical Union: Guidebook for excursions in the Modena and Verona areas, p. 103-107.
- Cendrero, A., and Dramis, F., 1996, The contribution of landslides to landscape evolution in Europe: *Geomorphology*, v. 15, p. 191-211.
- Chase, C.G., 1992, Fluvial landsculpting and the fractal dimension of topography: *Geomorphology*, v. 5, p. 39-57.
- Ciccacci, L.D., Fredi, P., Palmieri, E.L., and D'Alessandro, P., 1992, Relations between morphometric characteristics and denudational processes in some drainage basins of Italy: *Zeitschrift fur Geomorphologie*, v. 36(1), p. 53-67.
- Clarke, J.E., 1981, Stratigraphy, palaeontology and *Geology* of the central Santa Cruz Mountains, California Coast Ranges: *U.S. Geological Survey Professional Paper*, v. 1168.
- Cockburn, H., Seidl, M., and Summerfield, M., 1997, Assessing denudation rates across ancient landscapes: Be-10 and Al-26 data from Central Namibia: *Geological Society of America Abstracts*, v. 29, p. 170.
- Curtis, W., Culbertson, J., and Chase, E., 1973, Fluvial-sediment discharge to the oceans from the conterminous United States: *U.S. Geological Survey Circular*, 607, pp. 17.
- Dade, W., and Friend, P., 1998, Grain-size, sediment-transport regime, and channel slope in alluvial rivers: The Journal of Geology, v. 106, p. 661-675.
- Dahlen, F.A., and Suppe, J., 1988, Mechanics, growth and erosion of mountain belts, *in* Clarke, S.P.J., Burchfiel, B.C., and Suppe.J, eds., *Processes in continental lithospheric deformation*, Volume 218, Geological Society of America, p. 161-178.
- Davis, W., 1892, The convex profile of badland divides: *Science*, v. 20, p. 245.
- Davis, W., 1902, Base-level, grade and peneplain: *Journal of Geology*, v. 10, p. 77-111.
- Denny, C.S., 1964, Alluvial Fans in the Death Valley Region, California and Nevada: Washington, *U.S. Geological Survey Professional Paper 466*, 59 p.
- Densmore, A.L., Anderson, R.S., McAdoo, B.G., and Ellis.MA, 1997, Hillslope evolution by bedrock landslides: *Science*, v. 275, p. 369-372.
- Densmore, A.L., Ellis, M.A., and Anderson, R.S., 1998a, Landsliding and the evolution of normal-fault bounded mountains: *Journal of Geophysical Research*, v. 103(B7), p. 15203-15219.
- Densmore, A.L., and Hovius, N., 1998b, The topographic fingerprint of bedrock landsliding: *Eos Transactions, AGU*, v. 79 (45), p. F357.
- Di Dio, G., Lasagna, S., Preti, D., and Sagne, M., 1997, Carta Geologica dei depositi quaternari della provincia di Parma.: Bologna, Servizio Cartografico e Geologico della Regione Emilia-Romagna.

- Dietrich, W.E., Wilson, C.J., Montgomery, D.R., McKean, J., and Bauer, R., 1992, Erosion thresholds and land surface morphology: *Geology*, v. 20, p. 675-679.
- Dietrich, W., and Dunne, T., 1993, The channel head, *in* Beven, K., and Kirkby, M., eds., Channel Networls Hydrology: Chichester, Wiley, p. 175-219.
- Dietrich, W.E., Wilson, C.J., Montgomery, D.R., and McKean, J., 1993, Analysis of erosion thresholds, channel networks, and landscape morphology using a digital terrain model: *Journal of Geology*, v. 101, p. 259-278.
- Dietrich, W.E., Reiss, R., Hsu, M.-L., and Montgomery, D.R., 1995, A process-based model for colluvial soil depth and shallow landsliding using digital elevation data: *Hydrological Processes*, v. 9, p. 383-400.
- Dikau, R., 1989, The application of digital relief model to landform analysis in Geomorphology, *in* Raper, J.F., ed., *3-Dimensional Applications in G.I.S.* London, Taylor & Francis, p. 51-76.
- Dinklage, B., 1991, *The evolution of drainage density on Wheeler Ridge, an active fault-bend anticline, southern San Joaquin Valley,* Minor Comps Paper.
- Dole, R., and Stabler, H., 1909, *Denudation*, United States Geological Survey, 78-93 p.
- Ellen, S.D., Paterson, D.M., and Reid, G.O., 1982, Map showing areas susceptible to different hazards from shallow landslides, Marin County and adjacent parts of Sonoma County, California: *United States Geological Survey Miscellaneous Field Studies Map*, v. MF-1406.
- Ellen, S.D., and Wentworth, C.M., 1983, Hillside materials and slopes of the San Francisco Bay Region, California: *U. S. Geological Survey Professional Paper*, v. 1357.
- Ellen, S.D., Wieczorek, G.F., Brown, W.M., and Herd, D.G., 1988, Landslides, floods and marine effects of the storm of January 3-5, 1982, in the San Francisco Bay Region, California, *in* Ellen, S.D., and Wieczorek, G.F., eds., *Landslides, floods and marine effects of the storm of January 3-5, 1982, in the San Francisco Bay Region, California*: Washington, D.C., USGS.
- Ellen, S.D., Mark, R.K., Wieczorek, G.F., Wentworth, C.M., Ramsey, D.W., and May, T.E., 1997, Map showing principal debris-flow source areas in the San Francisco Bay Region, California: *U.S. Geological Survey Open-File Report 97-745E.*
- Ellis, M., Densmore, A., and Anderson, R., 1999, Development of mountainous topography in the Basin Ranges, USA: Basin Research, v. 11, p. 21-41.
- Evans, I.S., 1972, General geomorphometry, derivatives of altitude and descriptive statistics, *in* Chorley, R.J., ed., *Spatial analysis in Geomorphology*: London, Methuen & Co., p. 17-90.
- Formento-Triglio, M.L., and Pazzaglia, F.J., 1998, Tectonic *Geomorphology* of the Sierra Nacimiento: Traditional and new techniques in assessing long-term landscape evolution in the southern Rocky Mountains: *Journal of Geology*, v. 106, p. 433-453.
- Fournier, F., 1960, *Climat et erosion*: Paris, Presses Universitaires de France, 201 pp.
- Francis, S.L., 1987, Slope development through the threshold slope concept, *in* Anderson, M.G., and Richards, K.S., eds., *Slope Instability*: London, Wiley, p. 601-624.

- Fried, A., and Smith, N., 1992, Timescales and the role of inheritance in long-term landscape evolution, northern New England, Australia: *Earth Surface Processes and Landforms*, v. 17, p. 375-385.
- Gao, J., 1993, Identification of topographic settings conducive to landsliding from DEM in Nelson County, Virginia, U.S.A: *Earth Surface Processes and Landforms*, v. 18, p. 579-591.
- Gardner, T.W., Sasowsky, K.C., and Day, R.L., 1990, Automated extraction of geomorphometric properties from digital elevation data: *Zeitschrift fur Geomorphologie Supplement-Band*, v. 80, p. 57-68.
- Gilbert, G.K., 1877, *Report on the Geology of the Henry Mountains: Washington DC*, United States Department of the Interior.
- Gilbert, G., 1909, The convexity of hilltops: *Journal of Geology*, v. 17, p. 344-350.
- Giles, P.T., 1998, Geomorphological signatures: Classification of aggregated slope unit objects from digital elevation and remote sensing data: *Earth Surface Processes and Landforms*, v. 23, p. 581-594.
- Gilchrist, A.R., Summerfield, M.A., and Cockburn, H.A.P., 1994, Landscape dissection, isostatic uplift and the morphological development of orogens: *Geology*, v. 22, p. 963-966.
- Goldrick, G., and Bishop, P., 1995, Differentiating the roles of lithology and uplift in the steepening of bedrock river long profiles: an example from southeastern Australia: *Journal of Geology*, v. 103, p. 227-231.
- Gomez, B., and Church, M., 1989, An assessment of bed load transport formulae for gravel-bed rivers: *Water Resources Research*, v. 25, p. 1161-1181.
- Granger, D., Kirchner, J., and Finkel, R., 1996, Spatially averaged long-term erosion rates measured from in-site-produced cosmogenic nuclides in alluvial sediments: *Journal of Geology*, v. 104, p. 249-257.
- Gunnell, Y., 1998, Present, past and potential denudation rates: is there a link? Tentative evidence from fission-track data, river sediment loads and terrain analysis in the South Indian Shield: *Geomorphology*, v. 25, p. 135-153.
- Guzzetti, F., and Reichenbach, P., 1994, Towards a definition of topographic divisions for Italy: *Geomorphology*, v. 11, p. 57-74.
- Hack, J.T., 1957, *Studies of longitudinal stream profiles in Virginia and Maryland*: Washington, United States Government Printing Office, 97 p.
- Hack, J.T., 1973, Stream-profile analysis and stream-gradient index: *Journal of Research of the United States Geological Survey*, v. 1, p. 421-429.
- Hagstrum, J.T., and Murchey, B.L., 1993, Deposition of Franciscan Complex cherts along the palaeoequator and accretion to the American margin at tropical palaeolatitudes: *Geological Society of America Bulletin*, v. 105, p. 766-778.
- Hancock, G.S., Anderson, R.S., and Whipple, K.X., 1998, Beyond power: bedrock river incision process and form, *in* Tinkler, K., and Wohl, E.J., eds., *Rivers Over Rock: Fluvial Processes in Bedrock Channels*, AGU, Washington, DC.
- Hansen, A., 1984, Landslide hazard analysis, *in* Brunsden, D., and Prior, D.B., eds., *Slope Instability*: New York, Wiley, p. 523-602.
- Heimsath, A., Dietrich, W., Nishiizumi, K., and Finkel, R., 1997, The soil production function and landscape equilibrium: *Nature*, v. 388, p. 358-361.
- Hoffman, P.F., and Grotzinger, J.P., 1993, Orographic precipitation, erosional unloading, and tectonic style: *Geology*, v. 21, p. 195-198.

- Hooke, R.L., 1972, Geomorphic evidence for late-Wisconsin and Holocene tectonic deformation, Death Valley, California: *Geological Society of America Bulletin*, v. 83, p. 2073-2098.
- Hovius, N., 1995, *Macro scale process systems of mountain belt erosion and sediment delivery to basins* [Ph.D. Thesis], Oxford University, UK.
- Hovius, N., 1996, Regular spacing of drainage outlets from linear mountain belts: Basin Research, v. 8, p. 29-44.
- Hovius, N., Stark, C.P., and Allen, P.A., 1997, Sediment flux from a mountain belt derived by landslide mapping: *Geology*, v. 25(3), p. 231-234.
- Hovius, N., and Leeder, M.R., 1998, Clastic sediment supply to basins: *Basin Research*, v. 10, p. 1-5.
- Hovius, N., Stark, C.P., and Weissel, J.K., 1998, Topographic controls on hydro-meteorologically and seismically induced landslides: *Eos Transactions, AGU*, v. 79 (45), p. F357.
- Howard, A.D., and Kerby, A., 1983, Channel changes in badlands: *Geological Society of America Bulletin*, v. 94, p. 739-752.
- Howard, A.D., 1994, A detachment limited model of drainage basin evolution: *Water Resources Research*, v. 30(7), p. 2261-2285.
- Howard, A.D., Dietrich, W.E., and Seidl, M.A., 1994, Modelling fluvial erosion on regional to continental scales: *Journal of Geophysical Research*, v. 99, p. 13971-13986.
- Howard, A.D., 1997, Badland morphology and evolution: interpretation using a simulation model: *Earth Surface Processes and Landforms*, v. 22, p. 211-227.
- Howe, E., 1909, Landslides in the San Juan Mountains, Colorado: *U. S. Geological Survey Professional Paper*, v. 67, p. 58.
- Howell, D., and Murray, R., 1986, A budget for continental growth and denudation: *Science*, p. 446-449.
- Ijjasz-Vasquez, E.J., and Bras, R.L., 1995, Scaling regimes of local slope versus contributing area in digital elevation models: *Geomorphology*, v. 12, p. 299-311.
- Mather, P., 1992, "Long term" land surface processes: erosion, tectonics and climate history in mountain belts, *in* Isacks, B., ed., *TERRA-1: Understanding the terrestrial environment: the role of Earth observations from space*: London, Taylor and Francis.
- Iverson, R., Reid, M., and LaHusen, R., 1997, Debris flow mobilization from landslides: *Annual Review of Earth and Planetary Sciences*, v. 25, p. 85-138.
- Jacobson, R.B., Cron, E.D., and McGeehin, J.P., 1989, Slope movements triggered by heavy rainfall, November 3-5, 1985, in Virginia and West Virginia, USA: *Geological Society of America Special Paper*, v. 236, p. 1-13.
- Jaeger, H., and Nagel, S., 1992, Physics of the granular state: *Science*, v. 255, p. 1523-1530.
- James, E.W., 1992, Cretaceous metamorphism and plutonism in the Santa Cruz Mountains, Salinian Block, California, and correlations with the southernmost Sierra Nevada: *Geological Society of America Bulletin*, v. 104, p. 1326-1339.
- Jensen, S.K., and Domingue, J.O., 1988, Extracting topographic structure from digital elevation data for geographic information system analysis: *Photogrammetric Engineering and Remote Sensing*, v. 54(11), p. 1593-1600.
- Jibson, R.W., and Keefer, D.F., 1989, Statistical analysis of factors affecting landslide distribution in the New Madrid seismic zone, Tennessee and Kentucky: Engineering *Geology*, v. 27, p. 509-542.

- Jorgensen, D., 1998, Dynamic equilibrium between an active uplift and the Sevier River, Utah: Journal of Geology, v. 106, p. 181-194.
- Judson, S., and Ritter, D., 1964, Rates of regional denudation in the United States: *Journal of Geophysical Research*, v. 69, p. 3395-3401.
- Keefer, D.K., and Johnson, A.M., 1983, Earth Flows: Morphology, Mobilization and Movement: *U.S. Geological Survey Professional Paper 1264*, 55 p.
- Keller, J.V.A., Minelli, G., and Pialli, G., 1994, Anatomy of late orogenic extension: the Northern Apennines case: *Tectonophysics*, v. 238, p. 275-294.
- Keller, E.A., and Pinter, N., 1996, *Active tectonics: Earthquakes and landscape*: New Jersey, Prentice Hall, 333 p.
- Keller, E., Zapeda, R., Rockwell, T., and Ku, T.-L., 1998, Active tectonics and soil chronology of Wheeler Ridge, Southern San Joaquin Valley, California: Geological Society of America Bulletin, v. 110, p. 298-310.
- Kelsey, H.M., 1978, Earthflows in Franciscan melange, Van Duzen River Basin, California: *Geology*, v. 6, p. 361-364.
- Kelsey, H.M., 1980, A sediment budget and an analysis of geomorphic process in the Van Duzen River Basin, north coastal California, 1941-1975: *Geological Society of America Bulletin*, v. 91(2), p. 1119-1126.
- Kidson, C., 1977, The coast of South-West England, *in* Kidson, C., and Tooley, M., eds., *The Quaternary History of the Irish Sea*, Volume 7: Geological Journal Special Issue: Liverpool, Seel House Press.
- King, L., 1951, *South African Scenery*: London, Oliver and Boyd.
- Knighton, A., 1987, *Fluvial forms and processes*: London, Arnold.
- Kodema, Y., 1994, Downstream changes in the lithology and grain size of fluvial gravel, the Watarase River, Japan: Evidence for the role of abrasion in downstream fining.: Journal of Sedimentary Research. Section A, v. 64, p. 68-75.
- Kooi, H., and Beaumont, C., 1994, Escarpment evolution on high-elevation rifted margins: Insights derived from a surface process model that combines diffusion, advection, and reaction: *Journal of Geophysical Research*, v. 99, p. 12191-12211.
- Kooi, H., and Beaumont, C., 1996, Large-scale geomorphology: Classic concepts reconciled and integrated with contemporary ideas via a surface processes model: Journal of Geophysical Research, v. 101 (B2), p. 3361-3386.
- Koons, P.O., 1989, The topographic evolution of collisional mountain belts: a numerical look at the Southern Alps, New Zealand: *American Journal of Science*, v. 289, p. 1041-1069.
- Koons, P., 1995, Modelling the topographic evolution of collisional belts: *Annual Review of Earth and Planetary Sciences*, v. 25, p. 375-408.
- Kooi, H., and Beaumont, C., 1996, Large-scale Geomorphology: Classic concepts reconciled and integrated with contemporary ideas via a surface processes model: *Journal of Geophysical Research*, v. 101 (B2), p. 3361-3386.
- Krauskopf, K.B., Feitler, S., and Griggs, A.B., 1939, Structural features of a landslide near Gilroy, California: *Journal of Geology*, v. 47(6), p. 630-648.
- Lane, S., Richards, K., and Chandler, J., 1995, Morphological estimation of the time-integrated bed load transport rate: Water Resources Research, v. 31, p. 761-772.
- Langbein, W., and Schumm, S., 1958, Yield of sediment in relation to mean annual precipitation: *Transactions American Geophysical Union*, v. 39, p. 1076-1084.

- Leeder, M., 1997, Sedimentary basins: tectonic recorders of sediment discharge from drainage catchments: Earth Surface Processes and Landforms, v. 22, p. 229-237.
- Leopold, L., and Maddock, T., 1953, The hydraulic geometry of stream channels and some physiographic implications: *U.S. Geological Survey Professional Paper 600D*, p. 45-47.
- Leopold, L.B., Wolman, M.G., and Miller, J.P., 1964, *Fluvial Process in Geomorphology*: San Francisco, Freeman & Co.
- Lifton, N.A., and Chase, C.G., 1992, Tectonic, climatic and lithologic influences on landscape fractal dimension and hypsometry: implications for landscape evolution in the San Gabriel Mountains, California: *Geomorphology*, v. 5, p. 77-114.
- Mackin, J.H., 1948, Concept of the graded river: *Bulletin of the Geological Society of America*, v. 59, p. 463-512.
- Margheriti, L., Nostro, C., Cocco, M., and Amato, A., 1996, Seismic anisotropy beneath the Northern Apennines (Italy) and its tectonic implications: *Geophysical Research Letters*, v. 23(20), p. 2721-2724.
- Martin, Y., and Church, M., 1997, Diffusion in landscape development models: On the Nature of basic transport relations: *Earth Surface Processes and Landforms*, v. 22, p. 273-279.
- Martz, L.W., and Garbrecht, J., 1998, The treatment of flat areas and depressions in automated drainage analysis of raster digital elevation models: Hydrological Processes, v. 12, p. 843-855.
- Masek, J.G., Isacks, B.L., Gubbels, T.L., and Fielding, E.J., 1994, Erosion and tectonics at the margins of continental plateaus: *Journal of Geophysical Research*, v. 99(B7), p. 13941-13956.
- Meade, R., 1982, Sources, sinks, and storage of river sediment in the Atlantic drainage of the United States: *Journal of Geology*, v. 90, p. 235-252.
- Medwedeff, D.A., 1992, Geometry and kinematics of a active, laterally propagating wedge thrust, Wheeler Ridge, California, *in* Mitra, S., and Fisher, G.W., eds., *Structural Geology of fold and thrust belts*: Baltimore, John Hopkins University Press, p. 3-28.
- Meigs, A., Brozovic, N., and Johnson, M., 1999, Steady, balanced rates of uplift and erosion in the Santa Monica Mountains, California: Basin Research, v. 11.
- Menard, H., 1961, Some rates of regional erosion: *Journal of Geology*, v. 69, p. 154-160.
- Merrits, D., and Vincent, K., 1987, Geomorphic response of coastal streams to low, intermediate and high rates of uplift, Mendocino Triple Junction region, northern California: *Geological Society of America Bulletin*.
- Meyer-Peter, E., and Muller, R., 1948, *Formulas for bedload transport*, 3rd Annual Conference of the International Association for Hydraulic Research: Proceedings: Stockholm, p. 39-64.
- Miller, J.R., 1991, The influence of bedrock Geology on knickpoint development and channel-bed degradation along downcutting streams in south-central Indiana: *Journal of Geology*, v. 99, p. 591-605.
- Milliman, J.D., and Syvitski, J.P.M., 1992, Geomorphic/tectonic control of sediment discharge to the ocean: The importance of small mountainous rivers: *Journal of Geology*, v. 100, p. 525-544.
- Milliman, J., and Meade, R., 1983, World-wide delivery of river sediment to the oceans: *Journal of Geology*, v. 91, p. 1-21.

- Molnar, P., and England, P., 1990, Late Cenozoic uplift of mountain ranges and global climate change: chicken or egg?: *Nature*, v. 346, p. 29-34.
- Molnar, P., England, P., and Martinod, J., 1993, Mantle dynamics, uplift of the Tibetan Plateau, and the Indian Monsoon: *Reviews of Geophysics*, v. 31, p. 357-396.
- Montgomery, D.R., and Dietrich, W.E., 1989, Source areas, drainage density, and channel initiation: *Water Resources Research*, v. 25(8), p. 1907-1918.
- Montgomery, D., and Dietrich, W., 1992, Channel initiation and the problem of landscape scale: Science, v. 255, p. 826-830.
- Montgomery, D., and Dietrich, W., 1994, A physically-based model for the topographic control on shallow landsliding: Water Resources Research, v. 30, p. 1153-1171.
- Montgomery, D.R., and Foufoula-Georgiou, E., 1993, Channel network source representation using digital elevation models: *Water Resources Research*, v. 29(12), p. 3925-3934.
- Montgomery, D.R., 1994, Valley incision and the uplift of mountain peaks: *Journal of Geophysical Research*, v. 99(B7), p. 13913-13921.
- Montgomery, D.R., and Buffington, J.M., 1997, Channel-reach morphology in mountain drainage basins: *Bulletin of the Geological Society of America*, v. 109(5), p. 596-611.
- Montgomery, D.R., Sullivan, K., and Greenberg, H.M., 1998, Regional test of a model for shallow landsliding: *Hydrological Processes*, v. 12, p. 943-955.
- Moore, I.D., Grayson, R.B., and Ladson, A.R., 1991, Digital terrain modelling: a review of hydrological, geomorphological, and biological applications: Hydrological Processes, v. 5, p. 3-30.
- Morisawa, M., 1985, *Fluvial Geomorphology*: London, Allen and Unwin.
- Mueller, K., and Talling, P.J., 1997, Geomorphic evidence for tear faults accommodating lateral propagation of an active fault-bend fold, Wheeler Ridge, California: *Journal of Structural Geology*, v. 19(3-4), p. 397-411.
- Nash, D., 1980, Forms of bluffs degraded for different lengths of time in Emmet County, Michigan, U.S.A.: *Earth Surface Processes and Landforms*, v. 5, p. 331-345.
- Nelson, B., 1970, Hydrography, sediment dispersal, and recent historical development of the Po River delta. Italy, *in* Morgen, J., ed., Deltaic Sedimentation: Modern and Ancient, Volume 15, Society of Economic Petrologists and Mineralogists, p. 152-185.
- Nilsen, T.H., and Wright, R.H., 1979, *Relative slope stability and land use planning in the San Francisco Bay Region, California*: U.S. Geological Survey Professional Paper 944.
- Nogami, M., 1995, Geomorphometric measures for digital elevation models: *Zeitschrift fur Geomorphologie Supplement-Band*, v. 101, p. 53-67.
- O'Callaghan, L., and Mark, D.M., 1984, The extraction of drainage networks from digital elevation data: *Computer Vision Graphics and Image Processing*, v. 28(30, p. 323-344.
- Oguchi, T., 1997, Drainage density and relative relief in humid steep mountains with frequent slope failure: *Earth Surface Processes and Landforms*, v. 22, p. 107-120.
- Ohmori, H., 1983, Erosion rates and their relation to vegetation from the viewpoint of world-wide distribution: *Bulletin of the Department of Geography, University of Tokyo*, v. 15, p. 77-91.

- Ohmori, H., and Saito, K., 1993, Morphological development of longitudinal profiles of rivers in Japan and Taiwan: *Bulletin of the Department of Geography, University of Tokyo.*
- Ohmori, H., and Sugai, T., 1995, Towards geomorphometric models for estimating landslide dynamics and forecasting landslide occurrence in Japanese mountains: *Zeitschrift fur Geomorphologie Supplement-Band*, v. 101, p. 149-164.
- Paola, C., Hellert, P.L., and Angevine, C.L., 1992, The large scale dynamics of grain-size variation in alluvial basins, 1: theory: *Basin Research*, v. 4, p. 73-90.
- Paola, C., and Mohrig, D., 1996, Palaeohydraulics revisited: palaeoslope estimation in coarse-grained braided rivers: Basin Research, v. 8, p. 243-254.
- Park, A.J.C., 1995, *The application of a geographical information system approach to the modelling of tropical slope instability over wide areas* [Ph.D. Thesis], University of Bristol, Bristol.
- Parker, G., Klingeman, P., and McLean, D., 1982, Bedload and size distribution in paved gravel-bed streams: Journal of Hydraulic Engineering, v. 108, p. 544-571.
- Parker, G., Paola, C., Whipple, K., and Mohrig, D., 1998, Alluvial fans formed by channelised fluvial and sheet flow. I: Theory: Journal of Hydraulic Engineering, v. 124, p. 985-995.
- Pavlis, T.L., Hamburger, M.W., and Pavlis, G.L., 1997, Erosional processes as a control on the structural evolution of an actively deforming fold and thrust belt: An example from the Pamir-Tien Shan region, central Asia: *Tectonics*, v. 16(5), p. 810-822.
- Pazzaglia, F., and Brandon, M., 1996, Macrogeomorphic evolution of the post-Triassic Appalachian mountains determined by deconvolution of the offshore basin sedimentary record: Basin Research, v. 8, p. 255-278.
- Pazzaglia, F., Gardner, T., and Merrits, D., 1998, Bedrock fluvial incision and longitudinal profile development over geologic time scales determined by fluvial terraces, *in* Wohl, E., and Tinkler, K., eds., *Rivers Over Rock: Fluvial Processes in Bedrock Channels*, AGU, Washington, DC.
- Penck, W., 1924, Die Morphologische Analyse: Ein Kapital der Physikalischen Geologie: Stuttgart, Engelhorn.
- Peters, J.J., 1978, Discharge and sand transport in the braided zone of the Zaire Estuary: *Netherlands Journal of Sea Research*, v. 12, p. 273-272.
- Peuker, T.K., and Douglas, D.H., 1975, Detection of surface specific points by local parallel processing of discrete terrain elevation data: *Computer Graphics and Image Processing*, v. 4, p. 375-387.
- Pieri, M., and Groppi, D., 1981, Subsurface geological structure of the Po Plain, Italy: *CRNR P.F. Geodinamica*, v. 414.
- Pike, R.J., and Wilson, S.E., 1971, Elevation-relief ratio, hypsometric integral, and geomorphic area-altitude analysis: *Geological Society of America Bulletin*, v. 82, p. 1079-1084.
- Pike, R.J., 1987, Toward geometric signatures for geographic information systems: *IGIS Symposium Proceedings*, v. Vol. III, p. III-15-III-26.
- Pike, R.J., 1988, The geometric signature: Quantifying landslide terrain types from digital elevation models: *Mathematical Geology*, v. 20(5), p. 491-511.
- Pike, R.J., 1997, Index to detailed maps of landslides in the San Francisco Bay Region, California: *Open-File Report 97-745D.*
- Pilotti, M., Gandolfi, C., and Bischetti, G.B., 1996, Identification and analysis of natural channel networks from digital elevation models: Earth Surface Processes and Landforms, v. 21, p. 1007-1020.

- Pizzuto, J., 1992, The morphology of graded gravel rivers: a network perspective: Geomorphology, v. 5, p. 457-474.
- Pizzuto, J., 1995, Downstream fining in a network of gravel-bedded rivers: Water Resources Research, v. 31, p. 753-759.
- Powell, D., and Ashworth, P., 1995, Spatial pattern of flow competence and bed load transport in a divided gravel-bed river: Water Resources Research, v. 31, p. 741-752.
- Powell, D., 1998, Patterns and processes of sediment sorting in gravel-bed rivers: Progress in physical geography, v. 22, p. 1-32.
- Pratson, L., and Ryan, W., 1996, Automated drainage extraction in mapping the Monterey Submarine drainage system, California Margin: Marine Geophysical Researches, v. 18, p. 757-777.
- Rantz, S.E., 1968, Average annual precipitation and runoff in north central California, scale 1:1,000000: *United States Geological Survey Hydrological Atlas*, v. 298.
- Raymo, M.E., and Ruddiman, W.F., 1992, Tectonic forcing of late Cenozoic climate: *Nature*, v. 359, p. 117-122.
- Reichenbach, P., Pike, R.J., Acevedo, W., and Mark, R.K., 1993, A new landform map of Italy in computer-shaded relief: *Rivista Dell'Istituto Geografico Militare*, v. 52, p. 21-45.
- Reid, I., and Laronne, J., 1995, Bed load sediment transport in an ephemeral stream and a comparison with seasonal and perennial counterparts: Water Resources Research, v. 31, p. 773-781.
- Rhea, S., 1993, Geomorphic observations of rivers in the Oregon Coast Range from a regional reconnaissance perspective: *Geomorphology*, v. 6, p. 135-150.
- Richards, K., 1982, *Rivers: Form and Process in alluvial channels*: London, Methuen.
- Rice, R.M., Corbett, E.S., and Bailey, R.G., 1969, Soil slips related to vegetation, topography and soil in southern California: *Water Resources Research*, v. 5, p. 649-659.
- Rice, S., 1998, Which tributaries disrupt downstream fining along gravel-bed rivers: Geomorphology, v. 22, p. 39-56.
- Rieger, W., 1998, A phenomenon-based approach to upslope contributing areas and depressions in DEMs: Hydrological Processes, v. 12, p. 857-872.
- Rigon, R., Rinaldo, A., and Rodriguez-Iturbe, I., 1994, On landscape self-organisation: Journal of Geophysical Research, v. 99, p. 11971-11993.
- Rodgers, J., 1997, Exotic nappes in external parts of orogenic belts: *American Journal of Science*, v. 297, p. 174-219.
- Roering, J.J., Kirchner, J.W., and Dietrich, W.E., 1997, Evidence for a non-linear mass wasting transport law and implications for hillslope evolution in the Oregon Coast Range: *Eos Transactions, AGU*, v. 78(46), p. F287.
- Roering, J.J., Sklar, L., Kirchner, J.W., and Dietrich, W.E., 1998, A laboratory simulation of diffusive sediment transport on hillslopes: non-linear transport and the evolution of convex hilltops (abstract): *Eos Transactions, AGU*, v. 79 (45), p. F338.
- Roering, J., Kirchner, J., and Dietrich, W., 1999, Evidence for nonlinear, diffusive sediment transport on hillslopes and implications for landscape morphology: *Water Resources Research*, v. 35, p. 853-870.

- Rosenbloom, N.A., and Anderson, R.S., 1994, Hillslope and channel evolution in a marin terraced landscape, Santa Cruz, California: *Journal of Geophysical Research*, v. 99(B7), p. 14013-14030.
- Ruxton, B.P., and McDougall, I., 1967, Denudation rates in northeast Papua from potassium-argon dating of lavas: *American Journal of Science*, v. 265(7), p. 545-561.
- Schlocker, J., 1974, Geology of the San Francisco North Quadrangle, California: *U. S. Geological Survey Professional Paper 782*.
- Schmidt, K.M., and Montgomery, D.R., 1995, Limits to relief: *Science*, v. 270, p. 617-620.
- Schumm, S.A., 1964, Seasonal variations of erosion rates and processes on hillslopes in western Colorado: *Zeitschrift fur Geomorphologie Supplement-Band*, v. 5, p. 213-238.
- Schumm, S., Mosley, M., Zimpfer, G., and Trimble, S., 1976, Unsteady state denudation: *Science*, v. 191, p. 871.
- Seidl, M.A., and Dietrich, W.E., 1992, The problem of channel erosion into bedrock, *in* Schmidt, K.H., and de Ploey, J., eds., *Functional Geomorphology: Landform Analysis and Models*: Catena Supplementband: Cremlingen, Catena-Verlag, p. 101-125.
- Seidl, M.A., Dietrich, W.E., and Kirchner, J.W., 1994, Longitudinal profile development into bedrock: an analysis of Hawaiian channels: *Journal of Geology*, v. 102, p. 457-474.
- Sharpe, C.F.S., 1938, *Landslides and related phenomena: a study of mass movements of soil and rock*: New York, Columbia University Press, 136 p.
- Shaw, G., and Wheeler, D., 1994, *Statistical techniques in geographical analysis*: London, David Fulton Publishers, 359 p.
- Shields, A., 1936, Anwendung der Ahnlichkeitsmechanik und der Turbulenzforschung auf die Geschiebedewegung: Preuss: Versuchsanstalt fur Wasserbau und Schiffbau (Berlin), Mitteleiungen, v. 26, 26pp.
- Skempton, A., and Hutchinson, J., 1969, Stability of natural slopes and embankment foundations, International conference on soil and foundation engineering, A.A. Balkema, p. 291-340.
- Slaymaker, O., 1987, Sediment and solute loads in British Columbia and Yukon: their geomorphic significance reexamined, *in* Gardiner, V., ed., *International Geomorphology*: Chichester, Wiley, p. 925-945.
- Snow, R., and Slingerland, R., 1987, Mathematical modelling of graded river profiles: *Journal of Geology*, v. 95, p. 15-33.
- Sowter, M.J.., 1996, *Geomorphic controls on long-term landscape evolution in Southern Africa: Case study of the Tugela River, Natal* [MA thesis]: University of Edinburgh, UK.
- Sowter, M.J., Talling, P.J., Reichenbach, P., and Guzzetti, F., 1997, The use of digital elevation models in quantitative topographic analyses within orogenic mountain belts: *Supplementi di Geografia Fisica e Dinamica Quaternaria Supplemento III, 359.*
- Sowter, M.J., and Talling, P.J., 1998, Topographic fingerprinting of erosional processes in mountainous regions: *Eos Transactions, AGU*, v. 79(45), p. F366.
- Strahler, A., 1950, Equilibrium theory of erosional slopes approached by frequency distribution analysis: *American Journal of Science*, v. 248, p. 673-696.
- Strahler, A.N., 1952, Hypsometric (area-altitude) analysis of erosional topography: *Bulletin of the Geological Society of America*, v. 63, p. 1117-1142.

- Summerfield, M.A., 1991, *Global Geomorphology*: New York, John Wiley & Sons, 537 p.
- Summerfield, M.A., and Hulton, N.J., 1994, Natural controls on fluvial denudation rates in major world drainage basins: *Journal of Geophysical Research*, v. 99(B7), p. 13871-13883.
- Talling, P.J., 1994, *Sedimentation and tectonic Geomorphology in areas of active tectonic compression* [Ph.D. thesis], University of Leeds, UK.
- Talling, P.J., and Sowter, M.J., 1998, Basin-wide variations in stream power and shear stress: *Basin Research*, v. 10, p. 87-108.
- Talling, P., and Sowter, M., in press:a, Temporal evolution of drainage density on surfaces with different gradients, Wheeler Ridge, California: *Earth Surface Processes and Landforms*.
- Talling, P., in press, Self-organization of river networks to threshold states: Water Resources Research.
- Tarboton, D.G., Bras, R.L., and Rodriguez-Iturbe, I., 1991, On the extraction of channel networks from digital elevation data: *Hydrological Processes*, v. 5, p. 81-100.
- Tinkler, K., and Wohl, E., 1999, A primer on bedrock channels, *in* Tinkler, K., and Wohl, E., eds., Rivers over Rock: Fluvial processes in bedrock channels: Washington DC, AGU.
- Topping, D., 1993, Palaeogeographic reconstruction of the Death Valley extended region: evidence from Miocene large rock-avalanche deposits in the Armagosa Chaos Basin, California: *Geological Society of America Bulletin*, v. 105, p. 1190-1213.
- Tribe, A., 1992, Automated recognition of valley heads from digital elevation models: *Earth Surface Processes and Landforms*, v. 16, p. 33-49.
- Trimble, S., 1975, Denudation studies: can we assume steady state?: *Science*, v. 188, p. 1207-1208.
- Trimble, S., 1977, The fallacy of stream equilibrium in contemporary denudation studies: *American Journal of Science*, v. 277.
- Trimble, S., 1983, A sediment budget for Coon Creek Basin in the Driftless area, Wisconsin, 1853-1977: *American Journal of Science*, v. 283, p. 454-474.
- Tucker, G.E., and Slingerland, R.L., 1994, Escarpment dynamics, flexural isostasy, and long-lived escarpments: A numerical modelling study: *Journal of Geophysical Research*, v. 99, p. 12229-12243.
- Tucker, G.E., and Slingerland, R., 1996, Predicting sediment flux from fold and thrust belts: *Basin Research*, v. 8, p. 329-349.
- Tucker, G.E., and Bras, R.L., 1998, Hillslope processes, drainage density, and landscape morphology: Water Resources Research, v. 34(10), p. 2751-2764.
- van Asch, T.W.J., Haak, W.J.C., and Simon, J., 1989, The viscous creep component in shallow clayey soil and the influence of tree load on creep rates: *Earth Surface Processes and Landforms*, v. 14, p. 557-564.
- van der Beek, P., and Braun, J., 1998, Numerical modelling of landscape evolution on geological time-scales: a parameter analysis and comparison with the south-eastern highlands of Australia: *Basin Research*, v. 10, p. 49-68.
- van der Beek, P., and Braun, J., 1999, Controls on post mid-Cretaceous landscape evolution in the southeastern Highlands of Australia: Insights from numerical surface process models: *Journal of Geophysical Research*, v. 104, p. 4945-4966.
- van Wamel, W.A., 1987, On the tectonics of the Ligurian Apennines (northern Italy): *Tectonophysics*, v. 142, p. 87-98.

- Varnes, D.J., 1958, Landslide types and processes, *in* Eckel, E.B., ed., *Landslides and engineering practice*: Washington, D.C., Highway Research Board Special Report 29, p. 20-47.
- Vogel, G.K., Rinaldo, A., Rigon, R., and Rodriguez-Iturbe, I., 1995, Can one gauge the shape of a basin?: *Water Resources Research*, v. 31(4), p. 1119-1127.
- Warren, A., 1976, Morphology and sediments of the Nebraska sand hills in relation to pleistocene winds and the development of aeolian bedforms: *Journal of Geology*, v. 84, p. 685-700.
- Weissel, J.K., and Seidl, M.A., 1998, Inland propagation of erosional escarpments and river profile evolution across the southeast Australian passive margin, *in* Tinkler, K., and Wohl, E.J., eds., *Rivers Over Rock: Fluvial Processes in Bedrock Channels*, AGU, Washington, DC.
- Wentworth, C.M., Graham, S.E., Pike, R.J., Beukelman, G.S., Ramsey, D.W., and Barron, A.D., 1997, Summary distribution of slides and earth flows in the San Francisco Bay Region, California: *U.S. Geological Survey Open-File Report 97-745C.*
- Wilkin, J.C., 1995, *Sedimentation, Geomorphology and tectonics of active, extensional tilt blocks, basin and range, Nevada* [Ph.D. thesis], University of Leeds, UK.
- Willgoose, G., Bras, R.L., and Rodriguez-Iturbe, I., 1991, A coupled channel network growth and hillslope evolution model: 1. Theory: *Water Resources Research*, v. 27, p. 1671-1684.
- Willgoose, G., 1994, A statistic for testing the elevation characteristics of landscape simulation models: Journal of Geophysical Research, v. 99, p. 13987-13996.
- Willgoose, G.R., and Hancock, G., 1998, Revisiting the hypsometric curve as an indicator of form and process in transport-limited catchment: *Earth Surface Processes and Landforms*, v. 23, p. 611-623.
- Wilson, L., 1972, Variations in mean annual sediment yield as a function of mean annual precipitation: *American Journal of Science*, v. 272, p. 335-349.
- Wolman, M., 1954, A method of sampling coarse river-bed material: Transactions of the American Geophysical Union, v. 35, p. 951-956.
- Yatsu, E., 1955, On the longitudinal profile of the graded river: *American Geophysical Union Transactions*, v. 36, p. 655-663.
- Zavoianu, I., 1985, Hypsometric curves and longitudinal stream profiles, *in* Zavoianu, I., ed., *Morphometry of Drainage Basins*: Amsterdam, Elsevier,, p. 185-200.
- Zevenbergen, L.W., and Thorne, C.R., 1987, Quantitative analysis of land surface topography: *Earth Surface Processes and Landforms*, v. 12, p. 47-56.
- Zhang, W., and Montgomery, D.R., 1994, Digital elevation model grid size, landscape representation, and hydrologic simulations: Water Resources Research, v. 30, p. 1019-1028.
- Zhou, A.A., and Stuwe, A.A., 1994, Modeling the dynamic uplift, denudation rates, and thermomechanical consequences of erosion in isostatically compensated mountain belts: *Journal of Geophysical Research*, v. 99(B7), p. 13923-13939.
- Zoetemeijer, R., Cloetingh, S., Sassi, W., and Roure, F., 1993, Modelling of piggy-back stratigraphy: record of tectonic evolution: *Tectonophysics*, v. 226, p. 253-269.

APPENDIX 1

ARC MACRO LANGUAGE SCRIPTS (AMLS)

A1.1 FILL AML

```
/* DEM Pit Filling AML*/
/* The input grid : a grid of elevations*/
/* The output : a grid of elevations void of pits and sinks*/

/* Define the input DTM - 'return' for exit.*/
&setvar ingrid := [getgrid * 'Enter the grid name - 'none' for quit' -none]

/* Set the GRID extent*/
mape %ingrid%

/* If the grid exists, then continue*/
&if [exists %ingrid% -grid] &then
&do

/* Calculate the flow direction  of the input DEM*/
flow_dir = flowdirection (%grid%)

/* Define the sinks on the DEM*/
sink_areas = watershed (flow_dir, sink(flow_dir))

/* Calculate the sink depths of the DEM*/
sink_depth = zonalfill (sink_areas, %grid%) - (zonalmin (sink_areas, %grid%))

/* List the maximum sink depth*/
list sink_depth.sta

/* Kill off the temporary GRIDs*/
kill flow_dir
kill sink_areas
kill sink_depth

/* Define the filled GRID's name*/
&setvar new_grid := [response 'Enter the filled grid's name']

/* Define the maximum depth to which sinks are to be filled*/
&setvar sink_dep := [response 'Enter the sink_depth']

/* Fill the input GRID*/
fill %grid% %new_grid% sink %sink_dep%

&return
```

A1.2 LOCAL RELIEF AML

```
/* Local Relief AML*/
/* The input grid : a grid of elevations*/
/* The output : a grid of local relief within a defined range*/

/* Define the input grid of elevations - 'return' for exit.*/
&setvar ingrid := [getgrid * 'Enter the grid name - 'none' for quit' -none]

/* Define the calculation area*/
mape %ingrid%

/* If the selected GRID exists, then continue*/
&if [exists %ingrid% -grid] &then
&do

/* Define the size of the 'window' to calculate local relief within*/
&sv window := [response 'Enter the window radius size']

/* Calculate the local relief based on pixels surrounding a central pixel by calculating the range of
values within a selected window radius*/
focal = focalrange (%ingrid%, circle, %window%, data)

/* Define the output grid's name*/
&sv relief_grid = [response 'Enter the output relief grid's name']
rename focal %relief_grid%

&return
```

A1.3 DISPERSION OF ALTITUDE AML

```
/* Dispersion of Altitude AML*/
/* The input grid : a grid of elevations
/* The output : a grid of dispersion of altitude values within a defined window range*/

/* Define the input DTM - 'return' for exit.*/
&setvar ingrid := [getgrid s* 'Enter the slope grid - 'none' for quit' -none]

/* Set the GRID extent*/
mape %ingrid%

/* If the grid exists, then continue
&if [exists %ingrid% -grid] &then
&do

/* Define the calculation window's radius*/
&sv window := [response 'Enter the window radius size']

/* Calculate the dispersion of altitude within a defined window size*/
focal = focalstd (%ingrid%, circle, %window%, data)

/* List the range of dispersion calculated.*/
list focal.sta

/* Enter the minimum dispersion value*/
&setvar min := [response 'Enter the min standard deviation']

/* Enter the maximum dispersion value*/.
&setvar max := [response 'Enter the max standard deviation']

/* Count the number of pixels between the minimum and maximum dispersion values*/
count = con (focal > %min% && focal <= %max%, 1)

/* Perform check that there are values within the range !*/
&setvar check := [response 'enter the checking number-10 for nodata']

/* If there are values continue*/
&if %check% eq 10  &then
&do
      kill count
          kill focal
&end
&else
&do

/* List the number of pixels in the specified range*/
list count.vat

/* Kill off temporary GRIDs*/
kill count
kill focal

/* If there are no values then return.*/
&end
&return
```

A1.4 ELEVATION-RELIEF RATIO AML

```
/* Elevation-Relief Ratio / Hypsometric Integral Value AML*/
/* The input grid : a grid of elevations*/
/* The output : a grid of elevation-relief ratios within a defined window size*/

/* Define the input DTM - 'return' for exit.*/
&setvar ingrid := [getgrid * 'Enter the grid name - 'none' for quit' -none]

/* Set the GRID extent*/
mape %ingrid%

/* If the grid exists, then continue
&if [exists %ingrid% -grid] &then
&do

/* Define the size of the 'window' to calculate elevation-relief values within*/
&sv window := [response 'Enter the window radius size']


/* Calculate the minimum elevation within the window range*/
focalmin = focalmin (%ingrid%, circle, %window%, data)

/* Calculate the mean elevation within the window range*/
focalmean = focalmean (%ingrid%, circle, %window%, data)

/* Calculate the maximum elevation within the window range*/
focalmax = focalmax (%ingrid%, circle, %window%, data)

/* Calculate the elevation-relief ratio*/
el_relief = (focalmean - focalmin) / (focalmax - focalmin)

/* Multiply the output values by 100 to enable output to TABLES*/
el = (el_relief * 100)

/* List the elevation-relief values' range to calculate values for each 'slice' of the relief range*/.
list el.sta

/* Define the minimum relief threshold*/
&sv min := [response 'Enter the minimum relief threshold']

/* Define the maximum relief threshold*/
&sv max := [response 'Enter the maximum relief threshold']


/* Count the number of pixels between the relief ranges set.*/
count = con (el > %min% && el <= %max%, 1)

/* Check that there are values within the defined relief range*/
&setvar check := [response 'enter the checking number-10 for nodata']

/* If there are, continue*/
&if %check% eq 10  &then
&do
      kill count
          kill focalmin
          kill focalmax
          kill focalmean
          kill el_relief
          kill el
```

```
&end
&else
&do

/* List the number of pixels in the specified range
list count.vat

/* Kill off temporary GRIDs*/
kill count
kill focalmin
kill focalmax
kill focalmean
kill el_relief
kill el

/* If there are no values within the defined relief range, then return.*/
&end
&return
```

A1.5 DISSECTION INDEX AML

```
/* Dissection Index.AML*/
/* The input grid : a grid of elevations*/
/* The output : a grid of dissection indices*/

/* Define the input grid of elevations - 'return' for exit.*/
&setvar ingrid := [getgrid * 'Enter the grid name - 'none' for quit' -none]
/* Define the size of the 'window' to calculate the dissection indices within*/
&sv window := [response 'Enter the window radius size']

/* Calculate the minimum elevation within the window range*/
focalmin = focalmin (%ingrid%, circle, %window%, data)

/* Calculate the mean elevation within the window range*/
focalmean = focalmean (%ingrid%, circle, %window%, data)

/* Calculate the maximum elevation within the window range*/
focalmax = focalmax (%ingrid%, circle, %window%, data)

/* Calculate the dissection ratio, subtract the maximum window value from the mean window value
and divide by the result of the window maximum minus the window minimum*/
dis = (focalmax - focalmean) / (focalmax - focalmin)

/* Multiply the dissection indices by 100*/
diss = (dis * 100)

/* Kill off the temporary grids*/
kill focalmax all
kill focalmin all
kill focalmean all
kill dis all

/* Return to program*/
&return
```

A1.6 NOGAMI INDEX AML

```
/* Nogami Index AML*/
/* The input grid : a grid of elevations*/
/* The output : a grid of dissection ratios.*/

/* Define the input DTM - 'return' for exit.*/
&setvar ingrid := [getgrid * 'Enter the grid name - 'none' for quit' -none]

/* Calculate the minimum elevation within the 3*3 window range*/
focalmin = focalmin (%ingrid%, rectangle, 3, 3, data)

/* Calculate the maximum elevation within the window 3*3  range*/
focalmax = focalmax (%ingrid%, rectangle, 3, 3, data)

/* Calculate the Nogami Index values*/
/* Subtract the minimum window value from the central pixel's value*/
a = %ingrid% - focalmin
/* Subtract the maximum window value from the minimum pixel's value and multiply by 9*/
b = (focalmax - focalmin) * 9
/* Divide the two values*/
diss = a / b
/* Multiply 'diss' by 9*/
dis = diss * 9

/* Kill off temporary grids*/
kill diss all
kill focalmax all
kill focalmin all
kill a all
kill b all

/* Multiply 'dis' by 1000 to enable output to Tables*/
diss = dis * 1000

/*Kill 'dis'*/
kill dis all

/* Create integer GRID of diss*/
dis = int (diss)

/* Kill off temporary GRIDS*/
kill diss all

&return
```

A1.7 SLOPE VARIABILITY AML

```
/* Slope Variability Index*/
/* The input grid : a grid of elevations*/
/* The output : a grid of slope variability within a defined window range*/

/* Define the input grid of elevations - 'return' for exit.*/
&setvar ingrid := [getgrid * 'Enter the grid name - 'none' for quit' -none]

/* Define the size of the 'window' to calculate slope variability within*/
&sv window := [response 'Enter the window radius size']

/* Calculate slope values within the GRID*/
slope = slope (%grid%)

/* Calculate the mean value within a rectangular window of length defined above*/
focal4 = focalmean (slope, rectangle, %window%, %window%, data)

/* Subtract the mean value from the calculated slope values over the GRID*/
a = slope - focal4

/* Output a description of the output GRID*/
describe a

/*  From the output table input the value of the minimum pixel*/
&sv value = [response 'enter the minimum value']

/* Make the output GRID 'a' have positive values*/
b = a + %value%

/* Sum all the values within the window*/
focal5 = focalsum (b, rectangle, 3, 3, data)

/* Calculate the sum of values divided by the slope value for each value*/
matt = focal5 / slope

/* Calculate the value of the window's sum divided by the window's mean*/
matt2 = focal5 / focal4

/* Make the output GRID have integer values*/
int = int (matt)

/* Make output GRID 'matt2' integer*/
int2 = int (matt2)

/* Kill off temporary GRIDs*/
kill matt all
kill matt2 all
kill slope all
kill focal5 all
kill focal4 all
kill a all
kill b all

rename int matt
rename int2 matt
```